PATTERNS AND DRIVERS OF MARINE PHYTOPLANKTON CHANGE OVER THE PAST CENTURY

by

Daniel G. Boyce

Submitted in partial fulfillment of the
requirements for the degree of
Doctor of Philosophy

at

Dalhousie University
Halifax, Nova Scotia
October 2013

To my parents Dave and Sylvia, and my wife Tania,

for always supporting and encouraging me.

Table of Contents

List of Tables

List of Figures

Abstract

Marine phytoplankton produce the vast majority of primary production in the world's oceans and sustain virtually all marine ecosystems. Despite this importance, it is currently unclear how global marine phytoplankton concentrations have been changing over the available oceanographic record, and what the causes and consequences of any such changes may be. In this thesis I use observational datasets, statistical modeling, theory, and experiments, to estimate how the global standing stock of marine phytoplankton (referenced by chlorophyll) has changed over the past century, and what the causes and consequences of any changes may be.

I inter-calibrated shipboard measurements of upper ocean chlorophyll, transparency, and colour to generate a publicly-available global chlorophyll database spanning from 1890 to 2010. Generalized additive models and multi-model inference were used to estimate the magnitude and nature of changes over the available record, and to explore the effects of multiple oceanographic and climatic variables on these changes. Finally, I worked collaboratively to design and run a mesocosm experiment to test the mechanisms by which rising ocean temperatures influence phytoplankton and plankton community structure.

I observed declining trends in upper ocean chlorophyll concentrations at local, regional, and global scales over the past century. Increasing trends were observed closer to coastlines, and were possibly related to increased land-based nutrient deposition there. I also observed inter-annual to multi-decadal fluctuations overlying the long-term trends, which were partly related to climate variability. Sea surface temperature was a consistently strong driver of observed chlorophyll trends. Strong negative effects of rising ocean temperatures on chlorophyll concentration were observed at mid, and low latitudes, and positive effects were observed at high latitudes. The overall effect of increasing temperature on chlorophyll was negative, yet the mesocosm experiment revealed that the primary mechanisms explaining this effect depend on the nature of the ecosystem. Under nutrient limitation, the physically-mediated effects (stratification) of increasing SST were dominant, while under nutrient saturation, the biologically-mediated effects (trophic) were dominant.

This thesis provides new evidence that sustained declines in marine phytoplankton over the past century have occurred across multiple spatial scales and that rising ocean temperatures have contributed to this trend. The possible implications of this sustained decline are wide-ranging, with likely impacts on climate, geochemical cycling, fisheries, and ecosystem structure.

List of Abbreviations and Symbols Used

AAO	Antarctic oscillation
AIC	Akaike Information Criterion
AMM	Atlantic meridional mode
AMO	Atlantic multidecadal oscillation
ANOVA	Analysis of variance
AO	Arctic oscillation
AOI	Arctic oscillation index
BATS	Bermuda Atlantic Time-series Study
BIC	Bayesian Information Criterion
CalCOFI	California Cooperative Oceanic Fisheries Investigations
CDOM	Coloured dissolved organic matter
Chl	Chlorophyll
$\mathbf{Chl}_{CZCS}$	Coastal zone colour scanner-derived chlorophyll
$\mathbf{Chl}_{C}$	Calibrated chlorophyll
$\mathbf{Chl}_{F}$	Forel-Ule derived chlorophyll
$\mathbf{Chl}_{I}$	*in situ* chlorophyll
$\mathbf{Chl}_{SeaWiFS}$	Sea-viewing wide field of view sensor-derived chlorophyll
$\mathbf{Chl}_{T}$	Transparency derived chlorophyll
CPR	Continuous Plankton Recorder
CTD	Conductivity temperature depth
CZCS	Coastal Zone Colour Scanner
DIN	Dissolved inorganic nitrogen
DMI	Dipole mode index
DOM	Dissolved organic matter

EKE	Eddy kinetic energy
ENSO	El Niño southern oscillation
EU	European Union
FU	Forel-Ule
GAM	Generalized additive model
GCV	Generalized cross validation
GEBCO	General Bathymetric Chart of the Oceans database
GLM	Generalized linear model
GLS	Generalized least squares
GMT	Generic Mapping Tools
GPP	Gross primary production
GSHHS	Global Self-consistent, Heirarchical, High-resolution Shoreline database
HadISST	Hadley Centre Sea Surface Temperature database
HNF	Heterotrophic nanoflagellate
HOTS	Hawaii Ocean Timeseries
HPLC	High performance liquid chromatography
ICES	International Council for the Exploration of the Seas
IOD	Indian ocean dipole
IPCC	Intergovernmental Panel on Climate Change
KE	Kinetic energy
km	Kilometers
m	Meters

MA	Major axis
MIRC	Marine Information Research Institute
ML	Maximum likelihood
ml	Milliliters
MLD	Mixed layer depth
MMI	Multi-model inference
MTE	Metabolic theory of ecology
N	Nitrate
NAO	North Atlantic Oscillation
NASA	National Aerononautics and Space Administation
NOAA	National Ocean and Atmospheric Administration
NODC	National Oceanographic Data Center
NPP	Net primary production
OAFlux	Objectively Analyzed air-sea Fluxes
OGCM	Ocean general circulation model
OLS	Ordinary least-squares
P	Phosphorous
P-IRLS	Penalized iteratively re-weighted least squares
PCA	Principal component analysis
PCD	Programmed cell death
PCI	Plankton colour index
PDO	Pacific decadal oscillation
PL	Penalized likelihood
POC	Particulate organic carbon
POM	Particulate organic matter
PON	Particulate organic nitrogen
POP	Particulate organic phosphorous

RMA	Ranged major axis
RPCA	Rotated principal components analysis
s	Seconds
SE	Standard error
SeaWiFS	Sea-viewing Wide Field of view Sensor
SST	Sea surface temperature
SST$_G$	Sea surface temperature spatial gradients
TDS	Temperature-driven stratification
TN	Total nitrogen
TP	Total phosphorous
TSR	Temperature-size rule
TZCF	Transition zone chlorophyll front
UBRE	Un-biased risk estimation
VIF	Varaiance inflation factor
WOOD	Worldwide Ocean Optics Database
Yr	Year
Z$_D$	Secchi depth

Acknowledgements

This thesis would not have been possible without the help and guidance of many people. I am incredibly grateful to everyone who helped me along the very interesting and rewarding path leading to the completion of this thesis.

Firstly, I am enormously thankful and indebted to Boris Worm, my PhD supervisor. We have worked together since I was an undergraduate student, and he has greatly influenced and shaped my approach to science and life. Throughout my initial stumbling and faltering progress, Boris has been an excellent supervisor and mentor. I have enjoyed our many conversations and have appreciated his balanced and positive approach to research, which I hope to carry forth in my own life. Boris, I am very grateful for your time, patience, support, enthusiasm, and generosity. Thank you.

I would also like to thank Ransom (RAM) Myers and Marlon Lewis, whom I worked very closely with at various stages of my thesis. Ransom (RAM) Myers was my former employer and academic co-supervisor. While our time together was sadly brief, I will always remember his boundless energy, generosity, and passion. I am also very grateful to Marlon Lewis, whom I have worked closely with throughout my thesis. I have learned immensely from our talks, and have been amazed and inspired by his ability to remain scientifically productive, maintain a family, and still find the time to enjoy the many pleasures of life. Thank you to my committee members Sandra Walde, Tamara Romanuk, Marlon Lewis, and Hal Whitehead, whose insightful comments and questions have greatly improved this thesis.

I am also very grateful to all those with whom I have collaborated with and co-authored a paper during my thesis: Marlon Lewis, Michael Dowd, Ulrich Sommer, Aleksandra Lewandowska, Mattias Hofmann, and Birte Matthiessen. I would particularly like to thank Aleksandra Lewandowska and Birte Matthiessen who were incredibly warm, welcoming, and supportive to my family and me during the six week running of experiments in Kiel, Germany.

I am very grateful to many friends and colleagues in the Myers, Lotze, and Worm labs. I am particularly thankful to Dan Riccard, Coilin Minto, Derek Tittensor,

Francessco Ferretti, Ian Jonson, Luis Lucifora, and Travis Sheperd for generously helping me during my initial, painstaking entry into the intimidating world of computer programming and statistics. I am also very grateful to many additional past and present lab members including Sean Anderson, Stephanie Bourdreau, Allison Schmidt, Jennifer Ford, Catherine Miur, Brendal Davis, Aurelie Godin, Marta Coll-Monton, Camilo Mora, Julia Baum, Ian Jonsen, Anna Magera, Greg Britten, Greg Breed, Trevor Davies, Arliss Winship, Gretchen Fitzgerald, and Zoey Zaharodny for their abundant help, support, and friendship during my thesis.

I would very much like to thank Mike Dowd, Joanna Mills-Flemming, Keith Thompson, Bruce Smith, Hong Gu, for generously allowing me to audit their statistical courses. Particular thanks to Joanna Mills-Flemming, Mike Dowd, Wade Blanchard, and Chris Field for donating their time and statistical expertise; their hep enabled me to attain the quantitative tools necessary to undertake my thesis work. I would also like to thank Heike Lotze, Joanna Mills-Flemming, Bill Li, and Ken Frank, for providing valuable feedback and suggestions for improvement of my research. I would like to thank Balagopal Pillai and Justin Breen for providing expert and timely computing support at all hours of the day (or night) throughout my studies.

Thank you to Tim Boyer, Jeffrey Smart, for assisting me with data acquisition during my thesis. I would also like to thank the many dedicated researchers who have been collecting valuable oceanographic data throughout the global oceans for over 120 years; without this immense effort this thesis would not have been possible.

Lastly, I would like to sincerely thank my parents, Dave and Sylvia, for supporting and encouraging me to follow my interests to the fullest, even when they took me far afield. I would like to thank my wife Tania for being my best friend and constant support throughout the many ebbs and flows of this thesis and of life. Finally, thank you to my little daughter Hazel, for unwittingly helping me complete my thesis by 'motivating' me to manage my time as efficiently as possible, providing me with lots of comic relief when I needed it most, and for helping me to remember the important things in life.

Chapter 1

Introduction

1.1 General Introduction

> "Man eats the mackerel, which may feed upon young herring, and these upon copepods, and the copepoda again upon diatoms. .... All such chains of food matter from the sea seem to bring one through the copepods to the diatoms, which may be regarded as the ultimate 'producers' of food in the ocean. Thus our living food from the waters of the globe may be said to be the diatoms and other microscopic organisms as much as the fishes."
>
> - W.A. Herdman, Science, 1909

Since the late 1800's marine scientists onboard the *Challenger* expedition began to observe and document the link between the characteristics and colour of the ocean and the presence of ubiquitous, floating microalgae - the phytoplankton (Buchanan, 1910); (Figure 1.1A, B). At this time, the role of phytoplankton was completely unknown, and the theory of the ocean as a productive system supported entirely by the phytoplankton (see above quote) was a radical new idea (Herdman and Url, 1909). Since this time, there has been an enormous broadening in our understanding of the important roles marine phytoplankton play in global processes. Throughout the 1930's a series of oceanographic expeditions ultimately led to the startling discovery that the activities of marine phytoplankton not only reflected the chemical composition of the deep oceans, but actually formed it (Redfield, 1958). The activities of phytoplankton over geological time horizons have also profoundly shaped the composition of our atmosphere (Falkowski, 1998), and continue to influence global climate patterns today (Charlson et al., 1987; Murtugudde et al., 2002). By generating 46% of global annual primary production (Field et al., 1998), and more than 90% of marine production (Charpy-Roubaud and Sournia, 1990), marine phytoplankton establish

the upper limits for fisheries harvests (Chassot et al., 2010, 2007; Ryther, 1969), fuel deep-sea communities, and strongly influence the structure and functioning of all marine ecosystems (Chavez et al., 2003; Richardson and Schoeman, 2004). Despite our burgeoning understanding of the important roles that marine phytoplankton play in a diverse range of global processes, one of the most fundamental questions remains unresolved: are the oceans becoming more, or less abundant with phytoplankton? The difficulty in addressing this seemingly simple question has severely constrained our ability to quantify the effect of changing phytoplankton on climate, geochemical, and ecosystem processes and to identify the factors which may drive long-term phytoplankton changes.

Resolving long-term phytoplankton change has proven challenging for a number of reasons. Marine phytoplankton closely track and may sometimes amplify very subtle environmental changes (Taylor et al., 2002). Because of this, long-term changes on phytoplankton abundance are often small relative to any natural environmental variability. For instance, environmental disturbances can drive large transient Chl changes over days or weeks (Hamme et al., 2010), and intra-annual phytoplankton variability can span many orders of magnitude in some locations, such as at high latitudes (D'Ortenzio et al., 2012). Further, oscillatory climate fluctuations can induce 20-fold changes in Chl over time intervals ranging from monthly to multi-decadal (Barber and Chavez, 1986), and have been observed to explain a large proportion of the variability of shorter-term phytoplankton trends (Behrenfeld et al., 2006; Boyce et al., 2010; Chavez et al., 2011; Martinez et al., 2009). It has recently been estimated that phytoplankton time series of between $\sim$27 to $\sim$40 years is required to separate phytoplankton trends that are driven by transient environmental variability from those which are sustained and long-term (Beaulieu et al., 2013; Henson et al., 2010). Estimating such long-term changes requires a comprehensive database, robust analysis methods and long-term time-series of phytoplankton abundance or biomass. Appropriate analysis methods are now widely available, but consistent, accurate, large scale, long term measurements of phytoplankton abundance are scarce. Although different indices of phytoplankton biomass are available since the late 1800's, the availability of these data has changed considerably over time and space. For

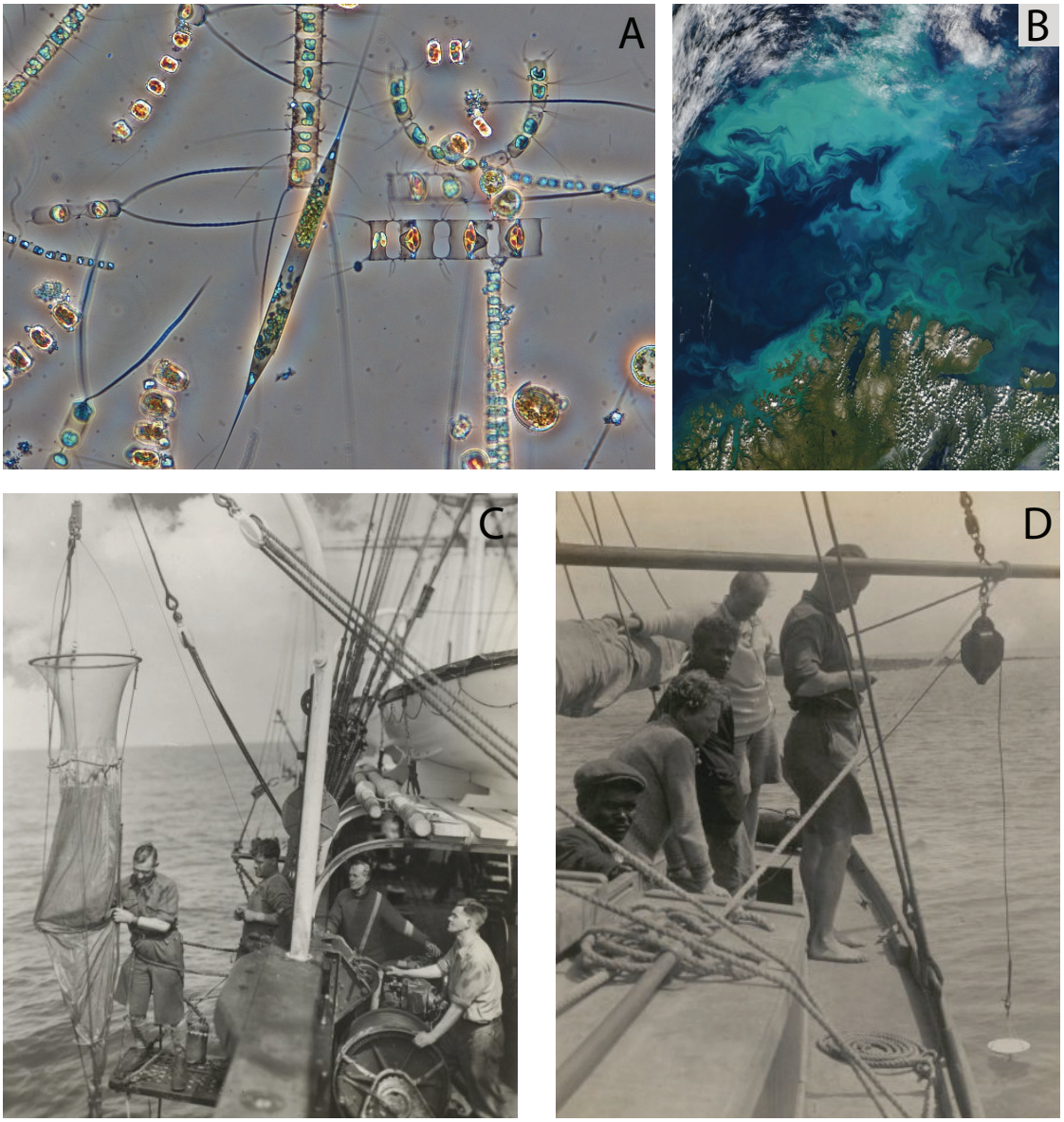

Figure 1.1: Marine phytoplankton.
(A) Marine diatom cells (*Rhizosolenia setigera*), which are an important group of phytoplankton in the oceans (Karl Bruun, Nostoca Algae Laboratory, photo courtesy of Nikon Small World). (B) A large phytoplankton bloom in the Barents Sea as viewed from space (NASA Earth Observatory Collection). (C) Scientists collecting plankton ca. 1929 using a vertical net (Hurley, F., Part of B.A.N.Z. Antarctic Research Expedition photographs, 1929-1931, photo courtesy of the National Library of Australia). (C) Scientists measuring water transparency using a Secchi disk, ca. 1928. Historical Secchi disc measurements are one of the main data sources in this analysis (Yonge, C.M., Part of Album of the Great Barrier Reef Expedition in the Low Islands region, Queensland, 1928-1929, photo courtesy of the National Library of Australia).

instance, changes in phytoplankton concentration have been inferred from measurements of upper ocean chlorophyll concentration (Chl; mg m^{-3}; ~1950 onward); (*i.e.* Venrick et al., 1987), transparency (1889 onward; Figure 1.1D); (*i.e.* Falkowski and Wilson, 1992), visual estimates of ocean colour (1889 onward); (*i.e.* Reid et al., 1998; Wernand et al., 2013), and remotely-sensed water-leaving radiances (1978 to 1983 and 1997 onward); (*i.e.* Antoine et al., 2005; Behrenfeld et al., 2006; Gregg and Conkright, 2002). This lack of sampling consistency has resulted in considerable uncertainty regarding the nature of long-term marine phytoplankton change. For instance, despite numerous published studies, both the direction and magnitude of marine phytoplankton change remains unresolved.

Based on this situation, the overarching goal of this thesis is to resolve how marine phytoplankton have been trending over the long term and globally, and what factors may be driving any observed changes.

1.2 Thesis Research Questions

In my thesis I attempted to better understand long-term and global marine phytoplankton change by addressing the following main research questions:

1. How has the global standing stock of marine phytoplankton changed over the past century? This includes quantifying the nature, magnitude, and spatial patterns of temporal phytoplankton change.

1. What factors relate to temporal changes in marine phytoplankton standing stock? Specifically, I am interested in identifying what physical or biological variables most strongly relate to phytoplankton changes over time, and in quantifying the nature, magnitude, and spatial patterns of the effects of drivers on phytoplankton.

1. What is the effect of ocean warming on marine phytoplankton? I am interested in understanding both the overall effect of ocean warming on phytoplankton, as well as the pathways by which changes in temperature influences phytoplankton. Spatial patterns in the temperature effects will also be explored.

1.3 Thesis Outline

Following this introduction, my thesis is organized into 7 more chapters:

Chapter 2 (*Global phytoplankton decline over the past century*) is an analysis of phytoplankton changes over the past century, and a preliminary analysis of the possible drivers of the observed changes. Ship-based measurements of upper ocean chlorophyll and transparency (Figure 1.1C, D) were used in combination with statistical models to estimate global phytoplankton changes from 1899 to 2009. The effect of several leading climate oscillations and 3 long-term oceanographic variables on estimated trends was also explored.

Chapter 3 (*Integrating global chlorophyll data from 1890 to 2010*) is an in-depth description of the data and methods used to generate the currently longest-running publicly-available global chlorophyll database, available from 1890 to 2010. Measurements of upper ocean chlorophyll, ocean colour, and transparency were intercalibrated to create a long-term and global database of chlorophyll measurements. A range of sensitivity analyses and comparisons against widely used remote sensing measurements of chlorophyll were undertaken to test the accuracy of the calibrated chlorophyll measurements.

Chapter 4 (*Global chlorophyll changes over the past century*) makes use of this new database (chapter 3) in combination with updated analysis methods to estimate the nature, magnitude, and spatial pattern of marine chlorophyll change from 1890 to 2010. The new database encompasses a wider spatial and temporal range than what has been compiled for Chapetr 2, and the use of multi-model inference allows for more complex phytoplankton dynamics to be incorporated within the trend analysis.

Chapter 5 (*Oceanographic drivers of chlorophyll change over the past century*) uses an expanded suite of oceanographic variables and new statistical methods to examine the factors contributing to long-term marine chlorophyll change. I used high-resolution time-series of 8 oceanographic variables and 4 leading climate variables in combination with long-term global chlorophyll measurements (chapter 4) to estimate the effect of the oceanographic variables on chlorophyll trends from 1890 to 2010. I also explored the timescales over which these drivers influence marine chlorophyll.

Chapter 6 (*Effects of sea surface warming on marine plankton*) presents a mechanistic analysis conducted in collaboration with the GEOMAR facility in Germany

examining the effects of ocean warming on a plankton community. This chapter combines ocean general circulation modeling, empirical analysis, and experimentation to explore the overall effects and pathways by which increasing temperature affects phytoplankton. This quantifies the influence of both physically- and biologically-mediated effects of increasing ocean temperatures on phytoplankton.

Chapter 7 (*Patterns, drivers and ecosystem consequences of marine phytoplankton change*) provides a broad overview of the state of our understanding of the drivers and consequences of marine phytoplankton change, as well as a quantitative analysis of past, present, and expected future changes in phytoplankton biomass as reported from the published literature.

Chapter 8 (*Conclusions*) provides a general summary and synthesis of my thesis findings and identifies the management implications and possible directions for future scientific investigation.

1.4 Thesis Miscellanea

This thesis has been shaped by the feedback received following the publication of Chapter 2. Chapters 3 to 5 were conducted in response to the interest and comment from the scientific community (see Appendix for published commentaries and response); these chapters test the robustness and validity of the chapter 2 findings, and expand upon them. Appendices to this thesis include supplementary materials for chapters 2, 5, 6, and 7, and a published reply to chapter 2, as well as all necessary permissions to reproduce chapters which have been published. Lastly, most of the chapters are published or submitted to peer-reviewed journals. Details of all published or submitted chapters are provided on the first page of each chapter or appendix. The references for each chapter and appendix are provided in a single reference list at the end of the thesis.

Chapter 2

Global Phytoplankton Decline Over the Past Century

2.1 Abstract

In the oceans, ubiquitous microscopic phototrophs (phytoplankton) account for approximately half of the production of organic matter on earth (Beaugrand, 2002; Sibert et al., 2006). Analyses of satellite-derived phytoplankton concentration (available since 1979) have suggested decadal-scale fluctuations linked to climate forcing, but the length of this record is insufficient to resolve longer-term trends. Here, we combine available ocean transparency measurements and *in situ* chlorophyll observations to estimate trajectories of phytoplankton biomass at local, regional, and global scales since 1899. We observed declines in eight of ten ocean regions, and estimated a global rate of decline of $\sim$1% of the global median per year. Our analyses further revealed interannual to decadal phytoplankton fluctuations superimposed on long-term trends. These fluctuations were strongly correlated with leading climate indices, while long-term declining trends were related to increasing sea surface temperatures. We conclude that global phytoplankton concentration has declined over the past century with implications for marine ecosystems, geochemical cycling, and fisheries.

2.2 Introduction

Generating roughly half of the planetary primary production (Field et al., 1998), marine phytoplankton affect the abundance and diversity of marine organisms, drive marine ecosystem functioning, and set the upper limits to fishery yields (Chassot et al., 2010). Phytoplankton strongly influence climate processes (Murtugudde et al., 2002) and biogeochemical cycles (Sabine et al., 2004; Roemmich and McGowan, 1995), particularly the carbon cycle. Despite this far-reaching importance, empirical estimates of long-term temporal trends in phytoplankton abundance remain limited.

Published as: Boyce, D. G., M. R. Lewis, and B. Worm. 2010. Global phytoplankton decline over the past century. Nature 466: 591596.

Estimated changes in marine phytoplankton using satellite remote sensing (1979-1986 and 1997-present) have been variable, with reported global decreases (Gregg and Conkright, 2002), increases (Gregg et al., 2005; Antoine et al., 2005), and large interannual (Behrenfeld et al., 2006) and decadal-scale variability (Martinez et al., 2009). Despite differences in scale and approach, it is clear that long-term estimates of phytoplankton abundance are a necessary, but elusive prerequisite to understanding macroecological changes in the ocean (Behrenfeld et al., 2006; Falkowski, 1998; Raitsos et al., 2005).

Phytoplankton biomass is commonly inferred from measures of total chlorophyll pigment concentration (Chl). Since Chl explains much of the variance in marine primary production (Ryther and Yentsch, 1957) and captures first-order changes in phytoplankton biomass, it is considered a reliable indicator of both phytoplankton production and biomass (Henson et al., 2010). Shipboard measurements of upper ocean Chl have been made since the early 1900s, first using spectrophotometric and then fluorometric analyses of filtered seawater residues, and more recently through in vivo measurements of phytoplankton fluorescence (Jeffrey et al., 1997). Additionally, measurements of upper ocean transparency using the standardized Secchi disk are available from 1899 to present and can be related to surface Chl through empirically-based optical equations (Falkowski and Wilson, 1992; Lewis et al., 1988). Although the Secchi disk is one of the oldest and simplest oceanographic instruments, Chl concentrations derived from Secchi depth observations are closely comparable to those estimated from direct *in situ* optical measurements or satellite remote sensing (Lewis et al., 1988).

We compiled publicly available *in situ* Chl and ocean transparency measurements collected in the upper ocean over the last century (Figure 2.1A-C, see Appendices for data sources). Transparency measurements were converted to depth-averaged Chl concentrations using established models (Falkowski and Wilson, 1992). Systematic filtration algorithms were applied to remove erroneous and biologically unrealistic Chl measurements, and to exclude those in waters <25 m deep or <1 km from the coast, where terrigenous and re-suspended substances introduce optical errors. *In situ* and transparency-derived Chl measurements (monthly averages for each year, 0.25° resolution) were strongly correlated ($r=0.52$; $P<0.0001$). After log transforming these

data to achieve normality and homoscedasticity, model II major axis regression analysis revealed linear scaling of transparency- and *in situ*-derived Chl (intercept=0.18; slope=1.08±0.016; r^2=0.60). This, and additional analyses indicated that both data sources were statistically similar enough to combine (see Methods and Appendix figure A.2 & A.3). The blended data consisted of 445,237 globally distributed Chl measurements collected between 1899 and 2008 (Figure 2.1A). Data density was greatest in the North Atlantic and Pacific Oceans and after 1930 (Figure 2.1B, C), and broadly reproduced spatial patterns of phytoplankton biomass derived from remote sensing (Gregg and Conkright, 2002); (Figure 2.1D and Appendix Figure A.3).

Chl trends were estimated using generalized additive models (GAMs) (Hastie and Tibshirani, 1986). These models are extensions of generalized linear models that do not require prior knowledge of the shape of the response function. To ensure robustness, Chl trends were estimated at three different spatial scales, (*i.*) local, (*ii.*) regional, and (*iii.*) global.

2.3 Methods

2.3.1 Data

Available upper ocean (<20m) *in situ* Chl data were extracted from the National Oceanographic Data Center[1] (NODC) and the Worldwide Ocean Optics Database [2] (WOOD). After removing duplicate observations, mean *in situ* Chl over the upper 20 meters was calculated for each cast. Ocean transparency data were extracted from NODC, WOOD, and the Marine Information Research Center[3] (MIRC). Chl (mg m^{-3}) was estimated from transparency measurements as

$$Chl = 457 \times Z_D^{-2.37}, \tag{2.1}$$

where Z_D is Secchi depth in meters (ref. Falkowski and Wilson, 1992). Since data may be affected by sampling and data entry errors, we filtered erroneous or biologically implausible measurements.

[1] www.nodc.noaa.gov
[2] www.wood.jhuapl.edu/wood
[3] www.mirc.jha.jp/en/outline

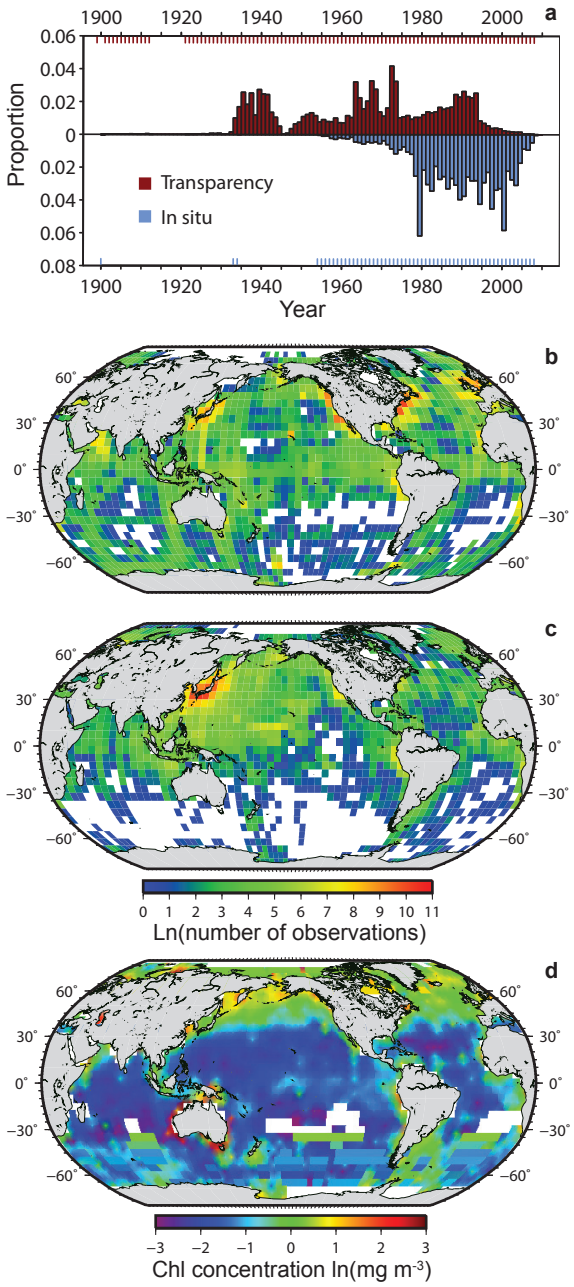

Figure 2.1: Data availability.
(A) Temporal availability of ocean transparency (red), and *in situ* Chl (blue) measurements. Bars represent the proportion of total observations collected in each year, ticks on x-axes represent years containing data. Spatial distribution of (B) *in situ* Chl, and (C) transparency data. Colors depict the number of measurements per 5° x 5° cell (ln-transformed). (D) Averaged Chl concentration from blended transparency and *in situ* data per cell.

2.3.2 Analysis.

Chl trends were estimated for each 10° x 10° cell containing adequate data ('local' models) and for each regional area ('regional' models). GAMs were fit to the blended data to estimate Chl trends as follows:

$$\eta(\mu_i) = \beta_0 + \beta_1 Year_i + \beta_2 Bathymetry_i + f_2(Latitude, Longitude) + f_3(Day) + \epsilon_i, \quad (2.2)$$

where η is the monotonic link function of the expected mean Chl concentration, β_0 is the model intercept, β_i are parametric and f_i, are nonparametric effects estimated from the data and ϵ_i is an error term. A Gamma-distributed error structure and a log link were used. The global mean rate of Chl change was estimated by calculating an inverse variance-weighted random-effects meta-analytic mean (Cooper and Hedges, 1994) from the 10 regional estimates (see Appendices for full details).

SST changes were estimated by fitting linear models to data in each 1° x 1° cell and area-weighted additive models to data in each of the 10 regions. To examine the effects of physical drivers (SST, MLD, wind), Chl and physical datasets were merged by location (1° cell) and time (year, month), and GAMs were fitted with an added effect for the physical driver in question.

2.4 Results and Discussion

2.4.1 Local-scale Phytoplankton Trends

To estimate 'local' Chl trends, blended data were binned onto a 10° x 10° global grid and GAMs of Chl as log-linear functions of covariates were fit to data within each cell. Phytoplankton declines were observed in most (59%; n=214) of the cells containing sufficient data (Figure 2.2A, B). Clusters of increasing cells were found across the Eastern Pacific, and the Northern and Eastern Indian Ocean (Figure 2.2B). High-latitude areas (>60°) showed the greatest proportion of declining cells (range: 78–80%).

Due to sparse observations in early years, local trends were also estimated using post-1950 data only. This yielded almost identical results, although the magnitude of change was amplified in some cells (see Appendices, Figure A.7).

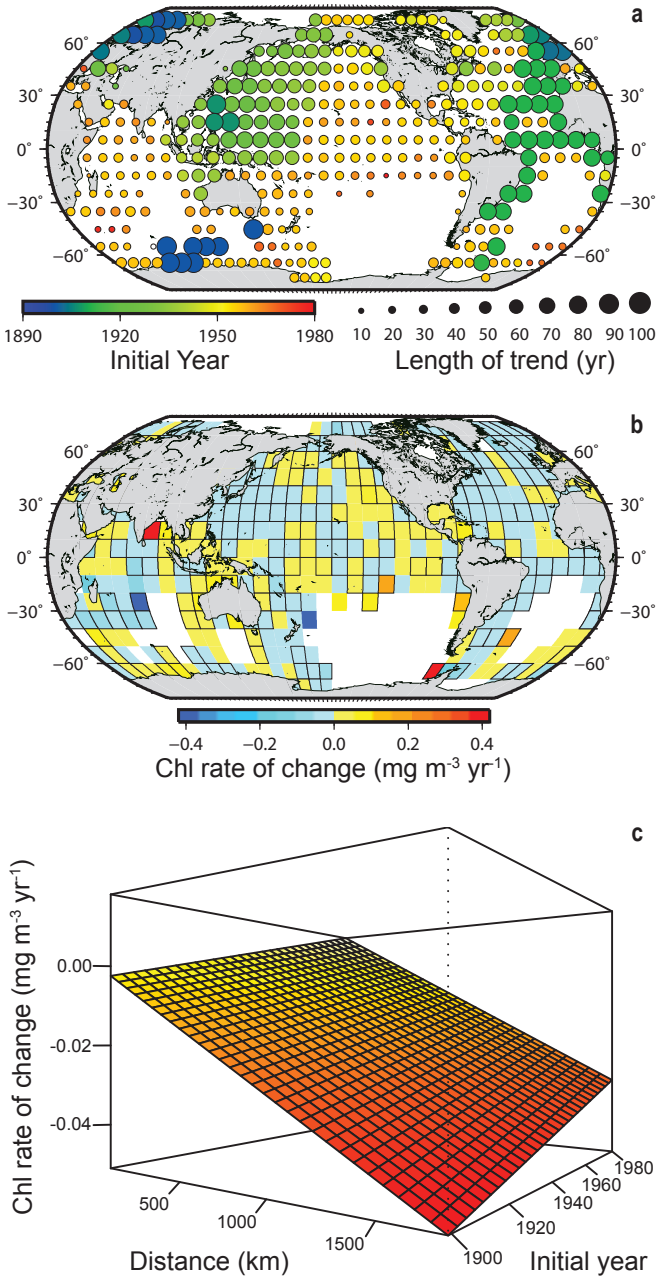

Figure 2.2: Loacal-scale trends in phytoplankton
(A) Baseline year and temporal span of Chl data used in local models. (B) Mean instantaneous rates of Chl change in each 10° x 10° cell (n=364). Yellow and red represent cells where Chl has increased while blue represents a Chl decrease. Cells bordered in black denote statistically significant rates of change ($P<0.05$) and white cells indicate insufficient data. (C) Mean instantaneous rates of Chl change for each 10° x 10° cell, estimated as a function of distance from the nearest coastline (km) and baseline year of trend. Color shading depicts the magnitude of change per year. All effects used to fit the trend surface were statistically significant ($P<0.05$).

Local models further suggested that Chl has declined more rapidly with increasing distance from land (Figure 2.2C). This agrees with results derived from satellite data, documenting declining phytoplankton in the open oceans (Gregg et al., 2005; Ware and Thomson, 2005; Vantrepotte and Melin, 2009), and expansion of oligotrophic gyres, likely due to intensifying vertical stratification and ocean warming (Behrenfeld et al., 2006; Polovina et al., 2008). These trends are noteworthy since the majority (75%) of aquatic primary production occurs in these waters (Pauly, 1995). In shelf regions Chl trends switched from negative to positive in more recent years (since ∼1980), consistent with reported Chl increases due to intensifying coastal eutrophication and land runoff (Gregg et al., 2005).

2.4.2 Regional and Global Phytoplankton Trends

To estimate 'regional' Chl trends, we divided the global ocean into 10 regions, exhibiting similar variability in phytoplankton biomass in response to seasonality and climate forcing (Behrenfeld et al., 2005); (Figure 2.3A). To capture the range of potential Chl trajectories, regional trends were estimated from GAMs as linear functions of time on a log scale in three different ways: as (*i.*) continuous (linear trend), (*ii.*) discrete (mean year-by-year estimates), and (*iii.*) smooth functions of time (non-monotonic trend). This approach is comprehensive; it allows both the quantitative (magnitude) and qualitative nature (shape) of trends to be estimated.

Estimation of Chl trends as continuous log-linear functions of time revealed phytoplankton declines in 8 of 10 regions. The largest rates of decline were observed in the South Atlantic (-0.018±0.0015 mg m^{-3} yr^{-1}), Southern (-0.015±0.0016 mg m^{-3} yr^{-1}), and Equatorial Atlantic (-0.013±0.0012 mg m^{-3} yr^{-1}) regions ($P<0.0001$ for all trends; Figure 2.3B). Increases were observed in the North (0.0018±0.0015 mg m^{-3} yr^{-1}; $P=0.268$) and South Indian regions (0.02±0.0011 mg m^{-3} yr^{-1}; $P<0.0001$). The global meta-analytic mean rate of Chl change derived from individual regional model estimates was -0.006±0.0017 mg m^{-3} yr^{-1}($P<0.0001$; Figure 2.3B), representing an annual rate of decline of ∼1% relative to the global median chlorophyll concentration (∼0.56 mg m^{-3}).

Regional trends were also estimated using data since 1950 only, but the direction of all trends remained unchanged and the magnitude of changes was minimal (Figure

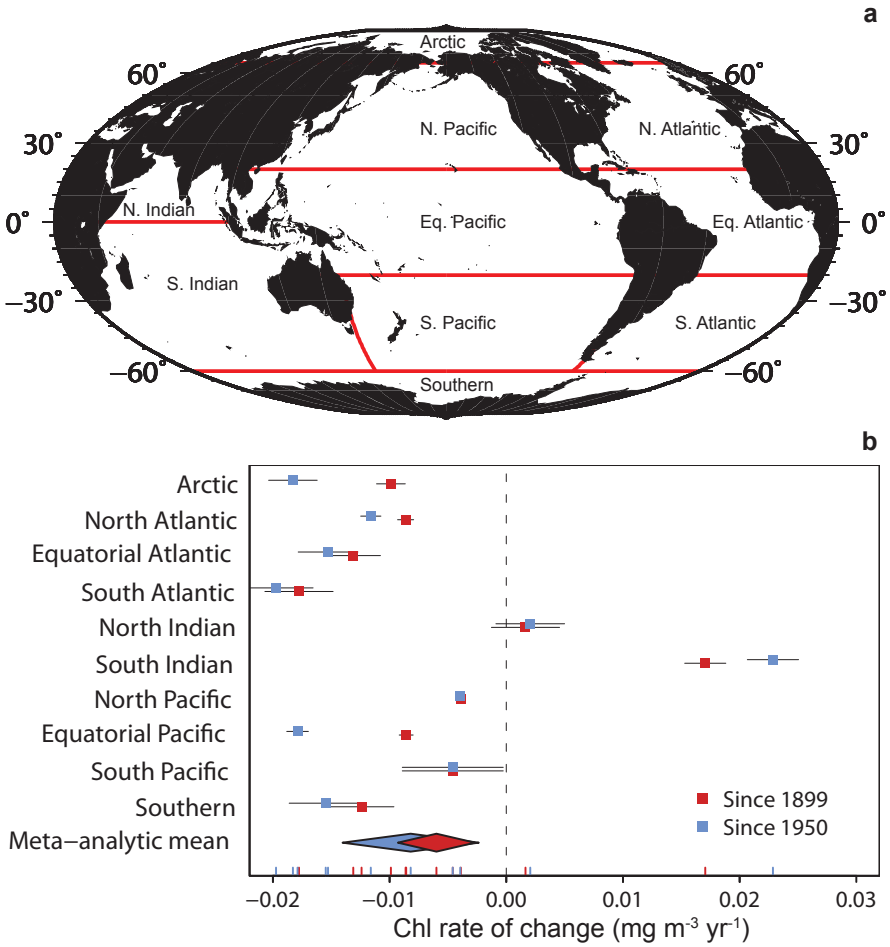

Figure 2.3: Regional and global trends in phytoplankton.
(A) Ocean regions (n=10) used to estimate regional trends in Chl. (B), Mean instantaneous rates of Chl change estimated for each region, with 95% confidence limits. Diamonds indicate the global meta-analytic mean rate of Chl change with 95% confidence intervals. Trends were estimated using all available data (red symbols) and data since 1950 only (blue symbols). Individual estimates are tick-marked on the x-axis. All estimates were statistically significant ($P<0.05$), except for the North Indian region ($P=0.27$).

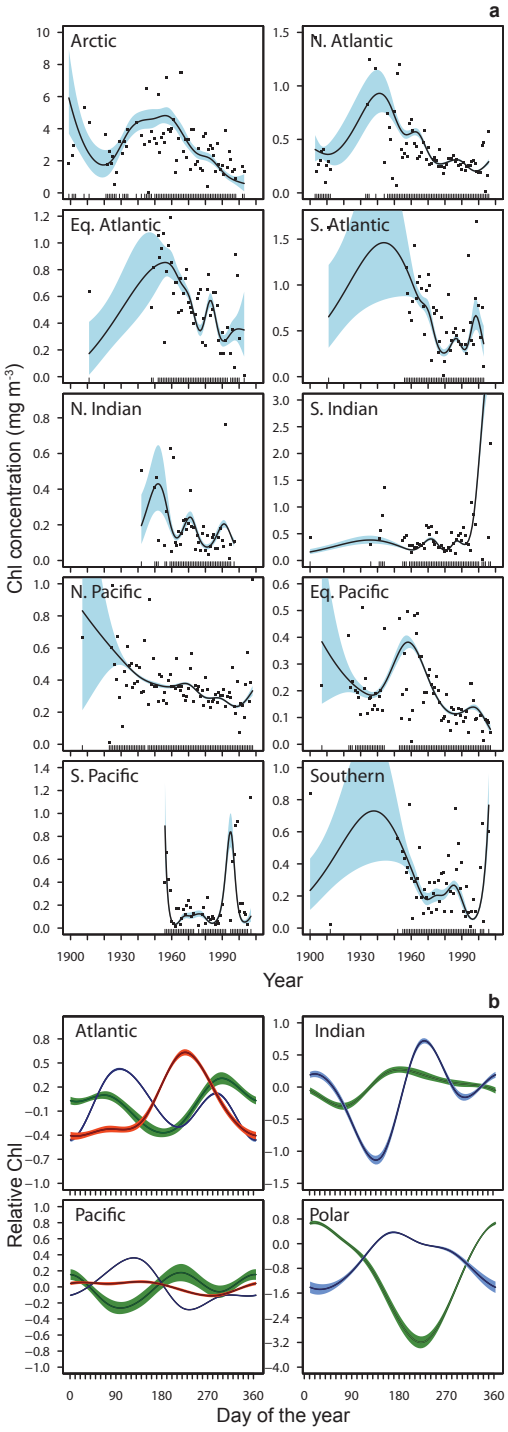

Figure 2.4: Temporal variability in phytoplankton trends.
(A) GAM estimates of Chl as a discrete (points) or smooth function (lines) of yearly variability in each region (n=10). For each initial year, Chl is the arithmetic, rather than model-estimated mean. Temporal data availability is tick-marked on the x-axis. (B) Seasonal patterns of Chl as a smooth function of day of year in each northern (blue), equatorial (red), and southern (green) ocean. Shaded areas represent approximate 95% Bayesian credible limits around each estimate.

2.3B). Post-1950 trends were amplified in some regions, resulting in a greater but more variable global rate of decline (-0.008±0.0068 mg m^{-3} yr^{-1}; P<0.0001). Estimating regional trends separately for each data source yielded similar results (see Appendices Figure A.4).

Modeling Chl trends as both discrete and smooth functions of time revealed pronounced interannual to decadal fluctuations superimposed on long-term trends (Figure 2.4A). We observed greater Chl fluctuations in the southern hemisphere regions and greater uncertainty about estimates prior to 1950; both issues likely reflect limitations in data availability for these regions and time periods. In the polar and Atlantic regions, Chl increased until ∼1950, before undergoing prolonged declines (ca. 1950-1995). After ∼1995, sharp increases were observed in the South Indian and Southern Ocean regions (Figure 2.4A).

GAMs also accounted for mean seasonal variation in Chl (Figure 2.4B) and closely reproduced known patterns (Behrenfeld et al., 2005; Yoder and Kennelly, 2003), providing a measure of confidence in our approach. Strong seasonality in polar regions reflects pronounced variability in mixing, irradiance and ice cover (Behrenfeld et al., 2001) while weak seasonality in equatorial regions is a function of near-constant solar irradiance. Complex seasonality in the Indian Ocean relates to the effects of monsoon dynamics and freshwater inputs on nutrient delivery (Wiggert et al., 2006). Temperate regions are affected by seasonally changing solar irradiance and trade winds, and their effects on upper ocean nutrient delivery (Mann and Lazier, 1991).

2.4.3 Climate Effects on Phytoplankton

Regional phytoplankton trends display both short-term variation and longer-term trends. We hypothesized that the short-term (interannual to decadal) component in Chl variation may be explained by the effects of leading climate oscillators, such as the El Niño Southern Oscillation (ENSO) or the North Atlantic Oscillation (NAO). After de-trending and removing seasonal variation, yearly Chl anomalies were strongly negatively correlated with the bivariate ENSO index in the Equatorial Pacific (r=-0.45; P<0.0001; Figure 2.5A). Positive ENSO phases are associated with warming sea surface temperatures (SST), increased stratification, and a deeper nutricline, leading to negative Chl anomalies in the Equatorial Pacific (Behrenfeld et al., 2006; Martinez

et al., 2009). Negative correlations were also found between the NAO index and Chl in the North (r=-0.31; P=0.0002; Figure 2.5B) and Equatorial (r=-0.44; P=0.001) Atlantic in accordance with results from Continuous Plankton Recorder (CPR) surveys (Dickson et al., 1988). Positive NAO phases are associated with intensifying westerly winds and warmer SST in Europe and the central North Atlantic (Fromentin and Planque, 1996). Possibly, the observed effects relate to increased westerly wind stress during the winter months when annual phytoplankton productivity is limited by light availability associated with deep mixed layer depths (MLD) (Dickson et al., 1988). We further hypothesize that an observed coupling of NAO and wind intensity to regional zooplankton abundances (Fromentin and Planque, 1996; Dickson et al., 1988) represents a trophic response to the observed phytoplankton fluctuations. No significant relationship was found between the Indian Ocean Dipole (IOD) index and Chl in the North Indian region (r=-0.23; P=0.18). The Atlantic Multidecadal Oscillation (AMO) was positively correlated with Chl in all Atlantic regions (range: r=0.31-0.43; P<0.05 for all). Chl anomalies in the Arctic region were negatively correlated with the Arctic Oscillation (AO) index (r=-0.31; P=0.01; Figure 2.5C). Chl anomalies in the Southern region were negatively correlated with the Antarctic Oscillation (AAO) index (r=-0.48; P=0.029; Figure 2.5D), again, possibly due to intensifying westerly winds and deep mixed layer depths. The strength of all relationships increased after 1950, indicating that phytoplankton may be increasingly driven by climate variability or, alternatively, that model accuracy increased due to increased data availability.

2.4.4 Physical Drivers of Phytoplankton Trends

Long-term trends in phytoplankton could be linked to changes in vertical stratification and upwelling (Behrenfeld et al., 2006; Martinez et al., 2009; Polovina et al., 2008), aerosol deposition (Paytan et al., 2009), ice, wind, and cloud formation (Gregg et al., 2005; Montes-Hugo et al., 2009), coastal runoff (Ware and Thomson, 2005), ocean circulation (Broecker et al., 1999), or trophic effects (Frank et al., 2005). For parsimony, we focus on three variables that may reflect the coupling between physical climate variability and the chlorophyll concentration in the upper ocean: (*i.*) ocean mixed layer depth (MLD; 1955-2009), (*ii.*) wind stress at 10 m (1958-2009), and (*iii.*)

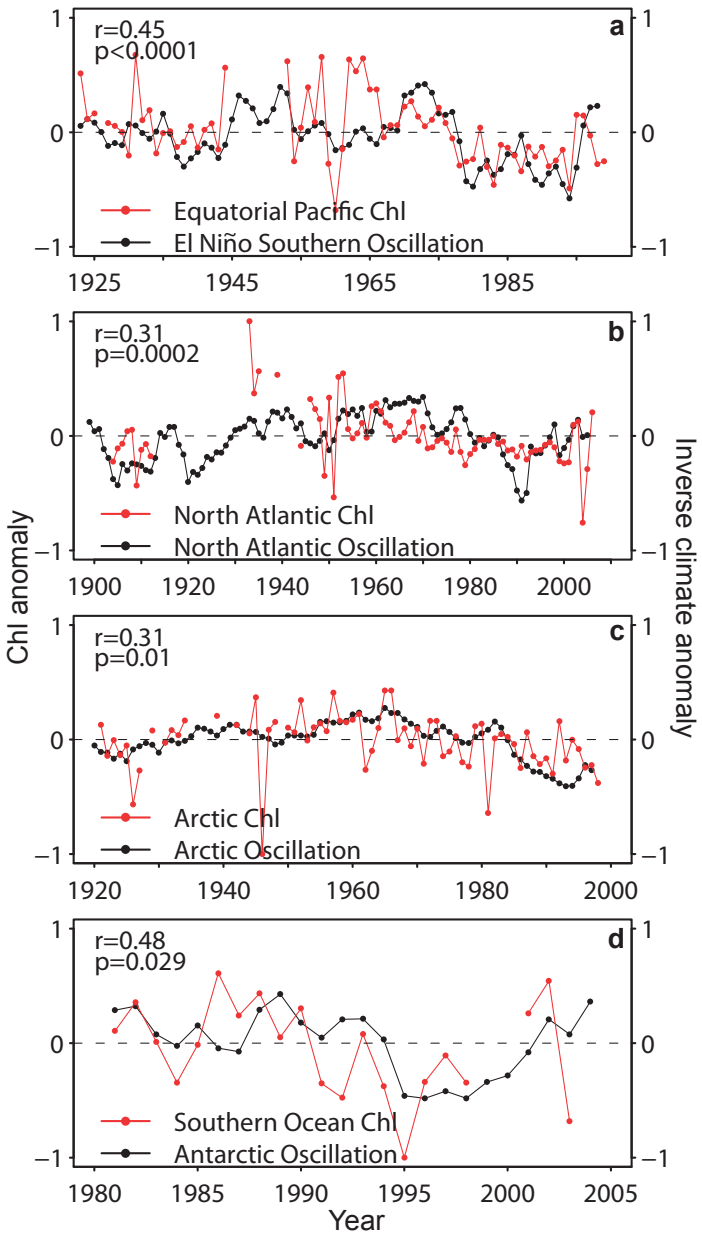

Figure 2.5: Effects of climate variability on phytoplankton.
Linear relationships between normalized and de-trended yearly Chl anomalies (red) and smoothed climate indices (black) for (A) the Equatorial Pacific, (B) the North Atlantic, (C) the Arctic, and (D) the Southern Ocean regions. Pearson correlation coefficients and P-values are shown. Climate indices and correlation coefficients have been inverted in order to better visualize correlations.

sea surface temperature (SST; 1899-2009). These physical variables (monthly averages, 1° resolution) were matched by time (year, month) and location (1° cell) with Chl data in order to estimate their effects on Chl within a single model framework (see Appendices for details). SST was the strongest single predictor of Chl. Rising SSTs over most of the global ocean (Figure 2.6A) were associated with declining Chl in 8 of 10 regions (range: -0.21 to -0.019 mg m^{-3} $°C^{-1}$; $P<0.0001$ for all). Positive relationships between SST and Chl were found in the Arctic (0.067 mg m^{-3} $°C^{-1}$; $P<0.0001$) and Southern regions (0.002 mg m^{-3} $°C^{-1}$; $P=0.11$). Likewise, inclusion of SST as a covariate in our local models revealed negative SST effects on Chl in 76% (n=118) of 10°x10°cells (Figure 2.6B), with negative relationships at low latitudes and strong positive effects at high latitudes, particularly in the Southern Ocean ($P<0.05$ for all; Figure 2.6B, C).

The effects of SST on Chl are likely explained by its influence on water column stability and MLD (Behrenfeld et al., 2006; Polovina et al., 2008). Increasing SST leads to a shallower mixed layer which further limits nutrient supply to phytoplankton in already stratified tropical waters, but may benefit phytoplankton at higher latitudes where growth is constrained by light availability and deep mixing (Doney, 2006). Indeed, in our local models MLD was a significant, but weaker predictor of Chl concentrations compared with SST, possibly due to the reduced time series span (1955-2009). Latitudinal gradients in MLD effects were also observed, with predicted positive effects between 20°N and 20°S and negative effects in polar areas ($r^2=0.1$; $P=0.018$; Figure 2.6D). Cumulatively, these findings suggest that warming SST and reduced MLD may be responsible for phytoplankton declines at low latitudes. This mechanism, however, does not explain observed phytoplankton declines in polar areas, where ocean warming would be predicted to enhance Chl (Figure 2.6C). This may partially be explained by concurrent increases in MLD and wind stress there (see Appendices; Figure A.9). Further work is needed to understand the complex oceanographic drivers of phytoplankton trends in polar waters.

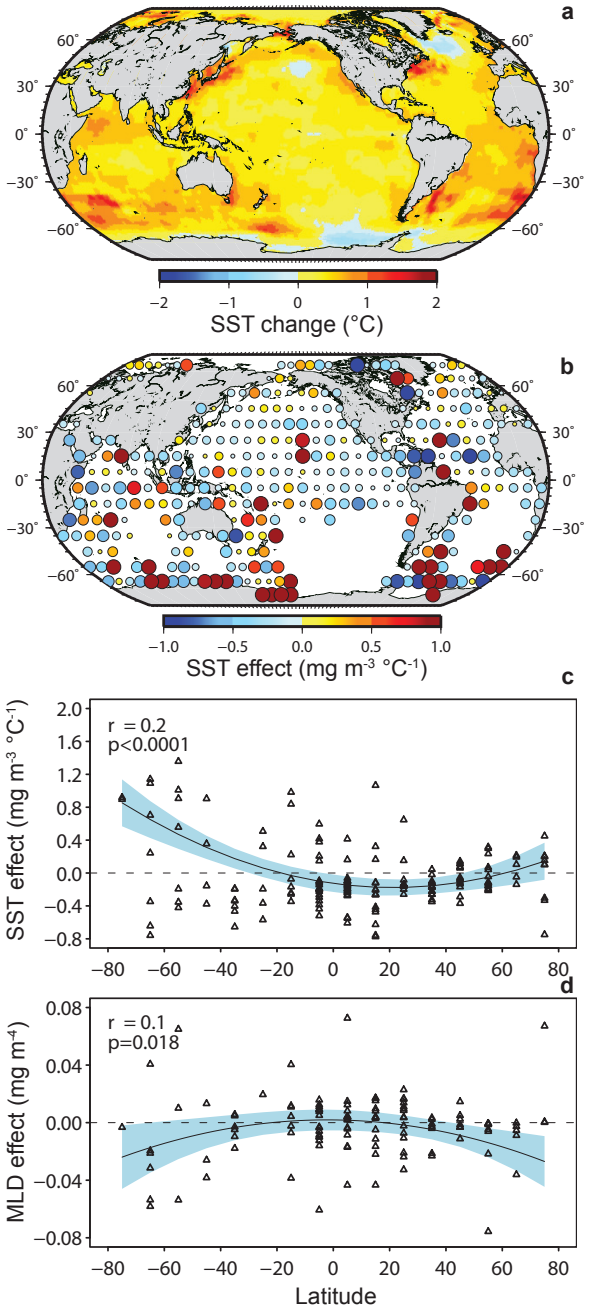

Figure 2.6: Physical drivers of phytoplankton trends.
(A) Estimated SST change at 1° resolution from 1899 to 2009. Blue represents cells where SST has declined while yellow and red represents increases. (B) Effects of SST changes on Chl estimated for each 10° x 10° cell with >10 yr of data (n=205). Size of circles represents the magnitude and colors depict the sign of the standardized SST effect on Chl in each cell. (C to D) Effects of SST (C), and MLD (D), on Chl as a function of latitude (points). Relationships were best approximated as quadratic functions of latitude (fitted lines and test statistics). Shading represents 95% confidence limits.

2.5 Conclusions

Our analysis suggests that global chlorophyll concentration has declined since the beginning of oceanographic measurements in the late 1800s. Multiple lines of evidence suggest that these changes are generally related to climatic and oceanographic variability and particularly to increasing SST over the last century (Figure 2.6). The negative effects of SST on Chl trends are particularly pronounced in tropical and subtropical oceans where increasing stratification limits nutrient supply. Regional climate variability can induce variation around these long-term trends (Figure 2.4), and coastal processes such as land-runoff may modify Chl trends in nearshore waters. The long-term global declines observed here are, however, unequivocal. These results provide a larger context for recently observed declines in remotely sensed Chl (Gregg and Conkright, 2002; Behrenfeld et al., 2006; Polovina et al., 2008), and are consistent with the hypothesis that increasing ocean warming is contributing to a restructuring of marine ecosystems (Richardson and Schoeman, 2004; Worm et al., 2009), with implications for biogeochemical cycling (Henson et al., 2010), fishery yields (Brander, 2007), and ocean circulation (Murtugudde et al., 2002). Such consequences provide incentive for an enhanced *in situ* and space-borne observational basis to reduce uncertainties in future projections.

2.6 Acknowledgements

We are grateful to all data providers, to J. Mills-Flemming, W. Blanchard, M. Dowd, C. Field and C. Minto for statistical advice, to T. Boyer, J. Smart, D. Ricard and D. Tittensor for help with data extraction, and to J. Mills-Flemming, W. Blanchard, W. Li, H. Lotze, C. Muir and M. Dowd for critical review. Funding was provided by the Natural Sciences and Engineering Research Council of Canada, the US Office of Naval Research, the Canada Foundation for Climate and Atmospheric Sciences, the National Aeronautics and Space Administration, the Sloan Foundation (Census of Marine Life FMAP Program), and the Lenfest Oceans Program.

Chapter 3

Integrating Global Chlorophyll Data From 1890 to 2010

3.1 Abstract

Understanding large-scale phytoplankton dynamics requires accurate, multi-decadal measurements of abundance and distribution. Since 1890, marine phytoplankton abundance has been assessed using a diverse range of sensors and observational platforms, and inter-calibrating these data has been challenging. Consequently, syntheses of historical phytoplankton data have been rarely attempted, and the need for accurate, long-term assessments of phytoplankton abundance and distribution is commonly acknowledged. Here, we derive quantitative indices of phytoplankton abundance from measurements of upper ocean transparency and colour calibrated with direct measurements of surface chlorophyll. The strong correlation and linear scaling of the predicted data enabled the construction of a comprehensive, globally inter-calibrated chlorophyll time series from 1890 to 2010. The calibrated chlorophyll data reproduced the well-established spatial features of phytoplankton surface biomass and were strongly correlated with chlorophyll concentration derived from two independent remote sensing platforms discontinuously available since 1978. These results suggest that with careful statistical treatment, it is possible to generate a globally integrated chlorophyll time series extending 120 years into the past. This database, which is available in the web appendices of this paper, may enable new insights in the areas of climate science, biogeochemical cycling, and marine ecosystem structure and functioning over the past century.

3.2 Introduction

Marine phytoplankton play a key role in the functioning of the Earth‘s ecosystem, through their effects on climate (Murtugudde et al., 2002; Charlson et al., 1987),

Published as: Boyce, D. G., M. Lewis, and B. Worm. 2012. Integrating global chlorophyll data from 1890 to 2010. Limnology and Oceanography: Methods 10: 840852.

geochemical cycling (Sabine et al., 2004; Roemmich and McGowan, 1995), fisheries yield (Chassot et al., 2007, 2010), and other important processes. Yet our understanding of macroecological phytoplankton dynamics is limited by the availability of accurate, large-scale, long-term measurements of abundance, particularly from the era pre-dating the operations of satellite sensors (ocean colour radiometry; available since 1978). Here, we construct a multi-decadal time-series of chlorophyll concentration, an indicator of phytoplankton abundance, by statistically integrating historical shipboard measurements from different sensors and sampling platforms.

Measurements of total chlorophyll pigment concentration (Chl) capture first-order changes in phytoplankton Carbon biomass, and despite some known variations in the Chl-to-carbon ratio (Geider, 1987) are considered to be the best indicator of phytoplankton C biomass (C) available on a global scale (Huot et al., 2007; Henson et al., 2010). Direct shipboard measurements of upper ocean Chl have been made since the early 1900s, first using spectrophotometric (Stokes, 1864) and then fluorometric analyses of filtered seawater residues, and more recently through *in vivo* measurements of phytoplankton fluorescence (Yentsch and Menzel, 1963; Lorenzen, 1966; Jeffrey et al., 1997). Measurements of upper ocean transparency using the standardized Secchi disk have been made since 1866 (Tyler, 1968; Collier et al., 1968) and have been used as a predictor of surface ocean Chl through empirically-based optical equations (Falkowski and Wilson, 1992; Lewis et al., 1988). Although the Secchi disk is one of the oldest and simplest oceanographic instruments, Chl concentrations derived from Secchi depth observations (Z_D) are closely comparable to those estimated from direct *in situ* optical measurements or satellite remote sensing (Lewis et al., 1988; Boyce et al., 2010). Finally, standardized measurements of ocean colour using the Forel-Ule (FU) comparator scale are available from 1890 to present (Forel, 1890) and have been used as an indicator of biological activity (Wernand and Woerd, 2010).

Modelling results indicate that a phytoplankton time series of ∼40 years is necessary to separate natural variability from long-term change (Henson et al., 2010). Since the available continuous ocean colour satellite record (currently 1997 to 2011) is presently too short, direct measurements of Chl, transparency, and colour represent the only available data to assess multi-decadal phytoplankton dynamics. To this end, efforts have been directed towards developing methods to reliably merge

different ocean colour data (I.O.C.C.G., 2007), and several studies have combined historical and contemporary Chl data to produce synthetic Chl time series (Raitsos et al., 2005; Gregg and Conkright, 2002; Gregg et al., 2003; Boyce et al., 2010). Such approaches require a good knowledge of the accuracy, precision, and comparability of Chl measurements sampled from different observational platforms.

Here, we build and expand upon the methods developed in a previous study (Boyce et al., 2010), taking into account suggested improvements (Mackas, 2011; McQuatters-Gollop et al., 2011; Rykaczewski and Dunne, 2011; Boyce et al., 2011). By using a larger, more spatially and temporally comprehensive database and improved statistical methods, we predict Chl concentrations from available measurements of upper ocean transparency (Z_D) and colour (FU), available since 1890. After affirming the accuracy of the predictive methods, both directly measured and predicted Chl data were combined to create a globally integrated and inter-calibrated Chl database (see Appendices). We then examine the accuracy of the calibrated Chl data against more recent and spatially extensive remote sensing estimates of Chl.

3.3 Materials and Procedures

3.3.1 Data

All data used in this analysis were extracted from publicly available databases (Table 3.1):

1. *In situ* measurements: Direct shipboard measurements of upper-ocean, *in situ*-derived Chl (Chl_I, mg m^{-3}) were extracted from the National Oceanographic Data Center (NODC), the Worldwide Ocean Optics Database (WOOD), and the International Council for the Exploration of the Sea[1] (ICES). Chl_I measurements were made on discrete water samples collected at different depths, from vertical profiling instruments, or continuous observations by shipboard flow-through systems. Chl_I values were derived by spectrophotometric techniques (Stokes, 1864), *in vitro* and *in vivo* fluorometric techniques (Yentsch and Menzel, 1963; Lorenzen, 1966; Jeffrey et al., 1997), or chromatographic methods such as high-performance liquid chromatography (HPLC) or filtered

[1] www.ices.dk/Pages/default.aspx

Table 3.1: Data sources.

Parameter	Symbol	Source	N Extracted	N Final	Span	Website
Chlorophyll	Chl_I	WOOD	1,665,895	5,315	1900-2003	wood.jhuapl.edu/wood
Chlorophyll	Chl_I	NODC	2,524,096	155,493	1934-2010	nodc.noaa.gov
Chlorophyll	Chl_I	ICES	349,308	20,532	1933-2010	ices.dk/indexfla.asp
Chlorophyll	Chl_{CZCS}	NASA			1978-1986	oceandata.sci.gsfc.nasa.gov
Chlorophyll	Chl_{SWFS}	NASA			1997-2011	oceandata.sci.gsfc.nasa.gov
Transparency	ZD	WOOD	41,388	22,266	1903-2008	wood.jhuapl.edu/wood
Transparency	ZD	NODC	160,383	128,988	1899-2007	nodc.noaa.gov
Transparency	ZD	ICES	38,385	17,432	1903-1998	ices.dk/indexfla.asp
Transparency	ZD	MIRC	121,436	101,053	1923-1998	mirc.jha.jp/en/outline
Transparency	ZD	BIDA	8,389	304	1890-1898	links.baruch.sc.edu
Colour	FU	NODC	203,763	193,533	1890-2008	nodc.noaa.gov

samples (Mantoura and Llewellyn, 1983). Chl_I measurements were derived using different instrumentation, on different platforms, and by different observers, but are collectively regarded as the most accurate Chl measurements available, and are commonly used to inter-calibrate Chl estimates from more indirect sources, such as remote sensing platforms. To allow comparability with Chl estimates from other sources, which almost exclusively estimate Chl in the uppermost layers of the oceans, only Chl_I collected in the upper 20 m were used in our analysis. All duplicated measurements were removed from the database prior to the analysis.

2. Transparency measurements: Measurements of upper ocean transparency (Z_D,m) were collected with the standardized Secchi disk and were extracted from several publicly available databases. Z_D measurements are collected by lowering a white Secchi disk into the seawater and recording the depth at which the disk is no longer visible. Measurements of upper ocean transparency collected with the Secchi disk have been collected using a standardized methodology since 1866 and have been related to inherent and apparent optical properties measured by modern oceanographic instruments in the context of a "theory" of the Secchi disk (see Preisendorfer, 1986). Secchi disk measurements have been used to infer changes in biological productivity and phytoplankton abundance in both freshwater and oceans (Tyler, 1968; Collier et al., 1968; Lewis et al., 1988; Falkowski and Wilson, 1992; Boyce et al., 2010). The linkage between observations of transparency and chlorophyll is through the dominant influence of marine phytoplankton on absorption and scattering of light in the upper ocean, similar to the basis of using ocean colour radiometry in the inference of chlorophyll concentration in the upper ocean.

3. Ocean colour measurements: Measurements of upper ocean colour have been recorded since 1890 using the Forel-Ule colour index scale (FU). The FU observations have been collected using a standardized methodology designed to quantitatively assess the colour of the upper ocean against a Forel-Ule scale of 21 discrete colours ranging from dark blue (FU=1) through different shades of green to brown (FU=21); (Forel, 1890). FU measurements are derived by

subjectively matching the colour of the seawater to that of the Forel-Ule colour scale. Although the optical characteristics of the Forel-Ule measurements are largely unresolved, they have been useful in inferring long-term changes in biological activity (see recent review by (Wernand and Woerd, 2010), and may be useful in deriving upper ocean chlorophyll concentrations.

4. Radiometry measurements: Measurements of Chl derived from remotely-sensed ocean-leaving radiances were extracted from the National Aeronautics and Space Administration's (NASA) ocean colour database. Chl measurements derived from the Coastal Zone Colour Scanner (CZCS; Chl_{CZCS} 1978-1986; (Hovis et al., 1980), and the Sea-viewing Wide Field-of-view Sensor (SeaWiFS; Chl_{SWFS}; 1997-2010; (McClain et al., 2004) were used. Remote sensing Chl data were extracted as monthly 9 km^2 resolution reprocessed Chl measurements, and were spatially interpolated to 1° x 1° cells for each year and month using nearest neighbour algorithms.

3.3.2 Analysis

The steps in this analysis included:

1. Quality control: Chl_I, Z_D and FU measurements are adjusted or eliminated from the database based on objective quality-control procedures.

2. Corrections and standardizations: Chl_I, Z_D, and FU Measurements are objectively standardized to common spatial and temporal resolutions.

3. Calibration: Chl fields are predicted from Z_D and FU based on available spatial and temporal matchups with Chl_I measurements.

4. Validation: The precision and accuracy of calibrated Chl measurements are compared against independent Chl measurements to assess their validity.

Quality control: Z_D and FU measurements

To eliminate the optically-confounding effects of suspended particles and dissolved organic material associated with terrigenous sources, all near-shore ($<$ 20 m water depth or $<$ 1 km from the nearest coastline) Z_D and FU measurements were removed

from the database. If the time or location of the Z_D or FU measurements were erroneous those measurements were also removed. All FU measurements less than one or greater than 21, and all Z_D measurements less than zero or greater than 60 m were treated as biologically implausible and removed from the database.

Quality control: Chl_I measurements

The Chl_I measurements used here have been collected since 1900 by different institutions and methods, and their accuracy may be affected by weather conditions, incorrectly calibrated instrumentation, sampling technique, data digitization errors, the optical complexity of seawater, and other factors. Due to the central importance of the Chl_I measurements to the subsequent calibration exercise and the larger number of factors potentially affecting their accuracy, the Chl_I measurements were rigorously filtered to remove any erroneous measurements. As for FU and Z_D measurements, all near-shore Chl_I measurements (< 20 m depth or < 1 km from the nearest coastline) and those with erroneous locations and time were removed. Chl_I measurements were identified as statistical outliers if they (*i.*) were greater than 75 mg m^{-3}; (*ii.*) were below the published limit of detection (0.01 mg m^{-3}; (Wiltshire et al., 1998); or (*iii.*) were identified as outliers by NODC quality control methods (details in Conkright et al., 2002). Our analysis revealed that a small fraction of the Chl_I database contained outlying values which were likely un-calibrated fluorescence measurements (Boyer et al., 2009). Such errors are likely systematically dependent on the cast, cruise, or observer associated with the outlying Chl_I measurement. To account for this, Chl_I measurements collected in casts or cruises where over 10% of all measurements were flagged as outliers by the previous criteria were removed from the database. While some erroneous measurements will remain, these represent a small fraction of the entire Chl_I database, and constitute a random, rather than systematic departure from the mean. Following this step, all remaining outlying individual Chl_I measurements in the database were removed.

Chl measurements of 0 mg m^{-3} accounted for a small fraction ($\sim$0.4%) of all Chl_I data, but are biologically implausible in even the most oligotrophic marine waters. These measurements may either reflect data collection or digitization errors, or valid measurements which are below the detection limit of the sampling instrument. To

identify and remove erroneous zero-Chl values and to estimate the true but unknown zero-Chl values, we fit an objective function relating Chl to sampling depth for each individual cast according to the number of Chl_I measurements in each cast:

1. For casts containing more than six unique Chl_I measurements, zero-Chl_I values were assessed based on an empirically-based function relating Chl_I to the sampling depth. Zero Chl_I values falling within the 95% confidence levels of the fitted function were assumed to be true data which were below the limit of detection and were readjusted to 50% of the minimum Chl value within the cast. If this adjusted value was greater than the lowest limit of detection (0.01 mg m^{-3}) then the values were again readjusted to 0.005 mg m^{-3}. Zero Chl_I values falling outside of the confidence limits of the function were identified as erroneous and removed from the database.

2. For casts containing between one and six additional measurements, if the lowest recorded Chl_I value was greater than 0.01 mg m^{-3} then the zero-Chl_I value was assumed to be erroneous and was removed from the database. Otherwise, the zero Chl_I values were adjusted to 50% of the minimum Chl_I value in the cast. If this adjusted value was greater than 0.01 mg m^{-3} then the values were again readjusted to 0.005 mg m^{-3}.

These corrective algorithms were visually inspected for each individual cast to ensure adequate performance. All zero-Chl_I measurements contained within casts with less than two additional measurements were eliminated from the database.

Even within the upper 20 m of the water column, Chl_I values can vary over several orders of magnitude, in part due to non-photochemical quenching of fluorescence. To account for this variability, mean Chl_I measurements were calculated over depth for each individual cast under an assumption of a well-mixed surface layer. Alternate depth interpolations such as the depth-weighted mean, median, Akima method (Akima, 1978), wavelets, polynomials, and generalized additive models (Wood and Bretherton, 2006; Hastie and Tibshirani, 1986) relating Chl_I to the sampling depth were used but did not improve the results.

Global spatial patterns of Chl at intra-annual timescales vary in a distinct and

well-established manner (Doney et al., 2003; Mahadevan and Campbell, 2002). Spatial filters were used to identify extreme outlying Chl_I measurements. For each annual season (n=4) a flexible spatial trend surface was fitted to the Chl_I data. This was accomplished by fitting an additive model (Wood and Bretherton, 2006) to the data as follows:

$$Ln(\mu_i) = \beta_0 + f_i(Longitude_i, Latitude_i) + \epsilon_i \tag{3.1}$$

where μ_i is the expected mean log-transformed Chl_I concentration, B_0 is the model intercept, f_1 is the nonparametric effect estimated from the data and ϵ_i is an error term. Measurements which were more than 12 standard deviations from the fitted spatial surface were flagged as extreme outliers and removed from the database (n=930). This technique is comparable to the Boolean 'range checking' methods which are a common quality control method for oceanographic data (Conkright et al., 2002).

Throughout these analyses, Chl_I collected using 'underway' methods (undulating ocean recorder or towed CTD) displayed atypical frequency distributions and many statistically outlying observations. Since the accuracy of these data could not be empirically verified they were removed from the analysis.

Standardizations

To examine the relationship between Chl_I,Z_D, and FU data, all measurements were binned to a common spatial and temporal resolution. To balance the fine resolution necessary to accurately capture small-scale spatial variations against the coarse resolution required to obtain representative sample sizes, datawere individually binned into 1° x 1° cells. Mean values per year and month for each cell ($\mathrm{Data}_{M,jkl}$) were calculated:

$$Data_{M,jkl} = \frac{\sum Data_{i,jkl}}{\sum N_{i,jkl}} \tag{3.2}$$

where $Data_{i,jkl}$is the data value and $N_{i,jkl}$is the number of measurements for cell j, month k, and year l. Objectively weighted binning algorithms were also implemented (Levy and Brown, 1986; Lewis et al., 1988; Boyce et al., 2010), but did not change the resulting parameter values within three decimal points. Hence we used the simpler un-weighted binning procedure here.

Calibration

Previous Chl calibration algorithms have used a linear relationship on a logarithmic scale between Secchi depth and Chl_I, provided that measurements are made in optically non-complex case I waters (Lewis et al., 1988; Falkowski and Wilson, 1992). The basis for this relationship is best explained through the equation relating Z_D to the optical properties of marine waters which to first order:

$$Z_D \propto \frac{1}{c + K} \tag{3.3}$$

where c is the average (photopic) beam attenuation coefficient (m^{-1}), and K is the average (photopic) diffuse attenuation coefficient (m^{-1}) and the proportionality depends weakly on illumination, contrast of the disk and water, and visual acuity (Preisendorfer, 1986; Falkowski and Wilson, 1992). Variations in $c + K$ explains the majority of the variability in transparency depths and co-varies with the amount of attenuating material in the water through its influence on the inherent optical properties such as scattering and absorption. For case I ocean waters, phytoplankton cells and co-varying biogenic dissolved matter are the principal sources of variation in the optical properties and empirically-based algorithms have consequently been used to derive accurate upper ocean chlorophyll concentrations (Chl_T) from transparency measurements (Lewis et al., 1988; Falkowski and Wilson, 1992; Boyce et al., 2010). The non-linear nature of the relationship reflects changes in the average size of phytoplankton cells, where rich coastal waters have a larger percentage of large cells relative to low chlorophyll waters where small cells dominate.

Forel-Ule ocean colour data are positively correlated with both the transparency and chlorophyll concentration of the upper ocean but have not yet been used to derive quantitative measurements of Chl. Before attempting to calibrate these data, we examined them along with the Z_D data to establish relationships between Z_D or FU measurements and Chl_I measurements.

To derive Chl values from Z_D or FU, model II ranged major axis (RMA) linear regression models were fitted to the (1° x 1° x month x year) binned data (Legendre and Legendre, 1998; Sokal and Rohlf, 1995). Model II RMA regression methods are appropriate when both variables in the regression equation are subject to error

(Ripley and Thompson, 1987), are expressed in different units, or the error variances differ (Legendre and Legendre, 1998). This technique accounts for the fact that Chl_I, Z_D, and FU measurements were all measured with some error and that these errors were probably unequal. Chl_I, Z_D, and FU measurements were log-transformed to achieve bivariate normality, and homoscedasticity and linearity were confirmed, as required by the regression analysis. The regression parameters from these models were estimated to predict individual Chl values from each discrete quality-controlled FU and Z_D value. Error statistics for the estimated model parameters were generated using randomized permutation tests with 1000 replicates (Legendre and Legendre, 1998). The suitability of alternate models and transformations were explored, but model fit statistics indicated that they did not fit the data as well as the linear RMA models. The resulting calibrated data are denoted as Chl_T and Chl_F, derived from Secchi depths and Forel-Ule indices respectively.

Validation

To explore the accuracy and linear scaling of Chl measurements derived from different methods, two separate validation analyses were undertaken. The first analysis compared the accuracy of calibrated Chl_T and Chl_F measurements against each another and against the direct Chl_I measurements (three comparisons). The second analysis compared the resulting integrated calibrated Chl measurements (Chl_C) against remotely sensed Chl_{SWFS} and Chl_{CZCS} measurements (three comparisons). Both validation analyses employed the same statistical methods and are described below.

Chl measurements derived using different observational platforms were individually objectively binned (Equaation 3.2) and matched spatially (1° cell) and temporally (month and year) to the Chl dataset under comparison. RMA regression models were then fitted to the log-transformed Chl matchups to examine the linear relationship between them. We used RMA as opposed to alternate model II regression techniques since it was the method used to derive Chl_T and Chl_Fvalues, and the statistical assumptions remain valid. A Pearson correlation coefficient of 1, an estimated slope of 1, and an intercept of 0 would indicate that the Chl values from the two data sources were identical. The bias of the estimated correlation coefficients and slopes was calculated using a bootstrapping procedure with 1000 replicates (Legendre and Legendre,

1998). The difference between the estimated parameter and the mean of the bootstrapped estimates provides an estimate of the bias. To further examine patterns of similarity, the standardized Euclidean residuals from RMA regression fits were calculated. These values correspond to the average difference between the two variables under comparison while minimizing the confounding effects of spatial and temporal variation. These differences were initially explored by visually inspecting the spatial distribution of the mean and absolute mean Euclidean residuals, here defined as the shortest distance between the residual and the fitted regression line. To further explore factors that may explain any systematic differences between the variables, spatially-explicit univariate and multivariate linear models were fit to the residuals. Temporal (year, month), spatial (distance from the nearest coast, bathymetry, latitude, Chl), and optical (climatological CDOM index; Acker and Leptoukh, 2007; Siegel et al., 2005; Morel and Gentili, 2009) factors were included as possible explanatory variables. An autocovariate was included within the models to account for any potential spatial dependence in the residuals. The autocovariate for each geographic cell (A_i) was calculated as the weighted average of the measurements within a pre-specified geographical radius of 8 nearest neighbours as:

$$A_q = \frac{\sum w_{qr} y_r}{\sum w_{qr}} \tag{3.4}$$

where y_r is the measurement of y at location r among location q's set of k_q neighbours; w_{qr} is the weight given to location r's influence over location q (Augustin et al., 1996; Gumpertz et al., 1997; Dormann, 2007). Individual weights for the autocovariate were derived as:

$$w_{qr} = \frac{1}{h_{qr}} \tag{3.5}$$

where w_{qr} is the weight given to cell r's influence over cell q, and h_{qr} is the Euclidean distance between cells q and r (Augustin et al., 1996).

Sensitivity analyses were undertaken to determine how robust the results of these comparisons were to variation in the initial conditions of the model. The sensitivity of the estimated slopes and correlation coefficients to changing sample sizes was estimated by bootstrapping estimates (1000 replicates) at each of 18 sample sizes ranging

from 10% to 100% of available matchups. Additionally, the sensitivity of the estimates to the ocean basin, bathymetry, month, and decade when the measurements were collected was also examined.

3.4 Results

After removing erroneous or biologically implausible measurements and those collected in nearshore waters, Chl_I, Z_D, and FU measurements were distributed most densely in northern temperate waters (>30° N) and closer to shore (Figure 3.1A, D, G). Chl_I measurements were most abundant in the North Atlantic, while Z_D and FU measurements were concentrated in the North Pacific. Spatial patterns of Chl_I measurements were similar to those of Z_D and FU measurements (Figure 3.1B, E, H), however, the oligotrophic gyres were less clearly delineated by the relatively sparser FU measurements (Figure 3.1H). Chl_I measurements were sampled since 1900, but their availability decreased markedly prior to 1955. The Z_D and FU measurements extended back to 1890 (Figure 3.1C, F, I), but were less available since the 1990s. The data density for all series was greater in Northern Hemisphere summer months and since 1950.

Regression analysis revealed that the relationship between available Chl_I and Z_D matchups (n=12,841) was linear (log-transformed) for Z_D >6 m (Figure 3.2A). Z_D measurements less than 6 m are rare in open ocean waters and are likely erroneous or associated with coastal waters with complex optical properties. Examination of available Z_D, Chl_I, and FU matchups (n=6,710) confirmed that most Z_D values less than 6 m corresponded to FU values greater than 10 (Figure 3.2C), indicative of optically complex green or brown waters located close to coastlines (Figure 3.2E). In fact, 86% of Z_D values under 6 m were located on continental shelves (<200 m depth). To eliminate Z_D measurements in optically complex waters and to ensure a linear relationship between available log-transformed Chl_I matchups, all Z_D measurements less than 6 m were removed from the final database product (n=20,748; 7% of Z_D measurements).

Likewise it was determined that the relationship between available log-transformed Chl_I and FU matchups (n=6,943) was linear for FU values between 2 and 10 (Figure 3.2B). FU measurements greater than 10 corresponded to yellow and brown waters.

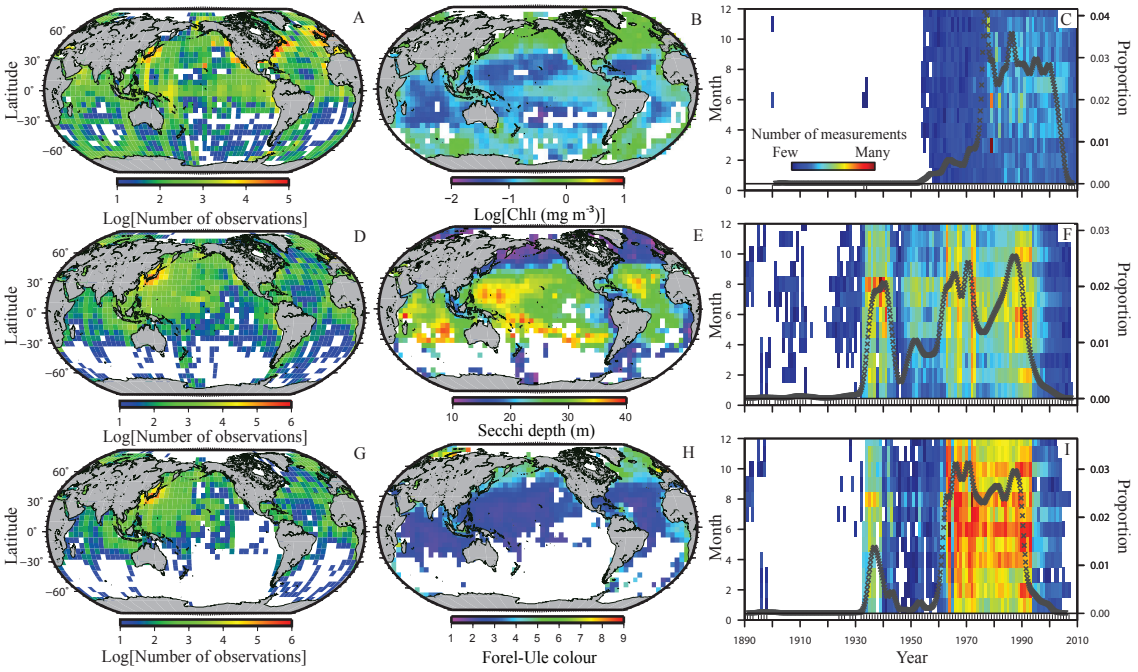

Figure 3.1: Temporal and spatial availability of data.
(A, D, G) Spatial availability of (A) Chl_I, (D) Z_D, and (G) FU colour measurements. Colours depict the number of available measurements per 5° cell. (B, E, H) Average (B) Chl_I, (E) Z_D, and (H) FU colour per 5° cell. Chl was derived using B-spline interpolation; white indicates lack of data. (C, F, I) Time-varying availability of (C) Chl_I, (F) Z_D, and (I) FU measurements. Left axis and colours depict the number of available measurements by month and year. Right axis and points depict the proportion of total observations collected in each year, smoothed with kernel density. Ticks on x-axes represent years containing data.

Examination of available FU, Chl_I, and Z_D matchups confirmed that most FU values above 10 corresponded to extremely low Z_D depths (Figure 3.2D), again indicative of optically complex waters located closer to coastlines (Figure 3.2E), which can confound Chl derivation techniques. In fact, 78% of FU values over 10 were located on continental shelves (<200 m depth). In contrast, FU measurements below 2 corresponded to indigo blue waters which contain the lowest Chl concentrations. The FU technique is likely unreliable in resolving subtle variations in Chl at these very low phytoplankton concentrations, as the primary determinant of ocean colour is the absorption and scattering associated with pure seawater. Although these waters may appear uniformly dark blue on the FU scale, Chl concentrations may vary over an order of magnitude or more, resulting in large variability at these FU values (Figure 3.2A). To eliminate FU measurements associated with optically complex waters and to ensure a linear relationship between available Chl_I matchups, FU values greater than 10 or less than 2 were removed from the final database (n=10,123; 5% of all FU measurements). The removal of these FU and Z_D measurements was necessary to ensure that the requisite statistical assumptions of the predictive models were satisfied.

The RMA regression was then used to predict Chl_T. The regression explained 64% ($p<0.0001$) of the variance in Chl_I (Figure 3.3A) and resulted in

$$Chl_T = 143.29 Z_D^{-2.082} \tag{3.6}$$

where Chl_T is the transparency-derived Chl (mg m^{-3}). Likewise, the RMA regression used to derive Chl_F explained 46% ($p<0.0001$) of the variance in Chl_I (Figure 3.3B), and resulted in

$$Chl_F = 0.016 FU^{2.44} \tag{3.7}$$

where Chl_F is the FU-derived Chl (mg m^{-3}). All RMA regressions conformed to the necessary statistical assumptions, such as linearity, normality, constancy of variance, and independence. Examination of the absolute Euclidean residuals from the RMA regressions indicated that the discrepancies between the predicted Chl fields (Chl_T or Chl_F) and Chl_I were random, and could not be explained by any of the explanatory variables. Chl_I matchups used to predict Chl_T or Chl_F values were

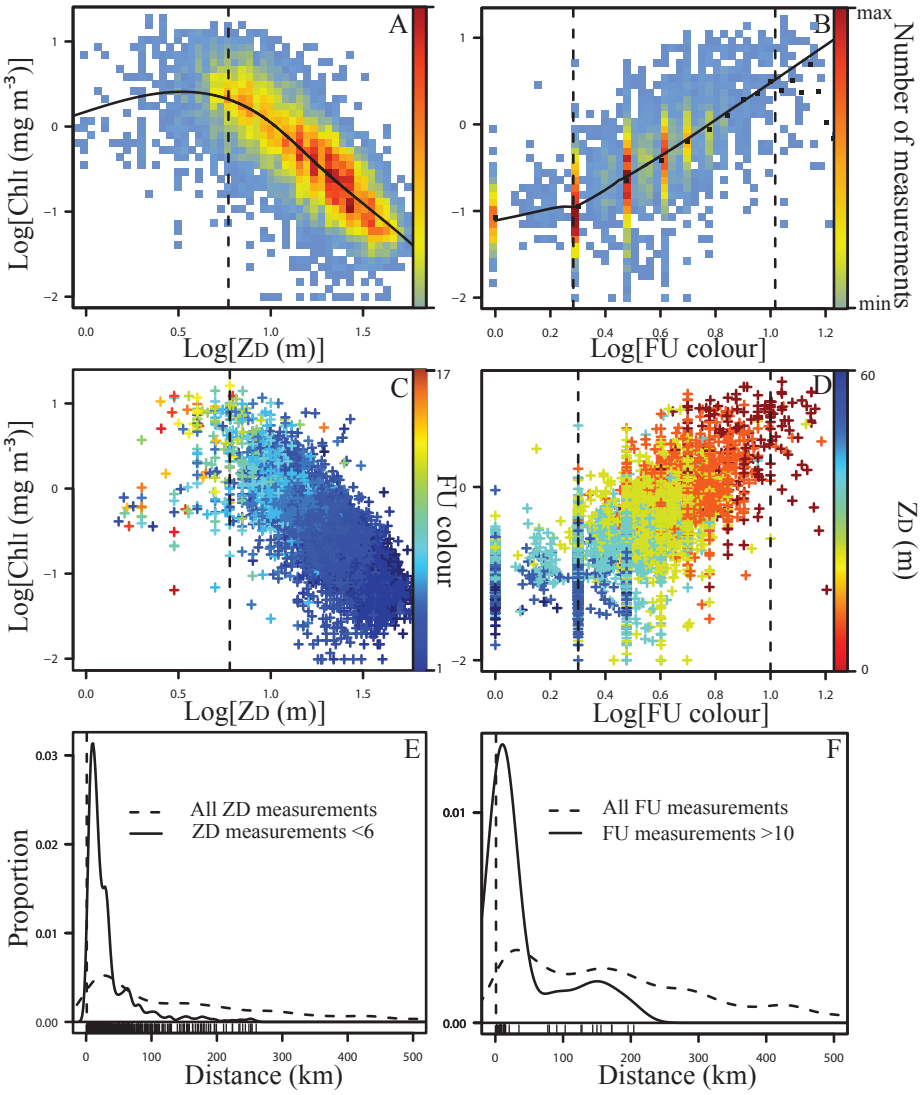

Figure 3.2: Comparing different data types.
Relationship between (A) Z_D and (B) FU and Chl_I. Relationships are approximated by a B-spline (knots=4). Vertical dashed lines represent the thresholds, beyond which the linear relationships break down. (C-D) Relationships between Z_D, FU, and Chl_I. (C) Z_D is plotted against Chl_I with corresponding FU values indicated as colours. (D) FU is plotted against Chl_I with corresponding Z_D values indicated as colours. Dashed lines represent thresholds, beyond which the linear relationships deteriorate. (E-F) Sampling effort of (E) Z_D and (F) FU measurements as a function of distance from the nearest coastline. Solid lines indicate all available data and dashed lines are the data which are eliminated from the database. Ticks on x-axes are the depths where the eliminated data are sampled; dashed vertical lines indicate a distance of 1 km from the nearest coastline.

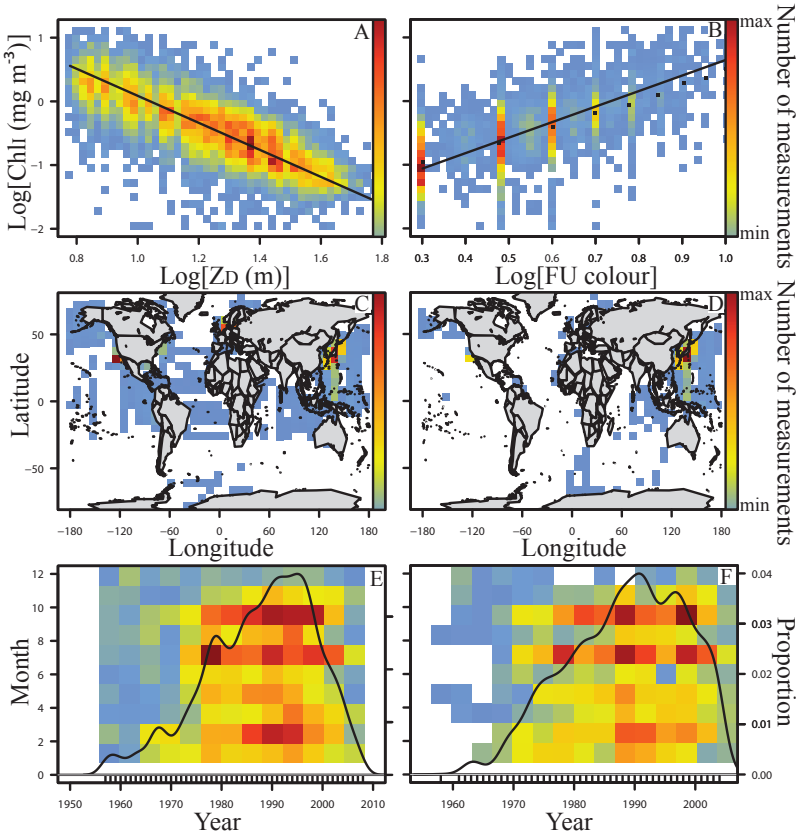

Figure 3.3: Predicting chlorophyll from transparency and colour data.
Linear RMA regression models used to derive Chl from (A) Z_D, and (B) FU. Confidence intervals are too narrow to visually detect. Spatial availability of Chl_I and (C) Z_D, and (D) FU matchups. Time-varying availability of Chl_I and (E) Z_D and (F) FU matchups. Left axes and colours depict the number of available measurements by month. Right axes and lines depict the proportion of total available measurements for each year. For all plots colours depict the number of available observations per pixel.

available globally, but were more heavily distributed in the northern hemisphere, and in near shore waters for both Z_D (Figure 3.3C), and FU (Figure 3.3D. Chl_I and FU matchups were notably lacking in open ocean waters (Figure 3.3D). Chl_I matchups were slightly less available in boreal winter months for both datasets (Figure 3.3E, F).

Chl_T and Chl_F are by definition inter-calibrated with Chl_I (slope=1, intercept=0; Figure 3.4). The accuracy of these inter-calibrations was further verified by the strong positive correlation (r=0.70; p<0.0001) and linear scaling observed between log-transformed Chl_F and Chl_T (intercept=0.002, slope=1.07±0.01, r^2=0.48). These

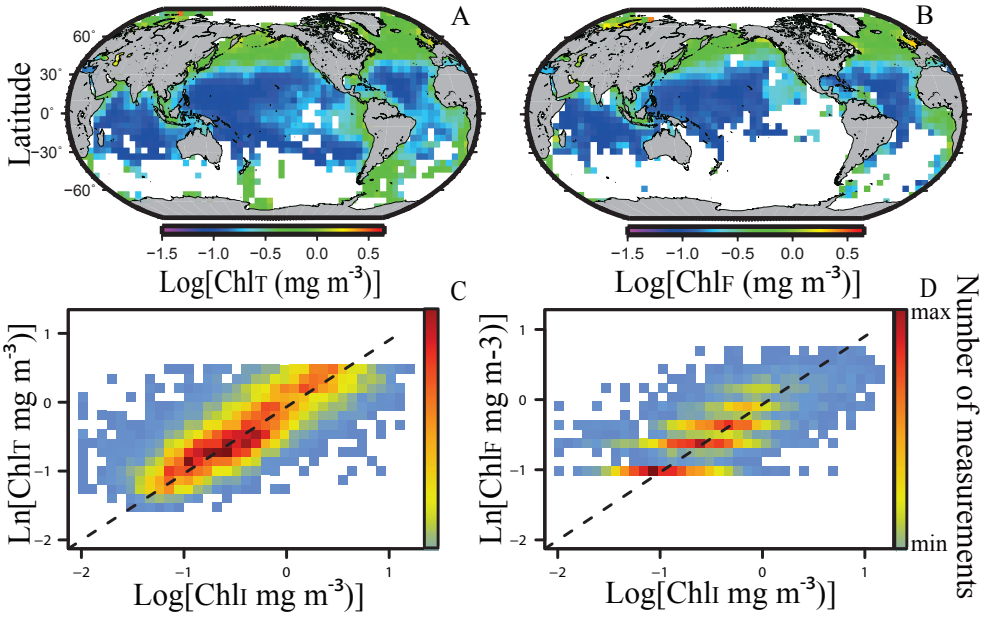

Figure 3.4: Spatial patterns of derived chlorophyll.
Mean Chl concentration from (A) Chl_T, and (B) Chl_F per 5° cell. Relationships between available Chl_I matchups and (C) Chl_T and (D) Chl_F. Idealized relationships are plotted as dashed lines and are identical to fitted RMA regression lines. Colours depict the number of observations per pixel.

calibrations were found to be insensitive to the number of measurements used, except at extremely low sample sizes. The strength of the linear relationships did not change with decreasing sample size, nor did they appreciably change with changes in the bathymetry, ocean basin, month, or decade when the measurements were collected. The magnitude of the estimated slopes varied randomly, rather than systematically. These results suggest that no further inter-calibration was required prior to combining historical Chl_I measurements with those predicted from Z_D or FU.

The resulting calibrated database (Chl_C) consisted of 644,916 globally distributed Chl measurements collected between 1890 and 2010. Similar to the individual Chl datasets, the sampling effort of Chl_C was heavily distributed over boreal summer months, and in more recent decades (>1930; Figure 3.5A). Despite the greatly increased spatial availability of Chl_C measurements, the sampling effort remained concentrated in the northern hemisphere (>30° S latitude), over mid- to low-latitude regions, and in waters closer to coastlines (Figure 3.5B). The Chl_C measurements

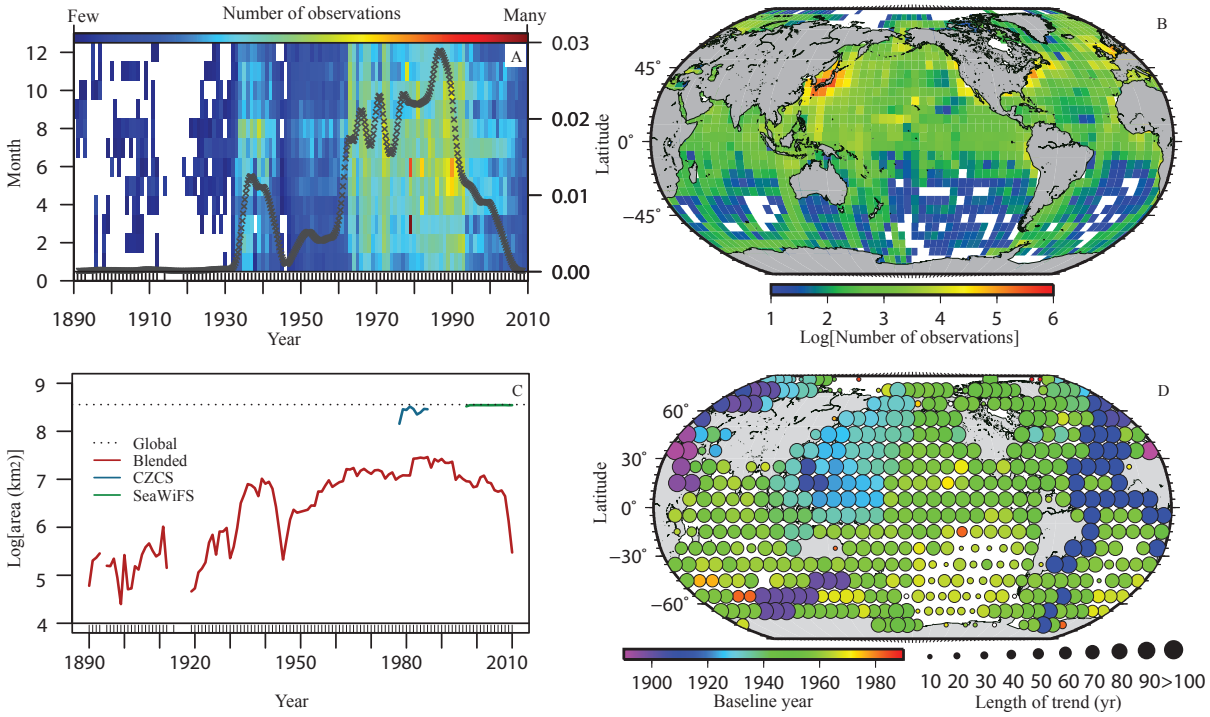

Figure 3.5: Availability of integrated chlorophyll measurements.
(A) Time-varying availability of Chl_C measurements. Left axis and colours depict the number of available measurements by month and year. Right axis and points depict the proportion of total observations collected in each year, smoothed with kernel density. Ticks on x-axis represent years containing data. (B) Spatial availability of Chl_C data. Colours depict the number of available measurements per 5° cell. (C) Spatial availability of Chl_C, Chl_{SWFS}, and Chl_{CZCS} measurements through time. Colours depict the observational platform, dashed line indicates the maximum available ocean area. Tick marks on x-axis represent years containing Chl_C data. (D) Spatio-temporal availability of Chl_C measurements. Colours depict the baseline year, size of the circles depicts the temporal span of available data per 10° cell.

are available since the 1950s in most ocean regions and since before 1930 in many North Atlantic and Pacific waters (Figure 3.5C). The data span more than 50 years in most regions of the ocean and 112 years in some regions of the North Atlantic. Importantly, the spatial and temporal availability of the Chl_C measurements is considerably increased after combining available historical data.

Spatial patterns of Chl_C closely reproduced the well-known spatial patterns of Chl derived from Chl_{CZCS} and Chl_{SWFS} (Figure 3.6); these include elevated chlorophyll in coastal, high-latitude, and upwelling regions, as well as low chlorophyll in the oligotrophic gyres. Although there are potential issues regarding the inter-calibration of

Chl_{CZCS} (Antoine et al., 2005; Gregg and Conkright, 2001), the Chl_C fields were positively correlated with concurrent (1^o x 1^o x 1 month bins) Chl estimates from CZCS (Chl_{CZCS} ; r=0.76, p<0.0001), and exhibited approximate linear scaling on a log-scale (intercept=-0.01, slope=0.84, r^2=0.58; Figure 3.6C; Table 3.2). Likewise, Chl_C measurements were positively correlated with Chl_{SWFS} (r=0.81, p<0.0001), and exhibited approximate linear scaling (intercept=0.01, slope=0.97, r^2=0.65; Figure 3.6D; Table 3.2). Interestingly, eliminating Chl_{FU} from the database led to improved correspondence between Chl_C and Chl_{CZCS} (r=0.77; intercept=-0.14; slope=0.86), and Chl_{SWFS} (r=0.82; intercept=-0.07; slope=1). Due to the large number of matchups, all correlation coefficients were statistically significant.

Spatial examination of the standardized Euclidean residuals from the RMA regressions indicated that there was a greater discrepancy between Chl_C and Chl_{SWFS} or Chl_{CZCS}in more coastal areas where Chl concentrations are on average greater and more variable (Figure 3.6E, F). Spatially explicit models fitted to the residuals confirmed that residuals were on average larger in areas closer to coastlines, at higher latitudes, and where Chl values are greater. Since latitude, distance from the nearest coast, and Chl are collinear, univariate models were also fitted to the residuals. The strongest single explanatory variable to explain the residual variation in Chl_C relative to Chl_{CZCS} or $Chl_{SWFS}$was the average Chl concentration (Chl_{SWFS}: r^2=0.05; p<0.0001 and Chl_{CZCS}: r^2=0.16; p<0.0001; Figure 3.7). For both matchups, the magnitude of the residuals was insensitive to the average concentration of coloured dissolved organic matter (CDOM) in the water, or to changes in the year of sampling. The relationship between Chl_C and Chl_{SWFS} or Chl_{CZCS} was found to be insensitive to the number of measurements used. The strength of the relationships was largely insensitive to reduced sample size, and to the bathymetry, ocean basin, month, or decade when the measurements were collected.

The reliability of the Chl_C database rests on the assumption that the function used to predict Chl is insensitive to the time and location of sampling and that the error associated with that relationship is random. We were fortunate that the large temporal and spatial overlap between available matchups allowed for a robust test of these assumptions; however, matchups were not available for all times and locations. Although matchups of Chl_I with water transparency or colour were unavailable prior to

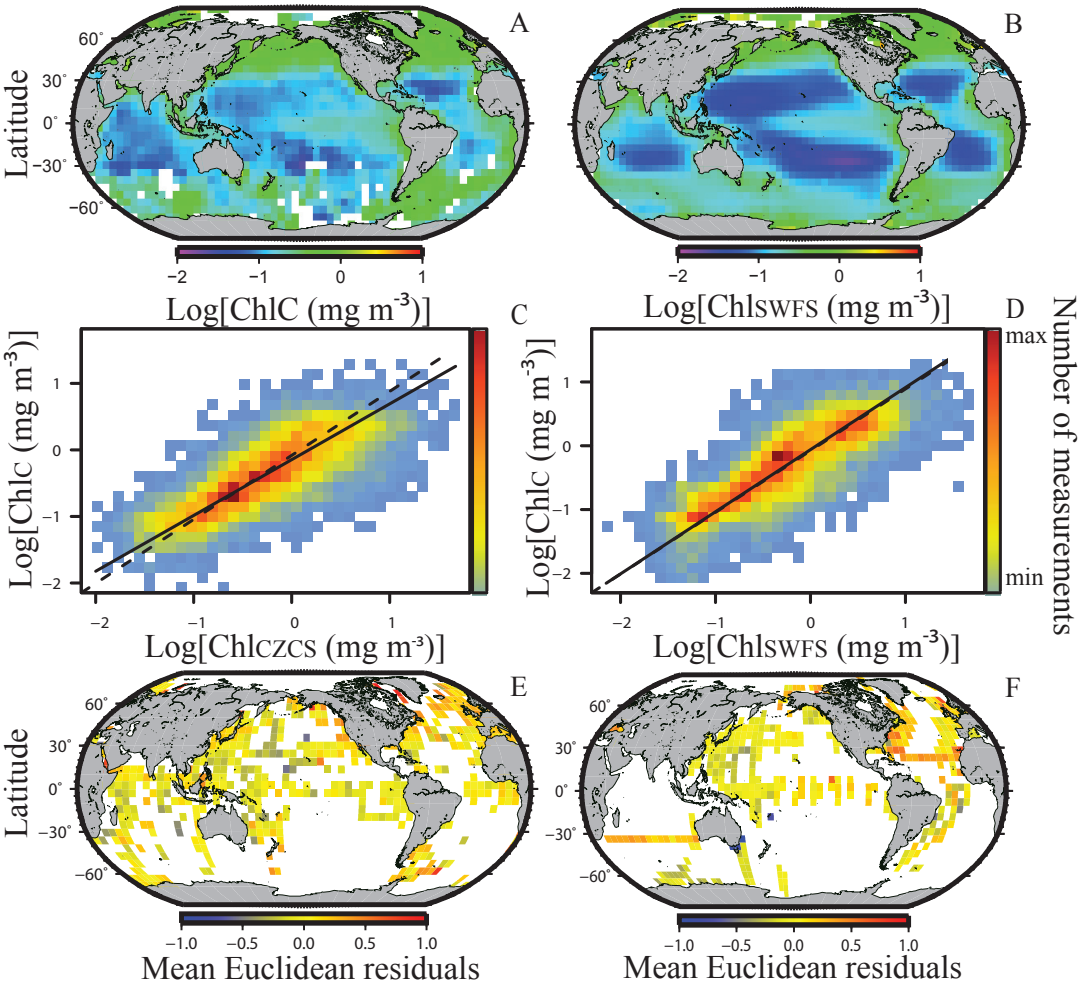

Figure 3.6: Comparison with satellite data.
Mean Chl concentration from (A) Chl_C, and (B) Chl_{SWFS} per 5° cell. Chl was derived using B-spline interpolation; white indicates lack of data. Relationships between Chl_C and (C) Chl_{CZCS}, and (D)Chl_{SWFS}. Idealized relationships are plotted as dashed lines and fitted RMA regressions are shown as solid lines. Colours depict the number of data per pixel. (E-F) Spatial patterns of the average mean Euclidean residuals from regression fits of Chl_C and (E) Chl_{CZCS}, and (F) Chl_{SWFS} per 5° cell.

Table 3.2: Regression results of model II RMA models fitted to the Chl matchups from different observational platforms.

Estimated regression coefficients, error estimates, bias estimates, coefficient of determination, correlation coefficient, number of matchups, and the temporal and latitudinal span of the available matchups are given.

Comparison	β_1	β_1 SE	β_1 bias	β_0	R^2	r	r(raw)	N	Yr Span	Lat Span
Chl_I/Chl_T	1.01	0.01	0.00	0.04	0.60	0.78	0.58	13425	51	154
Chl_{CZCS}/Chl_T	0.85	0.02	0.00	-0.39	0.57	0.76	0.49	4376	8	141
Chl_{SWFS}/Chl_T	0.95	0.02	0.00	-0.11	0.74	0.86	0.65	3234	10	84
Chl_F/Chl_I	1.00	0.03	0.00	0.01	0.44	0.67	0.56	7204	46	146
Chl_{CZCS}/Chl_F	0.96	0.05	-0.02	-0.45	0.35	0.59	0.30	3057	8	121
Chl_{SWFS}/Chl_F	0.87	0.02	0.00	0.09	0.71	0.84	0.71	2309	10	54
Chl_{CZCS}/Chl_I	1.08	0.02	-0.16	0.39	0.61	0.78	0.46	9502	8	145
Chl_{SWFS}/Chl_I	0.88	0.01	0.25	0.01	0.66	0.81	0.52	12804	12	160
Chl_F/Chl_T	1.02	0.01	-0.04	-0.12	0.48	0.69	0.53	46180	117	156
Chl_{CZCS}/Chl_B	0.87	0.01	0.00	-0.41	0.62	0.78	0.45	13364	8	148
Chl_{SWFS}/Chl_B	1.03	0.01	0.00	-0.02	0.67	0.82	0.53	13946	12	160

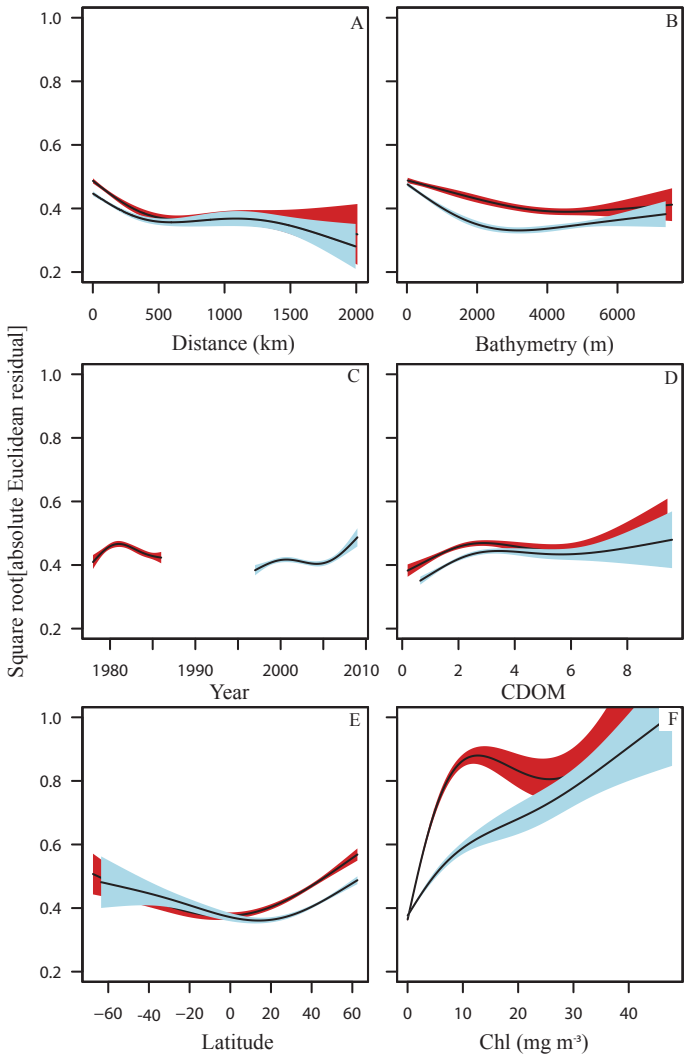

Figure 3.7: Variability in absolute Euclidean residuals.
GAM estimates of the square root-transformed absolute Euclidean residuals from linear RMA models of Chl_C versus Chl_{SWFS} (red) and Chl_{CZCS} (blue) as a function of (A) distance from the nearest coastline; (B) bathymetry; (C) year; (D) coloured dissolved organic material (CDOM); (E) latitude; and (F) mean Chl. The estimated trends are plotted as solid lines and shaded areas represent the 95% Bayesian credible limits for the trends.

1950, the strong correlation and approximately linear scaling between log-transformed Chl_T and Chl_F matchups since 1890 confirmed the efficacy of the algorithms used to calibrate them (Table 3.2). Additionally, the methods used here require accurate measurements of Chl_I to calibrate Chl_T and Chl_F. Chl_I measurements derived from high performance liquid chromatography (HPLC) are generally regarded as the best performing *in situ* technique, but are not readily available over long time scales. To generate a large enough database of historical measurements, Chl_I values derived from several *in situ* instruments were used here. Although some methods have been found to underestimate Chl, relative to HPLC techniques, this error is believed to be small (Trees et al., 1985), with the main source of Chl_I variability resulting from methodological differences among investigators (Welschmeyer, 1994). Although systematic quality control techniques were used to remove measurements associated with these sources of variability, some erroneous Chl_I measurements may persist, and contribute to the unexplained variation in the data.

To enable comparison of the various shipboard and remote sensing methods, the analysis was restricted to the surface layer (upper 20 metres). The Chl_C data therefore may not reflect the integrated chlorophyll values, since the Chl maximum occurs much deeper in some low-latitude ocean regions (Cullen, 1982). Additionally, Chl_I measurements below 20 m are usually derived from CTD profiles of *in vivo* fluorescence, and variability in the chlorophyll-to-phytoplankton biomass (organic carbon) relationship at these depths is known to produce more uncertain abundance estimates. The use of Chl_I measurements in the upper 20 m of the water column to infer phytoplankton biomass is a common practice (Behrenfeld et al., 2006; Falkowski and Wilson, 1992; Martinez et al., 2009), but it is possible that changes in major oceanographic features such as the mixed layer depth (MLD) may cause corresponding vertical shifts in phytoplankton to waters deeper than 20 m (Saba et al., 2010). If such shifts were occurring, this could cause underestimates of phytoplankton in some ocean regions and would provide a strong incentive for *in situ* observational platforms to expand the vertical sampling range.

3.5 Discussion

Here, we have demonstrated that shipboard measurements of upper ocean water transparency and colour can be integrated to derive accurate Chl fields at global scales, and extending 120 years into the past. Following careful calibration, measurements of Chl derived from different observational platforms have been combined into a single publicly-available database (see Appendices). This study was conducted using similar approaches to those developed in a previous study (Boyce et al., 2010), but incorporating additional data and several suggested improvements (Mackas, 2011; McQuatters-Gollop et al., 2011; Rykaczewski and Dunne, 2011; Boyce et al., 2011). Firstly, the calibrated database presented here was generated from a larger and more comprehensive set of measurements, and includes the FU-derived Chl measurements not previously used. Consequently, our calibrated Chl database is more spatially and temporally complete, and contains an additional 199,679 measurements. Unfortunately, we could not include plankton color measurements from the continuous plankton recorder (CPR) dataset (see Reid et al., 2003) in our analysis. Our goal was to produce a publicly-available database of Chl measurements, and as the raw CPR data are proprietary, we were unable to include them here. Furthermore, the size of the CPR silk (>250 mm) is designed to sample large zooplankton, and may not quantitatively sample smaller size fractions of the phytoplankton.

Secondly, several improvements have been made to the statistical methods used to identify implausible Chl measurements. Such improvements include, for instance, the treatment of zero Chl_I measurements, the identification of erroneous CTD-derived Chl_I measurements, and the use of spatial filters. Lastly, the Chl measurements presented here were directly calibrated from a database of independent, quality verified *in situ* Chl measurements, rather than from a previously established algorithm. Further, the calibration algorithms were developed using an unprecedented number of quality-controlled *in situ* Chl measurements (n=12,841 Secchi matchups; n=6,943 Forel-Ule matchups); this represents a considerable improvement over the number of matchups typically used to calibrate chlorophyll fields from remotely sensed water-leaving radiances (n=60 CZCS matchups; n=2,853 SWFS matchups); (Evans and Gordon, 1994; O'Reilly et al., 2000). This increases confidence in our approach, and allows for a robust verification of the statistical assumptions of the calibration and

validation methods.

The database of calibrated chlorophyll measurements presented here remains undersampled, as there are still some large data gaps, particularly in the Southern hemisphere. Despite this, we believe that the available data can and should be used to explore trends in global or regional phytoplankton dynamics prior to the satellite era (1979–86, 1997–2010). The separation of yearly-to-decadal fluctuations from longer-term phytoplankton dynamics is a frequently acknowledged challenge (Behrenfeld et al., 2006; Martinez et al., 2009; Henson et al., 2010), and is directly related to the scarcity of calibrated phytoplankton abundance measurements in the pre-satellite era (<1978). This lack of an adequate dataset may be partially responsible for the large variability in estimated trends in regional or global phytoplankton concentrations or primary production (Behrenfeld et al., 2006; Gregg et al., 2005; Gregg and Conkright, 2002; Gregg et al., 2003; Antoine et al., 2005; Falkowski and Wilson, 1992; Venrick et al., 1987). Accordingly, the calibrated global phytoplankton time series presented here may enable the assessment of ocean biological variability over a range of time and spatial scales, and help in establishing the 'missing baseline' (Pauly, 1995) against which to compare contemporary trends and estimates. Given the broad importance of phytoplankton to global marine ecosystems and processes (Behrenfeld, 2011; Falkowski, 2012), the potential applications of the calibrated phytoplankton time-series are considerable. In order to facilitate optimal use of the described dataset, we make it available as a web appendix to this paper. The data set is presented as a user-friendly text file which can be easily imported into most software platforms or in a spreadsheet. The associated metadata is also contained in the header of this file and includes a description of the variables included in the data set, the units they are measured in, the relevant citation for the data set, and contact information if users have any relevant questions.

3.6 Conclusions

For those seeking to analyze these data, several attributes must be considered. Firstly, to accurately calibrate Secchi and Forel-Ule measurements, we eliminated all measurements close to coastlines, all *in situ* Chl measurements below a depth of 20 m, all Secchi measurements less than 6 m, and all Forel-Ule measurements with a color

value of less than 2 and greater than 10. Although this was necessary to ensure the accuracy of calibration algorithms, the resulting database should not be considered to represent a complete phytoplankton inventory. Secondly, since the calibrated Chl values were derived from deterministic models, they contain no measurement error and are thus considered non-random. Alternately, the *in situ* Chl measurements were not derived from a model; thus, they contain measurement error and are considered random. Hence the calibrated values will, on average, contain the same mean as the *in situ* measurements but will have a lower variance. Lastly, spatial and temporal matchups between Chl measurements derived from different sensors and observational platforms are necessary for calibration and validation, but may violate the assumption of non-independence required by many statistical analyses.

3.7 Acknowledgements

We are very grateful to all data providers, to J. Mills Flemming for statistical advice. Funding was provided by the Natural Sciences and Engineering Research Council of Canada, and the Sloan Foundation (Census of Marine Life Program).

Chapter 4

Estimating Global Chlorophyll Changes over the Past Century

4.1 Abstract

Marine phytoplankton account for approximately half of the production of organic matter on earth, support virtually all marine ecosystems, constrain fisheries yields, and influence climate and weather. Despite this importance, long-term trajectories of phytoplankton abundance or biomass are difficult to estimate, and the extent of changes is unresolved. Here, we use a new, publicly-available database of historical shipboard oceanographic measurements to estimate long-term changes in chlorophyll concentration (Chl; a widely used proxy for phytoplankton biomass) from 1890 to 2010. This work builds upon an earlier analysis (Boyce et al., 2010) by taking published criticisms into account, and by using recalibrated data, and novel analysis methods. Rates of long-term chlorophyll change were estimated using generalized additive models within a multi-model inference framework, and *post hoc* sensitivity analyses were undertaken to test the robust of results. Our analysis revealed statistically significant Chl declines over 62% of the global ocean surface area where data were present, and in 8 of 11 large ocean regions. While Chl increases have occurred in many locations, weighted syntheses of local- and regional-scale estimates revealed that on average, chlorophyll concentrations have declined globally over the past century. Sensitivity analyses indicate that these changes do not arise from any bias between data types, nor do they depend upon the method of spatial or temporal aggregation, nor the use of a particular statistical model. The wider consequences of this long-term decline of marine phytoplankton are presently unresolved, but will need to be considered in future studies of marine ecosystem structure, geochemical cycling, and fishery yields.

In review as: Boyce, D. G., M. Dowd, M. Lewis, and B. Worm. 2012. Estimating global chlorophyll changes over the past century. Progress in Oceanography.

4.2 Introduction

Despite accounting for only 0.2% of global producer biomass, marine phytoplankton account for 46% of annual primary production (Field et al., 1998). Changes in marine phytoplankton biomass or productivity may lead to corresponding changes in geochemical cycles (Redfield, 1958), climate and weather (Murtugudde et al., 2002), fisheries landings (Chassot et al., 2010; Ryther, 1969), and the structure and dynamics of marine ecosystems (Chavez et al., 2003; Richardson and Schoeman, 2004). Although there is mounting evidence that marine phytoplankton concentration is changing at the scale of ocean basins and possibly globally, there is considerable debate regarding the direction and magnitude of change (Antoine et al., 2005; Behrenfeld et al., 2006; Boyce et al., 2010; Falkowski and Wilson, 1992; Gregg and Conkright, 2002; Gregg et al., 2005; Mackas, 2011; McQuatters-Gollop et al., 2011; Rykaczewski and Dunne, 2011; Venrick et al., 1987). This uncertainty likely results in part from the lack of consistent, long-term time series of estimates of phytoplankton concentration.

Changes in phytoplankton concentration have been inferred from measurements of upper ocean chlorophyll concentration (Chl; mg m^{-3}); (Venrick et al., 1987), transparency (Falkowski and Wilson, 1992), visual estimates of ocean colour (Reid et al., 1998; Wernand and Woerd, 2010), and remotely-sensed water-leaving radiances (Antoine et al., 2005; Behrenfeld et al., 2006; Gregg and Conkright, 2002). Recent trends estimated primarily from satellite data (<30 years) are strongly driven by transient climate fluctuations (Behrenfeld et al., 2006; Boyce et al., 2010; Chavez et al., 2011; Martinez et al., 2009), and longer series are required to resolve long-term trends (Beaulieu et al., 2013; Henson et al., 2010). To overcome this limitation, several studies have combined indices of phytoplankton concentration sampled over different time periods and from different observational platforms (Antoine et al., 2005; Boyce et al., 2010; Gregg and Conkright, 2002; Gregg et al., 2003; Raitsos et al., 2005; Saulquin et al., 2013). One such study combined shipboard measurements of ocean transparency and *in situ* Chl and concluded that average surface Chl had declined globally over the past century (Boyce et al., 2010). These findings were questioned by others, primarily because of possible calibration issues arising from the merging of two independent time series, available over different time intervals, to estimate trends

(Boyce et al., 2011; Mackas, 2011; Rykaczewski and Dunne, 2011). These criticisms were addressed in a follow-up study where time series were calibrated against each other, and their accuracy was compared against more recent satellite-derived measurements of surface Chl (Boyce et al., 2012). This procedure removed any potential bias introduced by merging of data types, and correlated strongly (r=0.81; ranged major axis slope=1) with the independently derived satellite record. In constructing this database we also introduced a range of methodological advancements and sensitivity analyses, which demonstrated the accuracy of the Chl measurements. Here, we use this larger, and expanded database of Chl measurements (Boyce et al., 2012) combined with newly developed analysis methods and robustness checks to provide new estimates of long-term changes in global upper ocean Chl over the last century.

4.3 Methods

4.3.1 Data

Due to the difficulty associated with direct enumeration of phytoplankton and in separating phytoplankton carbon from that contained in other living and detrital particles, the measured concentration of chlorophyll has been widely used as a first-order indicator of the abundance and biomass of oceanic phytoplankton. Despite variability in the phytoplankton Chl-to-carbon ratio (Geider, 1987; Saba et al., 2010), Chl is still the most practical and extensively used proxy of phytoplankton biomass over large spatial scales (Antoine et al., 2005; Behrenfeld et al., 2006; Gregg and Conkright, 2002; Gregg et al., 2005; Henson et al., 2010; Huot et al., 2007; Montes-Hugo et al., 2009; Raitsos et al., 2005; Reid et al., 1998).

We use a new and publicly-available database of integrated Chl values collected via shipboard sampling platforms from 1890 to 2010 (details in Boyce et al. 2012). The database is only briefly described here; full details of the data sources, temporal and geographic distribution, quality control and inter-calibration are given in Boyce et al. (2012). It consists of measurements of ocean transparency (derived from Secchi-depth measurements; Z_D) and colour (derived from the Forel-Ule color-matching scale; FU), which were both calibrated against a large and comprehensive database of quality-controlled *in situ* Chl measurements derived from spectrophotometric or fluorometric

analyses of seawater. Since the calibration methods used to derive Chl values are sensitive to the optical properties of the seawater, all near-shore measurements (<20 m water depth or <1 km from the nearest coastline) were removed from the database on the assumption that these waters would likely contain significant concentrations of other optically active constituents, that confound the optical detection of phytoplankton Chl. Statistical techniques were used to identify erroneous measurements; these were corrected or removed from the database.

This database (details in Boyce et al. 2012) has been expanded and improved over a previous version (used by Boyce et al., 2010), in a variety of ways, including :

1. The number of individual measurements, and the temporal and spatial coverage of the database has considerably increased, despite the use of more stringent quality control methods.

2. Transparency values in the database were calibrated directly against a large number of quality-controlled *in situ* Chl measurements (n=12,841); this is a large increase over the number of matchups used to calibrate globally distributed remotely sensed water-leaving radiance values from the Coastal Zone Colour Scanner (CZCS; n=60) or the Sea-viewing Wide Field-of-view Sensor (SeaWiFS; n=2, 853); (Evans and Gordon, 1994; O'Reilly et al., 2000), and ensures that our calibration equations accurately represent *in situ* Chl concentrations.

3. A range of new statistical methods (*i.e.* spatial filters) were developed to identify potential outlying or implausible Chl measurements in the database, and to subsequently remove or correct them. A range of Chl depth interpolation methods were also explored to verify the assumption that the mean Chl over 20 m was the appropriate metric.

4. Measurements in the database were subjected to a number of additional post-calibration analyses testing their quality, precision, and robustness (Boyce et al., 2012). This included testing their accuracy against widely used remote sensing estimates of Chl. These analyses indicated that the Chl values in this database are strongly correlated with Chl from SeaWiFS (r=0.81; ranged major axis slope=1) on log-log scales. The larger number of matchups and strong correspondence with remote sensing measurements attest to the improved quality

of the integrated Chl database (see Boyce et al. 2012 for further details).

Prior to our trend analyses, sensitivity analyses were undertaken to ensure that merging *in situ*, color, and transparency-derived Chl measurements would not bias the results of subsequent trend analyses. These sensitivity analyses suggested that Chl trends derived from Forel-Ule ocean colour measurements were atypical. Changes in Forel-Ule ocean color determinations are not sensitive to small changes in Chl observed in oligotrophic (blue) waters (FU<2) where the optical properties of pure water dominate, or in mesotrophic (green or brown) waters where other particles and dissolved substances are significant (FU>10). Oligotrophic blue waters contain the lowest Chl concentrations globally and are widely distributed.. Because the validity of these values could not be confirmed and to avoid any potential bias, we removed all FU-derived Chl values prior to the trend analysis. The resulting database used here contains 451,383 calibrated Chl values, is globally distributed, and spans over a century (1890 to 2010). Despite this, the measurements are sparse in many areas, particularly in the Southern hemisphere, and prior to 1950.

4.3.2 Statistical Analyses

Inter-annual changes in average Chl are often small relative to the naturally-occurring variability. For instance, stochastic natural disturbances can drive large transient Chl changes over days to weeks (Hamme et al., 2010), intra-annual Chl variability can span several orders of magnitude in some locations, and inter-annual to decadal climate fluctuations can induce 20-fold changes in Chl over varying time intervals (Barber and Chavez, 1986). Detection of any long-term trends that may underlie this large variability requires powerful and flexible analysis tools. Hence, we estimated changes in Chl over time using generalized additive models (GAMs). GAMs are an extension of widely-used generalized linear models, but enable the estimation of both linear trends as well as non-monotonic responses, (e.g. seasonal cycles) within the same model framework (Hastie and Tibshirani, 1986). In contrast to more traditional approaches, GAMs do not require the assumption of a fixed functional form (linear or otherwise), hence more complex (e.g. cyclical or bi-modal) dynamics can be captured.

As an additional improvement, we employed GAMs within a multi-model framework (Burnham and Anderson, 2002). This approach uses information theory to

rank and/or average across a set of statistical models. By eliminating the reliance on a single model, the robustness of the model inference is improved in much the same way as ensemble forecasts do for meteorological or climate projections. The advantages of this approach are considerable. The GAM approach enables Chl to vary as a linear or non-linear function of our model covariates, while accounting for the non-normality, as well as the spatial and temporal dependence of Chl measurements. The multi-model approach enabled us to allow for a very diverse array of dynamics to explain Chl variability at different ocean locations. For instance, our ensemble models allowed for the strength (magnitude) and nature (linear or smooth) of some important model effects, such as seasonality, or coastal distance to vary across space and through time.

As a first step in the analysis, an ensemble of competing GAM models to explain Chl variability in the upper oceans was selected. The ensemble model set was relatively small (maximum of 20-39 models) and defined a priori according to current knowledge of which factors influence Chl. Since we were interested in determining the rate of Chl change over time, all ensemble models contained an effect to explain inter-annual Chl variability. In addition to this, most ensemble models included effects to explain variability in Chl related to the location of measurements, the day of the year, water depth, and distance from the shore. Thus the general form of the GAMs used to estimate trends was as follows:

$$\eta(\mu_i) = \beta_0 + \beta_{year} \times year_i + \beta_1 x_{1,i} + f_1(x_{2,i}) + f_2(x_{3,i} x_{4,i}) + \epsilon_i \tag{4.1}$$

where i are the individual observations, η is the monotonic link function of the expected mean Chl concentration μ_i, $year_i$, x_1, x_2, x_3, and $x_4$are predictor variables, β_0 is the model intercept, β denotes parametric and f denotes functional effects estimated from the data, and ε_i represents the residual error term. The functional effects are continuous, smooth curves which can more closely track the response data, and thus accommodate a wide array of response functions ranging from linear to multi-modal (Wood and Bretherton, 2006; Wood, 2004, 2003). The predictors (x) in the above example may be spatial (*i.e.* longitude, latitude, bathymetry) or temporal (*i.e.* day of the year, decade) variables explaining Chl variability (Table 4.1). All

Table 4.1: Specification of effects to explain Chl variability.

The ensemble model set contained different combinations of covariates. The saturated model contained one effect from each category of variability explained (column 1); the minimum model contained only one effect of inter-annual variability. β are linear and f are functional model effects.

Variability explained	Effect estimation	Basis function	Dimension
Inter-annual	β(Year)		
	β(factor(Year))		
	f(Year)	Cubic	10
Intra-annual	f(Day)	Cyclic	5
	f(Day x factor(Space))	Cyclic	5
	f(Day x factor(Time))	Tensor product	5,3
	β(factor(Month))		
Nutrient re-suspension	f(Bathymetry)	Cubic	4
Land-based deposition	f(Coast distance)	Cubic	4
	f(Coast distance x factor(Time))	Cubic	4
Spatial	f(Longitude x Latitude)	Thin plate	Estimated
	f(Longitude)	Cubic	Estimated
	f(Latitude)	Cubic	Estimated

ensemble models contained β_{year}, which is a parametric effect capturing the long-term trend in average Chl. For all models we assumed a gamma-distributed error structure ($\mu_i \sim Gamma$) and a log link ($\eta(\mu_i) \sim ln(\mu_i)$); alternate distributions and link functions were fitted but did not perform as well. Using this method, we were able to estimate the average rate of Chl change over time while accounting for underlying aspects of Chl variability. Further, because the influence of the model covariates on the mean response is through the logarithmic link function such that $\eta(\beta_{year}) = e^{\beta_{year}}$, the estimated rate of Chl change over time was retrieved on a linear response scale (mg m^{-3} yr^{-1}). All model assumptions, including spatial and temporal dependence were verified by analysis of the model residuals.

All GAMs were fitted to the data using penalized likelihood approximation by penalized iteratively re-weighted least squares (Wood and Bretherton, 2006). The smoothing parameters used to scale the likelihood penalty of all functional effects were estimated by generalized cross-validation. To prevent over-fitting the influence of the effective degrees of freedom on estimation of functional effects was inflated by a factor of 1.4 (Kim and Gu, 2004). The basis dimensions of the functional effects were estimated *a priori* such that any patterns in the residuals as a function of the

functional predictor variables could not be explained by them. More information on the theory and technical aspects of GAMs can be found in, for example (Hastie and Tibshirani, 1986; Walsh and Kleiber, 2001; Wood and Bretherton, 2006; Litzow and Ciannelli, 2007), while details and examples on their implementation in an oceanographic context may found in, for example (Bigelow et al., 1999; Polovina et al., 2008; Irwin and Finkel, 2009).

The Bayesian information criterion (BIC) was calculated for each individual model within the ensemble (Schwarz, 1978) to evaluate its parsimonious performance. BIC is an information theoretic-based goodness of fit statistic and takes into account model fit, complexity, and sample size,

$$BIC = -2ln[L(\theta_p \mid y)] + pln(n) \tag{4.2}$$

where n is the sample size, $L(\theta_p \mid y)$ are the likelihood estimates of the model parameters θ_p, given the data y, and p is the number of free parameters estimated by the model. Normalized multi-model weights for each ensemble model (w_m) were then calculated as,

$$w_m = \frac{exp(\frac{1}{2\Delta_m})}{\sum_{m=1}^{R} exp(-\frac{1}{2\Delta_m})} \tag{4.3}$$

where R represents the total number of models fit, and

$$\Delta_m = BIC_m - BIC_{min} \tag{4.4}$$

Here BIC$_m$is the BIC score for model m, and BIC$_{min}$ is the minimum (top ranking) BIC score in the ensemble model set. The 'best' model was selected from the ensemble according to the information-theoretic weights (w_m, Equation 4.3), with $\beta_{year,B}$ extracted as the 'best' model estimated rate of Chl change over time. This approach selects the model containing the largest amount of 'information' (Burnham and Anderson, 2002; Burnham, 2004).

To determine how sensitive the estimated rate of change was to the model selection process, multi-model averaged estimates of Chl change over time were derived as

follows,

$$\overline{\beta}_{year,MM} = \sum_{m=1}^{R} w_m \beta_{year,m} \tag{4.5}$$

Where $\overline{\beta}_{year,MM}$ is the multi-model ensemble-averaged parameter estimate of the rate of Chl change over time, w_m are the model weights, and $\beta_{year,m}$ are the estimates of the rate of Chl change over time for each model.

Estimating trends across spatial scales

We estimated rates of Chl change at local, regional, and global spatial scales, using direct and weighted analysis methods. For the regional analyses Chl change was also estimated as linear, discrete, and smooth functions of time. This was done to evaluate robustness; estimates of change should be relatively insensitive to the use of different statistical methods and assumptions.

To resolve spatial patterns of Chl change, local-scale trends were estimated for individual 10° x 10° cells that contained adequate data. It has been suggested that a continuous Chl series spanning at least 27 (Beaulieu et al., 2013) to as many as 40 years (Henson et al., 2010) is required to separate long-term trends from shorter-term climate-driven fluctuations, with series length varying by ocean region. Hence we restricted our analysis to cells where the temporal range of measurements spanned at least 35 years. We also excluded cells containing <25 individual measurements or <5 individual years with measurements. The remaining database contained n=280 individual 10° x 10°cells with sufficient data. For each cell, up to 39 candidate models were fitted to the available data. From this ensemble model set, a multi-model average rate, and a best-model rate of Chl change were estimated (see above, equations. 2-4).

To estimate Chl trends at the 'regional' scale of ocean basins, the data were aggregated into 11 large regions which exhibit similar variability in Chl in response to seasonality and inter-annual to decadal climate variability (Behrenfeld et al., 2005; Boyce et al., 2010). Although 10 regions were initially selected, observed discontinuities in the Chl response between the eastern (> 20° W longitude) and western (< 20° W longitude) North Atlantic region led us to further subdivide this basin (see local and regional model results below for further details).

To capture the range of potential Chl trajectories over time, regional trends were

estimated from GAMs as linear functions of time (on a log scale) in three different ways: as (*i.*) continuous (linear trend), (*ii.*) discrete (decadal average estimates), and (*iii.*) smooth functions of time (functional trend). This approach allows both the quantitative (rate) and qualitative (shape) characteristic of trends to be estimated while accounting for the influence of the model covariates.

Rates of Chl change for each region were also determined by aggregating the local 10° x 10° estimates. Individual local scale estimates were heterogeneous in both the uncertainty of individual estimates, as well as the geographic area encompassed by them; statistical weighting methods were used to account for this heterogeneity. For each local estimate, statistical weights were calculated, taking account the sampled area, and the uncertainty weights. Standardized area weights ($w_{area(c,r)}$) were derived for each 10° x 10° cell (c) within each region (r),

$$w_{area(c,r)} = \frac{A_{c,r}}{A_{max(r)}} \tag{4.6}$$

where $A_{c,r}$ is the convex polygon area of all measurements in cell c within region r and $A_{\max(r)}$ is the maximum convex polygon area of all cells within region r. Standardized estimate uncertainty weights ($w_{uncertainty(c,r)}$) were calculated for each cell (c) within each region (r),

$$w_{uncertainty(c,r)} = \left(\frac{CV_{c,r}}{CV_{max(r)}}\right)^{-1} \tag{4.7}$$

where $CV_{c,r}$ is the coefficient of variation of cell c within region r, and $CV_{\max(r)}$ is the maximum coefficient of variation of all cells within region r. Coefficient of variation values were calculated using the estimated rates of Chl change and standard errors. Using this method, local estimates encompassing larger geographic areas and possessing less uncertainty are allocated greater statistical weight. Weighted mean rates of Chl change for each region ($\overline{\beta}_r$) were estimated as

$$\overline{\beta}_r = \frac{\sum_{i=1}^{n} w_{c,r}\beta_{c,r}}{\sum_{c=1}^{n} w_{c,r}} \tag{4.8}$$

where $w_{c,r}$ are the weights derived as the average of $w_{area(c,r)}$ and $w_{uncertainty(c,r)}$, and $\beta_{c,r}$ are local estimates for change for cell c within region r.

where $w_{c,r}$ are the weights derived as the average of $w_{area(c,r)}$ and $w_{uncertainty(c,r)}$, and $\beta_{c,r}$ are local estimates for change for cell c within region r. Global rates of Chl change were then derived by independently averaging local or regional estimates using the statistical weighting methods (Equations 4.5 to 4.7).

Finally, to determine the sensitivity of the estimated trends to the merging of transparency- and *in situ*-derived Chl measurements (Chl_T and Chl_I, respectively), model II major axis regression models were fitted to matched (1° x 1° x month x year) Chl_T and Chl_I measurements within each 10° x 10° cell. The estimated slope parameter from the model (β_{bias}) corresponds to the average change in Chl_T for each unit of Chl_I increase and is estimated as

$$\beta_{bias} = \frac{s_T^2 - s_I^2 + \sqrt{(s_T^2 - s_I^2)^2 + 4(S_{IT})^2}}{2s_{IT}} \tag{4.9}$$

where s_I^2 and s_T^2, are the estimated variances of Chl_I and Chl_T, respectively, and $s_{IT}^2$is their estimated covariance (Sokal and Rohlf, 1995; Legendre and Legendre, 1998).

4.4 Results

4.4.1 Local Trends

When considering the 280 10° x 10° cells with sufficient data for long-term trend analysis, 57.2 % (95% Wilson score confidence interval: 51.3-62.8%); (Wilson, 1927) showed declining Chl trends; this proportion increased to 60.1% (95% CI: 52.5-67.2%) when only statistically significant trends were considered (Figure 4.1A; Table 4.2). When all 348 available cells were considered irrespective of their trend length, 56.6% showed declining trends. This finding was robust to the estimation of changes using different subsets of the complete Chl database, or when considering all available trends or only statistically significant trends (Table 4.2). On an area basis, Chl declines were observed over 58.4% of the global ocean surface area where adequate data permitted trend analysis; this proportion increased to 62.1% when considering only areas where the rate of change was statistically significant.

The rate of Chl decline increased with distance from the nearest coastline (Figure 4.1B). Weighted linear regression of available local trends (n=280) as a function

Table 4.2: Summary statistics from local-scale estimates of Chl change estimated from different data sets.

Trends used	Data used	% Cells declining	N cells	Weighted rate	95% CI	Mean rate	95% CI	N cell	Span
All trends	ALL	57.00	280	-0.00	0.00	-0.00	0.04	321	1890 - 2010
	1950 Onward	55.00	254	-0.00	0.00	-0.00	0.05	311	1951 - 2010
	TRUNCATED	58.00	252	-0.00	0.00	-0.00	0.03	336	1890 - 2010
	ZD	51.00	153	0.00	0.00	0.00	0.03	329	1890 - 2008
	CHL	48.00	147	-0.00	0.00	-0.01	0.07	194	1900 - 2010
	SHELF	58.00	72	0.00	0.00	-0.00	0.03	474	1891 - 2010
	OCEANIC	57.00	208	-0.00	0.00	-0.00	0.05	268	1890 - 2010
Significant trends	ALL	60.00	168	-0.00	0.00	-0.01	0.05	478	1890 - 2010
	1950 Onward	57.00	152	-0.00	0.00	-0.01	0.06	433	1951 - 2010
	TRUNKATED	63.00	137	-0.00	0.00	-0.00	0.04	527	1890 - 2010
	ZD	51.00	91	0.00	0.00	0.00	0.04	445	1890 - 2008
	CHL	55.00	92	-0.01	0.00	-0.01	0.08	291	1900 - 2010
	SHELF	60.00	47	0.00	0.00	-0.01	0.04	809	1891 - 2010
	OCEANIC	60.00	121	-0.00	0.00	-0.01	0.06	434	1890 - 2010

Note: N cells are the number of 10° x 10° cells, % declining is the proportion of all cells that contain declining trends, weighted mean rate are the average weighted rates of Chl change (mg m^{-3} yr^{-1}), Mean rate is the arithmetic mean rate of Chl change, 95% CI are the confidence intervals for the weighted and average rates of change, N/cell is the median number of measurements per cell, year span is the years spanned by all data.

of distance from the nearest coastline yielded a negative trend, that was marginally non-significant (-4 x 10^{-6} mg m^{-3} yr^{-1} km^{-1}; P=0.06). When considering only statistically significant local-scale estimates of Chl change this relationship became stronger and statistically significant (-7 x 10^{-6} mg m^{-3} yr^{-1} km^{-1}; P=0.04; n=168). This general pattern was also observed when Chl changes were independently estimated from *in situ* or transparency derived Chl data, or using only measurements collected since 1950. Estimating local-scale rates of change separately using measurements collected in shelf (<200 m depth) or oceanic (>200 m depth) waters also suggested greater rates of Chl decline in remote open ocean waters (Table 4.2).

Despite the overall decline in Chl observed, statistically significant increases were observed in 39.9% of cells and (or 38.0% of the ocean surface) where adequate data permitted trend analysis. Clusters of increasing cells were observed in the temperate North Pacific, in the Northeast Atlantic, and across the subtropical warm pool (Figure 4.1A). Although rates of Chl increase were greater in waters closer to the shorelines (Figure 4.1B), there was a no change in the proportion of cells containing increasing Chl trends in coastal (< 200 m depth; 59.6%) or oceanic (>200 m depth; 60.3%) waters.

Estimated rates of Chl change were larger and more variable in the Southern Hemisphere, likely as a function of limited data availability. Spatial examination of the strength of inference for the main model effects suggested the seasonal effects were of large importance in most cells, but were especially significant in the Northern Hemisphere and in the Atlantic Ocean. Spatial effects were dominant in the tropical Pacific Ocean (20° N to 20° S), where seasonal effects were weaker.

When all local estimates were aggregated by ocean region (n=11; Figure 4.1C) using statistical weighting methods (Equations 4.5 to 4.7), declining trends were observed in 8 of 11 regions; five of those were statistically significant (Figure 4.1D). The largest rates of decline were observed in the Atlantic, the South Indian, and the Southern Ocean region. Conversely, the Northeast Atlantic and South Pacific showed increasing trends and the equatorial Pacific region appeared approximately stable. Estimates of change in the Southern hemisphere regions were found to be more variable and uncertain than elsewhere. The proportion of declining cells was also greater than 50% in 9 of 11 regions, with the largest proportional declines in

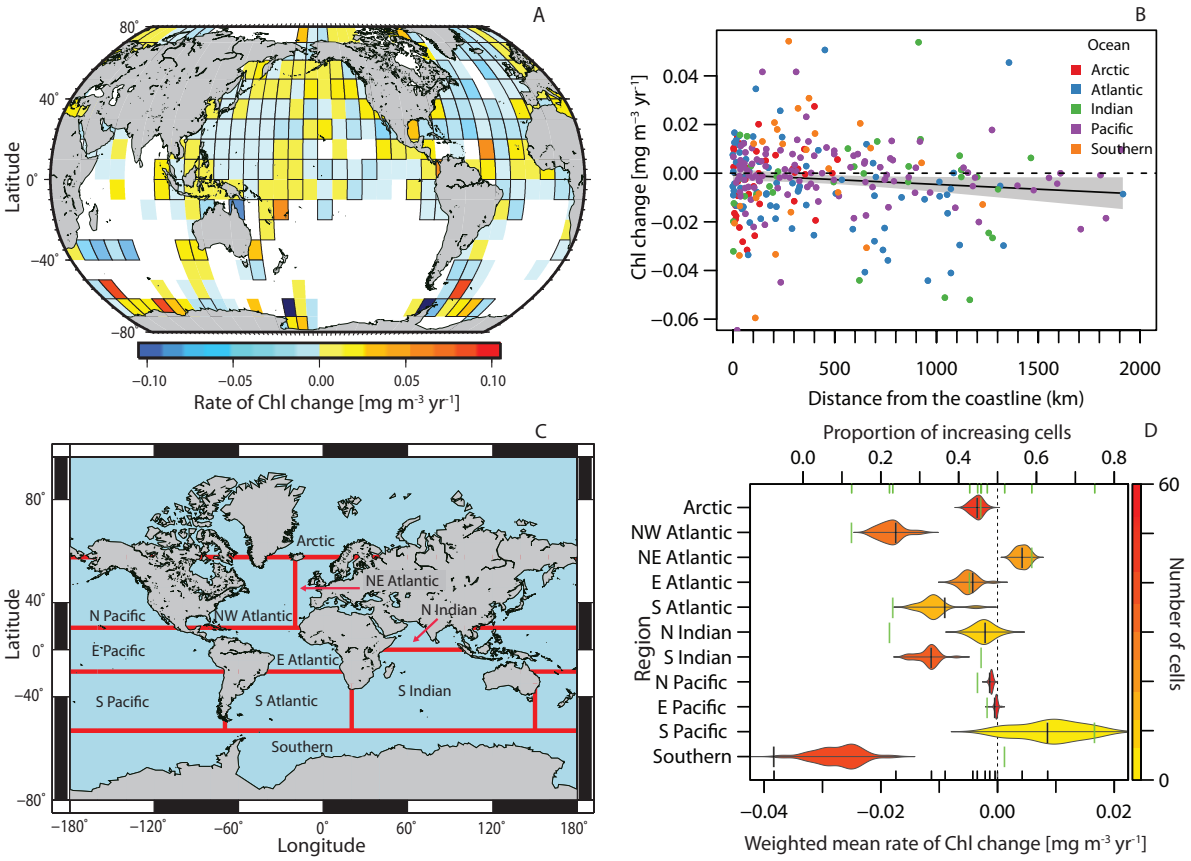

Figure 4.1: Local-scale phytoplankton trends.
(A) Estimated instantaneous linear rate of Chl change in each 10° x 10 cell (n=280). Color coding indicates the average rate of change over the available time series. Cells bordered in black denote statistically significant rates of change ($P<0.05$) and white cells indicate cells with insufficient data. (B) Chl change in each 10° x 10 cell as a function of distance from the nearest coastline (km). Colours indicate the ocean where the cell was located. Solid trend line was derived from a weighted linear model; shaded area is the 95% confidence interval; dashed line represents no change in Chl. (C) Ocean regions (n=11) used to estimate regional trends in Chl (D) Weighted mean Chl changes estimated by aggregating local estimates within each region. Shapes ('Raindrops') represent the probability distribution of the individual local estimates. The weighted mean rates of Chl change are depicted as black vertical lines, and the width of the raindrops and gray horizontal lines are the 95% confidence limits about the means. The colours of the raindrops depict the number of cells within each region. Green vertical lines are the proportion of increasing cells within each region. Black and green tick marks on the axes represent the individual rates or proportions of change, respectively. Dashed line represents no change.

Atlantic and North Indian regions (Figure 4.1D). The proportional changes of cells within each region was similar to weighted averages rates, except for the Southern Pacific and Southern regions, where the number of cells and measurements were small and estimates of change were variable (Figure 4.1D).

4.4.2 Regional Trends

Chl trajectories estimated as discrete, linear, or smooth functions of time suggested strong fluctuations in average Chl concentrations superimposed on long-term linear trends (Figure 4.2), with most trajectories declining over the last 60 years. Again, estimated Chl trends were more uncertain in the Southern Hemisphere regions and over earlier time periods, likely as a function of limited data availability. Estimated smooth Chl trajectories are strongly influenced by data-poor years and decades, possibly explaining the large fluctuations over the pre-1950 period (Figure 4.2). With the exception of the Pacific regions, Chl was observed to initially increase before undergoing prolonged decline. Most of these initial increases predated 1950, and appeared to be driven by a relatively small number of data points.

Estimates of change within large ocean regions described previously (Figure 4.1C), indicated statistically significant Chl decline in 8 of 11 regions (Figure 4.3A, B; Table 4.3). The largest instantaneous rates of decline were observed in the Northwest (-0.0096±0.001 mg m^{-3} yr^{-1}; P<0.001), equatorial (-0.0035±0.0018 mg m^{-3} yr^{-1}; P<0.001), and South (-0.0036±0.0029 mg m^{-3} yr^{-1}; P<0.001) Atlantic and the Arctic (-0.0046±0.002 mg m^{-3} yr^{-1}; P<0.001) and Southern Ocean (-0.0098±0.0033 mg m^{-3} yr^{-1}; P<0.001) regions (instantaneous rate of change and 95% confidence interval). Statistically significant rates of increase were observed in the Northeast Atlantic (0.0045±0.0016 mg m^{-3} yr^{-1}; P<0.001), South Indian (0.0058±0.0004 mg m^{-3} yr^{-1}; P<0.001), and South Pacific (0.0066±0.0005 mg m^{-3} yr^{-1}; P<0.001) regions. When extrapolating over the available trend length, these rates correspond to substantial cumulative upper ocean Chl changes. The largest proportional declines were observed in the Northwest Atlantic (-61%), Southern (-64.5%), and Arctic (-38.5%) regions (Table 4.3). Smaller declines were calculated for the equatorial Atlantic (-28.5%) and South Atlantic (-28.2%), North Indian (-19.5%), equatorial (-17.9%) and South Pacific (-4.5%) regions. Large increases were extrapolated for the Northeast

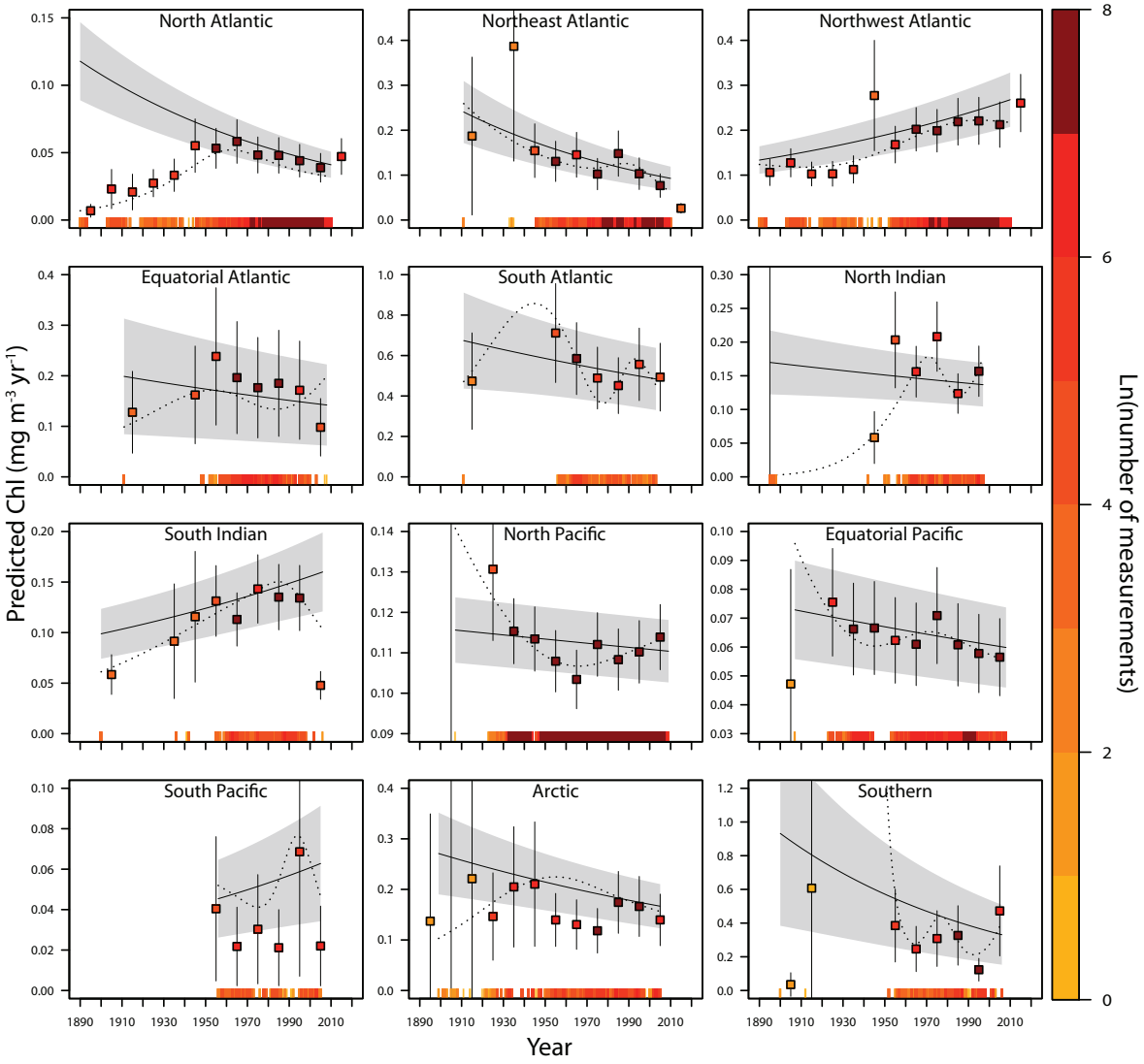

Figure 4.2: Temporal trajectories of phytoplankton.
Estimates of Chl as a discrete (points), log-linear (lines), and smooth (dotted lines) function of temporal variability in each region (n=11). Tick marks on the x-axis represent the availability of data through time. The color of tick marks and points represents the scaled number of observations available in each year (tick) and decade (point). Shaded areas represent approximate 95% Bayesian credible limits around each log-linear trend.

Table 4.3: Regional-scale estimates of Chl change.

Region	β_{year}	SE	P value	% Yr^{-1}	Deviance	Area	Span	N Yr
Arctic	-0.00	0.00	0.00	-0.37	35	177	1899 - 2005	111
NW Atlantic	-0.01	0.00	0.00	-0.62	48	295	1911 - 2010	781
NE Atlantic	0.01	0.00	0.00	0.84	45	183	1890 - 2010	730
E Atlantic	-0.00	0.00	0.00	-0.29	65	384	1911 - 2008	190
S Atlantic	-0.00	0.00	0.02	-0.31	43	299	1911 - 2003	60
N Indian	-0.00	0.00	0.02	-0.19	59	196	1895 - 1997	84
S Indian	0.00	0.00	0.00	0.58	76	760	1900 - 2006	131
N Pacific	-0.00	0.00	0.00	-0.04	52	478	1907 - 2009	2842
E Pacific	-0.00	0.00	0.00	-0.18	78	964	1907 - 2008	475
S Pacific	0.01	0.00	0.00	0.78	69	565	1956 - 2005	53
Southern	-0.01	0.00	0.00	-0.61	40	336	1900 - 2006	89

Note: Estimate, SE, and P-value are the instantaneous linear rate of Chl change (mg m^{-3} yr^{-1}), standard errors, and P-values for the rates of change. % per Year is the Chl change per year, reported as a proportion of the initial value, Deviance is the proportion of deviance explained by the individual models, Area is the maximum polygon area encompassed by the available data (km^2 x 10^4) and N/Year is the average number of measurements available in each year.

Atlantic (+100%), South Indian (61.9%) and South Pacific (38.4%) regions. These rates of change may be exaggerated for regions where data availability is low such as the Southern Ocean. In such instances, rates of change could be inflated due to the influence of measurements taken in more recent, data-rich decades.

4.4.3 Global Trends

When aggregated globally, both local and regional scale estimates of change were approximately Gaussian distributed (Figure 4.4A).Using statistical weighting methods to account for differences in the uncertainty and spatial coverage of estimates, we observed globally declining Chl trajectories. Synthesis of local estimates revealed a statistically significant global Chl decline of -0.0066±0.001 mg m^{-3} yr^{-1} (random-effects weighted mean and 95% confidence interval). This finding was insensitive to the use, or method, of weighting (Figure 4.4B). Synthesis of available regional estimates suggested that the global rate of change was smaller and not statistically significant (-0.0009±0.0027 mg m^{-3} yr^{-1}). The global rate of change derived from regional estimates was sensitive to the splitting of the North Atlantic region; when analyzing the North Atlantic as a whole, the global rate was greater and statistically significant (-0.0029±0.0025 mg m^{-3} yr^{-1}).

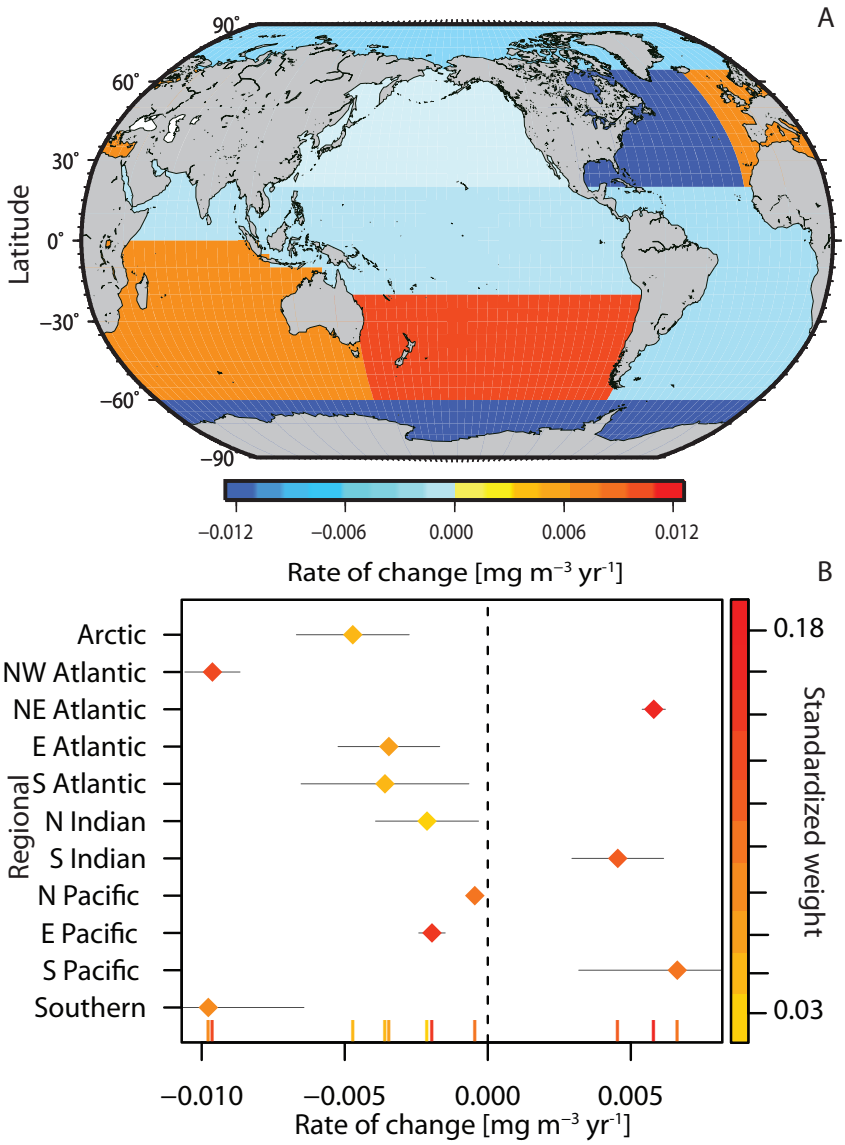

Figure 4.3: Regional-scale phytoplankton trends.
(A) Estimated instantaneous linear rate of Chl change in each of 11 ocean regions. Colors indicate rate of change; yellow and red are increasing regions, blue are declining regions. Trends for each region are plotted at 5° resolution (B) Chl changes estimated for each region (points), with 95% confidence intervals (gray lines). Individual estimates are displayed as tick marks on the x-axis. Colors depict the standardized statistical weight used in the derivation of the global average for each region. Dashed line represents no change.

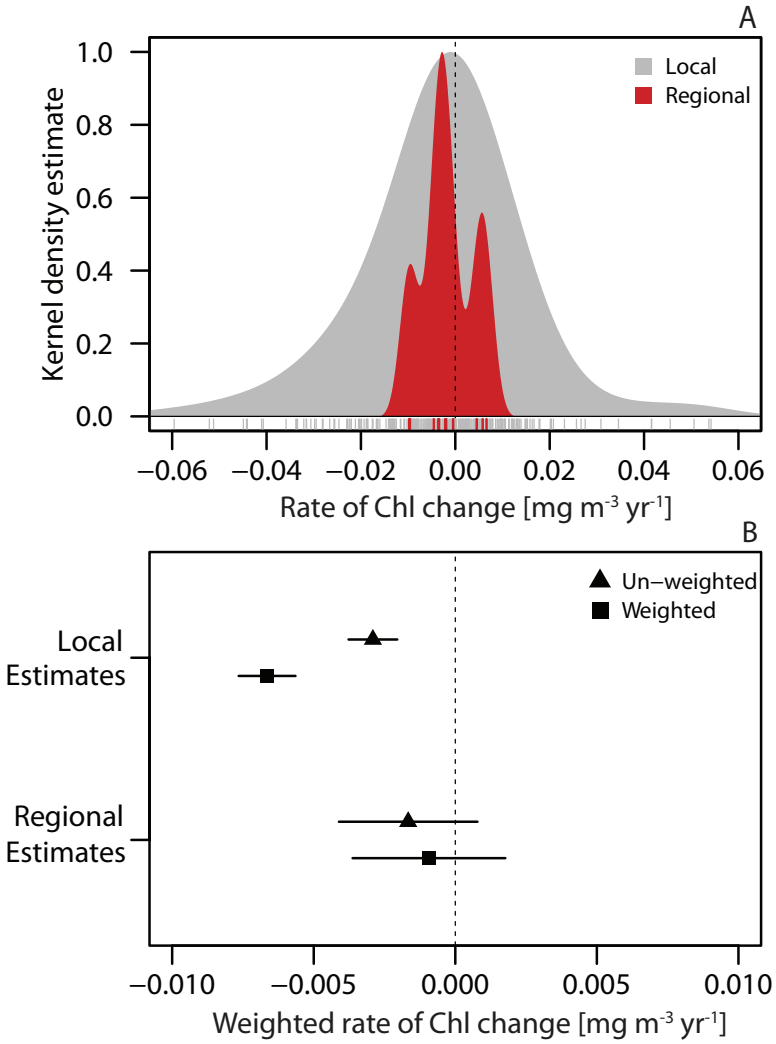

Figure 4.4: Average global phytoplankton change.
(A) Shaded areas represent the standardized kernel density distribution of individual local (gray) and regional (red) scale estimates of Chl change. Tick marks on the x-axis are the values of the individual estimates of change. Dashed line represents no change. (B) Global rates of Chl change estimated using local and regional scale estimates. Global rates of change were calculated as un-weighted (triangle points) and weighted (square points); random-effects were assumed. Horizontal lines are the 95% confidence limits around the mean rates; dashed line represents no change.

4.4.4 Sensitivity and Robustness Analyses

Analyses of all available 10° x 10° degree cells suggested that as the length of the available Chl time series decreases, the estimates of change become larger and more uncertain (Figure 4.5A). This supports the contention that Chl trends estimated over shorter timescales are strongly influenced by decadal-scale climate oscillations and may not necessarily represent long-term trends (Henson et al., 2010; Martinez et al., 2009). However, since sample size also co-varies with trend length, it is possible that the larger magnitude and uncertainty of estimates may be driven by data density, not just total time span. The estimated rates and patterns of Chl change at local scales were broadly insensitive to model specification, or the spatial resolution chosen (changes within 5° x 5° cells were also estimated). The proportion of declining cells and average global rate of Chl change were largely unchanged.

To determine the sensitivity of our analysis to model averaging, the estimates of Chl change over time from best models ($\beta_{year,B}$) were compared against those derived from multi-model averaging ($\overline{\beta}_{year,MM}$); (Figure 4.5B). In almost all instances, $\overline{\beta}_{year,MM}$ and $\beta_{year,B}$ were identical in direction, but differed slightly in magnitude. The $\overline{\beta}_{year,MM}$ estimates were generally smaller than $\beta_{year,B}$ estimates and the differences between them tended to increase with decreasing sample size (Figure 4.5C). However, since differences between $\overline{\beta}_{year,MM}$ and $\beta_{year,B}$ were small and because the statistical theory underlying single model selection is more robust, $\beta_{year,B}$ was used as the metric of Chl change. The overall results were insensitive to the use of $\overline{\beta}_{year,MM}$ or $\beta_{year,B}$.

Several analyses were performed to determine the sensitivity of the estimated trends to the blending of Chl measurements collected from different sampling platforms. It has been suggested that since the transparency- and *in situ*-derived Chl values are available over different time periods, any systematic difference between them could bias the overall rate of change over time (Mackas, 2011; Rykaczewski and Dunne, 2011). We conducted several analyses to explore this possible bias. Firstly, if temporal sampling differences were biasing the Chl trends, the magnitude of the bias should scale proportionally to the magnitude of the trends. To quantitatively test this, we examined the linear scaling of space- and time-matched Chl_T and Chl_I values on log-log scales in conjunction with the trend estimated from the integrated

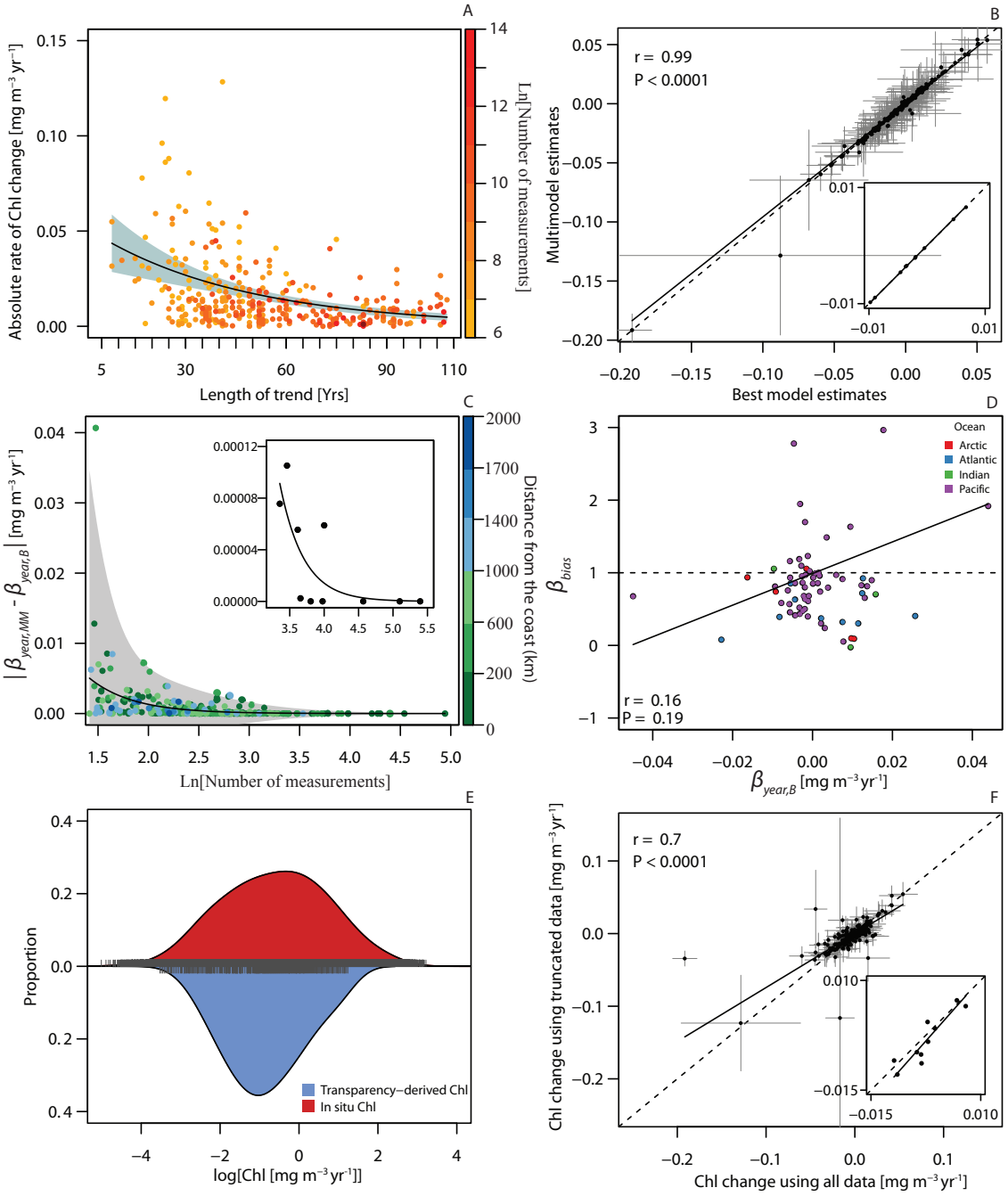
A
Absolute rate of Chl change [mg m⁻³ yr⁻¹]
Length of trend [Yrs]
Ln[Number of measurements]
B
r = 0.99
P < 0.0001
Multimodel estimates
Best model estimates
C
|β year,MM - β year,B| [mg m⁻³ yr⁻¹]
Ln[Number of measurements]
Distance from the coast (km)
D
Ocean
Arctic
Atlantic
Indian
Pacific
r = 0.16
P = 0.19
β bias
β year,B [mg m⁻³ yr⁻¹]
E
Proportion
Transparency−derived Chl
In situ Chl
log[Chl [mg m⁻³ yr⁻¹]]
F
r = 0.7
P < 0.0001
Chl change using truncated data [mg m⁻³ yr⁻¹]
Chl change using all data [mg m⁻³ yr⁻¹]

data ($\beta_{year,B}$) for each individual 10° x 10° cell. The linear scaling parameter was estimated as the model II major axis log-log regression slope of Chl_T against Chl_I (β_{bias}), whereby parameter values greater than 1 indicate Chl_T>Chl_I (Equation 4.8). If declining Chl trends were the result of a bias resulting from the blending of different data sources, β_{bias} should be negatively related to $\beta_{year,B}$. There was no indication that a systematic bias was present (r^2=0.01, P=0.19), suggesting that the estimated Chl trends ($\beta_{year,B}$) are not an artifact of the blending of Chl_T and Chl_I (Figure 4.5D).

Whereas the Chl_I measurements in the integrated database contain intrinsic measurement error, the Chl_T values are calibrated using a deterministic process and thus contain only an indirect form of measurement error. Consequently the means of Chl_T and Chl_I are identical, but their variances may not be (Figure 4.5E). Analyses were

---

Figure 4.5 ***(preceding page)*****:** (A) The absolute estimated rate of Chl change for each 10° x 10° degree cell is plotted as a function of trend length. Colors represent the number of measurements in each cell. The relationship was best approximated by a generalized linear model ($\mu_i \sim Gamma$ and $\eta(\mu_i) \sim ln(\mu_i)$; solid line); Shaded area depicts the confidence limits. (B) Rates of Chl change estimated by multi-model averaging plotted against best-model estimates for each 10° x 10° degree cell. Gray lines are the 95% confidence intervals for the estimates; dashed line represents idealized relationship (slope=1, intercept=0). Solid line is the model II regression fit (r=0.99; P<0.0001). Inset displays the same relationship for regional estimates. (C) Difference between multi-model averaged and best model rates of Chl change as a function of log sample size for each 10° x 10° degree cell. The relationship was approximated by a generalized linear model ($\mu_i \sim Poisson$ and $\eta(\mu_i) \sim ln(\mu_i)$; solid line); shaded area depicts the 95% confidence interval. Colours represent the distance of the cell to the nearest coastline. Inset displays the same relationship for regional estimates. (D) Estimated rates of change from all data plotted as a function of the average difference (model II major axis linear regression slope; equation 9) between Chl data types for each 10° x 10° cell. Fitted line represents the relationship estimated from a model II linear regression. Colour depicts the ocean where trends were estimated. (E) Probability distribution of log-transformed Chl_I (red) and Chl_T (blue) measurements estimated as a kernel density function. Area under each curve sums to 1. Tick marks represent the exact Chl values. (F) Rates of Chl change estimated using truncated data as a function of changes estimated from all available data for each 10° x 10° cell. Gray lines are the 95% confidence intervals for the estimates; solid line represents slope from a model II regression fitted to the data (r=0.7; p<0.0001). Dashed line represents idealized relationship (slope=1, intercept=0). Inset is the same relationship for regional estimates.

performed to determine the possible effect of this uneven variance on the estimated Chl trends. Trends were estimated using only Chl measurements that were within the extreme tails of the Chl_T distribution. This truncation simulation effectively standardized the variances of Chl_I and Chl_T. By comparing trends estimated from the truncated data against those estimated using all data, the sensitivity of the trends to the potentially uneven variances of Chl_T and Chl_I may be assessed. This analysis suggested that the trends were insensitive to the larger variance of Chl_I measurements (Figure 4.5F). The changes estimated from the truncated database indicated a slightly greater proportion of declining 10° cells and greater rates of Chl decline.

4.5 Discussion and Conclusions

This analysis presents comprehensive empirical evidence for a global decline in average Chl, particularly over the second half of the 20^{th} century. Importantly, this work builds upon previous estimates of long-term phytoplankton change (Boyce et al., 2010) and addresses all critical comments which were published in response (Boyce et al., 2011; Mackas, 2011; McQuatters-Gollop et al., 2011; Rykaczewski and Dunne, 2011). We have increased the robustness of this analysis in several ways including:

1. Using a larger Chl database with more stringent data quality control methods and direct Chl calibration methods (full details in: Boyce et al., 2012).

2. Implementing a range of new analyses to ascertain the sensitivity of the estimated trends to any possible biases (Mackas, 2011; Rykaczewski and Dunne, 2011).

3. Using multi-model analyses to eliminate the reliance on a single model of Chl change, and enabling for more complex Chl dynamics to be tested.

4. Restricting our analysis to Chl time-series that span at least 35 years, to minimize any confounding with cyclical climate variability (Beaulieu et al., 2013; Henson et al., 2010).

Following these improvements, the trajectories of Chl change reported here are similar, but not identical, to those estimated previously (Boyce et al., 2010). Statistically significant chlorophyll declines were observed in 60.1%±0.076 of 10° cells

examined, and over 62% of the global ocean surface area where trend analysis was possible. While Chl has declined globally, Chl trends were spatially heterogeneous. Large concentrations of declining cells were observed across the mid- to high-latitude Atlantic oceans, the western Pacific and the eastern tropical Pacific Oceans (Figure 4.1A). Patches of increasing cells were found in the North Pacific Ocean, northeast Atlantic Ocean, and Mediterranean Sea (Figure 4.1A). The greatest rates of Chl change were observed in the Southern Hemisphere (<50° S), and where the trend time span was shorter, likely as a function of limited data availability.

Weighted linear regression analysis suggested that the rate of Chl change became increasingly negative with increasing distance from land masses, ($p<0.01$). This suggests that Chl in the open oceans has been declining more rapidly than in shelf areas. This finding is in agreement with results derived from satellite data available over more recent time periods (1997 to 2010), documenting declining phytoplankton in the open oceans (Gregg et al., 2005; Vantrepotte and Melin, 2009; Ware and Thomson, 2005) and expansion of the oligotrophic gyres (Polovina et al., 2008). These declining trends have been generally related to ocean warming, intensifying vertical stratification and reduced vertical mixing (Behrenfeld et al., 2006; Boyce et al., 2010; McClain et al., 2004; Polovina et al., 2008), although they are largely unexplored over pre-satellite eras. Stable or increasing trends in shelf areas, could be, at least in part, due to the effects of anthropogenic eutrophication (Jickells, 1998; Nixon, 1995; Peierls et al., 1991), which may counteract the effects of increasing stratification on nutrient supply rates.

Regional estimates of change were in general agreement with local estimates, with the largest declines observed in the Atlantic (excluding the Northeast Atlantic) and polar regions (Figure 4.2 Figure 4.3). Due to the large spatial scale of these estimates, and because the minimum trend length of our analysis is 35 years, it is challenging to compare our results to independently published estimates, almost all of which are estimated at finer spatial scales (Reid, 1975; Reid et al., 1998; Saba et al., 2010; Venrick et al., 1987), or over shorter time intervals (Antoine et al., 2005; Behrenfeld et al., 2006; Goes et al., 2005; Gregg et al., 2005; Montes-Hugo et al., 2009). Despite this, some general patterns seem to emerge.

Local and regional declines in the North Pacific were broadly supported by independent long-term estimates derived from ocean transparency (Falkowski and Wilson, 1992) or colour (Wernand and Woerd, 2010). Our estimated rate of decline for the North Pacific region (-0.0005; mg m^{-3} yr^{-1}) is similar but smaller than that estimated over a shorter time interval (-0.002 mg m^{-3} yr^{-1}; 1900 to 1981) by Falkowski and Wilson (1992).

Long-term local and regional Chl changes in the North Atlantic are in agreement as well with estimated changes in the plankton colour index (PCI) from the North Sea and Northeast Atlantic using the continuous plankton recorder (CPR) survey (Raitsos et al., 2005; Reid, 1975; Reid et al., 1998), but at odds with PCI estimates from the Central Northeast Atlantic ($\pm 52^\circ$ to $\pm 58^\circ$ N and $\pm 10^\circ$ to $\pm 20^\circ$ E). Indeed, both our analysis and the plankton color index data suggest that phytoplankton changes across the North Atlantic are spatially heterogeneous, and that estimating a single aggregate trend for the entire region may be inappropriate. Our regional analysis supports this hypothesis, and suggests that different dynamics may explain phytoplankton variability in the eastern and western portions of the North Atlantic region (Figure 4.2). However, a Chl decline in the Northwest Atlantic is indirectly supported by the observed rapid expansion of the oligotrophic gyre there (McClain et al., 2004; Polovina et al., 2008).

Globally, the direction of long term secular trends described here is consistent with ocean general-circulation model (OGCM) projections of future changes in Chl over similar time horizons. Although there is substantial variability among OGCM projections, 15 of 18 published estimates report declining marine Chl or primary production into the future (median time interval: 100 yr; time interval range: 10 to 2000 yr); (Beaulieu et al., 2013; Bopp et al., 2001; Boyd and Doney, 2002; Cermeno et al., 2008; Cox et al., 2000; Henson et al., 2010; Hofmann et al., 2011; Olonscheck et al., 2013; Steinacher et al., 2010; Taucher and Oschlies, 2011). These models do not account for biological interactions, which may modify the Chl time trends (O'Connor et al., 2009; Olonscheck et al., 2013; Taucher and Oschlies, 2011).

We conclude that upper ocean chlorophyll concentrations have declined over the past century but that the absolute magnitude of this change remains uncertain (global averages from local and regional models were both negative, but varied by a factor

of 7). The rates of change we report are also heterogeneous in space and time and are overlaid by multi- decadal variability. Our analysis suggests that the direction of upper ocean Chl change is robust (*i.e.* consistently declining, on average), but the magnitude of changes is sensitive to the scale at which data are aggregated. A major source of this uncertainty stems from the limited availability of Chl measurements in many regions and years. This uncertainty and the fundamental importance of marine phytoplankton should provide a powerful incentive to increase global observational capabilities in order to more accurately resolve long-term phytoplankton change.

4.6 Acknowledgements

We are very grateful to all data providers, to J. Mills-Flemming for statistical advice. Funding was provided by the Natural Sciences and Engineering Research Council of Canada.

Chapter 5

Oceanographic Drivers of Chlorophyll Change over the Past Century

5.1 Abstract

There is mounting evidence that marine phytoplankton concentrations have been changing globally over the past century, yet it is unclear what factors may be driving these trends. Examination of contemporary satellite-derived ocean color data have yielded insight into the factors that may be responsible for changes in phytoplankton concentrations over shorter time periods (1978–1986 and 1997–2010), but analyses over longer time scales are constrained by a lack of global time series. In this study, we use the longest time series of chlorophyll measurements (a proxy for phytoplankton concentration) currently in existence to address this issue. We analyze these data along with time series of climate variability to determine the influence of eight oceanographic variables on temporal chlorophyll change from 1890 to 2010. Statistical time series models based on generalized linear and additive models were used to estimate changes in oceanographic variables and chlorophyll over time, and to test for statistical relationships between them. This was based on 10° x 10° grid cells containing sufficient data. Consistently strong correspondence was observed between temporal changes in sea surface temperature (SST), vertical stratification, and wind stress, with vertical stratification strongly influenced by the countervailing effects of SST and wind. Overall, SST was the strongest single correlate of chlorophyll changes. Increasing trends in SST and corresponding declines in chlorophyll were observed in 59% of cells, and SST was the strongest univariate driver of chlorophyll change in 26% of cells. Rising SSTs were found to be negatively related to chlorophyll over most of the ocean, except at high latitudes (>60°), where the effects were positive. We also observed a negative relationship between salinity on chlorophyll in coastal regions,

In review as: Boyce, D.G., M. Dowd, M. Lewis, and B. Worm. 2012. Oceanographic drivers of global chlorophyll changes over the past century. Progress in Oceanography.

likely due to river-borne nutrient inputs. The negative effect of rising temperature on chlorophyll remained consistent after accounting for the effects of seasonal cycles, spatial gradients, time trends, and climate oscillations. Our study provides new insight into the effects of long-term and large-scale physical oceanographic change on phytoplankton concentrations, and is consistent with the theory of ocean warming reducing the average concentration of global phytoplankton, particularly at lower latitudes.

5.2 Introduction

Macroecological changes in marine phytoplankton concentrations may influence climate patterns (Charlson et al., 1987; Murtugudde et al., 2002), elemental cycling (Falkowski, 1998), ecosystem structure (Ryther, 1969; Ware and Thomson, 2005), and fishery harvests (Chassot et al., 2010). Recently, the increased availability of publicly available databases coupled with advances in statistical and computing capacity has enabled improved assessment of the magnitude and nature of phytoplankton change through space and time. Published analyses suggest that marine phytoplankton concentration is changing at regional and global scales, but the factors and mechanisms driving these changes remain poorly explored and understood (Behrenfeld, 2011; Boyce et al., 2013, 2010; Falkowski, 2012; Henson et al., 2010).

Long-term changes in marine phytoplankton abundance may be influenced by a range of factors including changes in stratification (Behrenfeld et al., 2006; Polovina et al., 2008), temperature (Boyce et al., 2010; O'Connor et al., 2009; Sommer and Lengfellner, 2008), wind (Goes et al., 2005; Gregg and Conkright, 2002; Gregg et al., 2003), ocean mixing (McGillicuddy et al., 2007; Oschlies and Garcon, 1998), atmospheric nutrient deposition (Behrenfeld et al., 1996; Jickells, 1998), light availability (Montes-Hugo et al., 2009), ice concentration (Arrigo et al., 2012; Jacobs et al., 2002), grazing pressure (Frank et al., 2005; Roman and McCarthy, 2010), and climate variability (Boyce et al., 2010; Henson et al., 2010; Martinez et al., 2009). The strength and importance of these factors as drivers of phytoplankton time trends have generally been explored using short time series (<10 years), or empirical experiments (O'Connor et al., 2009; Sommer and Lengfellner, 2008). For instance, the relationship between increasing sea surface temperatures, enhanced stratification, and phytoplankton has been variously explored in observational time series ranging

from 5 to 12 years in length (Behrenfeld et al., 2006; Irwin and Finkel, 2009; Lozier et al., 2011; McClain et al., 2004; Polovina et al., 2008), but only rarely over longer time series (Boyce et al., 2010).

Analysis of time trends and drivers over these short intervals may be misleading, since phytoplankton variability is strongly determined by transient climate fluctuations (Behrenfeld et al., 2006; Martinez et al., 2009), which overly and may obscure any secular changes (Boyce et al., 2010). Thus, it is important to use longer time series in order to minimize the influence of inter-annual to multi-decadal climate fluctuations on phytoplankton dynamics. Resolving how marine phytoplankton responds to changing oceanographic conditions independent of transient climate variability is an important component to understanding and managing change in marine ecosystems.

In this study, we estimate global changes in eight physical oceanographic variables and chlorophyll over the available observational record (1890-2010), and explore the extent to which changes in physical variables may drive observed chlorophyll changes. Further, we explore the effects of these oceanographic variables on chlorophyll in relation to spatial, seasonal, inter-annual, and climate variability. Time trends in oceanographic variables were estimated using linear and generalized linear models, and trends in marine phytoplankton were estimated using multi-model ensemble inference applied to a new publicly available database of chlorophyll measurements collected from 1890 to 2010. All measurements used in this analysis were extracted from publicly available sources (Table 5.1).

5.3 Methods

5.3.1 Data

Chlorophyll data

Measurements of chlorophyll concentration (Chl, mg m^{-3}) were used as an indicator for phytoplankton concentration. Chl is the most practical and extensively used proxy to assess changes in phytoplankton at large spatial and temporal scales (Antoine et al., 2005; Behrenfeld et al., 2006; Gregg and Conkright, 2002; Gregg et al., 2005; Henson et al., 2010; Huot et al., 2007; Montes-Hugo et al., 2009; Raitsos et al., 2005;

Table 5.1: Published phytoplankton time series and associated metadata.

Variable	Symbol	Units	Spatial	Source
Chlorophyll	Chl	mg $m^{-}3$	-	www.aslo.org/lomethods/free/2012/0840.html
Sea surface temperature	SST	°C	0.25°	www.atmos.umd.edu/~ocean
Salinity	S	PSU	0.25°	www.atmos.umd.edu/~ocean
Stratification anomaly	-		0.25°	www.atmos.umd.edu/~ocean
Kinetic energy	KE	cm^2 s^2	0.25°	www.atmos.umd.edu/~ocean
Ice cover	-	%	1°	www.hadobs.metoffice.com
Temperature gradients	SSTg	°C $km^{-}1$	0.25°	www.atmos.umd.edu/~ocean
Cloud cover	-		2°	www.atmos.umd.edu/~ocean
Surface wind stress	WS	N m^2	0.25°	www.atmos.umd.edu/~ocean
Bathymetry	-	m	-	www.gebco.net
Coastline distance	-	km	-	www.ngdc.noaa.gov/mgg/shorelines.html
El Nino Southern Oscillation	ENSO		-	www.esrl.noaa.gov/psd/data/climateindices/list
North Atlantic Oscillation	NAO		-	www.cru.uea.ac.uk/cru/data/nao.htm
Indian Ocean Dipole	IOD		-	www.climexp.knmi.nl/selectindex.cgi
Pacific Decadal Oscillation	PDO		-	www.jisao.washington.edu/pdo
Arctic Oscillation	AO		-	www.atmos.colostate.edu/ao/Data/ao_index.html

Reid et al., 1998). In this study, we use a new and publicly-available database of integrated Chl values collected via shipboard sampling platforms from 1890 to 2010 (Boyce et al., 2012).

The database is only briefly described here; full details of the data sources, temporal and geographic distributions, quality control and inter-calibration are given in Boyce et al. (2012). It consists of measurements of ocean transparency (derived from Secchi-depth measurements; Z_D) and color (derived from the Forel-Ule color-matching scale; FU), which were both calibrated against a large and comprehensive database of intensively quality-controlled *in situ* Chl measurements derived from spectrophotometric or fluorometric analyses of seawater. All near-shore measurements (<20 m water depth or <1 km from the nearest coastline) were removed from the database on the assumption that these waters would likely contain significant concentrations of other optically active constituents that confound the optical detection of phytoplankton Chl. This database has been expanded and improved over a previous version (used by Boyce et al., 2010). These improvements are fully described in Boyce et al. (2012), and include the following changes:

1. The number of individual measurements and the temporal and spatial coverage of the database have increased considerably, despite the use of more stringent quality control methods.

2. Transparency values in the database were calibrated directly against a large number of quality-controlled *in situ* Chl measurements (n=12,841); this is a large increase over the number of matchups used to calibrate globally distributed remotely sensed water-leaving radiance values from the Coastal Zone Color Scanner (CZCS; n=60) or the Sea-viewing Wide Field-of-view Sensor (SeaWiFS; n=2, 853); (Evans and Gordon, 1994; O'Reilly et al., 2000), and ensures that our calibration equations accurately represent *in situ* Chl concentrations.

3. A range of new statistical methods (*i.e.* spatial filters) were developed to identify outlying or implausible Chl measurements in the database, and to remove or correct them. A range of Chl depth interpolation methods were also explored to verify the assumption that the mean Chl over 20 m was the appropriate metric.

4. Measurements in the database were subjected to a number of additional post-calibration analyses testing quality, precision, and robustness. This included testing the accuracy of the measurements against widely used remote sensing estimates of Chl. These analyses indicated that the Chl values in this database are strongly correlated with Chl from SeaWiFS (r=0.81; ranged major axis slope=1) on log-log scales. The larger number of matchups and strong correspondence with remote sensing measurements attest to the improved quality of the integrated Chl database (see Boyce et al., 2012) for further details).

Previously undertaken sensitivity analyses (Boyce et al., 2013) suggested that Chl time trends estimated from Forel-Ule ocean color measurements were inconsistent with those derived from transparency-derived or *in situ* Chl measurements. Changes in Forel-Ule ocean color determinations are insensitive to small changes in Chl observed in oligotrophic (blue) waters (FU<2) where the optical properties of pure water dominate, or in mesotrophic (green or brown) waters where other particles and dissolved substances are significant (FU>10). The validity of these values could not be confirmed, and to avoid any potential bias, we removed all FU-derived Chl values prior to the analyses in this study. The resulting database used here contains 451,383 calibrated Chl values, is globally distributed, and spans over a century (1890 to 2010).

Physical oceanographic data

We examined the influence of eight variables that have been hypothesized to affect long-term Chl trends: sea surface temperature (SST; °C; 1890-2010), wind stress (N m^2; 1890–2010), vertical stratification (dimensionless; 1890-2010), eddy kinetic energy (KE; m^2 s^{-2}; 1890-2010), ice cover (%; 1890-2010), cloud cover (dimensionless; 1890-2010), surface salinity (dimensionless (psu); 1890–2010), and spatial temperature gradients, (SST_G; °C km^{-1};1890–2010); (Oschlies and Garcon, 1998), which indicate frontal zones and warm- or cold-core eddies.

All physical oceanographic data were extracted from publicly available databases (Table 5.1). Ice cover measurements were obtained from the MET Hadley Centre[1], and were generated using a two-stage reduced space optimal interpolation analysis

[1] www.metoffice.gov.uk/climate-change/resources/hadley

applied to digitized sea ice charts, passive microwave retrievals, and *in situ* measurements (Rayner et al., 2003). Cloud cover data were generated from the International Comprehensive Ocean-Atmosphere Data Set (ICOADS version 2.5)[2]. Cloud cover measurements are generated using a combination of ship observations, ocean buoys, and other automated sampling platforms (Woodruff et al., 2011). Contrary to the other oceanographic data used in this study, cloud cover measurements are not predicted or interpolated fields, but are rather gridded averages. Ice and cloud measurements were extracted on 1° x 1° and 2° x 2° global grids, respectively.

All remaining variables were extracted or calculated from the Simple Ocean Data Assimilation model (SODA; Version 2.2.4)[3], which uses available hydrographic profile data, ocean station data, moored temperature and salinity time series, surface temperature and salinity observations, and nighttime infrared satellite SST data (Carton and Giese, 2008). SODA variables were obtained at a near-global (75° S to 90° N latitude) resolution as 0.5° x 0.5° monthly and yearly values.

The vertical stratification anomaly was calculated from SODA profiles of salinity and temperature as the difference between seawater density at the surface (depth of 6 m) and at a depth of 200 m (Behrenfeld et al., 2006). Interpolation was used to obtain exact density values at 6 m and 200 m. Total kinetic energy (KE) values were calculated as

$$KE_{c,m,y} = \frac{1}{2}\left({U_{i,c,m,y}}^2 + {V_{i,c,m,y}}^2\right), \tag{5.1}$$

where $U_{i,c,m,y}$ and $V_{i,c,m,y}$ are the ith zonal and meridional geostrophic velocities for cell c, month m, and year y, respectively (m s^{-1}); (Patterson, 1985).

SST_G was derived from the maximum rate of SST change between one grid cell and the eight surrounding cells using the average maximum method (Burrough, P. A., and McDonell, 1998). Average wind stress fields were calculated from the average monthly zonal and meridional downward wind stress components (N m^2).

All physical variables were interpolated over time using spline-based methods appropriate for high-frequency variations (Akima, 1978). This was performed to obtain daily values for each cell (0.25° for SODA, 1° for ice, and 2° for cloud) and year. This method is analogous to a piecewise function comprised of a series of polynomials and

[2]www.icoads.noaa.gov/
[3]www.atmos.umd.edu/ ocean/

is commonly used to interpolate irregularly spaced bivariate data (Akima, 1978). Following this, physical variables were merged with the Chl database by location (0.25° for SODA, 1° for ice, and 2° for cloud) and time (year and day).

Climate data

We extracted time series of several leading climate indices which have been hypothesized or observed to be related to phytoplankton concentrations over inter-annual, decadal, or multi-decadal timescales (Boyce et al., 2010; Martinez et al., 2009); (Table 5.1). Since we are interested in the influence of climate on long-term phytoplankton change, we used only series which were available over time periods >100 years. In the Pacific Ocean we extracted climate indices corresponding to the El Niño Southern Oscillation (ENSO), and the Pacific Decadal Oscillation (PDO). For the Atlantic Ocean we extracted the North Atlantic Oscillation (NAO) Index. For the Indian Ocean we extracted the Indian Ocean Dipole (IOD) Index and for the Arctic Ocean we extracted the Arctic Oscillation (AO) Index.

The ENSO index represents reconstructed SST anomalies across the eastern central Pacific Ocean. The IOD is the normalized anomalous SST gradient between the Western Equatorial Indian (50°E to70°E and 10°S to10°N) and the South Eastern Equatorial Indian oceans (90°E to 110°E and 10°S to 0°N); (Saji et al., 1999). The NAO represents the first principal component from a rotated principal components analysis applied to monthly standardized pressure anomalies across the North Atlantic (20° to 90°N); (Barnston and Livezey, 1987). The PDO is derived as the leading principal component of monthly SST anomalies across the North Pacific Ocean (>20°N). The AO represents sea level pressure anomalies across the Arctic and North Atlantic oceans (>20°N). Over the available record, all climate series are stationary through time. Following extraction, all series were standardized by normalizing to the maximum amplitude (range: -1 to 1) and were then merged to the database containing the Chl and physical measurements by location (ocean region of relevance) and time (year and month). For instance, since the PDO has effects centered on the North Pacific Ocean, the PDO time series was merged to physical and Chl measurements in the North Pacific region only.

5.3.2 Analysis

Effect of physical oceanographic variables on long-term phytoplankton trends

To examine the potential influence of physical oceanographic variables as drivers of long-term phytoplankton change, we examined the correspondence between estimated time trends in the physical variables and those of Chl at the same locations (10° x 10° cell) and over the same time intervals. It has been suggested that a continuous Chl time series spanning at least 27 (Beaulieu et al., 2013) to 40 years (Henson et al., 2010) is necessary to separate long-term trends from shorter-term climate-driven fluctuations. Since we are interested in the effect of oceanographic drivers on long-term Chl changes, we restricted our analysis to cells where the temporal range of oceanographic driver and Chl trends spanned at least 35 years.

Estimating term trends in physical oceanographic variables

We estimated long-term changes in physical variables over the entire available time period (1890 to 2010), and over the time period spanned by the Chl measurements in each 5° x 5° and 10° x 10° cell, respectively. In both instances, changes in physical oceanographic variables over time were estimated by the statistical model

$$\eta\left(\mu_i\right) = \ \beta_0 + \beta_1 year_i + \ \beta_2 month_i, \tag{5.2}$$

where $_i$are the individual observations, β_1 is the rate of response change as a function of time, β_2 is the rate of response change as a function of the month, and β_0 is the model intercept. η is the monotonic link function of the expected mean response, μ_i. Because the physical variables possess different statistical properties, we employed different statistical models to account for these differences (Table C.1). For instance, since ice cover measurements are proportions, we estimated time trends using generalized linear models (GLMs) with a binomial response distribution. For all variables, we attempted to use the simplest available model, and confirmed that all model assumptions were verified using residual diagnostic tests. Changes in physical drivers were estimated as continuous linear and discrete (year-by-year) functions of time.

Estimating chlorophyll trends

Changes in Chl through time were estimated using generalized additive models (GAMs) within a multi-model inference framework (Burnham and Anderson, 2002). Because this method has been described in detail previously (Boyce 2013), we briefly describe only the salient aspects of the method here. The general form of the GAMs used to estimate Chl changes in each 10° x 10° cell was

$$\eta(\mu_i) = \beta_0 + \beta_{year} year_i + \beta_1 x_{1,i} + f_1(x_{2,i}) + f_2(x_{3,i} x_{4,i}), \tag{5.3}$$

where i are the individual observations, η is the monotonic link function of the expected mean Chl concentration, μ_i, $year_i$, x_1, x_2, x_3, and x_4 are the model covariates, β_0 is the model intercept, and β are parametric and f are functional effects estimated from the data. The functional effects are continuous, smooth curves which can more closely follow the response over increasing values of the covariate, and thus accommodate a wide array of response functions ranging from linear to multi-modal (Wood and Bretherton, 2006; Wood, 2004, 2003). The predictors ($x's$) in the above example may be spatial (*i.e.* longitude, latitude, bathymetry) or temporal (*i.e.* day of the year, decade) variables that are believed to explain some Chl variability. All ensemble models contained β_{year}, which is a parametric effect capturing the average long-term rate of Chl change. For all models we assumed a gamma-distributed error structure ($\mu_i \sim Gamma$) and a log link ($\eta(\mu_i) \sim ln(\eta_i)$).

Using this method, we were able to estimate the average rate of Chl change over time while accounting for underlying aspects of Chl variability. Further, because the influence of the model covariates on the mean response is through the logarithmic link function such that $\eta(\beta_{year}) = e^{\beta_{year}}$, the estimated rate of Chl change over time was back-calculated to be on a linear response scale (mg m^{-3} yr^{-1}). All model assumptions, including spatial and temporal dependence, were verified by analysis of the model residuals. More details can be found in (Boyce et al., 2013); the theory and technical aspects of GAMs are described in, for example (Hastie and Tibshirani, 1986; Walsh and Kleiber, 2001), while details and examples on their implementation in an oceanographic context may found in, for example (Bigelow et al., 1999; Irwin and Finkel, 2009; Polovina et al., 2008).

The effects of physical drivers on temporal phytoplankton change

The influence of physical drivers on chlorophyll may occur at different temporal and spatial scales, and could be related to spatial gradients, seasonal cycles, interannual climate variability, or any processes responsible for long-term trends. Separating the influence of physical drivers on Chl into these different scales of variability is a challenging but necessary step in understanding their effect on long-term Chl change. It is worth noting that strong relationships between drivers and Chl may arise from, for instance, the spatial coherence between them, rather than from a causal relationship. While such approaches are common (Chassot et al., 2010, 2007; Ware and Thomson, 2005), they can potentially result in misinterpreting patterns of spatial coherence as cause-and-effect relationships. Likewise, recent studies have highlighted the importance of correctly accounting for patterns of seasonality (Lozier et al., 2011) or climate variability (Henson et al., 2010; Martinez et al., 2009) to avoid misinterpreting the effects of physical drivers on phytoplankton.

We explored the effect of oceanographic variables on Chl before and after accounting for different sources of variability. This was accomplished by generating four different analogues of the physical and Chl databases: (*1*) raw data with no variability accounted for, (*2*) spatial and seasonal variability accounted for, (*3*) spatial, seasonal, and inter-annual trends accounted for, and (*4*) spatial, seasonal, and inter-annual trends, and transient climate variability accounted for. This was accomplished by fitting statistical models to physical and Chl measurements in each 10° x 10° degree cell, and extracting the model residuals. Following this procedure, the model residuals are independent of the model covariates. This approach enables us to attribute the relationships between oceanographic variables and Chl to spatial, seasonal, long-term, or climate effects. For instance, this method allows us to better quantify the effects of stratification on phytoplankton through seasonal (Lozier et al., 2011), long-term (Boyce et al., 2010), and climate variability (Behrenfeld et al., 2006) stratification effects.

To generate the database with spatial and seasonal variability accounted for (database 2, described above), models containing a seasonal and spatial effect were

fitted to measurements in each 10° x 10° cell as

$$\mu_i = \beta_0 + \beta_2 month_i + f_1(Longitude_i, Latitude_i), \tag{5.4}$$

where $_i$ are the individual observations, μ_i is the predicted response, β_2 is the rate of response change as a function of the month, $f_1\left(Longitude_i, Latitude_i\right)$ is a functional effect corresponding to the rate of response change as a function of location, and β_0 is the model intercept. The residuals from the model are interpreted as spatially independent and de-seasonalized analogues of the response variable. We confirmed that this method was accounting for the seasonal cycle by plotting the model residuals against the month of data collection and verifying that no patterns were apparent. The spatial independence was also verified by calculating the spatial correlogram of the model residuals. This approach is useful because it enables the subsequent examination of the correspondence between physical variables and phytoplankton while accounting for different sources of variability.

Expanding on this, we de-trended the physical or Chl time series (database 3, described above), by adding $\beta_3 year_i$ to equation 4, where β_3 corresponds to the rate of response change over time. The rescaled residuals from the model are spatially independent, de-seasonalized, and de-trended analogues of the response variable. Lastly, the effects of leading climate oscillators on physical and Chl time series was accounted for (case 4, above), by including $\beta_3 year_i$, and $\beta_4 climate_i$ to equation 4, where β_4 represents the change in the response as a function of the leading climate oscillator. The rescaled residuals from the model are independent of spatial, seasonal, long-term, temporal, and oscillatory climate variability.

Following this procedure, we examined the relationship between the physical variables and Chl with and without different sources of variability accounted for both globally and at finer spatial scales. To quantify the nature and strength of the relationships between the physical variables and Chl spatially, we estimated simple ordinary least squares (OLS) linear univariate statistical models within each 10° x 10° cell as:

$$ln(Chl)_i = \beta_0 + \beta_1 Driver_i, \tag{5.5}$$

where $_i$are the individual observations, $ln(Chl)_i$ is the ln-Chl concentration, β_0

is the model intercept, and β_1 is the rate of response change as a function of the physical driver in question. This model was estimated within each cell, for each physical variable, and for each analogue of the database. Using this approach we quantified the direction, significance, and magnitude of the oceanographic effects on Chl (β_1), as well as the proportion of variance explained by them (R^2), both with, and without different sources of variability accounted for. Normalizing transformations were applied to physical covariates as required. All linear model assumptions were verified for each individual model by visual examination of the model residuals.

Although linear relationships between physical variables and Chl are frequently assumed, alternate functional forms may be present. To explore this possibility, we estimated Chl as a non-monotonic function of each physical driver within each 10° x 10° cell using GAMs as

$$\eta\left(\mu_i\right) = \beta_0 + f_1 driver, \tag{5.6}$$

where $_i$ are the individual observations, η is the monotonic link function of the expected mean Chl concentration μ_i, f_1 is the function determining the non-monotonic change in Chl as a function of the driver, and β_0 is the model intercept. Because the physical variables possess different statistical properties, we employed different statistical models to estimate changes over time (Table C.1). For all variables, we attempted to use the simplest available model, and confirmed that all model assumptions and residual diagnostic tests were verified. Changes through time were estimated as continuous and discrete functions of time.

5.4 Results

5.4.1 Changes in Physical Variables over Time

Estimated changes in physical oceanographic drivers over the past century (1890 to 2010) revealed coherent spatial patterns of change among several variables. SST increased over the majority of the ocean, particularly in the Atlantic and North Indian oceans, and closer to coastlines in all oceans (Figure 5.1). These spatial patterns of SST change appeared to broadly correspond to changes in stratification and wind stress. Increases in SST tended to coincide with increasing stratification over most of the ocean, and increases in wind stress appeared to have had a countervailing

Table 5.2: Summary of linear model estimation of the factors influencing phytoplankton time trend variability.

Variable	Mean	Mean SE	% Cells increasing	Upper 95% CI	Lower 95% CI
SST	0.004	0.007	72.0	74.0	70.0
EKE	0.004	0.007	72.0	74.0	70.0
MLD	0.002	0.004	66.0	68.0	64.0
Stratification	-0.000	0.001	30.0	33.0	28.0
Wind	0.001	0.002	72.0	74.0	70.0
Salinity	0.003	0.004	86.0	88.0	84.0
Cloud	0.006	0.007	87.0	89.0	85.0
SSTG	0.000	0.000	59.0	61.0	56.0
Ice	-0.005	0.014	19.0	22.0	16.0

effect (Figure 5.1). Spatial gradients in SST, here used as a proxy for thermal fronts, were estimated to have increased over most of the global ocean, with the largest increases observed in the open ocean gyres, and in the Southern Ocean (40° S to 70° S). Estimated changes in KE revealed increasing eddy kinetic energy over most of the ocean, particularly in the mid-latitudes (∼20° to 40° N and S latitude). KE has declined over large areas of the low-latitude ocean, especially in the Western Central Pacific. Cloud cover is estimated to have increased over most of the ocean, except for the Southern Ocean, where patches of decreasing cloud cover were observed. Ice cover mostly declined across polar oceans, with some increase in parts of the Southern Ocean. Salinity was estimated to have increased over most of the ocean with the largest increases observed in the open ocean gyres of the Pacific Ocean. Global average rates of change calculated from individual 5° x 5° cell estimates suggested that SST, wind stress, salinity, SST_G, and cloud cover have increased since 1890, while stratification and ice cover have decreased, on average (Table 5.2; see discussion for explanation).

5.4.2 Effect of Oceanographic Drivers on Long-term Phytoplankton Changes

Estimated corresponding long-term changes in physical oceanographic variables and Chl within each 10° x 10° cell over identical time intervals yielded insight into the influence of oceanographic variables on long-term Chl change. Increasing long-term trends in SST, KE, and cloud cover and declining trends in Chl were observed in

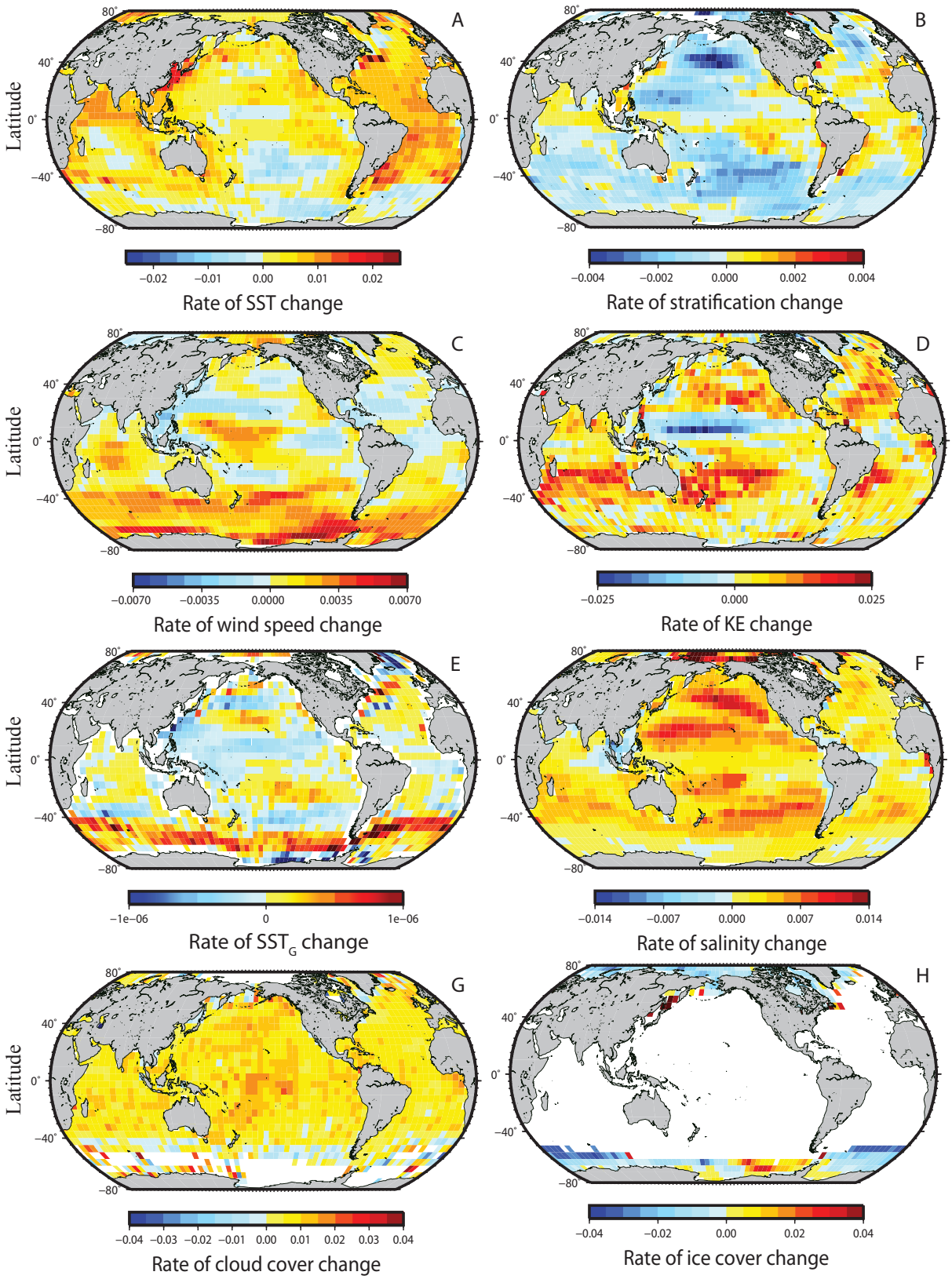
A
Latitude
80°
40°
0°
−40°
−80
−0.02 −0.01 0.00 0.01 0.02
Rate of SST change
B
80°
40°
0°
−40°
−80
−0.004 −0.002 0.000 0.002 0.004
Rate of stratification change
C
Latitude
80°
40°
0°
−40°
−80
−0.0070 −0.0035 0.0000 0.0035 0.0070
Rate of wind speed change
D
80°
40°
0°
−40°
−80
−0.025 0.000 0.025
Rate of KE change
E
Latitude
80°
40°
0°
−40°
−80
−1e−06 0 1e−06
Rate of SST$_G$ change
F
80°
40°
0°
−40°
−80
−0.014 −0.007 0.000 0.007 0.014
Rate of salinity change
G
Latitude
80°
40°
0°
−40°
−80
−0.04 −0.03 −0.02 −0.01 0.00 0.01 0.02 0.03 0.04
Rate of cloud cover change
H
80°
40°
0°
−40°
−80
−0.04 −0.02 0.00 0.02 0.04
Rate of ice cover change

58.2%, 50.9%, and 63.9% of 10° x 10° cells, respectively, where sufficient data permitted analysis (Figure 5.2). Long-term changes in stratification and wind did not appear to be correlated to changing Chl. Many of the cells where SST has increased and Chl has declined were located in low- and mid-latitude and coastal waters, and cells where SST has increased and Chl has increased were located at high latitudes and nearshore waters. The majority of the cells where cloud cover has increased and Chl has declined appeared to be located in waters far from coasts. Model II ranged major axis (RMA) regression analyses revealed negative relationships between estimated changes in SST, stratification, and ice cover and changes in Chl, and positive relationships between changes in wind stress and Chl, as well as ice cover and Chl (Figure 5.2).

5.4.3 Effect of Physical Drivers on Phytoplankton

Examination of all available data suggested that SST, KE, and salinity are negatively related to Chl, while SST_G and Chl were positively related (Figure 5.3A). The relationship between stratification and Chl was negative over most of the stratification range, but became positive as stratification levels increased (Figure 5.3A). Using this exploratory approach, the strongest relationship was found between SST and Chl, and was best approximated by a functional (*i.e.* non-linear) trend line. The nature of most relationships was similar after accounting for seasonal, inter-annual, or climate variability, except for wind and ice cover, which became more positive after seasonal effects were accounted for (Figure C.1).

Relationships between physical variables and Chl aggregated globally represent the net effect of specific regional relationships occurring throughout the global ocean (Figure C.2). To better understand such regional relationships, Chl estimated as a univariate log-linear function of each driver separately within each 10° x 10° cell

Figure 5.1 *(preceding page)*: (A) Estimated linear rate of Chl change in each 5° x 5° cell estimated for (A) SST, (B) stratification anomaly, (C) wind stress, (D) KE, (E) SST_G, (F) salinity, (G) cloud cover, and (H) ice cover. All trends are estimated from 1890 to 2010; model details are presented in Table C.1. Colors indicate the average rate of change over the available time series. White cells indicate cells with insufficient data.

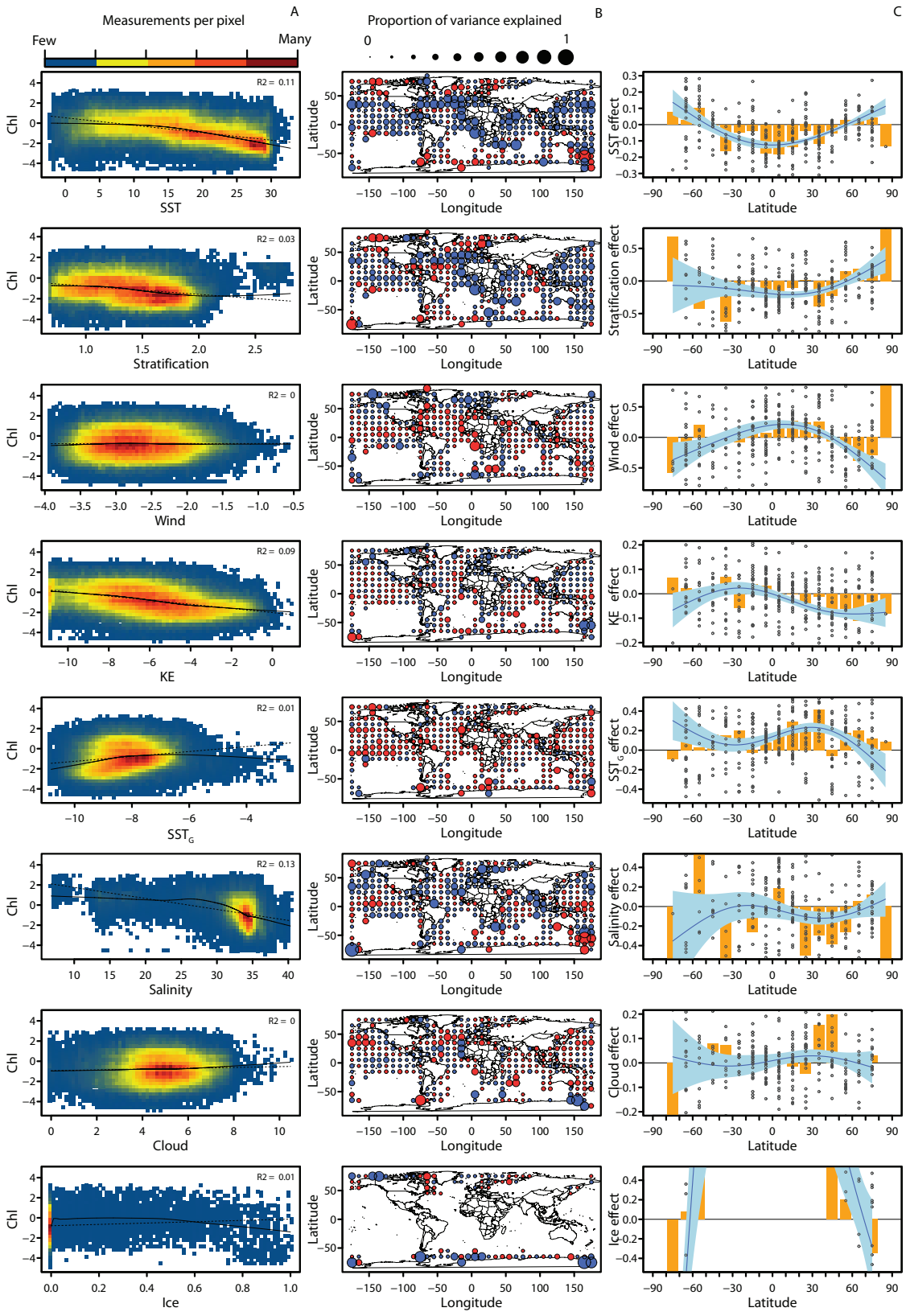
A
Measurements per pixel
Few
Many
B
Proportion of variance explained
0
1
C
Chl
SST
R2 = 0.11
Latitude
Longitude
SST effect
Stratification
R2 = 0.03
Stratification effect
Wind
R2 = 0
Wind effect
KE
R2 = 0.09
KE effect
SST$_G$
R2 = 0.01
SST$_G$ effect
Salinity
R2 = 0.13
Salinity effect
Cloud
R2 = 0
Cloud effect
Ice
R2 = 0.01
Ice effect

provided information regarding the spatial variability of the relationships observed globally. Using this approach SST, stratification, and salinity were observed to have negative impacts on, and to explain, a large proportion of the variability in Chl across large areas of the oceans (Figure 5.3B). Wind also explained a large proportion of Chl variability in many locations, and ice was a strong predictor of Chl at high latitudes (>70° N and S). The observed spatial pattern in the effect of SST, stratification, and wind on Chl was also apparent in this study; in waters where SST and stratification effects were negative, wind effects tended to be negative. These relationships were also manifest along a global latitudinal gradient, such that negative SST and stratification effects, but positive wind effects on Chl were observed at mid- and low-latitude waters (∼40° S to ∼40° N), and smaller but opposite effects were observed at high latitudes (Figure 5.3C). Latitudinal gradients were not observed for the remaining variables.

Estimating Chl as a univariate linear function of each driver (n=8) in each individual 10° x 10° cell suggests that SST is the strongest single predictor of Chl concentration globally (Figure 5.4). Prior to accounting for any sources of variability in the drivers or Chl, SST explained the greatest proportion of the variability in Chl in 25.5% of 10° x 10° cells where adequate data permitted analysis (n=337); (Figure 5.4C). Salinity, stratification, and wind were also strong drivers of Chl, and explained the largest proportion of the variability in Chl in 18%, 11.6 %, and 10.7 % of cells examined, respectively. Although ice cover was not a strong source of influence globally, it was an important determinant of Chl concentration at high latitudes. After

---

Figure 5.2 *(preceding page)*: (A) Spatial patterns of estimated long-term changes in physical oceanographic variables and Chl over the available record in each 10° x 10° cell. Yellow indicates cells where both the oceanographic variable and Chl have declined through time, red where they both have increased, green where the oceanographic variable has declined as Chl has increased, and blue where the variable has increased and Chl has declined. White cells indicate cells with insufficient data. (B) The proportions of cells where long-term changes in oceanographic variables and Chl have been synchronous or non-synchronous are illustrated using the same color representation as in A). The horizontal lines denote the 95% Wilson confidence intervals. (C) Estimated long-term changes in oceanographic variables (x-axes) are plotted against changes in Chk. Model II linear regression and spline regression lines are plotted. For A, B, and C, only statistically significant long-term trends spanning at least 35 years are used.

accounting for the effects of spatial, seasonal, inter-annual, and climate variability in both the drivers and Chl, SST remained the strongest single driver of Chl in 20.1% of cells examined (n=334). Again, wind, stratification, and salinity also emerged as strong univariate predictors of Chl, and were the strongest predictor in 12.6%, 12%, and12 % of cells examined, respectively. After removing sources of variability SST_G also emerged as a strong explanatory variable, and was the strongest driver in 9.7% of cells. Accounting for spatial, seasonal, temporal, or climate variability did not greatly influence the proportional representation of the drivers (Figure 5.4C), but the spatial locations where the various effects were dominant did change. SST effects were also statistically significant in the majority of the cells where data permitted analysis, prior to accounting for seasonal effects (Figure 5.4D). Although salinity and ice cover were strong drivers in many cells (Figure 5.4C), they were only statistically significant explanatory variables in ∼40% of cells prior to accounting for seasonal effects. Alternately, while SST_G was a weak influence, it was statistically significant in ∼60% of cells prior to accounting for seasonal effects (Figure 5.4D). The proportion of variance explained by the strongest drivers was also generally reduced after accounting for different sources of variability (Figure C.6). These findings were insensitive to the model used or to the specification of Chl as a linear or non-monotonic function of the physical variable. Prior to accounting for seasonal effects, Chl was found to vary as a non-monotonic function of several oceanographic drivers; however, accounting for seasonal influences resulted in linear relationships.

5.5 Discussion and Conclusions

Our results suggest that globally averaged values of SST, wind, salinity, cloud cover, and SST_G have increased from 1890 to 2010, while stratification and ice cover have declined (Figure 5.1 and Table 5.2). The observed long-term warming trend is consistent with previous estimates over similar timescales (Boyce et al., 2010; Levitus, 2000). Estimated increased wind stress and reduced stratification globally are consistent with past estimates of wind and mixed layer depth (MLD) over similar timescales (1958 to 2009 and 1955 to 2009, respectively). It is perhaps surprising, given the findings of recent studies (Behrenfeld et al., 2006; Martinez et al., 2009; Polovina et al., 2008), that when averaged globally, vertical stratification has declined as SST has

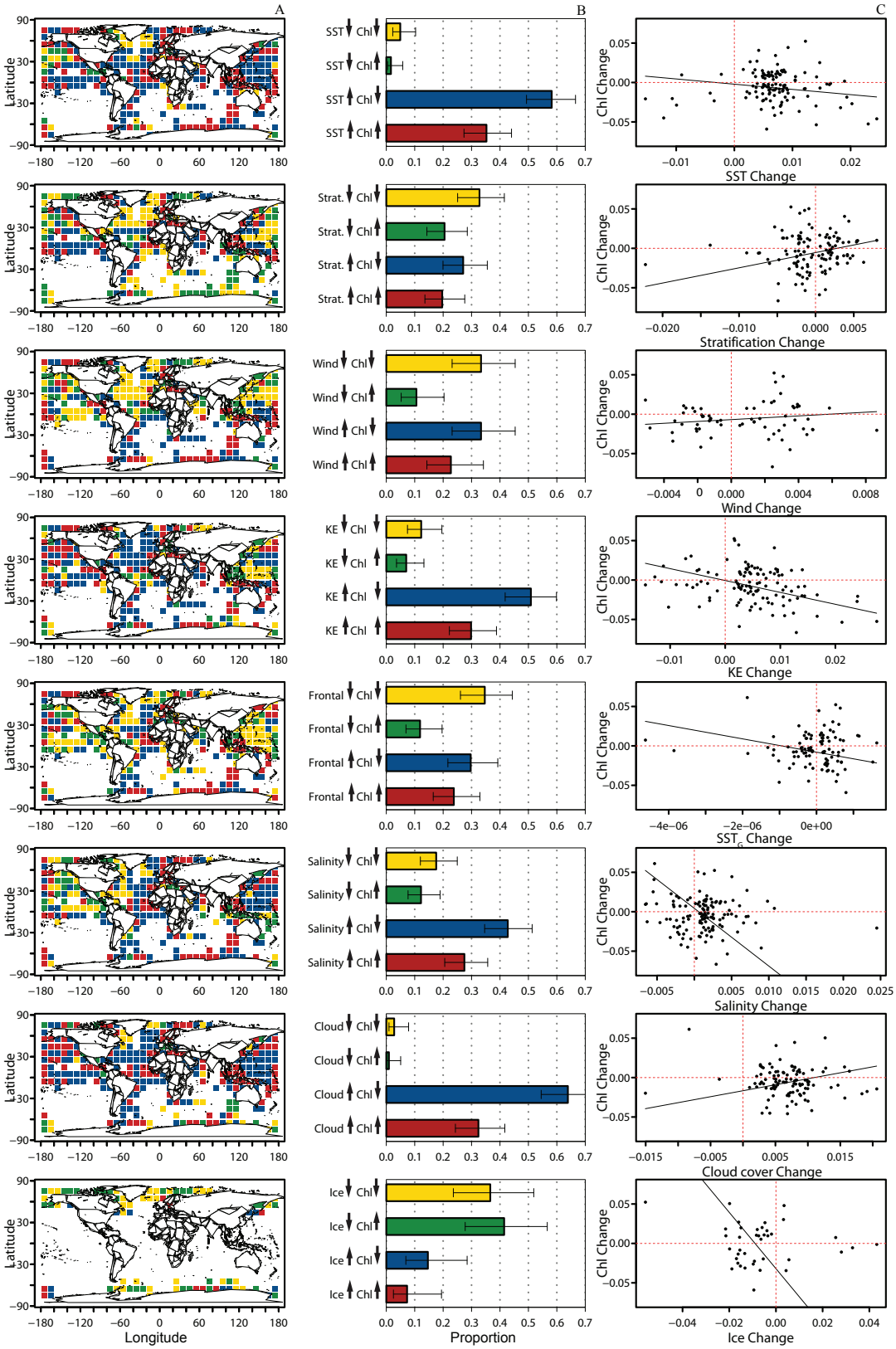
A
B
C
Latitude
Longitude
Proportion
Chl Change
SST Change
Stratification Change
Wind Change
KE Change
SST$_G$ Change
Salinity Change
Cloud cover Change
Ice Change
SST ↓ Chl
SST ↓ Chl
SST ↑ Chl
SST ↑ Chl
Strat. ↓ Chl
Strat. ↓ Chl
Strat. ↑ Chl
Strat. ↑ Chl
Wind ↓ Chl
Wind ↓ Chl
Wind ↑ Chl
Wind ↑ Chl
KE ↓ Chl
KE ↓ Chl
KE ↑ Chl
KE ↑ Chl
Frontal ↓ Chl
Frontal ↓ Chl
Frontal ↑ Chl
Frontal ↑ Chl
Salinity ↓ Chl
Salinity ↓ Chl
Salinity ↑ Chl
Salinity ↑ Chl
Cloud ↓ Chl
Cloud ↓ Chl
Cloud ↑ Chl
Cloud ↑ Chl
Ice ↓ Chl
Ice ↓ Chl
Ice ↑ Chl
Ice ↑ Chl

increased over the past century. However, much of the reduction in global vertical stratification is driven by large changes occurring at high latitudes, especially in the Southern Hemisphere (<50° S), where wind stress has also increased. It appears that the effects of increasing SST on stratification are outweighed by corresponding increases in wind stress over large regions of the ocean, particularly at high latitudes. This theory is consistent with analyses of long-term (Boyce et al., 2010) and contemporary (Montes-Hugo et al., 2009) time series, showing consistently increasing winds in the Southern Ocean, and reduced stratification. The observed global increases in cloud cover were similar to previous estimates covering the time period from 1948 to 2002, except at low latitudes (<20° N and S), where estimates of cloud cover are uncertain (Bedacht et al., 2007). The estimated global long-term declines in ice cover observed here are consistent with independent estimates (Post et al., 2013), some of which suggest that sea ice declines have been exceeding model projections (Stroeve et al., 2012), and may be accelerating (Perovich and Richter-Menge, 2009).

Within these average global trends, relationships between the location-specific rates of long-term change for several oceanographic variables were observed. Globally, rates of long-term SST change were negatively related to changes in wind stress (r=-0.43), and ice cover (r=-0.14), and positively related to stratification changes (r=0.35). Generally, the strong relationships between changes in SST, stratification,

Figure 5.3 *(preceding page)*: (A) All available space- and time-matched oceanographic variables (x-axes), are plotted against Chl (y-axes). Colors depict the number of observations per pixel. Dashed lines show the linear trend, and the dashed lines show the non-linear (spline) trend fitted to the data. Variables have been transformed to approximate the normal distribution where necessary. (B) Spatial distribution in the univariate effects of oceanographic variables on Chl. blue denotes negative effects of the driver on Chl and red denotes positive effects. The size of each circle depicts the proportion of variance explained by the oceanographic variable (range: 0 to 1). White areas contain insufficient data from analysis. (C) Latitudinal gradient in the univariate effects of the oceanographic variables on Chl estimated on a 10° x 10° grid. Points are the estimated effect of the variable on Chl within each 10° x 10° cell. The shaded bars are the median effect values for each 10° latitude bin. Trend lines are GAM estimates of the effects as weighted smooth functions of latitude; weightings are the inverse of the individual estimate standard errors. Blue shaded regions are the 95% confidence intervals for the trend lines.

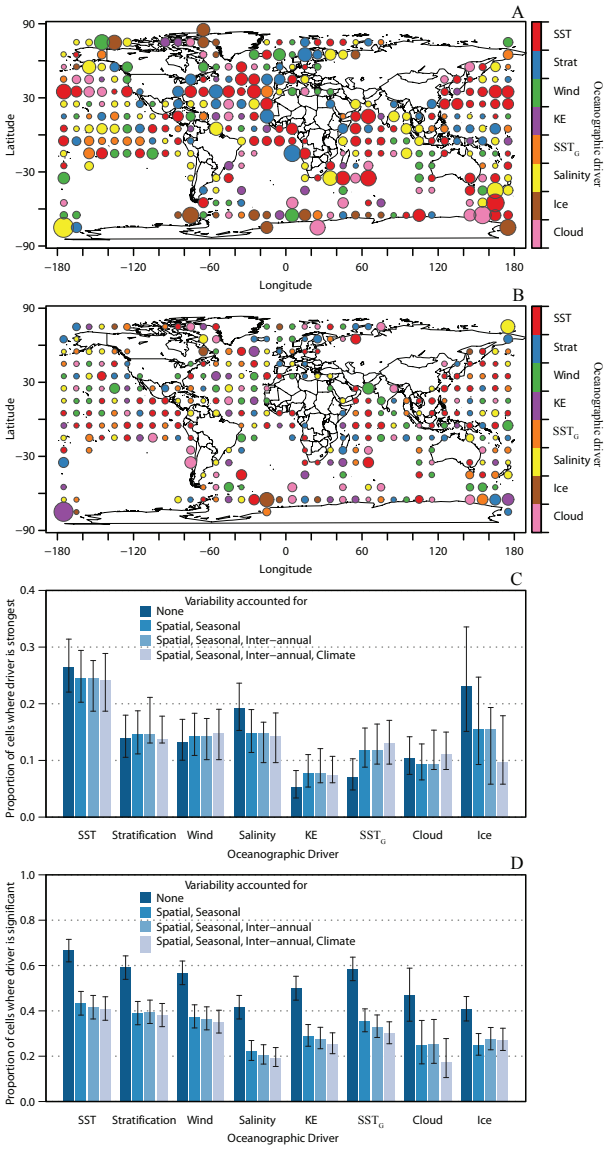

Figure 5.4: Strongest univariate drivers of chlorophyll.
(A and B) The oceanographic variables explaining the largest proportion of Chl variability within each 10° x 10° cell are plotted spatially. Colors depict the oceanographic driver and the size of each circle depicts the proportion of Chl variance explained by that oceanographic variable. This procedure was undertaken (A) using the raw data, and (B) after accounting for spatial, seasonal, inter-annual, and climate variability. (C and D) Shaded bars depict the proportion of 10° x 10° cells where (C) each oceanographic variable was the strongest single predictor of Chl, and (D) the effect of each oceanographic variable on Chl was statistically significant ($P<0.05$). For C and D, only the cells where analysis was possible were used. Colors depict the variability accounted for prior to the analysis, where dark blue is the raw data, and light blue is the data after accounting for spatial, seasonal, inter-annual, and climate variability. Vertical lines represent the 95% Wilson score confidence intervals for the proportions.

and wind suggest increasing SST and wind stress have countervailing effects on vertical stratification. Further analysis suggested that the positive correlation between SST and stratification was greater at low- and mid-latitudes (∼40° N and S). The relationship between estimated changes in stratification and surface salinity were also strongly related (r=-0.72).

Of the oceanographic variables examined, SST, stratification, and wind consistently explained a large fraction of Chl variability (Figures 5.2 to 5.4), both before and after accounting for spatial, seasonal, inter-annual, or climate variability (Figure C.1). The strong spatial and/or latitudinal gradients in the effects of SST, stratification, and wind observed here have also been observed previously, and have been linked to large-scale temporal changes in Chl in the North Pacific Ocean (Venrick et al., 1987), and globally (Behrenfeld et al., 2006; Boyce et al., 2010; Martinez et al., 2009; Polovina et al., 2008). These effects are believed to be a function of the countervailing effects of SST and wind on vertical stratification and mixing. Over most of the ocean, rising SST generally leads to enhanced stratification and reduced nutrient flux from deeper waters to phytoplankton in the euphotic zone, negatively affecting their growth. These effects may be less important in nearshore waters where land-based nutrients tend to dominate (Jickells, 1998; Peierls et al., 1991), or at high latitudes, where waters are generally well-mixed. Increased wind at higher latitudes may negatively influence phytoplankton by transporting them below their critical depth (Sverdrup, 1953). Substantial evidence for this SST-induced mechanism has emerged from analyses of the recent satellite record (Behrenfeld et al., 2006; McClain et al., 2004; Polovina et al., 2008) and from climate models (Boyd and Doney, 2002; Sarmiento et al., 2004). Given the limited timescales of observation for these studies, some of these relationships may reflect decadal climate variability (Beaulieu et al., 2013; Henson et al., 2010) rather than reflecting sustained long-term trends. Indeed, observed SST-induced expansions of the major oligotrophic gyres since 1997 (McClain et al., 2004; Polovina et al., 2008) were not observed over multi-decadal time scales (Antoine et al., 2005). Another analysis of observational data from the North Atlantic subtropical gyre also found that stratification was strongly linked to primary production at seasonal timescales, but only weakly on a year-to-year basis (Lozier et al., 2011). Such findings emphasize the need for long-term time series and

the use of appropriate analysis methods to more accurately account for the influence of seasonal and climate variability.

Our findings also suggest that rising SSTs negatively affect Chl via stratification through seasonal and climate forcing, but more weakly through long-term forcing. If SST and wind are influencing Chl indirectly by modifying vertical stratification, it would be expected that stratification would be the strongest correlate of Chl. Although stratification is a strong influence, SST consistently explains the largest proportion of Chl variability. Further, while long-term SST increases and Chl declines were observed in 58.2% of 10x10 cells, similar changes were not observed for changes in stratification or wind (Figure 5.2). This suggests that although there is a negative effect of increasing SST on Chl via increasing vertical stratification, other mechanisms may also be important. For example, theory and experimentation have shown that rising SST also speeds up heterotrophic metabolic processes faster than autotrophic ones, thus altering ecosystem dynamics (Klauschies et al., 2012). It is still uncertain if this will benefit marine phytoplankton by increasing nutrient recycling (Taucher and Oschlies, 2011), or negatively affect them by increasing grazing pressure (O'Connor et al., 2009).

Surface salinity also emerged as a strong correlate of Chl in many regions (Figure 5.4), and salinity effects were observed to co-vary with the effects of SST and stratification, likely because both SST and salinity determine the strength of vertical stratification. It is probable that part of the observed salinity effects are mediated by the stratification effects on Chl. For instance, surface water freshening can strengthen stratification and limit nutrient exchange (Ji et al., 2008). However, after accounting for any stratification effects on Chl, salinity continued to explain a large fraction of Chl variability (Figure C.6). Many of the locations where salinity effects were strong were located near major river outflows (Figure 5.4A), where salinity gradients are high and possibly co-vary with terrestrial nutrient inputs via river transport. This hypothesis is supported by the observed large negative effects of increasing salinity on Chl in regions close to major river outflows (Figure 5.3). In areas of river outflow, large river inputs would lower salinity, while providing terrestrial nutrient inputs, and hence increased Chl. After accounting for seasonal influences, the spatial pattern of these salinity effects appeared weaker, but persistent (Figure 5.4B).

At high latitudes, ice cover explained a large fraction of Chl variability through spatial, seasonal, and climate effects (Figure 5.4), but only weakly through long-term temporal forcing (Figure 5.2). Ice cover may influence phytoplankton through a range of pathways. Declining sea-ice exposes the ocean to the influence of wind, which in turn influences vertical stratification, nutrient supply, and light availability (Mitchell and Holm-Hansen, 1990; Montes-Hugo et al., 2009). However, melting sea-ice also freshens the upper ocean and has been linked with increased stratification, reduced nutrient availability and negative effects on phytoplankton (Lee et al., 2012). Ice-induced freshening of the upper oceans may also lead to reduced phytoplankton cell sizes, which would reduce the transfer efficiency to higher trophic levels (Li et al., 2009). Declining ice also reduces surface albedo which may lead to increased ocean warming, thus leading to further reductions in ice cover (positive feedback). Lastly, large phytoplankton concentrations have recently been observed beneath substantial ice cover (0.5 to 1.8 m thickness) in the Arctic Ocean (Arrigo et al., 2012). These under-ice phytoplankton blooms are likely widespread (Fortier et al., 2002; Mundy et al., 2009; Strass and Niithig, 1996), and strongly depend on the amount of light transmitted through the overlying ice. As such, the nature and thickness of overlying ice are likely important determinants of phytoplankton concentration in addition to ice cover (Arrigo et al., 2012).

We observed weak positive effects of increasing SST_G, a proxy for thermal fronts, on Chl across most of the ocean (Figure 5.4), and the effect of long-term SST_G change on Chl was equivocal (Figure 5.2). Previous work has suggested that ocean fronts may be associated with enhanced primary production, likely via entrainment or advection of nutrients and phytoplankton from adjacent, higher productivity waters (Hyrenbach et al., 2000; Polovina et al., 2001). Turtles and predatory fish also use fronts as migration routes (Polovina et al., 2001, 2000), and additional species may be attracted by elevated primary production and habitat heterogeneity (Etnoyer et al., 2004; Haney, 1986; Sund et al., 1981). It is possible that this elevated concentration of consumers regulates phytoplankton via grazing pressure. Further, some fronts, such as the transition zone chlorophyll front (TZCF), are associated with weak downwelling of phytoplankton to depths of over 50 m (Polovina et al., 2001), which is significantly below the maximum depth sampled by the chlorophyll database used here (20 m).

The observed relationships between most oceanographic variables and Chl became progressively weaker after accounting for different sources of variability (*i.e.* equation 4). Despite this, the overall relationships between the variables and Chl remained broadly consistent both at local scales and globally (Figure C.1). This suggests that the effects of changing oceanographic variables are not solely due to a single source of variability such as spatial gradients or seasonal cycle.

Most oceanographic variables used in this analysis were estimated from process-based models applied to empirical observations (Carton and Giese, 2008), and thus contain both measurement and model error. While the use of such analyses is common and necessary to provide more complete oceanographic databases, the error introduced in the estimation process may influence subsequent analyses. Further, while the process-based component of this method estimates oceanographic conditions for many dates and locations where empirical observations are lacking, the final oceanographic database remains incomplete. For example, stratification measurements were lacking for many times and locations where Chl measurements were available. Although we made efforts to account for these missing observations, it is still possible that missing physical measurements may influence the analyses.

Because long-term, large-scale time series of zooplankton, fish, or other organisms are scarce, in this study we focused on the effect of oceanographic variables in driving Chl change. However, numerous studies have found that 'top-down' effects can also be strong drivers of Chl (Frank et al., 2005). Consumers can influence phytoplankton both directly through grazing, or indirectly by modifying grazing pressure (Frank et al., 2005) or more subtly via ecosystem conditioning (Durham et al., 2009; Roman and McCarthy, 2010). Such top-down effects on phytoplankton are potentially important, but remain unexplored here.

The use of Chl as an indicator for phytoplankton biomass is long standing and widespread, yet the C-to-Chl relationship is non-linear and subject to the influences of light, nutrients, and temperature (Geider, 1987). Variation in the C:Chl ratio often occurs in the context of 'acclimation' to changing conditions, e.g. over a seasonal cycle. Although models to correct for acclimation exist, their applicability over long time scales is constrained by data availability. However, with all other factors held constant, increasing temperatures are expected to result in an overestimation

of phytoplankton C biomass (reduced C:Chl ratio); (Eppley and Sloan, 1965; Eppley, 1972). In practical terms this suggests that as temperatures increase, Chl may be biased upward relative to phytoplankton C due to the temperature effect on the C:Chl ratio. Thus, the negative relationships observed between SST and Chl likely did not arise from the influence of SST on the C:Chl relationship; this effect, however, depends on the constancy of other influential variables such as light and nutrients.

The effects of the oceanographic variables on phytoplankton may be more complex than the simple univariate linear models used here permit. For instance, there is evidence that the phytoplankton response to turbulence may also depend on wind strength and direction (McGillicuddy et al., 2007), and the response to ice cover may also depend on the type and thickness of ice (Arrigo et al., 2012). Additionally, since the response of phytoplankton to oceanographic change is generally rapid (Taylor et al., 2002), we did not explore any lagged relationships in our analysis. However, due to the potential for complex and interactive effects of oceanographic change on phytoplankton, it is possible that lagging effects may be present. Complex interactions between oceanographic drivers and lagged effects could not be fully explored in our analysis due to the very large number of models that would need to be fitted (364 10° cells x 9! full models per cell=1.3 x 10^7 models).

We conclude that SST is a predominant variable that explains a large proportion of the variability in chlorophyll concentrations across the global oceans. We observed consistent negative effects of SST on Chl via seasonal, inter-annual, and climate forcing. These negative effects were strongest at mid- and low-latitudes and tended to be weaker and slightly positive at higher latitudes. Over most of the ocean, increasing SSTs lead to increased vertical stratification, thus reducing deep mixing and the supply of nutrients to phytoplankton in near surface waters, negatively influencing them (Behrenfeld et al., 2006; Boyce et al., 2010; Martinez et al., 2009; Polovina et al., 2008). Our results support this mechanism, but the weak coupling between long-term stratification and Chl changes suggests that SST may be influencing long-term Chl trends through additional pathways. It is likely that rising ocean temperatures will also influence phytoplankton, and consumer growth rates. It is, however unclear if this effect will positively (Taucher and Oschlies, 2011) or negatively (O'Connor et al., 2009; Olonscheck et al., 2013) influence phytoplankton. It is also likely that

rising SSTs will reduce phytoplankton size structure (Li et al., 2009; Moran, 2010; Polovina and Woodworth, 2012) and alter phytoplankton seasonal cycles (Edwards, 2004), which may modify trophic structure and control. Lastly, rising SSTs may alter the distribution and abundance of consumers, leading to altered grazing pressure (Atkinson et al., 2004; Frank et al., 2005), and possible effects on phytoplankton via ecosystem conditioning (Durham et al., 2009; Roman and McCarthy, 2010; Smetacek, 2008). Our present analysis identifies rising sea surface temperatures as a strong correlate of observed phytoplankton declines over the past century, but does not resolve the multifarious pathways by which changing temperatures influence phytoplankton. Resolving the various responses of marine phytoplankton to ocean warming will be increasingly important, given that average sea surface temperatures are predicted to increase between 1 and 6° C by 2100 (I.P.C.C., 2007; Rosenzweig et al., 2008).

5.6 Acknowledgements

We are very grateful to all data providers. Funding was provided by the Natural Sciences and Engineering Research Council of Canada.

Chapter 6

Effects of Sea Surface Warming on Marine Plankton

6.1 Abstract

Global warming affects communities through many different pathways. Here, we implement results from global circulation models in a mesocosm experiment to determine the direct and indirect effects of ocean warming on marine phytoplankton. Our analysis reveals nutrients as a key factor controlling phytoplankton response to warming. In nutrient-limited ecosystems warming had positive direct effects on phytoplankton biomass, but these were overcompensated by the negative indirect effects via increasing nutrient limitation. In nutrient-replete ecosystems warming had negative effects on phytoplankton biomass via increased zooplankton grazing rates. We conclude that the negative effects of warming on nutrient availability and trophic interactions determine the overall response of phytoplankton biomass to sea surface warming, overriding direct positive effects. Effects on primary productivity were equivocal, however, likely due to more rapid turnover and nutrient recycling under warm conditions. Our results provide a mechanistic basis for improving predictive models and understanding global change in marine ecosystems.

6.2 Introduction

Marine phytoplankton contribute approximately half of the global primary production, form the basis of marine food webs, and strongly influence biogeochemical processes in the ocean (Field et al., 1998). Recently, there has been growing evidence that ocean warming is negatively affecting global phytoplankton biomass and productivity. Despite counter-examples showing increasing primary productivity in some regions (Chavez et al., 2011), observations, experiments and physical models suggest that at large scales, average phytoplankton biomass will decline as the oceans continue to

In review as: Lewandowska, A.M. Boyce, D.G. Hofmann,M. Matthiessen, B., Sommer,U., Worm, B. 2013. Effects of sea surface warming on marine plankton. Ecology Letters.

warm (Behrenfeld et al., 2006; Boyce et al., 2010; Henson et al., 2010; Steinacher et al., 2010; Sommer et al., 2012). At least two mechanisms drive this trend: a physically-mediated effect of upper-ocean warming on vertical mixing and nutrient supply, and a biologically mediated-effect on plankton metabolic rates.

The physically-mediated effect of temperature on phytoplankton is associated with enhanced vertical stratification, reduced mixed layer depth (MLD), and consequently reduced nutrient flux into the upper oceans (Behrenfeld et al., 2006; Doney, 2006; Boyce et al., 2010). This mechanism is believed to explain observed spatial expansion of the oligotrophic gyres of the ocean (Polovina et al., 2008), and reduced phytoplankton production in the Eastern Central Pacific during El Niño years (Behrenfeld2006). In a global model simulation progressive warming induced a shoaling of MLD, reduced vertical mixing, and weakening of deep-water circulation. This led to a projected 50% decline in average global chlorophyll *a* concentration from the year 2000-2200 (Hofmann et al., 2011).

The biologically-mediated effect of temperature on phytoplankton is driven by a growing imbalance between photosynthesis and respiration rates as temperature increases. Heterotrophic processes are more sensitive to temperature than autotrophic ones, leading to higher grazing rates by zooplankton and consequent reduction of phytoplankton biomass under warmer conditions (Sommer and Lengfellner, 2008; O'Connor et al., 2009). This mechanism may be partly offset by faster nutrient recycling by bacteria, which increases phytoplankton productivity (Taucher and Oschlies, 2011).

It is presently unclear how these two mechanisms interact, and what the cumulative effects on marine phytoplankton biomass and productivity will be. Here we combine global model simulations and mesocosm experiments to examine the strength and possible interactions between both physically-, and biologically-mediated effects of warming on a marine plankton community. Experimental treatments were established to mimic physical ocean conditions under continued global warming, as projected by a published ocean general circulation model (POTSMOM-C).

6.3 Methods

6.3.1 General Circulation Model

We employed a coarse-resolution ocean general circulation model (OGCM) which includes a state-of-the-art model of the ocean carbon cycle and marine ecosystem. While the former derives from an improved version of the Modular Ocean Model version 3.1 (Hofmann and Maqueda, 2006) the latter follows the parametrization of Six and Maier-Reimer (Six, 1996) utilizing a fixed elementary Redfield ratio between carbon, nitrogen, and phosphate. The model was extended to account for the effects of mineral ballast on the vertical export of organic matter (Hofmann et al., 2011). The horizontal resolution was 3.75° x 3.75° while the water column was sub-divided into 24 vertical layers, increasing in thickness with depth. Primary production was assumed to be constrained to the four uppermost layers with a uniform thickness of 25 m. In the steady state the model exports about 8.6 Pg of POC across the 100 m horizon into the deep ocean while an atmospheric CO_2 partial pressure of 282 atm is established.

The atmospheric forcing of the ocean is provided by the climatological NCEP/NCAR-reanalysis database (Kalnay, 1996). In order to consider the transient effects of anthropogenic global warming between years 1800 and 2100 in our simulations, we have utilized the atmospheric anomalies of surface temperature, precipitation and relative humidity from a former model run of the coupled Earth climate system model CLIMBER-3 (Kuhlbrodt et al., 2009), as forced by an IPCCs A1FI emissions scenario (Nakicenovic and Swart, 2000). The procedure is described in detail by Hofmann (Hofmann et al., 2011).

6.3.2 Experiment

We simultaneously filled twelve mesocosms (1500 l volume, 1 m depth) with sea water containing natural plankton communities from the Baltic Sea. Mesocosms were placed in temperature-controlled climate chambers. Mesozooplankton dominated by copepods were obtained from net catches (200 μm mesh) and added to each mesocosm in natural concentrations of 6 ind. l^{-1}. Computer-controlled light conditions mimicked daily and seasonal irradiance patterns calculated from astronomic equations

for above-cloud irradiance (Brock 1981), light reduction by clouds and attenuation coefficient typical for Baltic Sea waters. Six mesocosms were cooled by 3 °C and six were warmed by 3 °C above ambient sea temperatures to simulate a total 6 °C temperature gradient. Nitrate ($NaNO_3$), phosphate (KH_2PO_4) and silicate (Na_2O_3Si) were added every third day to simulate projected changes in nutrient flux. We ran the experiment over five weeks from 16 May to 18 June 2012 with six nutrient treatments: 100% (control, no nutrients added), 106%, 112%, 119%, 126%, and 134% of total nitrogen (TN).

Water temperature, pH, salinity and fluorescence were measured daily. Mesocosms were sampled three times per week for bacteria, phytoplankton, heterotrophic nanoflagellates (HNF), chlorophyll, TN, total phosphorous (TP), particulate organic carbon, nitrogen, and phosphorous (POC, PON, POP) and dissolved inorganic nutrients (NO_2^- and NO_3^-, NH_4^+, PO_4^{2-}, SiO_4^{2-}). Zooplankton, primary production and respiration were measured weekly. Bacteria and phytoplankton <5 μm cell size were counted using a flow cytometer (FACScalibur, Becton Dickinson), larger phytoplankton and microzooplankton were fixed with Lugol's iodine and counted after Utermohl (1958), using an inverted microscope. Biomass contribution of different phytoplankton and microzooplankton species were estimated from carbon content (Stoecker, 1989; Menden-Deuer and Lessard, 2000) after approximation of cell biovolumes to geometric standards (Hillebrand, 1999). Copepods were identified to genus level and counted with a binocular microscope. HNF were fixed with formaldehyde (2% final solution), stained by DAPI (1 μg l^{-1} final concentration) and counted using a fluorescence microscope. For estimation of primary production and community respiration rates, samples (100 ml) were incubated inside the mesocosms at mid depth (light bottles) or in closed containers inside the climate chambers (dark bottles) for 24 h. Subsequently, concentrations of dissolved oxygen were measured (Hansen, 1999).

6.3.3 Statistical Analyses

To quantitatively explore the linear relationships between temperature or nutrients and the plankton community a multivariate principal component analysis (PCA) was performed (Rao, 1964). The PCA analysis was estimated from the correlation matrix, so that the relative strength of effects could be better interpreted.

To test the effects of experimental treatments on individual variables (fluorescence, phytoplankton biomass etc.), we used generalized least squares (GLS) models with temperature and nutrients, as well as their interaction, as covariates. GLS models were selected in order to account for time dependence of the response variable within each mesocosm. Models were fit to the data according to

$$y = X\beta + \ \varepsilon$$

where y is the response vector, X is a matrix of model covariates, β are the model parameters estimated by maximum likelihood, and ε are the model errors which are specified as,

$$\varepsilon \sim N\left(0, \delta\right)$$

where 0 is the mean and δ is the error-covariance matrix. To account for autocorrelation, the covariance parameters of δ were assumed to follow a time-dependent autoregressive process (AR1). All AR1 parameters were estimated from the raw data *a priori* to model fitting. All response variables were checked for normality and transformed prior to model fitting where required. GLS model assumptions were verified by examination of the residuals. For each dependent variable, the best-fit model was selected using Akaike's Information Criterion (AIC) which takes into account both goodness of fit and model complexity.

6.4 Results and Discussion

6.4.1 Model Simulation.

We ran the POTSMOM-C model under the IPCC SRES A1F1 scenario. This business-as-usual scenario assumes continuing exponential increase in global carbon emissions until the year 2100 (for details see methods section), and approximates current trends in emission growth. Because our experiment was conducted using a North Atlantic (Kiel Bay, Baltic Sea) plankton community we simulated changes in average sea surface temperature (SST, Figure 6.1A), as well as average annual nutrient fluxes (Figure 6.1B) across the North Atlantic (0-60° N), for the years 1800, 2000, and 2100. Average SST there increased from 23.7 °C in 1800 to 24.6 °C in 2000, and was projected to

reach 29.8 °C in 2100 (Figure 6.1). Average dissolved inorganic nitrogen (DIN) flux into the North Atlantic surface layer (0-100 m) was 0.193 mol m^{-2} yr^{-1}in 1800. With increasing SST and stratification this average annual flux of DIN diminished by 13% until the year 2000 (0.168 mol m^{-2} yr^{-1}), and by 44% until 2100 (0.108 mol m^{-2} yr^{-1}, Figure 6.1B). In relative terms, this DIN flux equates to a renewal of ∼12% of the total nitrogen pool per month (TN=dissolved plus particulate nitrogen) in 1800 and 2000, and 10% in 2100. These values varied by region: total DIN flux into the surface layer can be as high as 30-40% of TN per month in some upwelling and coastal regions (Figure 6.1B). Model-simulated SST and nutrient trends in the North Atlantic were similar to those in other oceans, with the exception of polar seas, which showed very large, and possibly unrealistic, projected temperature increases by 2100 (Figure 6.1).

6.4.2 Mesocosm Experiment

Our mesocosm experiment was initiated during the period of seasonal thermal stratification during summer 2012. Initial conditions were typical for the temperate North Atlantic summer (T=15 °C, low dissolved nutrient concentrations, dominance by small-sized flagellates and copepods, see Appendices). Experimental temperature and nutrient treatments covered the range of model outcomes from 1800-2100, *i.e.* a temperature range of 6 °C (6 treatments were cooled 3 °C below and 6 treatments were warmed 3 °C above ambient temperature), and a monthly enrichment flux of DIN ranging between 0-34% of the TN pool. Other macronutrients (phosphate, silicate) were added in proportions 16N:1P:11Si, as they would during vertical mixing events in the ocean.

Results suggest that the net response of marine phytoplankton to ocean warming was mainly driven by temperature-driven changes in nutrient availability, rather than temperature *per se*. Principal component analysis (PCA) was used to explore multivariate response of the community to experimental treatments (Figure 6.2). This analysis suggested that nutrient supply was linked to changes in fluorescence, chlorophyll *a* concentration, POC, gross primary production (GPP) and community respiration. In contrast, changes in the abundance of consumers were more strongly related to temperature, but in opposite direction: copepods increased with warming, while ciliates and HNF were favored by cool conditions (Figure 6.2). Combined effects

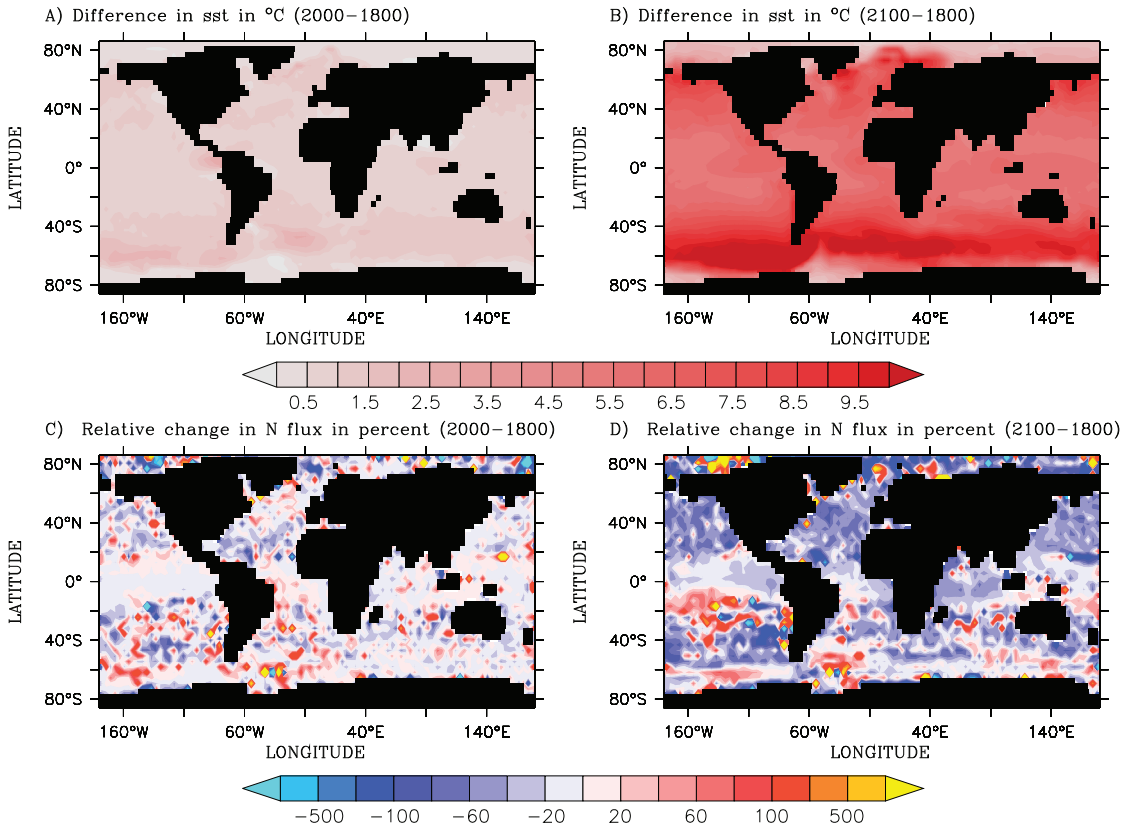

Figure 6.1: Ocean general circulation model.
(A) Absolute annual mean temperature changes projected from 1800-2000, and (B) from 1800 to 2100. Color bar indicates temperature increase in °C. (C) Relative changes in dissolved nitrogen flux into the euphotic zone 1800-2000, and (D) 1800-2100. Color bar indicates nitrogen flux increases (red) or decreases (blue) in percent, relative to the baseline year. Results from this model for the North Atlantic (0-60°N) were used to parameterize mesocosm experiments simulating future ocean conditions.

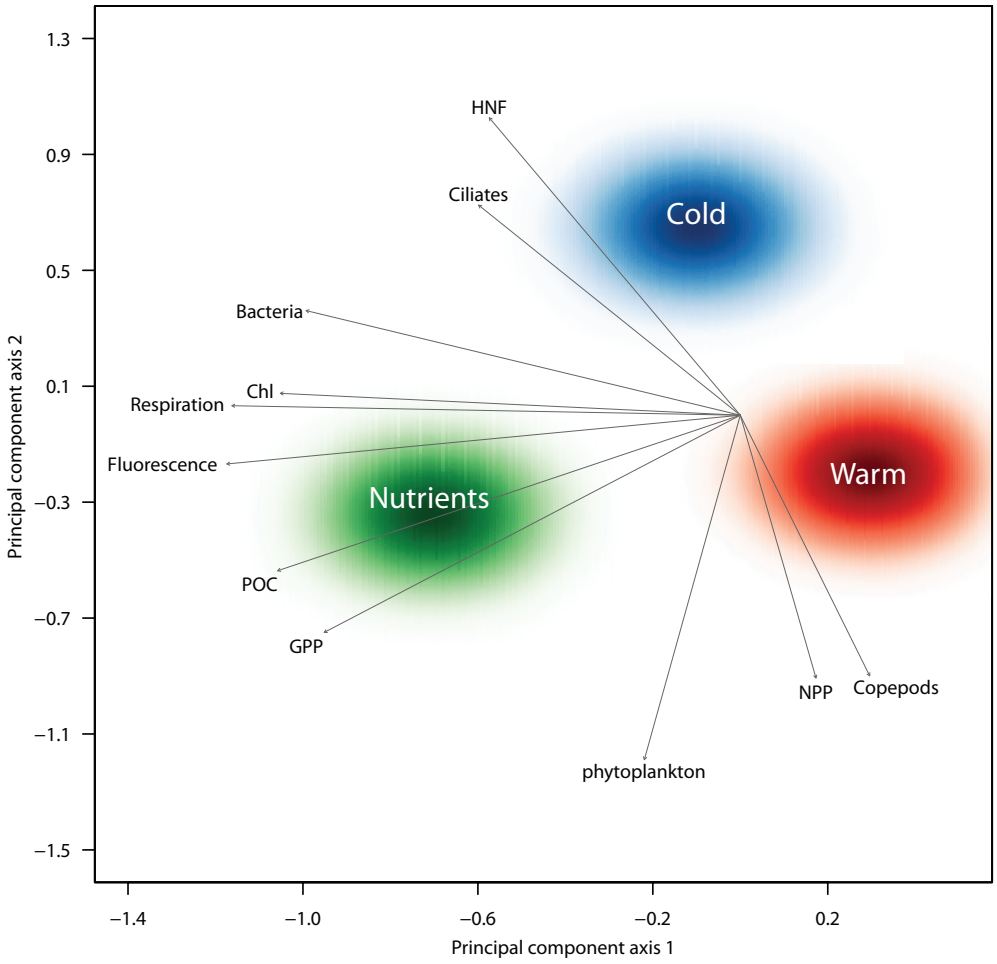

Figure 6.2: Principal component analysis of the experimental plankton community.
Positioning of a dependent variable close to colored regions indicates positive effects of experimental warming (red), cooling (blue) or nutrient enrichment (green). POC=Particulate organic carbon, GPP=Gross primary production, NPP=Net primary production, HNF=Heterotrophic nanoflagellates, Chl=Chlorophyll.

of nutrients and temperature were observed on phytoplankton biomass, and bacteria abundance.

Over the course of the experiment we observed an increase in phytoplankton biomass and a subsequent bloom, especially in treatments with a positive nutrient flux (Figure 6.3A, B). Maximum bloom biomass was nutrient-dependent, with a larger peak at higher nutrient supply. Generalized least squares (GLS) analysis accounting for temporal dependence of the individual time series showed a significant positive effect of nutrients on phytoplankton biomass, fluorescence, chlorophyll *a* concentration, and POC (Figure 6.2; Table 6.1). Temperature increase also had a positive effect on phytoplankton biomass. The timing of the bloom was temperature dependent, with more rapid development and an earlier peak in warm treatments.

Net primary production (NPP) followed the trajectory of phytoplankton biomass (Figure 6.3A, B). However, no statistically significant changes in NPP were observed in response to changes in temperature or nutrient supply (Table 6.1). Community respiration declined over the experimental period, (Figure 6.3) but trended higher in the warm treatments (non-significant trend, P=0.056). Both respiration and gross primary production (GPP) increased significantly with nutrient supply (Table 6.1).

Copepod abundance also increased over the course of the experiment (Figure 6.3A, B), due to new production of copepod nauplii larvae which rapidly developed into copepodites. This growth was accelerated in warm mesocosms (Figure 6.3B), and likely resulted in periodically increased grazing pressure there. Ciliates, in contrast, trended downwards over the course of the experiment (Figure 6.3A, B), and their abundances were strongly negatively correlated with copepods (model II major axis regression: r=-0.21, 2-tailed $P < 0.001$). This observation suggests copepods feeding heavily on ciliates, and less so on phytoplankton, which showed a positive correlation with copepod abundance (model II major axis: r=0.18, 2-tailed P=0.001). In addition to the effects of temperature on plankton abundance and biomass, temperature also increased temporal variability in most plankton groups (Figure 6.3A, B), significantly so for phytoplankton biomass, copepods, ciliates, and HNF (ANOVA, $P < 0.05$, see Appendices for details).

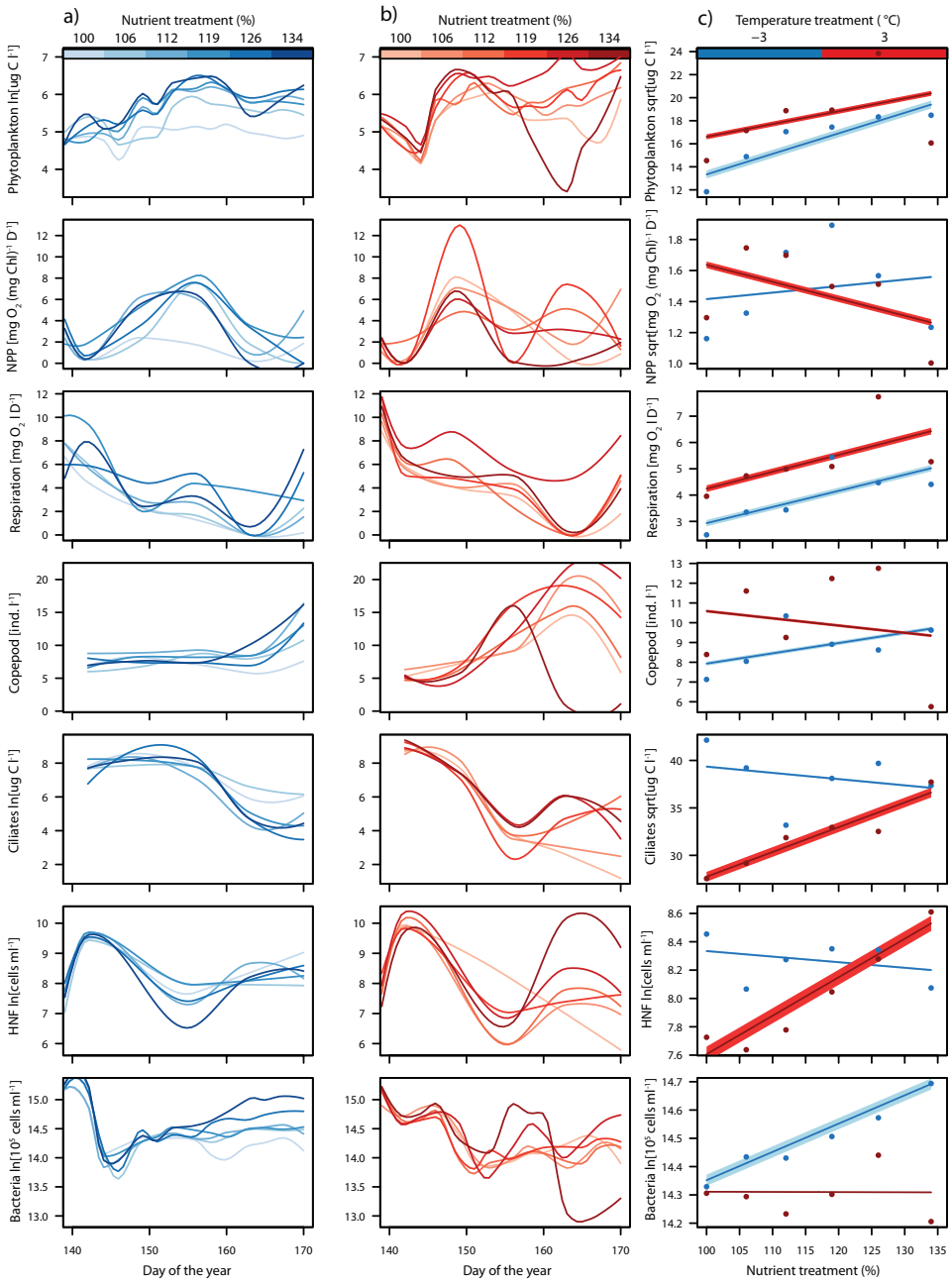

Figure 6.3: Time trends and responses of plankton community to changes in temperature and nutrient supply.
(A-B) Interpolated time series for the main biological variables are plotted for each mesocosm treatment (n=12). Blue trend lines depict cold mesocosm treatments and red lines depict warm treatments. The shading of the trend lines identifies the mesocosm nutrient treatment level (% of total nitrogen). (C) Generalized least squares model predicted trends in main biological variables as functions of temperature and nutrient treatment levels. Shaded areas represent the 95% confidence limits about the trend lines. Generalized least square statistical analysis results are reported in 6.1.

Table 6.1: Generalized least squares analysis.

Variable	Units	Predictor	Coefficient	SE	P
Phytoplankton biomass	ln(g C $L^{-}1$)	Nutrients	0.14	0.04	<0.001
		Temperature	2.17	0.90	0.017
POC	ln(mg C $L^{-}1$)	Nutrients	0.01	0.00	<0.001
Chlorophyll a	sqrt(mg $L^{-}1$)	Nutrients	0.01	0.00	0.005
Fluorescence	ln	Nutrients	0.01	0.00	0.005
NPP	sqrt(mg O2 [mg Chl]$^{-}1$ $D^{-}1$)	Temperature	-0.00	0.01	0.712
GPP	sqrt(mg O2 $L^{-}1$ $D^{-}1$)	Temperature	0.03	0.01	0.014
Respiration	mg O2 $L^{-}1$ $D^{-}1$	Nutrients	0.06	0.03	0.041
		Temperature	0.70	1.94	0.056
Copepod abundance	ind. $L^{-}1$	Temperature	1.22	1.18	0.304
Ciliate biomass	sqrt(g C $L^{-}1$)	Temperature	-6.33	7.30	0.39
HNF abundance	ln(cells $ml^{-}1$)	Nutrients	0.01	0.01	0.338
Bacteria abundance	ln(105 cells $ml^{-}1$)	Nutrients	0.01	0.00	0.024
		Temperature	0.97	0.73	0.186
		Nut x Temp	-0.01	0.01	0.108

Notes: Results represent the most parsimonious model selected from a base model including the effects of nutrients, temperature, and their interaction (Nut x Temp). POC=Particulate Organic Carbon. NPP=Net primary production. GPP=Gross Primary Production. HNF=Heterotrophic nanoflagellates.

6.4.3 Discussion

Our results contrast with experiments conducted with plankton of the same geographic origin during winter. These previous trials tracked the spring phytoplankton bloom under identical warming treatment (up to 6 °C temperature range), but produced opposite results (Sommer et al., 2012). There, warming caused a sharp increase in copepod grazing pressure which depressed phytoplankton biomass (Figure 6.4). Nutrients were abundant at that time, due to strong vertical mixing in the winter. Under such conditions (cold, mixed, nutrient-rich) warming increased consumer grazing rates and top-down regulation of phytoplankton biomass. In contrast, our summer experiment indicated that phytoplankton biomass was nutrient limited, and affected primarily by the rate of nutrient delivery via vertical mixing, as simulated here using nutrient delivery rates projected by ocean circulation models. Warming under such conditions (warm, stratified, nutrient-poor) had positive effects on phytoplankton biomass (Table 6.1). There was no evidence for increased top-down regulation of phytoplankton biomass, but some evidence of increased copepod grazing on ciliates, with possible cascading effects on the microbial loop. Copepods often feed on microzooplankton such as ciliates when large phytoplankton (20-200 μm) such as diatoms are rare (Stibor, 2004). Ciliates in turn, prey on HNF which consume bacteria in a food chain called the microbial loop (Azam et al., 1983). The countervailing trajectories of these trophic groups over time (Figure 6.3A, B) are consistent with a temperature-driven trophic cascade from copepods to bacteria, with ciliates and HNF as intermediary links. Yet, the effects of temperature on the microbial loop were statistically non-significant in the GLS analysis.

It has been suggested that the microbial loop might 'speed up' with warming, thereby supporting photosynthesis due to the faster turnover of nutrients (Taucher and Oschlies, 2011). However, the present results complicate this story: when copepods feed mainly on ciliates instead of phytoplankton, HNFs are released from grazing pressure by ciliates, and will reduce bacteria abundance. Consequently nutrients will not necessarily be recycled faster, except if that function is supplied by HNFs rather than by bacteria (Pane, 2003).

Our findings illustrate how sea surface warming affects marine plankton communities through both physical and biological mechanisms (Figure 6.4). We suggest these

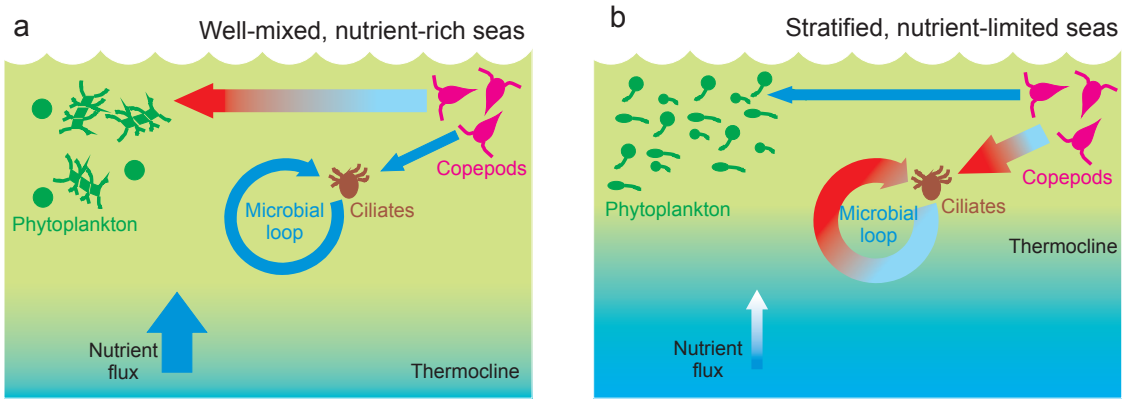

Figure 6.4: Trophic interactions in marine pelagic ecosystems in response to sea surface warming.
(A) In well mixed, nutrient-rich waters phytoplankton is dominated by medium to large diatoms, these are heavily grazed by copepods. (B) In stratified, nutrient limited waters small flagellates dominate phytoplankton biomass, copepods feed mainly on ciliates, increasing the relative importance of the microbial loop for energy flows. Warming (symbolized by gradient arrows) gradually elevates the thermocline, decreases nutrient supply and increases grazing pressure. This always leads to a reduction in phytoplankton biomass, with grazer effects on phytoplankton dominant in (A) and nutrient effects dominant in (B).

marked seasonal differences in phytoplankton response to warming are explained primarily by the large contrast in nutrient supply under well-mixed versus stratified conditions. Physical mechanisms (related to stratification and nutrient supply) tend to control phytoplankton biomass in ecosystems with low nutrient concentrations (Figure 6.3B), such as in the oligotrophic ocean or seasonally stratified shelf seas. Here bottom-up regulation via nutrient supply primarily drives phytoplankton growth and abundance. Low nutrient concentrations favor small phytoplankton, such as flagellates (Edwards et al., 2012). Due to the lack of preferred food, such as large diatoms (20-200 μm), copepods switch to feed on ciliates. Warming increases nutrient limitation, which results in reduction of phytoplankton biomass. Interestingly, there were no significant effects of warming on NPP in this experiment (Table 6.1), indicating that observed changes in plankton biomass may not necessarily impact oceanic uptake of carbon dioxide.

Biological mechanisms via increased grazing of phytoplankton may prevail in nutrient replete waters such as most coastal regions or seasonally mixed shelf seas (Figure

6.4A). In such systems the presence of overwintering consumers strongly influences phytoplankton response to warming as shown in mesocosm experiments with spring plankton (Sommer et al., 2012). Here phytoplankton communities are dominated by large diatoms (20-200 μm), which are the main food source for copepods. Warming acts primarily on plankton metabolic rates, specifically by creating a growing imbalance between grazing and phytoplankton growth that progressively reduces the standing stock of phytoplankton. This, in turn, may reduce food availability for higher trophic levels. Perhaps one of the most important challenges for next-generation earth system modeling is to suitably parameterize trophic interactions and their strengths. Our results provide a mechanistic basis for improving these models and could lead to improved predictions of the effects of climate change on oceanic biomass and productivity.

6.5 Acknowledgements

This study is a contribution to the EU project MESOAQUA. Technical assistance by T. Hansen C. Meyer, C. Eich, L. Berghoff and K. Bading is gratefully acknowledged.

Chapter 7

Patterns, Drivers and Ecosystem Consequences of Marine Phytoplankton Change

7.1 Abstract

Marine phytoplankton production strongly influences the structure and functioning of marine ecosystems, and establishes the biological carrying capacity of ocean ecosystems. There is growing evidence that average global phytoplankton concentrations have been changing over the past century, yet published trajectories of change are divergent. Here, we review and analyze 115 published phytoplankton trend estimates and time series to shed light on underlying patterns, drivers, and ecosystem consequences of long-term change. Our study integrates satellite- and *in situ*-derived chlorophyll measurements, Continuous Plankton Recorder measurements, and other methods to estimate marine phytoplankton change. Generally, observed phytoplankton concentrations tended to increase over time in nearshore waters and over more recent time periods, and decline in the open oceans and over longer time periods. Most published evidence suggests that changes in temperature and nutrient supply rates as leading causes of phytoplankton change. In nearshore waters, altered coastal runoff and increased nutrient loading are a dominant driver of change and may explain widespread increases in phytoplankton observed there. In the open oceans increasing surface temperatures are strengthening water column stratification, reducing nutrient flux from deep waters and negatively influencing phytoplankton. Multiple lines of evidence suggest that temporal phytoplankton change may in part be driven by biological processes, such as changes in grazing regimes and nutrient cycling, but these effects are less well studied. Documented ecosystem consequences of observed phytoplankton changes include altered species composition and abundance across multiple trophic levels, effects on fisheries yield, and changing patterns of export production.

In review as: Boyce, D. G., and B. Worm. 2010. Patterns, drivers and ecosystem consequences of marine phytoplankton change. Global Change Biology.

We conclude that there is broad empirical evidence for substantial changes in phytoplankton concentration over the past century, but that the overall magnitude of these changes remains uncertain. Rising temperatures are predicted to drive further declines in phytoplankton biomass and production over the coming century, with consequences for ecosystem structure and function.

7.2 Introduction

Marine phytoplankton are a diverse group of pelagic photosynthetic microbes that provide over 90% of marine primary production (Charpy-Roubaud and Sournia, 1990). Phytoplankton cells range over three orders of magnitude in size (∼2 to 200 μm; Figure 7.1A) and are distributed across the uppermost layers of the global oceans. Although marine phytoplankton account for only 0.2% of global photosynthetic carbon (C) biomass, they generate 46.2% of the primary production (Field et al., 1998). To achieve this, the global standing stock of phytoplankton turns over every two to six days on average (Behrenfeld and Falkowski, 1997). Due to this rapid turnover (Figure 7.1A), phytoplankton growth often depletes available nutrient resources.

Over a century of scientific research has shown that marine phytoplankton play an important role in determining the structure and functioning of marine ecosystems (Chavez et al., 2003; Richardson and Schoeman, 2004), and can have large effects on fisheries yields (Ryther, 1969; Chavez et al., 2003; Ware and Thomson, 2005; Chassot et al., 2007, 2010), biogeochemical cycles (Redfield, 1958; Falkowski, 1998), climate regulation (Charlson et al., 1987; Murtugudde et al., 2002), and weather patterns (Gnanadesikan et al., 2010). Reflecting this scientific interest, the proportion of peer-reviewed scientific studies of marine phytoplankton has increased over time (7.1B). Also apparent is a shift from phytoplankton studies largely focussed on ecological aspects to those aimed at understanding phytoplankton in the context of biogeochemical cycles, climate, the economy, and global change (Figure 7.1C).

Despite these increased research efforts, one of the most fundamental questions in phytoplankton research remains poorly resolved: How are marine phytoplankton biomass concentrations changing over the long term? Answering this seemingly simple question is complicated by the fact that phytoplankton concentrations are highly variable in space and time and are difficult to distinguish from other marine microbes

and particles, making it difficult to obtain direct measurements of their C biomass. As a consequence, the total concentration of the light-harvesting pigment chlorophyll (Chl), which is present in all phytoplankton cells, has been used as a first-order proxy of abundance and biomass. Despite documented variability in the phytoplankton Chl-to-carbon ratio (Geider, 1987), Chl continues to be the most practical and extensively used proxy of phytoplankton C biomass over large spatial scales (Huot et al., 2007; Henson et al., 2010). This review deals with large-scale changes in phytoplankton concentrations as indexed by changes in ocean color and chlorophyll. We do not attempt to integrate the literature on phytoplankton cell counts and species composition, and make only limited inferences on changes in primary production.

The natural variability of plankton coupled with the numerous challenges of quantitative sampling have contributed to a scarcity of consistent, long-term time series of phytoplankton standing stock and may partially explain the variable and sometimes conflicting estimates of change. Additionally, inter-annual phytoplankton changes are small when referenced to natural variability, and any long-term trends are confounded by transient seasonal or climate-driven variability (Behrenfeld et al., 2006; Martinez et al., 2009; Boyce et al., 2010; Chavez et al., 2011). Thus, the detection of long-term phytoplankton change requires accurate, consistently sampled measurements over a sustained period of time; it has been estimated that time series of between 27 and 40 years are required to separate any long-term trends from short-term variation (Henson et al., 2010; Beaulieu et al., 2013). Phytoplankton time series derived from satellite measurements of ocean color are spatially comprehensive but are currently decades too short (1978-1983 and 1997-present). Alternatively, phytoplankton series derived from shipboard measurements are available beginning in the late 19th century, but are unevenly distributed across time and space. Although several studies have combined time series to estimate phytoplankton changes over broader scales, the accuracy of the blended series can be difficult to empirically verify. In this study, we synthesize all published marine phytoplankton time series to identify patterns of phytoplankton change over the available observational record. We then review the drivers of such long-term marine phytoplankton change and conclude by summarizing some potential ecosystem consequences.

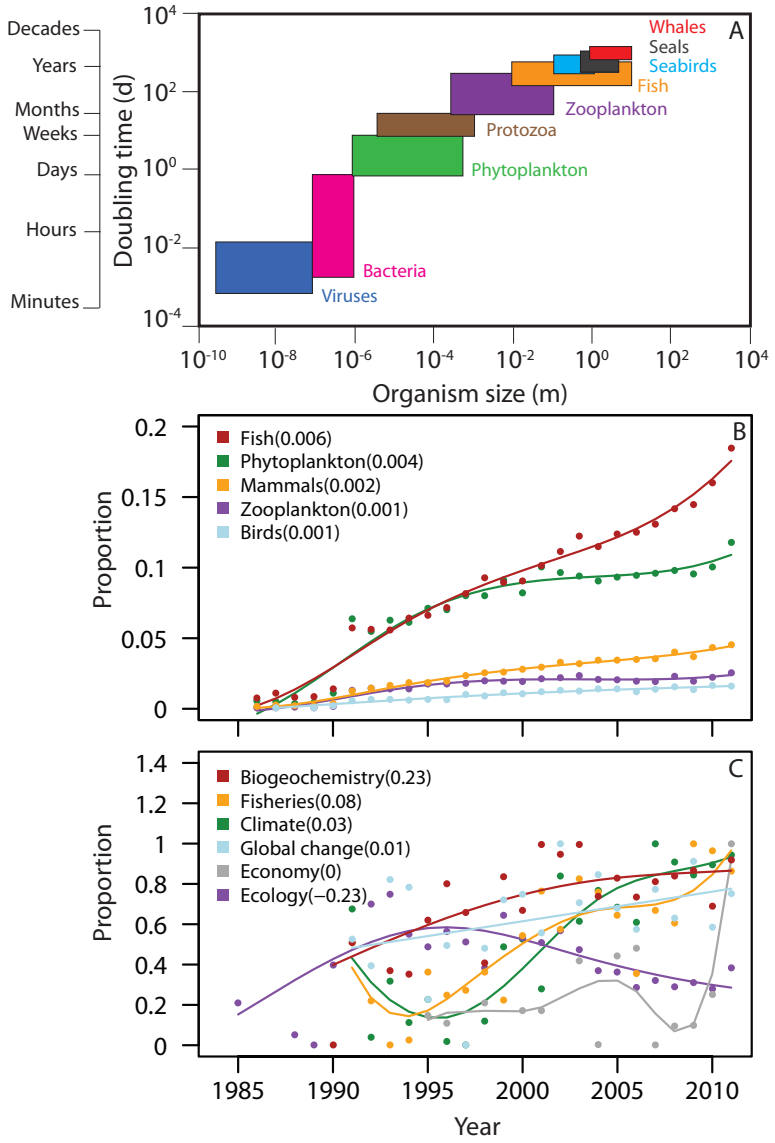

Figure 7.1: Phytoplankton in the scientific literature.
(A) Dominant space and time scales of major groups of marine organisms. The average size range (*x-axis*) is plotted as a function of the average doubling time (*y-axis*) for various marine groups. Phytoplankton are represented in green. Figure was adapted after (Murphy et al., 1988). (B) Temporal trends in the scaled proportion of major marine species groups (1985–2010; see Appendices for details). (C) Temporal trends in the scaled proportion of marine phytoplankton publications associated with different key words. Taxonomic groups and fields of study are represented as colors with the linear rates of change reported in brackets.

7.3 Materials and methods

7.3.1 Patterns of Phytoplankton Change

We systematically searched scientific databases to identify peer-reviewed studies of temporal marine phytoplankton change. Our literature search covered a minimum of ∼22 million titles from over 16,500 peer-reviewed journals. We limited our search to publications estimating phytoplankton change from chlorophyll concentrations (Chl; mg m^{-}3) collected from the upper ocean at multi-year scales (>5 years). Studies conducted in fresh or brackish waters were not included. We extracted 115 phytoplankton time series and estimates of temporal phytoplankton change from 24 publications (Table 7.1).

To standardize measurements that were reported in different units, we extracted the estimated total percentage change in phytoplankton over the available time span as reported by the authors. In some cases data extraction software was used to extract and calculate these rates[1]. Where we extracted the time-series from the publication, we fitted linear time series models to the observations, and calculated the total percentage change as the difference between the start and end of the fitted time series referenced to the initial value. The percent change was then divided by the length of the time series to yield the standardized percent change per year. To spatially standardize the rates of change, we binned all estimates into 5° x 5° cells. This resolution was selected because the majority of published phytoplankton time series were estimated over spatial domains equal or greater than 5°.

Studies of temporal phytoplankton trends are often widely conflicting in both the direction and magnitude of reported change (*i.e.* Wernand et al., 2013; Boyce et al., 2010; Behrenfeld et al., 2006; Antoine et al., 2005; Gregg et al., 2005; Conkright and Gregg, 2003; Falkowski and Wilson, 1992; Venrick et al., 1987). To better understand the factors that may explain these differences, we estimated the phytoplankton trend variability within each 5° x 5° cell as

$$CV_i = \frac{\mu_i}{\sigma_i} \tag{7.1}$$

where $CV_i$is the coefficient of variation, μ_i is the mean trend (% yr^{-1}), and σ_i is

[1]www.getdata-graph-digitizer.com

Table 7.1: Published phytoplankton time series and associated metadata.

Reference	Start year	End year	Span	Platform	Driver
Aebischer et al. 1990	1955	1987	32	CPR	BU
Aksnes & Ohman, 2009	1949	2007	58	Secchi	BU
Antoine et al. 2005	1979	2002	23	Satellite	-
Behrenfeld et al. 2006	1997	2006	9	Satellite	BU
Boyce et al. 2010	1899	2008	109	Blended	BU
Boyce et al. 2013	1890	2010	120	Blended	BU
Chavez et al. 2011	1989	2009	20	In situ	-
Falkowski & Wilson, 1992	1900	1981	81	Secchi	-
Frank et al. 2005	1962	2002	40	CPR	TD
Goes et al. 2005	1997	2004	7	Satellite	BU
Gregg & Conkright 2002	1979	2000	21	Blended	-
Gregg et al. 2005	1998	2003	5	Satellite	-
Head et al. 2010	1998	2006	8	CPR	-
Karl et al. 2001	1969	1998	29	In situ	BU
Lomas et al. 2010	1990	2007	17	In situ	B
Mcquatters-gollop et al. 2007	1948	2003	55	CPR	-
Mcquatters-gollop et al. 2011	1948	2008	60	CPR	-
Montez-hugo et al. 2009	1978	2006	28	Satellite	BU
Motoda et al. 1987	1949	1969	20	In situ	B
Raitsos et al. 2005	1948	2002	54	CPR	-
Shiomoto et al. 1997	1985	1994	9	In situ	TD
Sugimoto & Tadokoro, 1998	1972	1993	21	In situ	B
Suikkanen et al. 2007	1979	2003	24	In situ	BU
Venrick et al. 1987	1968	1985	17	In situ	BU
Wernand et al. 2013	1889	1999	110	Forel-Ule	-

Note: BU=bottom-up, TD=top-down.

the trend standard deviation within cell i. To explore which factors are most related to the variability of the trends, we estimated the trend variability as a function of several covariates within a linear model as

$$ln(CV)_i = \beta_0 + \beta_1 Driver_i + \varepsilon_i, \tag{7.2}$$

where $_i$are the individual observations, $ln(CV)_i$ is the coefficient of variation, β_0 is the model intercept, β_1 is the rate of response change as a function of the driver in question, and ε_i are the model errors. Using this approach, we quantitatively estimated which factors may be most related to discrepancies among phytoplankton time trend estimates. Based on this analysis, we calculated the mean rate of phytoplankton change from the extracted trend estimates for each individual 5° x 5° cell while accounting for the major factors influencing trend variation (see the Results and Discussion section for details). As a sensitivity check, we also calculated weighted mean rates of phytoplankton change, but this did not influence the results.

7.4 Results and Discussion

7.4.1 Patterns of Phytoplankton Change

The median trend length of the extracted phytoplankton trends was 23 years, with most estimates distributed over more recent years (Figure 7.2A). The majority of the trends were derived using *in situ* sampling (36%) or satellite remote sensing (32%); (Figure 7.2A, inset). The remaining trends were inferred from water column transparency measurements (15%); (Secchi, 1886), Continuous Plankton Recorder data (CPR; 13%), or semi-quantitative assessments of ocean color using the Forel-Ule color scale (3%); (Forel, 1890). A large fraction (31%) of the phytoplankton trend estimates were obtained by combining measurements from two or more of these methods. Although remote sensing is considered as a single observational platform, measurements from different satellite sensors collected over different time intervals are often combined (Gregg and Conkright, 2002; Antoine et al., 2005; Montes-Hugo et al., 2009). The extracted trend estimates were globally distributed, but concentrated in the Northern Hemisphere and closer to the coasts, and were sparsely distributed at high latitudes and in the Southern Hemisphere (Figure 7.2B).

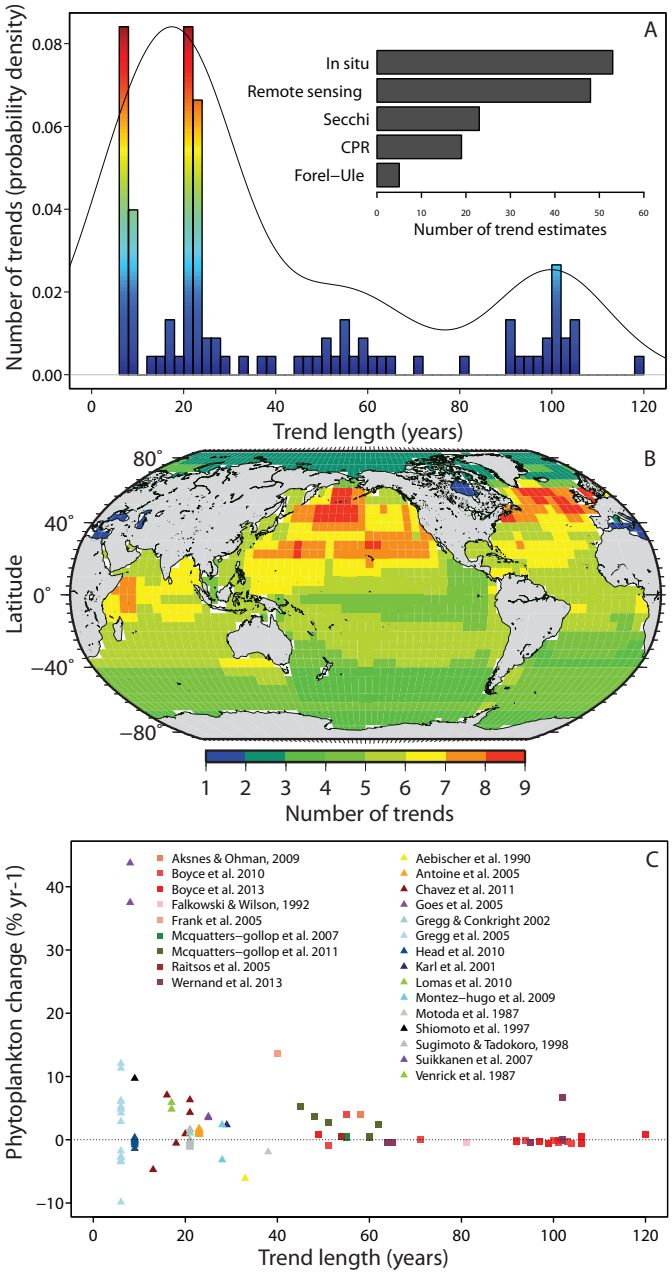

Figure 7.2: Time series data.
(A) Standardized number of phytoplankton trend estimates as a function of the trend length. Inset depicts the number of phytoplankton time trends estimated using different observational methods. (B) Spatial distribution of all phytoplankton trend estimates. Colors depict the number of trends per 5° x 5° cell. (C) Standardized phytoplankton change as a function of trend length. Long-term trends that transcend scales of cyclical variability (35 years Beaulieu et al., 2013; Henson et al., 2010) are shown as squares; all others are shown as triangles. Colors depict the source publication. The horizontal dashed line denotes no change.

The extracted estimates of change were observed to be larger and more variable when estimated over shorter time intervals (Figure 7.2C). We also observed increased variability in the Southern Hemisphere and in waters further from the coastlines (Figure 7.3A). Linear model analyses suggested that the observed variability in the estimates of temporal phytoplankton change was best explained by the number of observational platforms used and the mean temporal span of the trend (Figure 7.3; Table 7.2). The average rates of phytoplankton change within each 5° x 5° cell were more variable when calculated from estimates obtained from different observational platforms (Figure 7.3B), when the trend was estimated over more recent time periods (Figure 7.3C), or when the average temporal span of the estimates was shorter (Figure 7.3D). The specific type of observational platform used for trend analysis did not influence the variability. This suggests that the results of combining estimated rates of phytoplankton change derived from multiple observational platforms or estimated over different time intervals are highly variable and could be difficult to interpret. Accordingly, we calculated average rates of phytoplankton change by combining extracted trend estimates which were available over comparable time intervals, and/or using the same observational platforms. This allowed us to estimate time trends in phytoplankton over four intervals:

1. 1890–1920 to 1980–2010, derived from ocean color, Secchi, and *in situ* Chl measurements (4 studies).

2. 1975 to 2000–2010, derived using remote sensing measurements (3 studies).

3. 1995–2005 to 2005–2010, derived using remote sensing measurements (3 studies).

4. 1945–1955 to 1990–2010, derived using CPR measurements (4 studies).

This procedure reduced the number of extracted trends used in the trend analysis, but was necessary in order to minimize the influence of any biases on the average rates of phytoplankton change. Notably, most estimates of phytoplankton change derived from *in situ* measurements could not be incorporated into our analysis, because they tended to be available over a highly variable range of spatial and temporal scales.

Further, the long-term average rates of change were derived from multiple observational platforms; this was necessary in order to obtain average rates of change over these time intervals.

Long-term rates of change suggested declining trends over much of the ocean, except for the North Atlantic Ocean, where large increases were driven by possibly inflated estimates (6.7% yr^{-1}) derived from semi-quantitative ocean color measurements (Wernand et al., 2013); (Figure 7.4A). Most estimates over this period suggest declining trends across the North and Equatorial Pacific oceans. This contrasts greatly with satellite-derived estimates since the late 1970s, suggestive of large phytoplankton increases, except in the Southern Ocean (Figure 7.4B). Again, these trends were largely driven by one study, which reported large and coherent increases in phytoplankton biomass since 1979 (Antoine et al., 2005). Satellite estimates since 1997 suggest spatially variable rates of change, with declines in open ocean regions and increases in nearshore areas (Figure 7.4C). Lastly, estimates derived from CPR measurements indicate large increases across the North Atlantic Ocean since ∼1950 (Figure 7.4D).

Although the observed patterns of phytoplankton change were variable (Figure 7.4), some general patterns were identified. The rates of phytoplankton change were of greater magnitude and more variable when estimated over shorter intervals (Figures 2C, 3D, and 4). This likely reflects transient climate variability, which may strongly influence shorter-term (less than 27 to 35 years) trends (Behrenfeld et al., 2006; Martinez et al., 2009; Boyce et al., 2010; Henson et al., 2010; Chavez et al., 2011; Beaulieu et al., 2013). As such, some of the trends reported here (Figures 4B and 4C) may reflect climate-driven phytoplankton variability rather than sustained long-term changes. Phytoplankton trend estimates were observed to switch from negative to positive through time and with proximity to the nearest coastline (Figure 7.5), similar to the findings of other long-term studies (Boyce et al., 2010, 2013). Phytoplankton declines in open oceans have also been observed previously (Gregg and Conkright, 2002; McClain et al., 2004; Polovina et al., 2008), and are predicted to continue into the future (Polovina et al., 2011). Increases in nearshore waters have also been observed previously, and are likely related to increasing coastal eutrophication there (see environmental conditioning section below for further details). The direction of

Table 7.2: Summary of linear model estimation of the factors influencing phytoplankton time trend variability.

Covariate	Description	Effect	SE	P	R-squared
Platform	Number of sampling platforms used to derive estimates in the cell	2.464	0.061	<0.0001	0.19
Average series length	Mean trend length within cell	-0.039	0.001	<0.0001	0.13
Bathymetry	Bathymetry of cell	0.000	0.000	<0.0001	0.04
Range of series length	Difference between longest and shortest trend length within cell	0.006	0.001	<0.0001	0.01
Data: blended remote sensing	Inclusion of trends derived from multiple satellite platforms	-0.321	0.035	<0.0001	0.01
Distance	Distance of cell from the coastline	0.000	0.000	<0.0001	0.00
Data: Forel-Ule	Inclusion of Forel-Ule-derived trends	-0.357	0.064	<0.0001	0.00
Data: Remote sensing	Inclusion of remote sensing-derived trends	0.175	0.031	<0.0001	0.00
Variance of series length	Variance of trend lengths within cell	0.007	0.001	<0.0001	0.00
Spatial range	Difference betwen spatial coverage of estimates within cell	0.768	0.161	<0.0001	0.00
Data: blended	Inclusion of trends derived from multi-platform data	-0.141	0.031	<0.0001	0.00
Data: Transparency	Inclusion of transparency-derived trends	0.457	0.109	<0.0001	0.00
Data: In situ	Inclusion of in situ-derived trends	0.340	0.176	0.054	0.00
Data: Continuous Plankton Recorder	Inclusion of CPR-derived trends	0.072	0.138	0.602	0.00

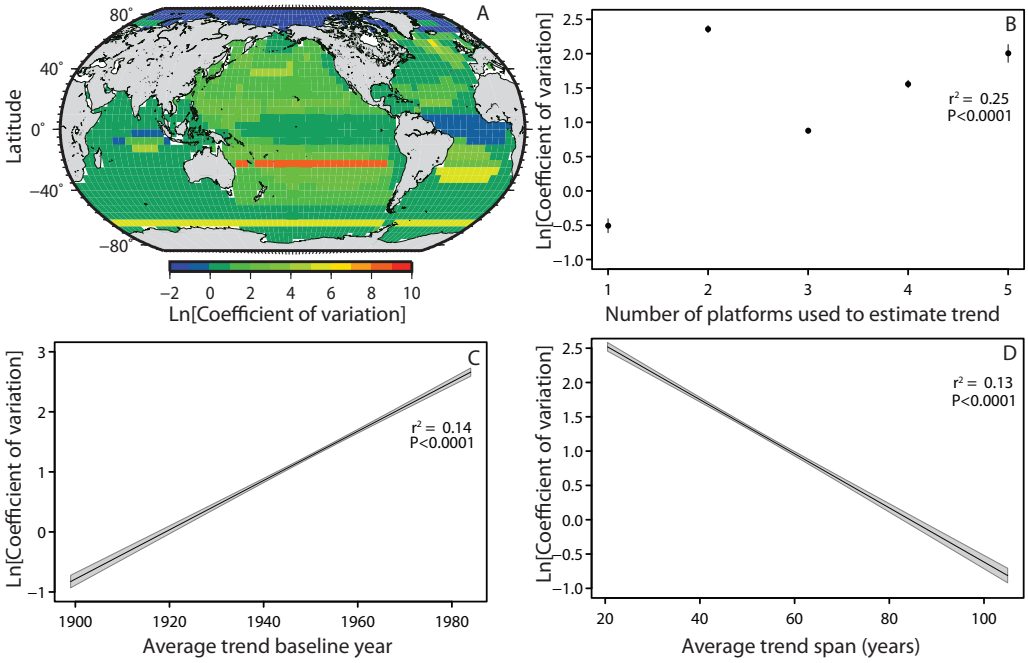

Figure 7.3: Influences on phytoplankton trend variability.
(A) The coefficient of variation for extracted trends within each 5° x 5° cell. Colors depict the log-transformed coefficient of variation calculated within each cell using all available phytoplankton trend estimates. (B–D) Strongest single predictors of phytoplankton trend variability across all 5° x 5° cells. (B) The number of sampling platforms present in the cell, (C) the average baseline year (initial year) for all trends in the cell, and (D) the average length of time spanned by all trends in a cell. For B–D, the points and trends lines are model-predicted phytoplankton trend variability values (coefficient of variation), and the vertical lines (B) or shaded regions (C–D) are the 95% confidence limits. All relationships are statistically significant (P<0.0001).

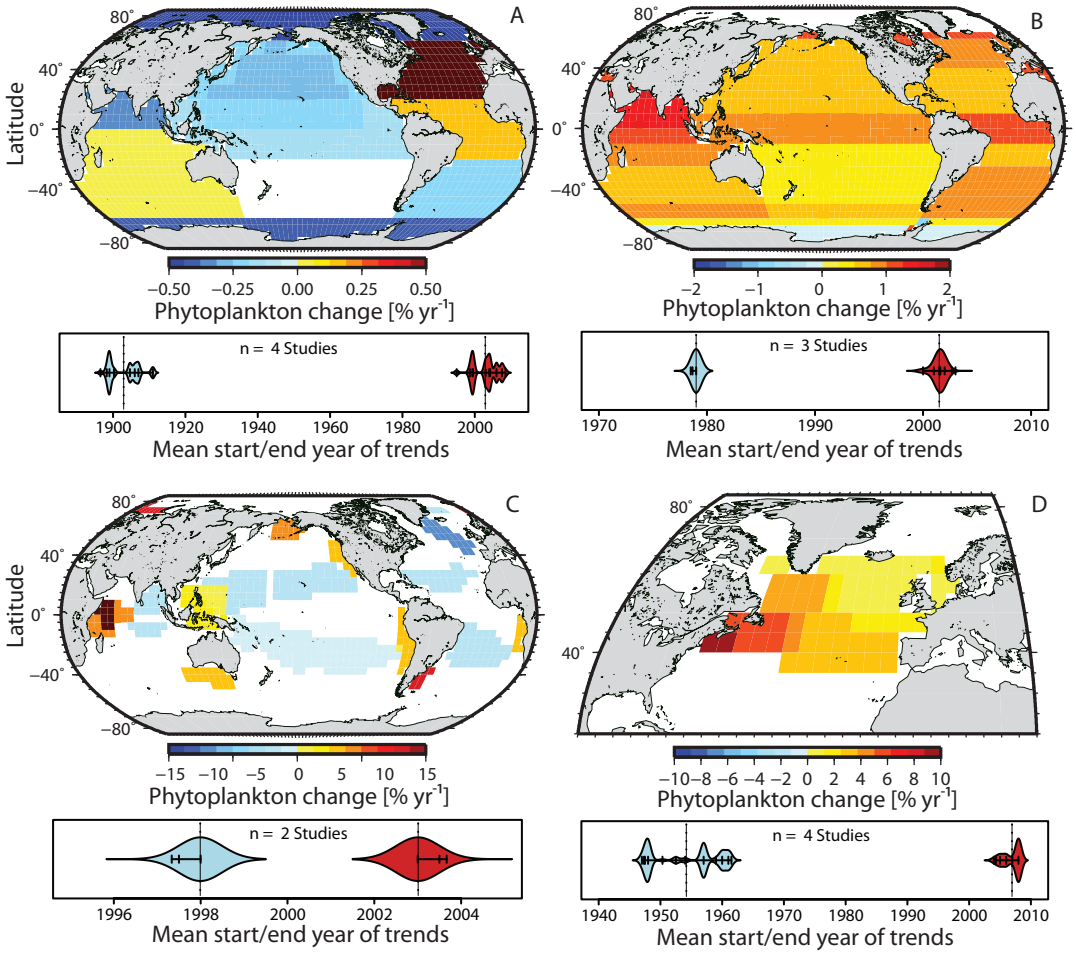

Figure 7.4: Average phytoplankton change over different space and time scales. Average rate of phytoplankton change from (A) 1890–1920 to 1980–2010, (B) 1975 to 2000–2010 derived using remote sensing measurements, (C) 1995–2005 to 2005–2010 derived using remote sensing measurement, and (D) 1945–1955 to 1990–2010 derived using CPR measurements. Colors within the maps depict the average rate of phytoplankton change within each 5° x 5° cell; white depicts no data. The plots below each map are the distributions of the start (blue) and end (red) years for all trends. The long vertical lines represent the averages and the vertical ticks are the actual start and end values.

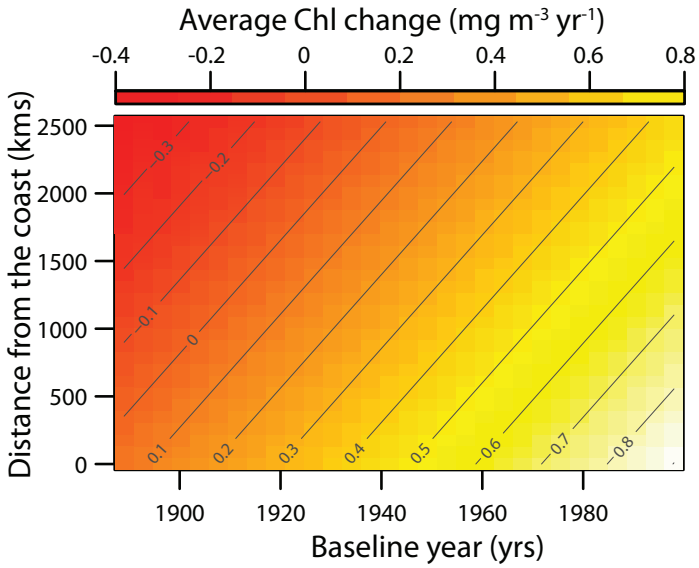

Figure 7.5: Effects of location and baseline year on phytoplankton trends. Shown are the modelled effects of distance from the nearest coastline and baseline year of time series on all extracted rates of phytoplankton change. Color depicts the magnitude of the mean rate of phytoplankton change.

the extracted phytoplankton trends from different studies within each 5° x 5° cell were generally different, except for at high latitudes (>60° N or S), where four spatially overlapping studies reported phytoplankton declines.

Similar to our estimates, predicted patterns of future phytoplankton change from process-based ocean models are variable. At global scales, 14 out of 17 studies (82%) predict a global phytoplankton decline over the next century (Table 7.3). Most predictions suggested phytoplankton increases at high latitudes and declines at low- and mid-latitudes (Schmittner et al., 2008; Henson et al., 2010; Steinacher et al., 2010; Hofmann et al., 2011). Some of the largest and most variable declines are predicted to occur in the North Atlantic Ocean (*i.e.* Henson et al., 2010; Steinacher et al., 2010), where our estimates are also highly variable. This suggests that temporal phytoplankton dynamics in the North Atlantic are particularly difficult to represent in both empirical and process-based models.

Table 7.3: Published estimates of future phytoplankton or primary production change.

Reference	Start year	End year	Span	Response	Change	Units	Forcing
Hoffman et al. 2011	2000	2200	200	Chl	-50.00	%	CO2
Schmittner et al. 2008	2000	4000	2000	Chl	5.00	%	CO2
Henson et al. 2010	2001	2100	99	Chl	-0.00	mg m-3 yr-1	T
Boyd et al. 2001	2000	2080	80	Chl	-8.50	%	CO2
Beaulieu et al. 2013	2001	2100	99	Chl	-1.53	mg m-3 yr-1	CO2
Olonscheck et al. 2013	2000	2100	100	Chl	-50.00	%	CO2
Henson et al. 2010	2001	2100	99	PP	-0.15	mg m-3	T
Sarmiento et al. 2004	2040	2060	20	PP	4.40	%	T
Taucher & Oschlies 2011	2000	2100	100	PP	-5.30	%	T
Bopp et al. 2001	2000	2080	80	PP	-8.90	%	CO2
Bopp et al. 2001	2000	2080	80	PP	-8.50	%	CO2
Boyd & Doney 2002	2060	2070	10	PP	-5.50	%	CO2
Steinacher et al. 2010	1860	2099	239	PP	-11.00	%	CO2
Schmittner et al. 2008	2000	4000	2000	PP	100.00	%	CO2
Boyd et al. 2001	2000	2080	80	PP	-8.90	%	CO2
Cermeno et al. 2008	2000	2100	100	PP	-14.00	%	CO2
Cox et al. 2000	2000	2100	100	PP	-5.00	%	CO2

7.4.2 Drivers of Phytoplankton Change

To first order, phytoplankton growth is determined by the availability of sunlight and macronutrients (bottom-up processes), as well as grazing, viral infection, auto-catalyzed programmed cell death (PCD); (Agusti et al., 1998; Bidle and Falkowski, 2004), pathogenic bacteria, and fungi (top-down processes). Based on this, we discuss drivers of plankton change in the context of changes in (*i.*) physical forcing and (*ii.*) biological forcing, which may alter the strength of bottom-up and top-down processes on marine phytoplankton.

Physical forcing

Particularly in the open oceans, which account for 90% of the ocean surface, studies have observed phytoplankton growth and productivity to be strongly driven by physical forces which control nutrient flux, such as mixing and upwelling (Oschlies and Garcon, 1998; McGillicuddy et al., 2007). Passive diffusion across the thermocline (Chavez and Toggweiler, 1995), biological nitrogen fixation (Capone et al., 1997), and the atmospheric deposition of iron, are often of regional importance (Behrenfeld et al., 1996). Hence it is likely that the observed declines in open ocean regions (Figures 7.4C and 7.5) are driven by factors affecting these processes. Primary among these is increasing sea surface temperature (SST), which generally leads to reduced mixing depth, enhanced stratification, and reduced nutrient flux from deeper waters. Studies using observational measurements have reported strong temperature-driven stratification (TDS) effects on phytoplankton concentration at seasonal (Lozier et al., 2011), inter-annual (Behrenfeld et al., 2006), and multi-decadal (Martinez et al., 2009) time scales. Stratification has also been observed to influence phytoplankton trajectories over geological time scales (Vermeij, 2011; Romero et al., 2011). Analyses of satellite observations suggest that TDS may also be leading to an expansion of the low-chlorophyll gyres of the open oceans (McClain et al., 2004; Polovina et al., 2008); bio-physical models also predict this expansion to continue over the coming century (Polovina et al., 2011). Studies using empirical observations (Behrenfeld et al., 2006; Boyce et al., 2010) and process-based models (Henson et al., 2010) have provided strong empirical evidence that TDS effects on phytoplankton also vary by latitude, with strong negative effects at low- and mid-latitudes, but positive effects

at high latitudes. This pattern of change is partly at odds with our observations, which mostly suggest declining trends at high latitudes (>70° N or S; Figures 7.4A and 7.4B). In well-mixed high latitude oceans, increasing TDS may positively influence phytoplankton growth by retaining phytoplankton cells above the critical depth (Sverdrup, 1953; Jacobs et al., 2002; Montes-Hugo et al., 2009; Arrigo et al., 2012). Process-based models also predict that over the coming century rising SSTs will lead to reduced ice cover and increased light availability, and a longer growing season may lead to increased phytoplankton biomass and productivity at high latitudes (Schmittner et al., 2008; Henson et al., 2010; Steinacher et al., 2010). Phytoplankton trends are generally less available at these high latitudes (Figure 7.2B), likely contributing to the variability of the empirical estimates of change there.

Experimental, field, and modeling studies suggest that TDS may also lead to declines in the concentration of larger species (*i.e.* diatoms), and increases in smaller phytoplankton species (*i.e.* cyanobacteria). These effects may be related to different nutrient uptake strategies between large and small phytoplankton species (Bopp et al., 2005; Cermeno et al., 2008; Li et al., 2009), the temperature-size rule (TSR) (Atkinson, 1994; Atkinson et al., 2003; Moran, 2010), or increased sinking rates of larger phytoplankton species (Rodriguez et al., 2001).

Changes in a range of additional physical variables such as wind intensity or salinity may modify the influence of temperature on stratification and nutrient flux in some locations. For instance, observations of changing wind intensity over the past century will have large effects on upwelling intensity, including highly productive Eastern Boundary Current systems (Bakun, 1990; Vecchi et al., 2006). In the Indian Ocean, warming of the Eurasian land mass has been linked to intensifying monsoon winds and upwelling, leading to reported phytoplankton increases of 300–350% (Goes et al., 2005); (Figures 7.4B and 7.4C; Table 7.1). Wind-driven atmospheric deposition of iron is of regional importance to phytoplankton growth (Behrenfeld et al., 1996). In polar oceans, melting sea ice has been linked to increased irradiance and reduced surface salinity, which may have stronger effects on phytoplankton than TDS (Lee et al., 2012; Post et al., 2013).

Biological forcing

Trophic control Consumers may drive phytoplankton change through their trophic (feeding) behaviour. These effects may be caused by modified grazing pressure (direct), or by changes to other consumers, which may propagate across multiple trophic links, ultimately modifying grazing pressure (indirect). For instance, the removal of a top predator from the Northwest Atlantic ecosystem led to cascading trophic effects which may have driven a long-term (∼40 year) increase in phytoplankton there (Table 7.1); (Frank et al., 2005). Such trophic cascades have been observed across diverse ecosystems but often attenuate at the plankton level (Baum and Worm, 2009), and it is unclear what factors determine their occurrence and strength. It is possible that short food chains with fewer trophic transfers between predators and producers may be more susceptible to cascading effects, with reduced diversity and lower functional redundancy rendering the systems generally less stable (*i.e.* Casini et al., 2008; Worm et al., 2006). High phytoplankton biomass during blooms may also affect the strength of trophic control. Grazing pressure (Loeb et al., 1997; Sommer et al., 2007), heterotrophic bacterial activity (Llewellyn et al., 2008), and viral infection (Suttle, 1994) can all be influential in controlling phytoplankton blooms. Experimental and modeling studies also suggest that ocean warming may induce metabolic changes, thereby increasing grazer control of phytoplankton (O'Connor et al., 2009; Lewandowska et al., 2013). Lastly, heavily exploited marine systems may be more susceptible to cascading effects (Baum and Worm, 2009).

Environmental conditioning Marine organisms further modify their environment through a range of non-trophic activities, thereby promoting or inhibiting phytoplankton growth in a process termed environmental conditioning (Smetacek, 2008). For instance, whales and seals forage at depth and excrete fecal plumes which float and become concentrated in surface waters. In this manner, essential macronutrients such as nitrogen and iron are transported from deeper to surface waters, promoting phytoplankton growth. Changes in this so-called 'whale pump' have been suggested as a possible driver of phytoplankton change (Smetacek, 2008; Roman and McCarthy, 2010). Particularly, long-term reductions in whale biomass in the Northwest Atlantic (Roman and Palumbi, 2003) and Southern Ocean (Smetacek, 2008) may have led

to reduced efficiency of the whale pump, and may explain (at least in part) observed long-term phytoplankton declines there (Boyce et al., 2010, 2013).

The activities of biological organisms may also influence phytoplankton through their effects on ocean mixing (Munk, 1966). Kinetic energy generated by swimming organisms could account for 33% of global ocean mixing; this is comparable to wind or tidal driven mixing (Dewar et al., 2006). Observational studies have also reported that the swimming activities of krill may induce four orders of magnitude increases in turbulence in nearshore waters (Kunze et al., 2006). Given the global distribution and large biomass of vertically migrating marine organisms (Gjosaeter and Kawaguchi, 1980), biologically generated turbulence may have larger impacts on the global flux of nutrients to phytoplankton in surface waters than is currently recognized. The harvesting of large-bodied consumers (Estes et al., 2011) may have disproportionately reduced ocean mixing, with possible effects on phytoplankton (Behrenfeld et al., 2006; Polovina et al., 2008; Boyce et al., 2010). This mechanism may have contributed to part of the observed phytoplankton declines in the open oceans (Figure 7.5), where vertical mixing is a particularly strong driver of phytoplankton change.

By accounting for 20% of all marine microorganism mortality, viruses may have large effects on nutrient fluxes in the oceans, with consequences for phytoplankton (Suttle, 2007). Viruses may negatively influence phytoplankton directly via cell lysis, or their presence may trigger phytoplankton programmed cell death (PCD) as an antiviral defence mechanism (Bidle and Falkowski, 2004).Viruses may also infect consumers ranging from bacteria to whales, thereby increasing the amount of dissolved and particulate organic matter available for phytoplankton growth (Suttle, 2007).

Lastly, the activities of humans provide perhaps the clearest example of environmental conditioning. Some examples concern strong effects on coastal nutrient inputs stemming from soil erosion, agriculture, and industrial activities. For instance, anthropogenic activity has led to global increases in the riverine deposition of nitrate (N) and phosphate (P) to nearshore waters by up to 300% (Duce et al., 1991) or more in some regions (Howarth et al., 1996), while atmospheric deposition of N has increased by up to 50% in some regions (Brimblecombe and Pitman, 1980). Such large-scale environmental conditioning by humans in nearshore oceans is likely driving the large phytoplankton increases observed there (Figures 7.4 and 7.5).

Synergistic forcing

Much of the physical and biological forcing of phytoplankton change is likely highly synergistic. For instance, despite the mostly negative effects of rising SST via TDS, some studies also suggest that ocean warming could lead to increased rates of phytoplankton growth (Sarmiento et al., 2004) or microbial metabolism (Taucher and Oschlies, 2011), both of which ultimately lead to increased phytoplankton biomass or production and could outweigh TDS effects. However, the metabolic theory of ecology (MTE; Brown et al., 2004), and experimental results (Sommer and Lengfellner, 2008; O'Connor et al., 2009), suggest that rising SST increases grazer metabolic rates faster than phytoplankton metabolic rates, leading to reduced phytoplankton through increased grazing pressure. It is important to distinguish clearly between the physically-mediated SST effects on phytoplankton via changes in stratification and nutrient delivery, and the biologically-mediated SST effects on phytoplankton via altered phytoplankton and consumer metabolism. One experimental study compared the relative importance of these processes, and found that that this varied depending on the nature of the ecosystem (Lewandowska et al., 2013). In nutrient-limited systems the effect of rising temperature on nutrient delivery was dominant, while in nutrient-replete systems, the effect of rising temperature on grazing pressure was stronger. However, in both systems, the overall effect of increasing SST on phytoplankton was negative. Such synergistic effects on phytoplankton may be widespread.

Case study: Global patterns of phytoplankton, nutrients, and grazers

To quantitatively explore selected controls on phytoplankton biomass, we examined spatial gradients in Chl (mg $m^{-}3$), in conjunction with spatial data for nitrate concentration (N; μmol l^{-1}), and total zooplankton C biomass (mg m^{-3}) at global scales. This approach has been used to show the strong positive relationship between phytoplankton and zooplankton concentration across the Atlantic Ocean (Irigoien et al., 2004), but to our knowledge had not yet been applied globally. All data were extracted from publicly available sources (see Appendices for details).

Based on this simple approach, global patterns in Chl appeared similar to those of nitrate and zooplankton (Figures 7.6A, 7.6B and 7.6C). Elevated levels in nearshore,

high latitude, and upwelling regions are well-delineated, as are the oligotrophic gyres of the major ocean basins, where nitrate and phytoplankton concentrations are lesser. Ordinary least-squares (OLS) regressions of log-transformed mean nitrate or zooplankton on phytoplankton measurements for each 1° x 1° cell statistically confirmed this relationship, a result suggestive of bottom-up control of both phytoplankton and zooplankton concentrations by nitrate (Figures 7.6D and 7.6F). The relationship between nitrate and chlorophyll was strongly positive ($r=0.51$, $p<0.0001$), and was best approximated by a polynomial regression ($r^2=0.39$; $p<0.0001$; Figure 7.6D). The non-linearity of the relationship likely relates to the phytoplankton requirement for additional resources such as phosphate, silicate, carbon, and iron. For example, despite high available nitrate concentrations in some regions, phytoplankton biomass is limited by, and responds strongly to, the addition of iron across 20-40% of the ocean (Behrenfeld et al., 1996; Boyd et al., 2000; Moore et al., 2009). It is therefore possible that changes in physically- or biologically-driven iron deposition may have influenced the observed phytoplankton trends, particularly in the Pacific, Atlantic, and Southern oceans (Figure 7.4).

7.4.3 Ecological Consequences of Phytoplankton Change

Ecosystem partitioning of primary production

Phytoplankton-generated primary production ultimately supports virtually all life in the oceans. There are three fundamental pathways by which phytoplankton production is channelled through the food web: (*i.*) the grazer food chain via zooplankton and fish, (*ii.*) the microbial food chain via bacterial processing of plankton organic matter, and (*iii.*) detrital export to deeper waters. Here, we focus on the importance of phytoplankton biomass and production with respect to these pathways and the possible consequences of phytoplankton changes for the structure and functioning of marine ecosystems.

By entering the grazer food chain, phytoplankton sustains pelagic organisms at higher trophic levels. As observed above, spatial gradients in phytoplankton concentration are positively related to zooplankton ($r=0.63$, $p<0.0001$), suggesting that phytoplankton biomass strongly influence zooplankton via bottom-up control (Figures 6B and 6C). The non-linear nature of the relationship may relate to different

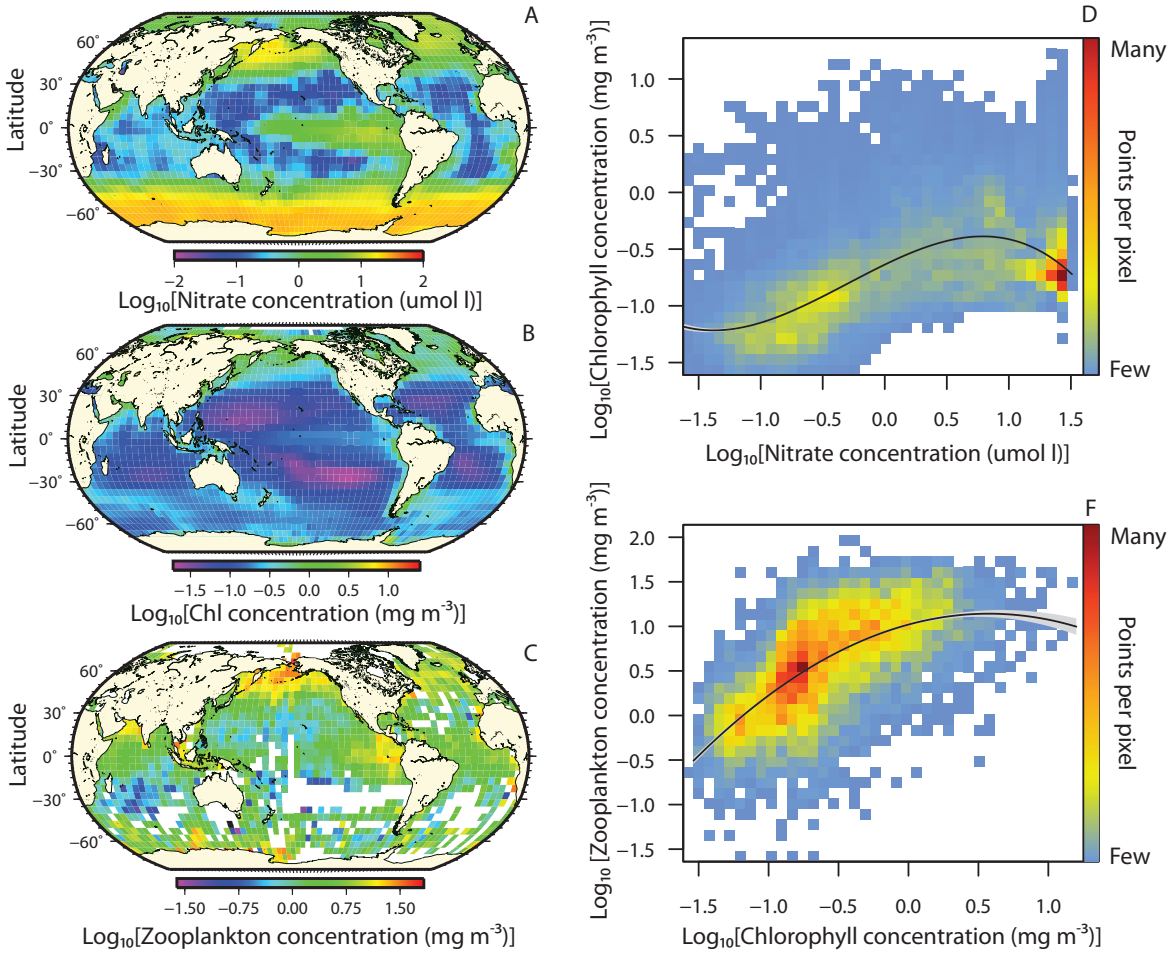

Figure 7.6: Global scaling of phytoplankton, zooplankton, and nutrient concentrations.

Averaged nitrate (A), Chl (B), and zooplankton (C) concentration per 5° x 5° cell depicted as colors. White represents areas with no data. (D) Chl as a function of nitrate, and (E) zooplankton as a function of Chl. All variables are (log10)-transformed average concentrations per 1° x 1° cell. Colors depict the number of measurements per pixel. Relationship in (D) was best approximated by a polynomial function and relationship in (E) by a quadratic function. Shading represents the 95% confidence limits.

controls of zooplankton across ecosystems. For instance, consumers may have strong effects on grazers in some ecosystems, while phytoplankton availability may dominate in others. We were unable to determine empirically if these observed relationships (Figures 7.6B and 7.6C) were maintained between adjacent higher trophic levels, but the strong positive relationship between zooplankton and fish for both the larval and adult stages is well-established (Lasker, 1975; Cushing, 1990; Beaugrand et al., 2003). Additionally, bottom-up linkages between phytoplankton primary production, zooplankton, and fish catches have been observed at regional (Ware and Thomson, 2005; Chassot et al., 2007) and global (Chassot et al., 2010) scales. Such correlations do not necessarily imply causation, but support the hypothesis that phytoplankton biomass sets the carrying capacity of the grazer food web via bottom-up control (Figures 7.6B and 7.6C).

However, other approaches have been used to show strong bottom-up regulation of the grazer food web by phytoplankton affecting such taxonomically distant organisms as leatherback turtles (Saba et al., 2008), octopuses (Otero et al., 2008), seabirds (Frederiksen et al., 2006), and fishes (Richardson and Schoeman, 2004). Phytoplankton concentrations also influence higher trophic levels via changes in the timing and magnitude of phenological cycles (Hjort, 1914; Cushing, 1990). Observational studies have demonstrated that the amount, species composition, and timing of phytoplankton blooms can strongly influence the survival of larvae and the subsequent population size of fish (Lasker, 1975; Platt et al., 2003). Such phenological changes in the concentration and quality of phytoplankton may be manifest as temporal changes in overall biomass and can also affect ecosystem structure from the bottom-up (Edwards, 2004).

Deep-sea ecosystems are almost entirely sustained by the rain of particulate organic matter (POM) from surface waters, the majority of which is produced by phytoplankton (Ruhl et al., 2008). The downward flux of particulate organic carbon (POC) accounts for up to 67% of deep-sea benthic biomass in some regions (Johnson et al., 2007). Studies have also documented positive relationships between spatial gradients of surface chlorophyll, POC flux, and deep-sea macro-faunal abundance (Johnson et al., 2007; Ruhl et al., 2008). Phytoplankton-derived POC flux may also influence inter-specific body size distributions of deep-sea macrofauna (Ruhl et al., 2008)

and diversity of deep-sea ecosystems. There is broad consensus among physically-based models, which predict declining export production over the coming century to be driven in part by rising temperature and changes in phytoplankton biomass and community composition (Steinacher et al., 2010). The strong dependence and the already food-stressed nature of deep-sea ecosystems would likely render them particularly sensitive to such reductions in export production.

Changes in phytoplankton concentration and composition will also affect the structure and functioning of the microbial food chain or 'microbial loop' (Azam et al., 1983). This is composed of pico-phytoplankton, viruses, bacteria, and small heterotrophic protists. Although a small fraction of the primary production entering the microbial chain reaches the traditional grazer chain, the majority is recycled and re-mineralized by heterotrophic bacteria, producing inorganic matter which fuels phytoplankton growth. Ultimately, this microbial loop increases the recycling efficiency of phytoplankton and other dissolved organic matter, but reduces the amount of primary production available to both the grazer and deep-sea ecosystems. Due to size-based predation constraints (Barnes et al., 2010), the microbial loop is more prevalent in systems where pico-phytoplankton are abundant, such as in the oligotrophic oceans (Pomeroy, 1998). In addition to changes in total phytoplankton standing stock, process-based models, field, and experimental studies suggest that continued warming will lead to increases in the abundance of pico-phytoplankton (Cermeno et al., 2008; Polovina and Woodworth, 2012), expansions of the oligotrophic oceans (Polovina et al., 2008, 2011), and increased microbial metabolism (Taucher and Oschlies, 2011). Such changes may increase the relative importance and turnover rate of the microbial loop, thereby increasing overall primary production, but limiting channeling to the grazer and deep-sea food chains.

Consequences of phytoplankton change across ecosystems

Our results thus far suggest that the phytoplankton biomass places first-order constraints on the carrying capacity of ecosystems, and that large-scale changes in phytoplankton biomass would alter the average biomass of zooplankton and likely fish across marine ecosystems (Frank et al., 2005; Ware and Thomson, 2005; Chassot et al., 2007, 2010). Within such broad phytoplankton biomass-driven alterations in

carrying capacity, additional factors such as the structure of the ecosystem, the degree to which productivity is affected, altered phenology, and changes in species composition and size structure will modify the ecological response to phytoplankton biomass changes across ecosystems.

In the open ocean oligotrophic gyres phytoplankton biomass is low, and is comprised mainly of pico- and nano-phytoplankton (<2 to 20 μm diameter). Due to the constraints of size-based predation (Barnes et al., 2010), primary production in the open ocean is inefficiently channelled to higher trophic levels through numerous trophic transfers (Ryther, 1969), limiting the overall size of top predators (Norris et al., 2013). Due to low nutrient availability, efficient recycling of organic matter, and long, complex flows of primary production from producers to grazers, fishery landings per unit area and export production of open ocean ecosystems are low (Ryther, 1969); hence they are sometimes referred to as biological deserts (Polovina et al., 2008). Since the open oceans are already food-stressed, ecosystems there may be particularly sensitive to any reductions in phytoplankton biomass. Declines in overall biomass in the oligotrophic open oceans may be exacerbated by predicted temperature-driven reductions in phytoplankton diversity over the coming century (Thomas et al., 2012). Such diversity losses may alter the structure (Hooper et al., 2012) and stability (Worm et al., 2006) of open ocean ecosystems, and may further reduce primary productivity in these ecosystems through the loss of productive species (Tilman, 1996), reduced complementarity (Reich et al., 2012), or increased grazer pressure (Hillebrand, 2004). Resolving the consequences of phytoplankton changes on the oligotrophic ocean ecosystems will be important, since studies suggest past (Boyce et al., 2010, 2013), present (McClain et al., 2004; Polovina et al., 2008), and future (Polovina et al., 2011) expansions of these already vast ocean regions.

In contrast to oligotrophic waters, nearshore ecosystems are supported by an abundance of large micro-phytoplankton species ($\sim$20 to 200 μm in diameter); (Cermeno et al., 2008). These ecosystems often have shorter food chains and are thought to be more efficient, with fewer trophic transfers between phytoplankton and predators. Large blooms of rapidly sinking diatoms, slower turnover, and 'sloppy grazing' by large zooplankton result in large fluxes of POC to benthic ecosystems (Ryther, 1969; Cermeno et al., 2008; Guidi et al., 2009; Chavez et al., 2011; Norris et al., 2013).

Our results suggest that phytoplankton may have increased in most nearshore waters (Figure 7.5), likely due to human-derived nutrient input (Jickells, 1998). Increasing phytoplankton in these nearshore systems is hypothesized to have a positive effect on global fishery landings, ∼50% of which derive from nearshore and shelf systems (FAO, 2010), but may also trigger negative effects in some regions. For instance, large phytoplankton blooms are known to increase heterotrophic bacterial activity and can lead to large subsurface anoxic regions known as 'dead zones' (Grantham et al., 2004). Such effects have been linked with decreased secondary biomass and fishery yield (Diaz and Rosenberg, 2008), particularly in nearshore waters. Additionally, some phytoplankton species can form harmful algal blooms, which negatively affect secondary production and fisheries (Nixon and Pilson, 1983).

Upwelling ecosystems occur in both nearshore and oceanic waters and contain characteristics of both systems. These ecosystems are predominantly driven by the wind-driven upwelling of nutrient-rich waters, resulting in large blooms of micro-phytoplankton, which support some of the world's largest fisheries and export large amounts of POM to the deep sea. Contrary to nearshore systems, phytoplankton trends in upwelling systems are largely driven by changes in upwelling intensity as driven by changes in wind, temperature, and stratification. Any increases in TDS here would reduce total phytoplankton biomass but may have disproportionate negative effects on larger phytoplankton, which are out-competed by pico-phytoplankton under conditions of warming, stratification, or prolonged nutrient limitation (Atkinson et al., 2003; Cermeno et al., 2008; Li et al., 2009; Moran, 2010). Since large grazers in these systems are often incapable of consuming pico-phytoplankton (Sommer, 2002; Sommer and Sommer, 2006), a shift towards smaller phytoplankton may decrease the transfer efficiency of primary production through the grazer food chain (Barnes et al., 2010; Ryther, 1969; Chavez et al., 2011). These size-selective negative effects are predicted to be strongest in the North Atlantic and tropical upwelling systems, possibly due to the proportionally larger contribution of micro-phytoplankton to phytoplankton standing stock (Cermeno et al., 2008). Studies of the relationship between phytoplankton changes and fisheries landings confirm these observations, with the average effect of changing Chl on fish yield being strongest in upwelling, temperate, and nearshore marine ecosystems (Ware and Thomson, 2005; Chassot

et al., 2007, 2010). Although model predictions for upwelling systems are variable and uncertain (Wang et al., 2010), many predict temperature-driven future declines in phytoplankton biomass and size (*i.e.* Henson et al., 2010; Steinacher et al., 2010). Such changes are hypothesized to have strong and negative effects on productivity.

Case study: Ecological effects of climate-driven phytoplankton variability

Some of the clearest examples of the drivers and ecological consequences of marine phytoplankton change stem from studies of the effects of transient climate variability on marine ecosystems (Barber and Chavez, 1986; Chavez et al., 1999; Behrenfeld et al., 2006; Martinez et al., 2009). Climate fluctuations wax and wane over short time scales, and hence represent 'natural experiments' which can be used to examine the drivers and consequences of climate-driven phytoplankton change.

One example of the effects of climate variability propagating up the food web comes from the North Sea (Aebischer et al., 1990). Here, the positive correspondence between standardized long-term (1955 to 1987) time series of westerly weather, phytoplankton, zooplankton, herring *Clupea harengus*, and breeding success of kittiwakes *Rissa tridactyla*, suggests that environmental effects are transmitted up the food chain. Although the study accounted for the influence of weather patterns, the potential effects of periodic climate variability were not realized at the time. The North Atlantic Oscillation (NAO) is a major mode of climate variability in the region and is characterized by shifting patterns of westerly wind and SST between 40° and 60° N. Although the mechanisms are unresolved, the NAO is negatively related to the concentrations of phytoplankton (Boyce et al., 2010) and zooplankton (Fromentin and Planque, 1996) in the North Atlantic. Alternatively, the Atlantic multi-decadal oscillation (AMO) may be the dominant mode of climate variability in the Atlantic Ocean (Martinez et al., 2009; Chavez et al., 2011). The AMO captures low-frequency (20- to 40-year cycle) SST variability in the North Atlantic Ocean and is positively related to marine phytoplankton concentration in the region (Martinez et al., 2009). To further examine the interplay between climate and ecosystem structure, we extracted time series of westerly weather, phytoplankton, zooplankton, herring, and kittiwake chicks (Aebischer et al., 1990), as well as time series for the NAO and AMO. All series were smoothed to remove any high-frequency variability and re-scaled such that

they ranged over the same interval (see Appendices for data source and full methods). Westerly weather was smoothed to linearity and had a low explanatory power and was thus removed from the analysis. All series were positively related (Figure 7.7A). The AMO emerged as the strongest climate driver of observed ecological change, showing a much tighter correlation than the NAO or westerly weather. However, it is unclear if it affects the ecosystem directly through physical processes, or indirectly by changing phytoplankton concentration. For instance, zooplankton may be influenced by climate-mediated changes in phytoplankton concentration, or by climate-mediated changes in ocean currents.

To more quantitatively address this issue, we examined the linear correlation between all series. If climate is driving consumer abundance via changes in phytoplankton, the correlation between adjacent trophic levels should be stronger than between individual trophic levels and climate. Using this simple approach, we observed strong evidence of bottom-up effects mediated by the influence of climate on phytoplankton (Figure 7.7B). Climate indices were the strongest predictors of phytoplankton concentration. For example, the AMO shows almost perfect positive correlation (NAO: r=-0.596; AMO: r=0.998). Zooplankton and herring were best predicted by the concentration of phytoplankton on which they graze (zooplankton: r=0.961; herring: r=0.781). Lastly, the number of Kittiwake chicks was most strongly predicted by their primary food source, herring (r=0.989). While these correlations do not imply causation, they do provide observational support for the hypothesis of climate-induced control of the ecosystem, and suggests that long-term changes in phytoplankton could cascade up the food web, ultimately influencing apex predators and humans. The strong influence of the AMO particularly highlights the importance of temperature variation in determining phytoplankton concentration in the upper ocean.

7.5 Summary and Outlook

Our analysis suggests that estimates of changes in marine phytoplankton over the past century have been variable, with this variability related to the number of observation platforms used and the time period over which the trend was estimated. Generally, we observed declines in studies conducted over longer time scales, in the open oceans, and at higher latitudes. Phytoplankton increases tended to occur in

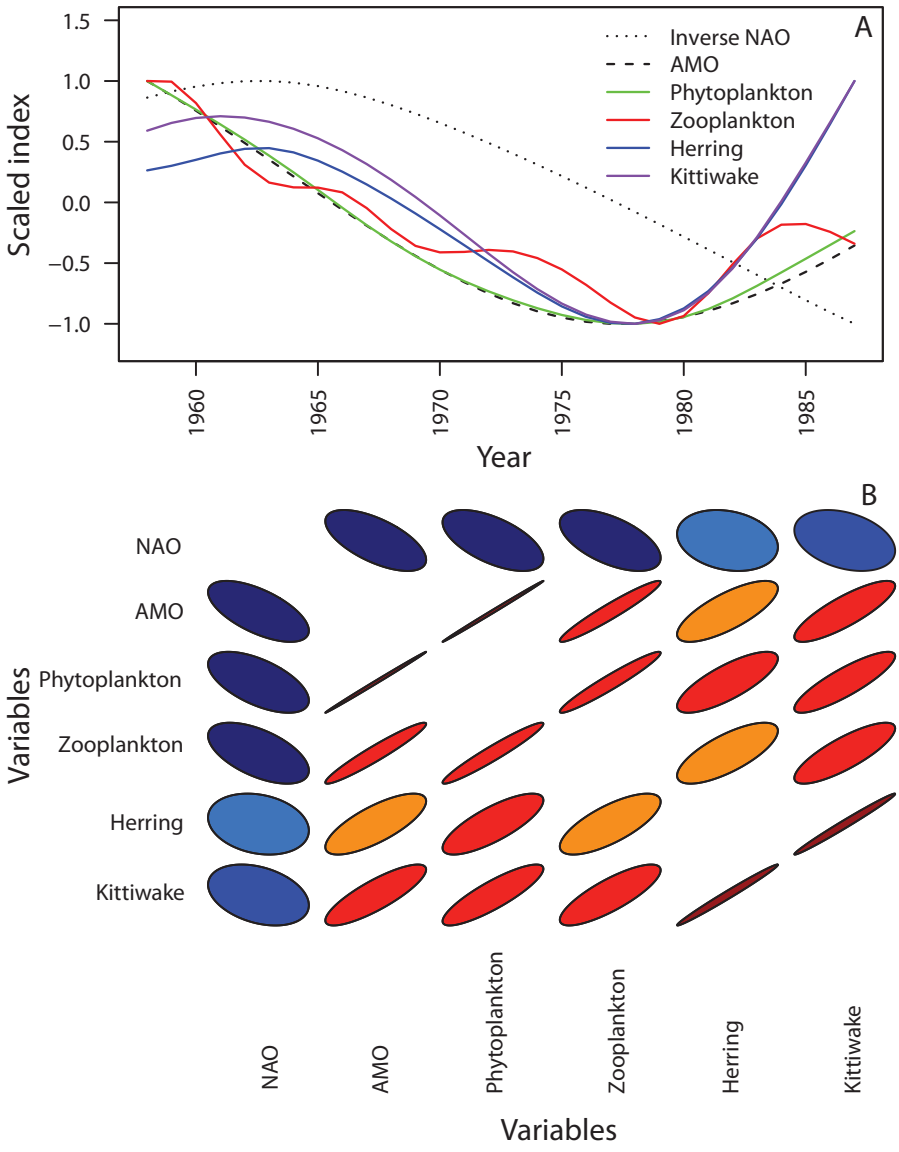

Figure 7.7: A bottom-up cascade driven by low-frequency climate effects on phytoplankton.
(A) Time series of climate and abundance across multiple trophic levels in the North Sea. Dashed lines represent climate indices and colors depict different trophic levels within the food web. Biological time series were extracted from Aebischer et al., (1990). Series were smoothed and normalized between -1 and 1 (see Appendices for full details). (B) Linear correlation between time series of climate and abundance presented in (A). The shape and color of the ellipses represent the strength and direction of the relationships. Blue depicts negative relationships and red depicts positive relationships. Flatter ellipses represent stronger relationships. White represents correlations of 1.

studies that concerned recent time periods, and were conducted in nearshore waters. Regionally, our analysis suggests that phytoplankton concentrations have declined across the North and Equatorial Pacific Oceans and at high latitudes, and increased in the South Indian Ocean. Estimates of change in the North Atlantic Ocean and in the Southern Hemisphere were highly variable, emphasizing the need for consistent measurements spanning multiple decades (Henson et al., 2010; Saulquin et al., 2013). While empirical estimates vary, most predictive models suggest that global phytoplankton concentrations will decline over the coming century (Table 7.3). Despite increases at high latitudes and in nearshore waters, future global phytoplankton declines are dominated by phytoplankton declines across the low- and mid-latitude oceans, and in the open oceans, where 82% of annual global ocean primary production occurs (Ryther, 1969).

Multiple lines of evidence suggest that SST is a dominant driver of contemporary phytoplankton changes. Increasing SSTs are predicted to induce shifts in phytoplankton diversity (Thomas et al., 2012), phenology (D'Ortenzio et al., 2012), species composition (Cermeno et al., 2008; Li et al., 2009), and expanding 'desertification' of the oceans (Polovina et al., 2008, 2011). The pathways by which temperature changes influence phytoplankton are multifarious, but temperature-driven stratification (TDS) emerges as a strong driver of global phytoplankton change over the geological record (Schmittner, 2005) and contemporary (Boyce et al., 2010) and future (Henson et al., 2010; Hofmann et al., 2011; Olonscheck et al., 2013) time horizons. This is supported by process-based models, which predict global declines in phytoplankton and primary production over the coming century, driven by TDS phytoplankton declines across the low- and mid-latitude oceans if the current rate of ocean warming is unabated (Schmittner et al., 2008; Steinacher et al., 2010; Hofmann et al., 2011). Warming is also shifting the balance of autotrophic to heterotrophic metabolism, which may exacerbate (O'Connor et al., 2009; Olonscheck et al., 2013) or counterbalancing (Taucher and Oschlies, 2011) any declines in biomass driven by TDS.

Such changes will likely propagate up the ocean food web and have large effects on the structure and functioning of both pelagic and deep-sea ecosystems. Declines in phytoplankton will reduce the overall carrying capacity of marine ecosystems, but this

will play out differently across regions. A robust examination of future phytoplankton change and the ecological consequences therein will depend on better resolving critical uncertainties, such as the influence of consumers on marine phytoplankton, the net effect of changing metabolic rates in a warmer ocean, and the effects of size-restructured phytoplankton communities on ecosystem functioning. Further, despite ample evidence to suggest strong biological effects on phytoplankton via trophic control or environmental conditioning, the scarcity of consistent, long-term measurements of consumer abundance across trophic levels limits any rigorous analysis of their relevance as drivers of long-term phytoplankton change. Such challenges and limitations may explain why relatively few studies have considered the importance of such effects. Further investigation may be facilitated by combining process-based models with experimentation and field observation.

7.6 Acknowledgements

We are very grateful to all data providers, and to Dr. Kenneth Frank for providing helpful comments and suggestions. Funding was provided by the Natural Sciences and Engineering Research Council of Canada.

Chapter 8

Conclusions

The overarching goal of this thesis was to better understand the nature, causes, and consequences of long-term changes in marine phytoplankton standing stock over the past century. In this final chapter, I attempt to synthesize the major findings of my thesis. Firstly, I will summarize the results of my thesis and interpret these in the context of previous work. Next, I will discuss the possible policy or management implications of my thesis research. Lastly, I will identify some remaining knowledge gaps in this field and discuss some directions for future work.

8.1 Thesis Summary

8.1.1 Publicly Available Databases

In chapters chapter 2 (*Global phytoplankton decline over the past century*) and 3 (*Integrating global chlorophyll data from 1890 to 2010*), I generated long-term, global Chl databases that are available for public use. To achieve this, all available shipboard measurements of upper ocean Chl, ocean colour, and transparency collected throughout the global ocean since from 1890 to 2010 were inter-calibrated and standardized. A range of sensitivity analyses and comparisons against widely used satellite remote sensing measurements of Chl were undertaken and suggested that the Chl values in this database were strongly correlated with Chl from SeaWiFS (r=0.81; ranged major axis slope=1). While publicly available databases of oceanographic measurements are now increasingly common, those generated during my thesis are currently the longest running and most spatially comprehensive available; the measurements span over 120 years in some locations and are globally distributed. This information within these databases represents millions of individual measurements painstakingly collected by hundreds of ocean-going marine researchers. The databases provide a much-needed resource, which may be used by the scientific community to explore phytoplankton

dynamics over the pre-satellite era. The use of such data will be a key component of understanding long-term changes in phytoplankton, particularly as the available satellite record is still decades too short to separate secular change from transient climate-driven variability (Beaulieu et al., 2013; Henson et al., 2010).

8.1.2 Changes in Phytoplankton Standing Stock over the Past Century

In chapter 2 (*Global phytoplankton decline over the past century*) and chapter 4 (*Global chlorophyll changes over the past century*) I estimated the nature and magnitude of marine phytoplankton (as indicated by Chl) change over the past century. Trajectories of Chl change were estimated across spatial scales ranging from local ($\sim$1000 km^2) to regional (ocean basin), using generalized additive models. Estimating Chl trends at local spatial scales revealed increasing Chl trends across the tropical warm pool region, throughout the Indian Ocean, in the Northeast Atlantic Ocean, and in closer proximity to coastlines. Alternately, large swaths of declining Chl trends were observed across most of the Atlantic Ocean, in the Western Pacific, and in the open oceans. These local scale estimates of change were generally consistent with the regional-scale estimates, which indicated Chl increase in the South Indian, and Northeast Atlantic regions and decline in the Arctic, Northwest Atlantic, Equatorial Atlantic, South Atlantic, North Pacific, and Equatorial Pacific regions. Estimates of change for the North Indian and South Pacific were particularly variable and uncertain, likely due to the limited amount of measurements available. These local- and regional-scale estimates corresponded to an average global Chl decline of between -0.0066$\pm$0.001 and -0.0009$\pm$0.0027 mg m^{-3} yr^{-1} over the past century. Although the direction of global Chl change was insensitive, the magnitude of change was dependent upon the method of spatial aggregation and the statistical weighting used. Thus, although an overall conclusion of Chl decline is supported, the precise magnitude of this decline remains uncertain.

Alternate empirical estimates of Chl change over the 20^{th} century have been interred from *in situ*, ocean colour, or remote sensing observations, but are different in spatial and/or temporal scope to my estimates making comparisons difficult (Antoine et al., 2005; Behrenfeld et al., 2006; Gregg and Conkright, 2002; Gregg et al., 2003; Montes-Hugo et al., 2009; Raitsos et al., 2005; Reid et al., 1998). Published

long-term (∼80 to 100 years) estimates derived from ocean transparency or Forel-Ule measurements in the North and Equatorial Pacific Ocean are similar in direction and magnitude to mine and suggest sustained phytoplankton declines over the past century (Falkowski and Wilson, 1992; Wernand et al., 2013). Observed Chl changes across the North Atlantic (>40° N) agree with long-term (∼50 years) continuous plankton recorder (CPR) derived changes from the North Sea and Northeast Atlantic (Raitsos et al., 2005; Reid, 1975; Reid et al., 1998), but are at odds with estimates from the Central Northeast Atlantic (∼52° to ∼58° N and ∼10° to ∼20° E). My estimates in the North and Equatorial Atlantic Ocean are also at odds with large, and possibly unrealistic increases derived from Forel-Ule measurements. However, it is worth noting that comparisons with these alternate estimates of phytoplankton change should be interpreted with caution. For instance, the CPR only retains the largest plankton cells (>270 μm) and under-samples smaller cells (Dippner and Krause, 2013). The spatial and temporal resolution of the Forel-Ule-, and CPR-derived trends are also different to mine, which may explain some of the discrepancy. Indeed, the observationally-based estimates of phytoplankton change presented in this thesis are among of the most spatially and/or temporally extensive available in the scientific literature to date (Figure 8.1), making any comparisons difficult. However, the availability of phytoplankton measurements over the past century may continue to grow, possibly allowing for further validation.

8.1.3 Drivers of Observed Marine Phytoplankton Change

In chapter 2 (*Global phytoplankton decline over the past century*), I observed strong correspondences between several leading inter-annual to multi-decadal climate oscillations and Chl trends at the scale of ocean basins. Previous to this, the relationship between Chl and the El Niño Southern Oscillation were firmly established, but the effect of climate variability on phytoplankton in other ocean basins and over longer-timescales were unknown.

These findings, in combination with studies using contemporary remote sensing time-series (Behrenfeld et al., 2006; Martinez et al., 2009) have highlighted the importance of climate variability in driving short-term marine Chl trends and have further

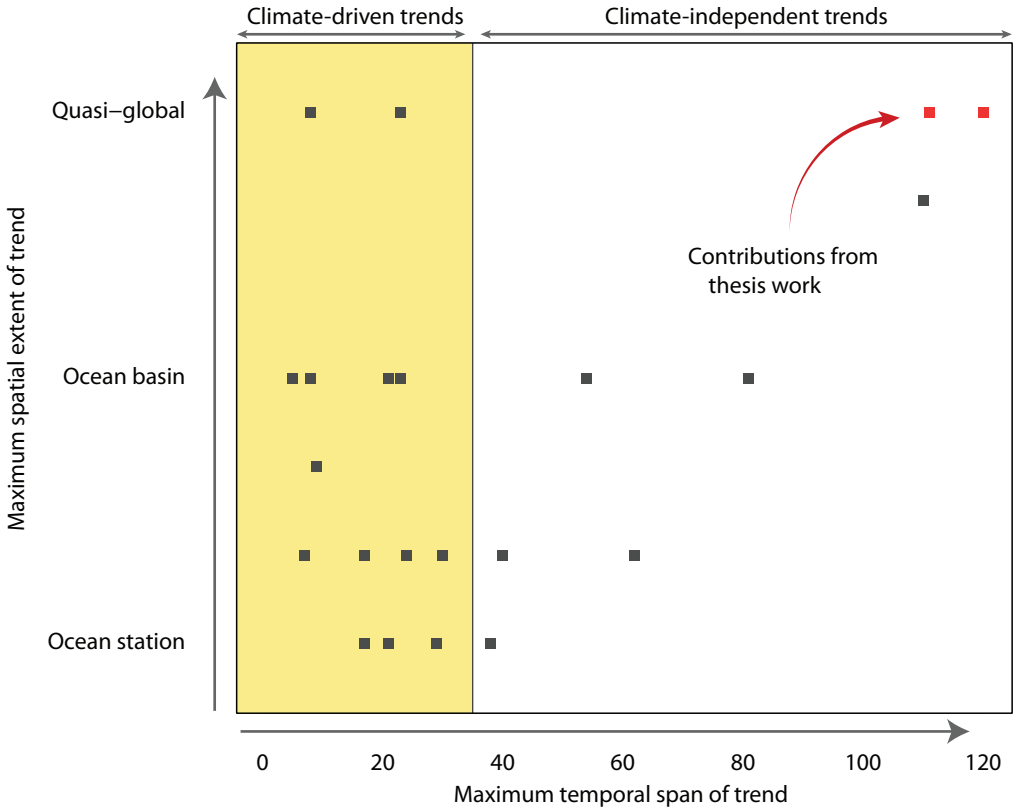

Figure 8.1: Contribution of thesis trend analyses to our understanding of phytoplankton change.
Points are the maximum spatial (*x-axis*) and temporal (*y-axis*) extent of available published estimates of phytoplankton change from chapter (7). Trend estimates within the yellow shaded region may be strongly influenced by transient climate variability, while estimates within the white are more likely to represent sustained climate-independent changes. Estimates of phytoplankton change derived in this thesis are denoted in red.

emphasized the need for continuous, long-term time-series to accurately resolve sustained climate-seperable trends (Beaulieu et al., 2013; Henson et al., 2010; Saulquin et al., 2013). As highlighted in my chapter 7 analysis, the majority of published estimates of phytoplankton change span less than 20 years, and therefore may not represent sustained long-term change (Figure 8.1).

In chapters 2 (*Global phytoplankton decline over the past century*), chapter 5 (*Oceanographic drivers of chlorophyll change over the past century*) I used a comprehensive suite of long-term oceanographic variables and integrated climate indices to explore the factors driving temporal Chl change over the past century. The correspondence between estimated long-term changes in oceanographic variables and Chl were quantitatively examined. Subsequent to this, the strength of oceanographic variables in explaining Chl variability before and after accounting for different sources of variability was estimated. Using this approach, sea surface temperature (SST) emerged as the strongest single correlate of Chl change via spatial, seasonal, climate, stochastic, and inter-annual forcing. My analyses revealed a strong latitudinal pattern to the SST effects on Chl, which co-varied to those of wind, mixed-layer depth, and stratification. This suggested that rising SST negatively influences Chl by intensifying vertical stratification and reducing nutrient delivery at low- and mid-latitudes, where phytoplankton growth is strongly driven by the rate of mixing which delivers nutrients from deeper waters. At higher latitudes, where waters are already well mixed, rising SSTs had weak positive effects on Chl. The SST-induced stratification effects on phytoplankton were generally weaker in nearshore waters, where land-based processes are a stronger determinant of phytoplankton growth (Jickells, 1998).

These observations are consistent with analyses of satellite observations (Behrenfeld et al., 2006; Martinez et al., 2009) and models (Hofmann et al., 2011; Schmittner et al., 2008; Steinacher et al., 2010) which have also observed or predicted negative effects of rising SSTs on phytoplankton via stratification and nutrient flux. Satellite observations also suggest that this mechanism is inducing an expansion of the lowest productivity 'deserts' of the ocean (McClain et al., 2004; Polovina et al., 2008), a trend which is projected to continue over the next century (Polovina et al., 2011). Rising SSTs are also predicted to induce shifts in phytoplankton diversity (Thomas et al., 2012), phenology (D'Ortenzio et al., 2012), and species composition (Cermeno

et al., 2008; Li et al., 2009). The negative effects of rising SSTs on phytoplankton via stratification will possibly be exacerbated by increased grazing pressure as heterotrophic metabolism will speed up (O'Connor et al., 2009). However, increasing SSTs may lead to faster turnover rates of phytoplankton and the microbial loop, which may modify or outweigh the effect of temperature on grazing rates (Taucher and Oschlies, 2011). There is evidence that rising SSTs will influence marine phytoplankton both by changing nutrient supply (physically forced) and metabolic rates (biologically forced), however it is unclear what the magnitude of the effects will be or how they will interact.

Based on the above condition, in chapter 6 (*Effects of sea surface warming on marine plankton*) I worked collaboratively at the GEOMAR facility in Germany to explore the effects of ocean warming on a plankton community. To complement the correlative approaches used in chapters 2 and 5, I used theory and experimentation to separate different mechanisms by which SST affects phytoplankton. The POTSMOM-C ocean general circulation model was run to project ocean temperature and nutrient changes between 1800 and 2100. These changes were then implemented as temperature and nutrient treatments to mimic the physically-mediated of nutrient limitation via stratification, as well as biologically-mediated effects of SST on plankton metabolic rates. A large mesocosm experiment containing a natural plankton community of bacteria, heterotrophic nanoflagellates, phytoplankton, and zooplankton was run over a 6 week period. Using this approach, we found that the effects of SST on phytoplankton were dependent upon the nature of the ecosystem. In nutrient-limited systems the effect of rising temperature on nutrient delivery was dominant. This is consistent with empirical (Behrenfeld et al., 2006; McClain et al., 2004; Polovina et al., 2008) and process-based studies (Polovina et al., 2011), which have found strong temperature-driven stratification effects on phytoplankton in oligotrophic systems, such as the ocean gyres. In nutrient-replete systems, the effect of rising temperature on grazing pressure was stronger. This is consistent with empirical studies, which have observed strong grazing effects triggered by increased nutrient availability, such as during phytoplankton blooms (Loeb et al., 1997; Sommer and Lengfellner, 2008). However, in both nutrient-limited and replete systems, the overall effect of increasing SST on phytoplankton was negative. This work emphasizes

the strength of merging experimental and theoretical modeling approaches to better understand the mechanistic underpinnings of any correlations and patterns observed in field data.

8.1.4 Thesis Results in the Context of the Oceans' Past and Future

My estimates of global phytoplankton decline over the past century using observational measurements are generally similar to predictions of phytoplankton changes over the next century using process-based general circulation models. Although the models generally agree on the direction of global phytoplankton change, the magnitude and spatial patterns of predicted change are highly variable (*i.e.* Henson et al., 2010; Steinacher et al., 2010). Most studies predict increases in phytoplankton concentration and primary production at high latitudes but widespread declines across low- to mid-latitudes and in the open oceans (*i.e.* Henson et al., 2010; Polovina et al., 2011; Steinacher et al., 2010). This is partially at odds with my results, which suggest sustained declines in phytoplankton concentration at high latitudes. Similar to empirical analyses, process-based model estimates of phytoplankton change in the North Atlantic Ocean are also highly variable. The North Atlantic is a dynamic ocean, strongly influenced by human use (Frank et al., 2011, 2005; Roman and Palumbi, 2003), and resolving phytoplankton change here appears to be particularly challenging. Similar to my thesis results, models suggest that if unabated, rising temperatures will drive global phytoplankton decline over the next century. Particularly, rising temperatures are predicted to reduce the productivity of vast areas in the open oceans (Polovina et al., 2011; Steinacher et al., 2010), and cause a shift towards smaller phytoplankton species (*i.e.* Moran, 2010; Woodworth-Jefcoats et al., 2013). Lastly, while process-based models are valuable for exploring physical forcing and future changes in marine phytoplankton, they are limited in some respects. For instance, with few exceptions (*i.e.* Olonscheck et al., 2013; Taucher and Oschlies, 2011), such models do not account for any biological effects, which may also drive observed phytoplankton change (Frank et al., 2005; Sommer and Lengfellner, 2008). These models also require assumptions regarding important, but unknown parameters, which may have large effects on the predictions and render them highly subjective. For instance, the variation in the assumed biological temperature-sensitivity within these models may

induce large changes in both the direction and magnitude of predicted phytoplankton trajectories (Taucher and Oschlies, 2011).

It is also important to interpret phytoplankton change over the past and coming centuries in the context of changes which have occurred over geologic or 'deep' time. Studies suggest that phytoplankton changes over geologic time are strongly driven by processes operating over longer timescale than those encompassed by the observational record used in this thesis. Such processes include, for instance, nutrient inputs by rock weathering, plate tectonics, change in the thermohaline circulation (Sachs and Anderson, 2005), or insulation cycles (Beaufort et al., 1997). The phytoplankton trends estimated in my thesis over the past century are also influenced by these slowly evolving processes. As such, the phytoplankton trends explored in my thesis as well as future trends over the coming century may be regarded as transient in the context of deep time.

While temporal phytoplankton trends over the past century and those over the deep time are not strictly comparable, insight can be gained by examining the influence of climate on phytoplankton and ecosystem structure over past eras. For instance, comparing past periods of warming and cooling allows for a 'natural experiments' whereby the effects of temperature on phytoplankton and other processes may be explored. One such comparison has been made between the warmer 'greenhouse' world (34 to 66 Ma), and the colder 'icehouse' world (0 to 34 Ma); (Norris et al., 2013). During the greenhouse world, when maximum ocean temperatures reached 34 °C, the oligotrophic gyres were larger than today, and ecosystems there were largely based on small phytoplankton cells, which limited the size of top predators (Norris et al., 2013). Organic matter was tightly cycled in these systems, thus reducing export production and limiting the carrying capacity of deep sea ecosystems. Subsurface anoxic zones were also likely more expansive than today. In the icehouse world, when maximum temperatures reached 31 °C, marine ecosystems were supported by larger phytoplankton cells (diatoms) which resulted in shorter food chains, with greater export production. The diatom-based food chains are believed to have fueled the recent diversification of whales, seals, fish, and seabirds (Fulton and Strobeck, 2010; Houben et al., 2013; Norris et al., 2013). Similar to my thesis results and predictive

models, temperature-driven stratification was a driver of phytoplankton declines during such past periods of warming (Norris et al., 2013; Vermeij, 2011). Such effects of increasing SST on marine systems are consistent with those over the past century and predicted into the future, and provide robust evidence that temperature is a leading driver of marine phytoplankton change.

8.1.5 Consequences of Changing Marine Phytoplankton Standing Stock

Due to the many interactive pathways by which phytoplankton influences climate processes, ecosystem dynamics, and biogeochemical cycles (Figure 8.2), predicting the consequences of a long-term decline in phytoplankton standing stock is extremely challenging. The ecological consequences of changing phytoplankton concentration will vary regionally, but documented effects include altered species composition and abundance across multiple trophic levels (Aebischer et al., 1990), effects on fisheries yield (Chassot et al., 2010), and changing patterns of export productivity (Steinacher et al., 2010). Declining phytoplankton trends may have particularly strong effects on the oligotrophic open oceans or deep-sea ecosystems, which are already tightly constrained by bottom-up processes. The ecological consequences of changing phytoplankton will also depend on changes in phytoplankton community composition, which is a strong determinant of ecosystem structure and export production (Barnes et al., 2010; Rodriguez et al., 2001; Ryther, 1969). Global changes in phytoplankton concentrations will also have important effects on climate systems, but again, the exact nature of these effects is unresolved. By contributing a large fraction of export production, phytoplankton production influences the oceanic drawdown and possible sequestration of atmospheric CO_2. Declining phytoplankton may lead to reduced pumping to the deep sea and more CO_2 in the atmosphere, with effects on climate systems (Falkowski, 2012). By producing dimethylsulphide, phytoplankton may also have effects on marine cloud formation (Charlson et al., 1987; Quinn and Bates, 2011). While the exact magnitude of such effects remain unclear (Quinn and Bates, 2011), long-term declines in phytoplankton may lead to altered cloud formation, with corresponding effects on albedo and upper ocean penetrative radiation. Since increasing temperatures are negatively related to phytoplankton concentration over much of the oceans, such changes may lead to a feedback on phytoplankton.

While it is clear that a sustained decline of phytoplankton standing stock over the past century will have certain effects on ecosystem dynamics and climate systems, the magnitude of these effects is unclear. This uncertainty provides strong motivation to increase our phytoplankton observational capabilities in order to better understand the consequences of phytoplankton change.

8.1.6 Caveats

The use of Chl as an indicator for phytoplankton biomass is widespread, yet the C-to-Chl relationship is non-linear and subject to the influences of light, nutrients, and temperature (Geider, 1987). Variation in the C:Chl ratio often occurs in the context of 'acclimation' to changing conditions, e.g. over a seasonal cycle. Although models to correct for acclimation exist, their applicability over the time scales encompassed by this thesis is constrained by data availability. However, with all other factors held constant, increasing temperatures are predicted to result in an overestimation of phytoplankton C biomass from Chl due to a reduced C:Chl ratio; (Eppley and Sloan, 1965; Eppley, 1972). In the context of my thesis findings, this suggests that as temperatures have risen over the past century (Levitus, 2000), the estimated Chl declines over this same period may be biased upward relative to phytoplankton C, thus potentially rendering our estimated global rates of decline conservative. This is, however, based on the strong assumption that SST has increased as other influential variables such as light, and nutrients have remained constant. This is certainly an unrealistic assumption in nearshore waters, where nutrient deposition has increased (Jickells, 1998). While efforts are being directed towards developing more accurate assessment methods (Siegel et al., 2013), Chl remains the most and best available metric to assess phytoplankton biomass changes over large spatial scales and multi-decadal time scales.

In this thesis, I compiled a database of Chl observations spanning 120 years in some locations and distributed globally. To accomplish this, measurements of ocean Chl and transparency were inter-calibrated and combined into a single database. The Chl and transparency observations were available at different spatial and temporal densities, and our trend analysis was based on the assumption that the relationship

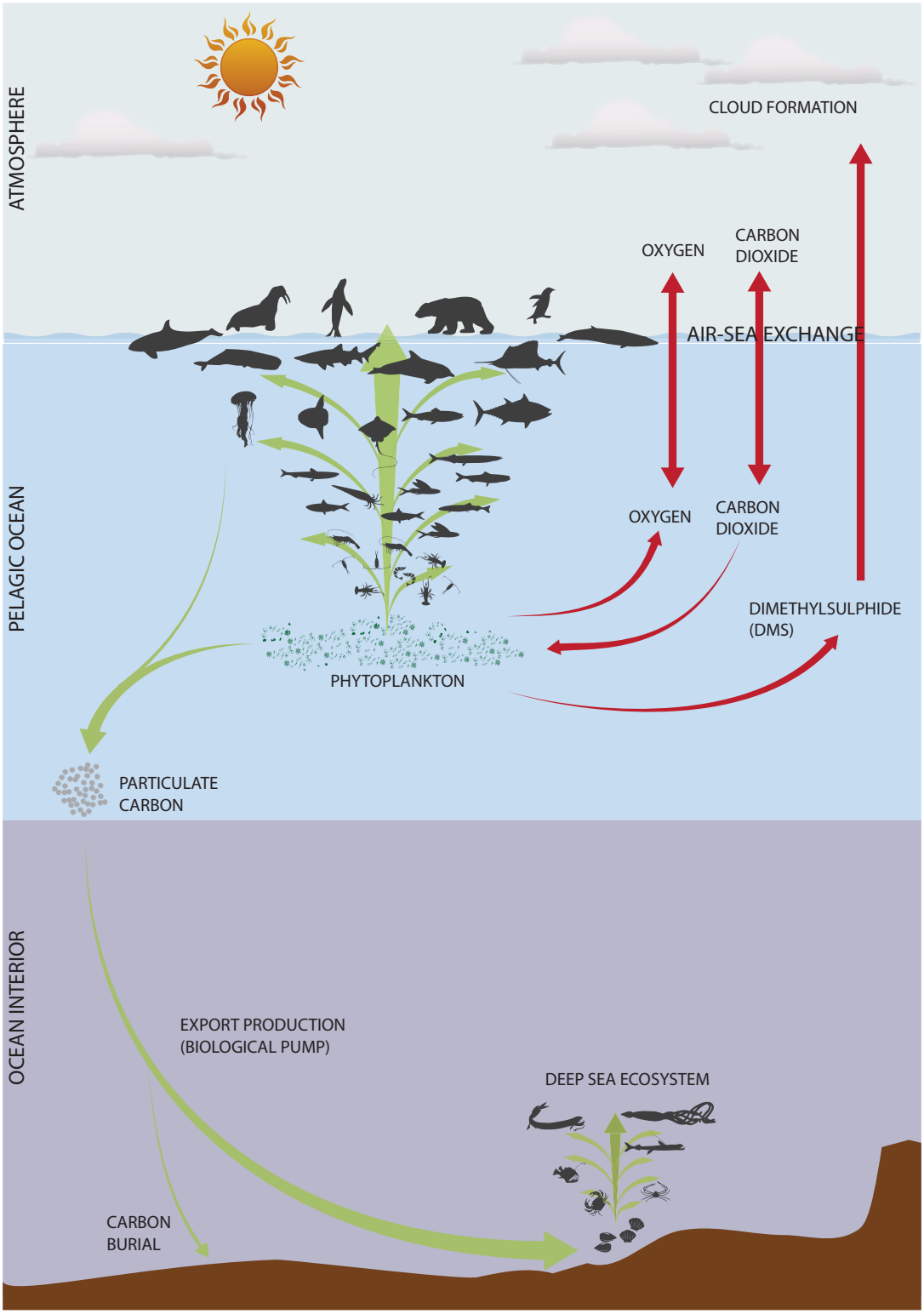

Figure 8.2: Ecosystem linkages of marine phytoplankton.
The organic matter generated through marine phytoplankton photosynthesis (green arrows) sustains virtually all marine ecosystems, as well as influencing ocean-atmosphere processes (red arrows).

between them was constant at all times and locations. In chapters 2 to 4, I performed a range of analyses and sensitivity checks which suggested that combining Chl and transparency observations did not influence the trend analysis. Despite this, corresponding Chl and transparency matchups were unavailable for many times and locations and it was thus impossible to directly test this assumption for some regions.

Despite the comprehensive spatial and temporal coverage of the Chl database generated in my thesis, many spatial locations and time periods remain under-sampled. Notably, measurements were less available prior to 1950, in the Southern Hemisphere, and in waters further from coastlines. The greater uncertainty of our estimates in these times and locations were accounted for as much as was possible in our analyses, and sensitivity analyses were undertaken to explore the robustness of our analyses. Despite this, yet the effect of under-sampling on the estimated trends could not be directly quantified and may influence the accuracy of the analysis.

8.2 Management Implications

Several potential management or policy implications emerge from this thesis. Although some of these are discussed in the individual chapters, I will briefly expand upon them here.

The consequences of the century-long decline of marine phytoplankton observed here may be of interest to marine managers and policy makers alike. Because the activities of phytoplankton are influential in many global processes, several of which are connected, the exact consequences of declining phytoplankton are difficult to predict. However, reduced phytoplankton concentrations are predicted to reduce the aggregate biomass available to fisheries (Chassot et al., 2010, 2007; Ware and Thomson, 2005), and altered ecosystem structure and function. The aggregate effect of phytoplankton declines on climate are likewise difficult to predict since changes in phytoplankton may influence carbon sequestration (Pollard et al., 2009), solar radiance distribution (Murtugudde et al., 2002), and marine cloud formation (Charlson et al., 1987; Quinn and Bates, 2011). This broad importance of phytoplankton coupled with the poorly constrained consequences of changing phytoplankton concentrations should provide a strong incentive for managers and policy makers to better monitor marine phytoplankton stocks.

One possible method of mitigating declining trends in marine Chl observed in this thesis and predicted into the future (Beaulieu et al., 2013; Henson et al., 2010; Hofmann et al., 2011; Olonscheck et al., 2013), would be to mitigate rising ocean temperatures. Throughout my thesis, I observed consistently negative effects of rising sea surface temperature on phytoplankton. Such negative effects of rising SST on phytoplankton have also been estimated over contemporary, (Behrenfeld et al., 2006; Li et al., 2009; Polovina et al., 2008; Thomas et al., 2012), geological (Finkel et al., 2005; Vermeij, 2011), and predicted future eras (Henson et al., 2010; Olonscheck et al., 2013; Steinacher et al., 2010). Although these effects were weaker or positive at high latitudes, the overall global effect or rising temperature was negative. (Chavez et al., 2011; Ryther, 1969). Additional temperature-driven shifts towards smaller phytoplankton species have also have effects on fisheries by limiting to overall size of marine predators (Norris et al., 2013). Sea surface temperature increases over the past century far exceed any of the previous 10,000 years (Marcott et al., 2013), and although human activities are likely contributing to this trend (I.P.C.C., 2007) the issue remains contentious and debated. Under circumstances such as this, where no consensus exists, taking the precautionary approach may be the best option. In this instance, the precautionary approach would entail taking efforts to limit future greenhouse gas emissions with the aim of mitigating global temperature increase.

In addition to mitigating declining phytoplankton trends, restoration may also be a desired objective. Particularly, the key roles of marine phytoplankton in the global carbon cycle has led some to advocate the 'fertilization' of vast areas of the ocean with iron for the purpose of stimulating phytoplankton growth and increasing carbon sequestration (Ney and Schoor, 2000). Indeed, there is strong evidence that iron availability and phytoplankton production are strongly related at regional scales over the past 1 million years (Murray et al., 2012). Contemporary studies using field measurements have also observed strong relationships between iron addition and phytoplankton (Behrenfeld et al., 1996; Martin and Fitzwater, 1988; Martin et al., 1994). However, while fertilization increases production, it is unclear how export production responds. Further, ocean fertilization has been the subject of much debate and controversy (Chisholm et al., 2001), and some rightly claim that a better understanding of the causes and consequences of altered marine phytoplankton

production is an important prerequisite to any fertilization efforts (Chisholm et al., 2001). Thus, better resolving how and why marine phytoplankton standing stocks are changing may assist policy makers in making more informed decisions regarding ocean fertilization and similar efforts.

Phytoplankton concentrations were observed to decline globally, yet increasing trends were apparent in many coastal locations and were hypothesized to be related to increases in land-based human activities and eutrophication (Jickells, 1998). Such increasing phytoplankton concentrations in coastal locations can lead to subsurface hypoxic regions or 'dead zones' and are associated with altered ecosystem structure and function. Our finding of coastal phytoplankton increase is indirectly supported by observations of an exponential increase in marine dead zones since the 1960's (Diaz and Rosenberg, 2008). Mitigating the spread of these dead zones may be possible by reducing the amount of land-based nutrient inputs.

8.3 Future Research Directions

Many interesting research questions have emerged from my thesis work. First and foremost, my thesis highlights the need for continued ocean- and space-borne observational platforms to assess marine phytoplankton abundance. As re-iterated throughout my thesis, the lack of consistently sampled and long-term phytoplankton time-series continues to severely constrain our ability to understand how marine phytoplankton is changing (Beaulieu et al., 2013; Henson et al., 2010; Saulquin et al., 2013). At the time of this thesis, the length of the currently available remote sensing Chl time-series is decades too short to accurately resolve sustained phytoplankton changes. Yet, continued space-borne monitoring is the most promising method to accurately assess future global marine phytoplankton dynamics. However, as is the case now the accuracy and validity of these remotely sensed observations will need to be verified against direct ship-based measurements. Further, Secchi depth measurements have been collected using standardized methods for over 120 years (Secchi, 1886), and provide accurate estimates of phytoplankton concentration which are closely comparable with *in situ* or remote sensing measurements (Boyce et al., 2010,

2012; Falkowski and Wilson, 1992; Lewis et al., 1988). Recent efforts to increase citizen participation in Secchi depth sampling worldwide (*i.e.* Secchi App[1]) may further increase the utility of these valuable data. Efforts such as these will ultimately enable the full and accurate resolution of long-term phytoplankton change.

Secondly, while my thesis addressed changes in marine phytoplankton standing stock and the drivers and consequences of this change, it did not explore any species-, or functional group-specific dynamics. Resolving the consequences of phytoplankton change on processes such as climate, geochemical cycles, or the structure and functioning of ecosystems will strongly depend on these species-specific dynamics. At the time of this thesis, resolving such dynamics over centennial timescales was unfeasible. However, recent methodological advances using remote sensing observations (Alvain et al., 2008, 2005; Masotti et al., 2011; Uitz et al., 2010, 2009), theoretical modeling (Bopp et al., 2005), and empirical observations (Cermeno et al., 2008) have increased our understanding of how phytoplankton functional groups are changing over contemporary timescales. These advances may pave the way for examination of these dynamics over longer and larger scales, ultimately yielding insight into the consequences of phytoplankton change.

Thirdly, in my thesis work I attempted to explore the drivers of marine phytoplankton change. Due to the limited availability of long-term, large-scale timeseries of zooplankton or fish, my analysis of phytoplankton drivers was limited to oceanographic variables which influence phytoplankton through 'bottom-up' processes. While this approach is common, grazer abundance has also been found to regulate phytoplankton abundance via 'top-down' processes in some instances (*i.e.* Frank et al., 2005). These top-down processes are less frequently explored and are thus poorly understood, but there is a pressing need to resolve the nature and relevance of top-down regulation of phytoplankton, particularly as rising ocean temperatures may increase grazing pressure (O'Connor et al., 2009).

Lastly, one of the strengths of the experimental approach is control, while one of the drawbacks is scalability. The GEOMAR facility where the experiment was run is state-of-the-art, and every attempt was made to establish a realistic representation of a plankton community. Despite this, some ecological complexities could not be

[1] www1.plymouth.ac.uk/marine/secchidisk/Pages/default.aspx

incorporated. It would be fruitful to attempt to 'scale-up' such experiments to more accurately represent the real world. Including higher trophic level predators in the experiments for instance may yield new information of the effects of warming on rates of predation and how these effects may propagate to phytoplankton. Mitigating the effects of algal wall growth on the experimental units may allow longer experiments to be run, and enable temporal community dynamics to be better resolved. Lastly, the experiment in my thesis was performed using a nearshore plankton community. Yet since 90% of the ocean is open ocean and the majority of primary production occurs there (Ryther, 1969), resolving the effects of ocean warming and climate change here will be important. Running experiments on an open ocean plankton community may be one way to achieve this.

Ultimately, fully resolving the patterns, drivers, and consequences of long-term marine phytoplankton change requires the collection and analysis of field observations. For over 120 years, scientists have invested incredible amounts of effort and expense to attain such data. Although such measurements are scattered in space and time, my thesis demonstrates that with careful and appropriate analysis, clear patterns and processes may be observable. This approach may be augmented by further experimentation, process-based predictive modelling, and examination of patterns over deep time, opening a wide arena for further investigation.

Appendices

Appendix A

Global Phytoplankton Decline Over the Past Century

A.1 Supplementary Methods

A.1.1 Overview.

An overview figure that summarizes data compilation and analyses steps and their rationale is presented as Figure A.1.

A.1.2 Chl Data Compilation.

Publicly available upper ocean transparency- and *in situ*-derived total chlorophyll (Chl) measurements were extracted from the National Oceanographic Data Center (NODC), the Worldwide Ocean Optics Database (WOOD), and the Marine Information Research Center (MIRC); (Table A.1). All duplicated Chl measurements were removed. These data were collected over the course of a century by different institutions and methods, hence their precision and accuracy may vary. The accuracy of *in situ*- (Chl_I) and transparency-derived (Chl_T) Chl concentration may be affected by several factors, including weather conditions, instrumentation, collection technique, collection depth, and temporal changes in sampling methodology. Furthermore, all Chl data sources can be subject to errors associated with data transcription and digitization. Both $Chl_T$and Chl_I data were systematically filtered to remove measurements associated with these sources of error. While some erroneous measurements may possibly persist, analysis indicates that these represent a small fraction of the total measurements and can be considered as random variation.

Only Chl_I collected in the upper 20 m were extracted. Mean Chl values were calculated over depth for each sampling cast to minimize statistical dependence. Following data extraction, we examined Chl_I to investigate the effect of collection methods on their accuracy. Chl collected using underway collection methods contained atypical

Table A.1: Details of data used.

Parameter	Organization	Temporal	Webpage
Chl	WOOD	1954-2008	wood.jhuapl.edu/wood/
Chl	NODC	1954-2008	nodc.noaa.gov/
Transparency	WOOD	1899-2004	wood.jhuapl.edu/wood/
Transparency	NODC	1899-2008	nodc.noaa.gov/
Transparency	MIRC	1899-2008	mirc.jha.jp/en/outline.html
Sea Surface Temperature	NODC/WOA	1955-2008	nodc.noaa.gov/OC5/3M_HEAT_CONTENT
Sea Surface Temperature	Met Office	1850-2009	hadobs.org/
Mixed Layer Depth	Met Office	1950-2009	hadobs.org/
Isothermal Layer Depth	Met Office	1950-2009	hadobs.org/
Bathymetry	GEBCO		gebco.net/
Coastal distance	NGDC		ngdc.noaa.gov/mgg/shorelines
Bivariate ENSO Index	NOAA	1871-2001	esrl.noaa.gov/psd/data/correlation
Multivariate ENSO Index	ESRL	1950-2009	esrl.noaa.gov/psd/people/klaus.wolter/MEI
North Atlantic Oscillation	NOAA	1950-2009	cpc.noaa.gov/products/precip/Cwlink
Indian Ocean Dipole	NOAA	1856-2007	jamstec.go.jp/frcgc/research/d1/iod
Atlantic multidecadal oscillation	NOAA	1856-2009	esrl.noaa.gov/psd/data/timeseries/AMO
Pacific Decadal Oscillation	JISAO	1900-2009	jisao.washington.edu/pdo
Arctic Oscillation	JISAO	1899-2002	jisao.washington.edu/ao
Antarctic Oscillation	NOAA	1979-2009	cpc.ncep.noaa.gov/products/precip

frequency distributions. The remainder of collection methods yielded log-normal distributions, which are more typical. Since the accuracy of underway data could not be empirically verified they were removed from the analysis (n=110,935).

All nearshore measurements (< 25 m depth or < 1 km from the nearest coastline) were removed from the analysis (n=252,640). Chl values which exceeded >50 mg m^{-3} globally or >5 mg m^{-3} in open ocean waters (> 200 m depth or >200 km from the nearest coastline) were flagged as biologically improbable outliers and removed (n=23,379). Chl measurements were also examined by their accession number (submitting institution) and cast number to determine the proportion of measurements which were outliers within each accession number and cast. If over 25% of measurements within a given accession number were flagged as questionable, all data from that accession number were removed. This same technique was applied to each individual *in situ* cast. This was aimed at removing data gathered from casts where the instrumentation might not have been calibrated correctly or from accession numbers where systematic data entry errors might have occurred.

A.1.3 Similarity of Chl Data.

For comparison, Chl_I and Chl_Twere individually binned into 0.25° x 0.25° cells. For each cell, monthly mean values were calculated individually for both Chl_I and $Chl_T$for each available year. Mean Chl values were calculated using a modified objective weighting algorithm developed for scatterometer data (Levy and Brown, 1986; Lewis et al., 1988). Spatial weighting functions were calculated as,

$$W_{S,ij} = \frac{(S^2 - sij^2)}{(S^2 + s_{ij}^2)} \tag{A.1}$$

Where S is the chosen value for the spatial distance scale (0.25°), and s_{ij} is the distance of the jth observation from the center of the ith cell. Temporal weightings were calculated as,

$$W_{T,kj} = \frac{(T_k^2 - t_{kj}^2)}{(T_k^2 + t_{kj}^2)} \tag{A.2}$$

Where T is the number of days in the kth month, and t_{kj} is the time separation of the jth observation from the center of the kth month. Weightings were combined

for each unique cell and month as,

$$Chl_{i,j,k} = \frac{(W_{S,ij} + W_{T,kj}}{2} \tag{A.3}$$

This produces weightings of 1 at the center of the grid point and middle of the month to near 0 at periphery of the cell and ends of the month. Great circle distances between observations and the center of each cell (s_{ij}) were calculated using the Haversine formula (Smart, 1960). Pearson correlation coefficients were then calculated to examine the strength of the linear relationship between Chl_I and Chl_T. Strong positive relationships were observed between mean Chl_I and Chl_T (r=0.52; P<0.001), with increasing strength through time. The linear relationship was insensitive to proximity to the coast, although the variability in Chl was slightly higher for shelf areas.

To further explore the linear scaling of these data, model II linear regression models were used (Legendre and Legendre, 1998; Sokal and Rohlf, 1995). Model II regression analysis is appropriate when both variables in the regression equation are random (*i.e.* subject to error). We log-transformed both Chl data sets in order to achieve bivariate normality and fitted major axis (MA) model II regressions to the data. If Chl estimates from the two data sources were identical, one would expect a Pearson correlation coefficient of 1, a linear slope of 1, and an intercept of 0. We observed strong linear relationships between Chl_I and Chl_T in shelf and oceanic regions, and globally (Figure A.2). To further examine spatial patterns of similarity, we extracted the standardized residuals from these regressions fitted to the entire dataset and calculated the absolute mean residual for each 5° x 5° cell. This value corresponds to the average difference between Chl_T and Chl_I,minimizing the confounding effects of spatial and temporal variation. Spatial examination of the mean residuals indicated that there was a greater discrepancy between Chl_I and Chl_T in more coastal areas (Figure A.2B). Excluding more coastal Chl_Tmeasurements had a minor effect on the linear regression statistics and the higher residual variability remained in coastal regions. Linear regression techniques were also used to examine the effects of *in situ* collection methods on the linear agreement between Chl_T and Chl_I. These differences were negligible.

Blended Chl were compared against satellite-derived Chl concentrations extracted

from the Sea-viewing Wide Field-of-view (SeaWiFS; Figure A.3A), and Coastal Zone Color Scanner projects (CZCS; Figure A.3B). Spatial patterns of the blended Chl data broadly approximated those from remote sensing radiometry and major spatial features such as the oligotrophic gyres, equatorial upwelling, and enhanced phytoplankton production in coastal and high latitude regions were well reproduced (Figure A.3C).

The similarity of Chl_T and Chl_I was also examined using regression trees. Regression trees use recursive partitioning to split data to explain the largest amount of variation possible. Regression trees were fit to each of our 10 focal regions and globally using the main model covariates and a dummy variable (β_D) corresponding to the data type (0=*in situ*; 1=transparency). This data type variable only appeared in 2 of 11 regression trees and was confined to the lowest branches, indicating that data type explained very little variation in overall Chl concentration.

A.1.4 Estimation of Chl Trends.

Trends in relative Chl concentration for each ocean region and 10° x 10° cell were estimated from blended data using generalized additive models (GAMs); (Hastie and Tibshirani, 1986). GAMs are a flexible extension of generalized linear models that allow the specification of the linear predictor (response) as a generalized linear or smooth function of covariates. This approach can be advantageous when it is suspected that the response varies as a complex non-monotonic function of covariates, or where one expects complex interactions among covariates. The application of GAMs to ecological data is rapidly growing in recently published works, especially in the field of biological oceanography (Polovina et al., 2008; Walsh and Kleiber, 2001).

A.1.5 Statistical Models

The model covariates were selected to explain the largest proportion of the variation in Chl while remaining parsimonious. Phytoplankton growth and abundance vary spatially and temporally with changes in photosynthetically active radiation and nutrient availability, among other factors. We attempted to explain variability related to these processes by including model covariates for mean seasonality (day or month of the year), the water depth of sampling locations where Chl observations were taken

(bathymetry), temporal change (year), and spatial changes (latitude and longitude).

Local-scale Chl trends were estimated by fitting individual GAMs to data in each 10° x 10° cell. For these models, we specified Chl as a linear function of year, as a smooth function of bathymetry, and as a discrete function of month of the year. Spatial Chl variability was explained by using individual smooth functions of latitude and longitude. Following this, local Chl trends for each cell containing adequate data (n=364) were estimated as follows:

$$\eta(\mu_i) = \beta_0 + \beta_1 Year_i + \beta_2 Month_i + f_1(Bathymetry_i) + f_2(Lat_i) + f_3(Lon_i) + \epsilon_i \quad \text{(A.4)}$$

where η is the monotonic link function of the expected mean Chl concentration μ_i, B_0 is the model intercept, B_i are parametric and f_i are nonparametric effects estimated from the data and ϵ_i is the model error term. A Gamma distributed error structure and a log link were used.

To estimate regional Chl trends, more abundant data within each basin-scale region (n=10) led to modified covariate specification. For bathymetry, we used a 3-level discrete variable defined as: *i*) less than 200 m, *ii*) between 200 and 1000 m depth, or *iii*) greater than 1000 m). Seasonality relates to variation in both sunlight and nutrients throughout each year. To explain variation in Chl associated with seasonality we assumed that Chl varied as a smooth function of day of the year. This allowed different patterns of seasonality to be fitted within each region. Since many regional patterns of phytoplankton seasonality are well-known (*i.e.* Arctic, versus temperate and tropical regions), examination of the estimated seasonality patterns provided a useful verification to ensure the model was correctly specifying mean seasonal Chl variability. Statistical dependence, whereby observations are not independently distributed, arises frequently in ecological data. For phytoplankton, spatial dependence not captured by bathymetry or seasonality may be due to physical oceanographic features such as fronts and eddies, or localized enrichment due to upwelling or anthropogenic contributions. A smooth spatial variable (latitude, longitude) was used to capture potential spatial dependence not explained by bathymetry or seasonality. The inclusion of this term also captured variability associated with spatial differences in sampling effort. Regional Chl trends were estimated by fitting GAMs to the blended data in each region, in order to estimate Chl as a log-linear function of time

Table A.2: Regional trends in Chl estimated by GAMs as a continuous log-linear time trend.

Region	β_{year}	SE	P	Deviance	R^2	GCV	EDF	Scale	Span
Arctic	-0.01	0.00	0.00	0.57	0.41	0.57	25547	0.55	1899 - 2003
N.Atlantic	-0.00	0.00	0.00	0.49	0.22	0.77	15527	0.74	1903 - 2006
E.Atlantic	-0.01	0.00	0.00	0.70	0.46	0.72	13223	0.68	1911 - 1999
S.Atlantic	-0.04	0.00	0.00	0.62	0.37	0.91	5647	0.84	1911 - 1994
N.Indian	-0.03	0.00	0.00	0.79	0.48	0.55	15210	0.52	1942 - 1997
S.Indian	0.03	0.00	0.00	0.73	0.51	1.16	9375	1.07	1941 - 2000
N.Pacific	-0.00	0.00	0.00	0.60	0.25	0.52	49067	0.52	1907 - 2008
E.Pacific	-0.01	0.00	0.00	0.85	0.47	0.45	36987	0.43	1907 - 2005
S.Pacific	-0.04	0.00	0.00	0.92	0.57	0.40	8002	0.36	1956 - 2003
Southern	-0.07	0.00	0.00	0.60	0.88	0.89	13293	0.83	1912 - 2002

Notes: The slope is the estimated instantaneous linear rate of change in abundance, SE=standard error, P is probability that the slope is not different from zero, R^2= the proportion of variance explained by the covariates, GCV=generalized cross validation score.

as

$$\eta(\mu_i) = \beta_0 + \beta_1 Year_i + \beta_2 Month_i + f_1(Bathymetry_i) + f_2(Lat_i, Lon_i) + \epsilon_i \quad \text{(A.5)}$$

and to estimate Chl as a log-smooth function of time as

$$\eta(\mu_i) = \beta_0 + f_1 Year_i + \beta_2 Month_i + f_1(Bathymetry_i) + f_2(Lat_i, Lon_i) + \epsilon_i \quad \text{(A.6)}$$

Additional details regarding the specification of parametric and nonparametric effects for local and regional models are presented in Table S2. Summary statistics for the regional model are also detailed in table A.2.

Global rates of phytoplankton change were derived by estimating the random-effects meta-analytic means (Cooper and Hedges, 1994) across the 10 individual regional estimates A.2. Global rates were estimated as both inverse variance- and geographic area-weighted means, but results obtained by these weightings were almost identical. Inverse variance-weighted means were used for inference.

A.1.6 Additional Robustness Analyses

Regional trends were estimated for Chl_T and Chl_I separately as a smooth function of time in each region to determine if trends were similar between data types. Despite large differences in the spatial and temporal coverage of the individual data types,

estimated regional Chl trends appeared similar (Figure A.4). There were minor discrepancies between trends derived from the two data sources in some regions. These differences were likely the result of limited data availability in these regions, rather than differences between data types. Regional models were also fitted to the blended dataset for global and open ocean areas individually for each region (Figure A.5). Although the overall global rate of change was similar, several Southern Hemisphere region estimates were different in the open oceans. Spatial analysis of the residuals from these regional models indicated more outlying residuals in the Southern Hemisphere (Figure A.5C). An emergent pattern from these analyses is an elevated degree of uncertainty for trends estimated for Southern Hemisphere regions where data availability is relatively low.

Local-scale trends were estimated for Chl_T and Chl_I individually as well (Figure A.6). Despite the variable temporal coverage of the data within each 10° x 10° cell, trends estimated from each data source individually were broadly similar in most areas. The magnitude of change in each cell was generally greater when estimated from Chl_I, which may reflect greater Chl changes over more recent time periods.

After blending *in situ* and transparency data, the temporal availability of data within each 10° x 10° cell was variable. Following our robustness approach for the regional models, we estimated local-scale trends from blended data using only data since 1950 as well as the full series (Figure A.7). The spatial patterns of Chl trends was largely unchanged. The linear correlation between estimates using all data against those using only data since 1950 was high ($r=0.985$; $P<0.0001$), and the estimated direction of temporal change different in only 2% (n=4) of all cells showing statistically significant effects (n=198). Using only data since 1950 resulted in 61% (n=120) of cells showing statistically significant declines and appeared to amplify the trends observed when using all data.

For *in situ* data, we also tested the effect of Chl sampling depth (m) and temporal changes in sampling methodologies within the local and regional model frameworks. Results indicated that there is little variability in Chl concentration associated with sampling depth within the upper 20 m.

A.1.7 Notes on Model Inference, Specification and Diagnostics

Because maximum likelihood (ML) estimation is inappropriate when including smooth functions as model covariates, all GAMs were fit using penalized likelihood (PL) approximation by penalized iteratively re-weighted least squares (P-IRLS). In PL approximation the model negative log likelihood is modified by adding a penalty which is scaled by a smoothing parameter (λ) for each nonlinear function. The λ parameter represents the tradeoff between model fit and model smoothness and is estimated by generalized cross-validation (GCV) or Un-biased Risk Estimation (UBRE). Because overfitting is common when using GCV estimation, the influence of the effective degrees of freedom on nonlinear estimation was inflated by a factor of 1.4 (ref. Kim and Gu, 2004). All additive and generalized additive models were estimated using the statistical software R[1] (V. 2.10) and packages (mgcv) developed by Wood (Wood and Bretherton, 2006).

Model assumptions were checked for all regions and all individual 10° x 10° cells, and residuals were examined against all covariates to determine if they were adequately specified. Regional model residuals were also examined spatially to examine any factors affecting model fits (Figure A.5C). Most outlying residuals occurred in the Southern Hemisphere, likely reflecting the relative scarcity of data in these regions, rather than improper model specification. The presence of collinearity among model covariates was examined by calculating the variance inflation factor (VIF); (ref. Heiberger and Holland, 2004) for all models. VIF values over 5 were considered evidence of collinearity.

Statistical autocorrelation, which violates the assumption of independence among observations, is common in spatio-temporal data sets. If not properly accounted for, autocorrelation can artificially inflate the degrees of freedom and bias the significance test. We accounted for temporal autocorrelation by including a temporal smooth effect and for spatial autocorrelation by including a latitudinal and longitudinal smooth effect within all GAMs. We then tested the effectiveness of these measures by examining the model residuals. If autocorrelation was still present, spatial and temporal patterns would be apparent in the model residuals. Omni-directional semi-variogram and correlogram analyses (Cressie, 1993) of model residuals in each region before and

[1] http://cran.r-project.org

after fitting the spatial variable indicated that our modeling approach was very effective at minimizing spatial autocorrelation (Figure A.8A). Although residuals from models without spatial effects exhibited clear spatial structure (Figure A.8B), those from models including spatial effects did not (Figure A.8C). Temporal autocorrelation was examined by calculating the mean model residual at 10-day intervals and fitting temporal autoregressive models. No significant temporal structure was observed in the model residuals.

A.1.8 Physical and Climate Data and Analyses.

To calculate the bathymetry associated with each Chl sampling station, we used global gridded bathymetry data (30-arc second resolution), extracted from the General Bathymetric Chart of the Oceans database (GEBCO_08). To calculate the distance from the nearest coastline, we used data extracted from the Global Self-consistent, Hierarchical, High-resolution Shoreline Database (GSHHS v1.10). The bathymetry and distance from the nearest coastline were calculated for each Chl measurement using Generic Mapping Tools software[2] (GMT); (Table A.1).

We extracted climate anomalies corresponding to the El Niño Southern Oscillation (ENSO); (Dec-Mar average), the Pacific Decadal Oscillation (PDO), the North Atlantic Oscillation Index (NAO), the Atlantic Multidecadal Oscillation (AMO), the Indian Ocean Dipole Index (IOD), the Arctic Oscillation Index (AOI), and the Antarctic Oscillation Index (AAO) from the standard sources listed in Table A.1. The bivariate ENSO index represents reconstructed SST anomalies and Southern Oscillation Index (SOI) anomalies. The IOD represents the normalized anomalous SST gradient between the Western Equatorial Indian (50°E to70°E and 10°S to10°N) and the South Eastern Equatorial Indian Oceans (90°E to 110°E and 10°S to 0°N) termed the Dipole Mode Index (DMO); (ref. Saji et al., 1999). The NAO represents the first principle component from a rotated principle components analysis (RPCA) applied to monthly standardized pressure anomalies across the North Atlantic (20° to 90°N); (ref. Barnston and Livezey, 1987). The AMO represents the area-weighted SST average over the North Atlantic (0° to 70°N). The PDO is described by the leading principal component of monthly SST anomalies in the North Pacific Ocean

[2]http://gmt.soest.hawaii.edu

(>20°N). The Arctic Oscillation (AO) index or Northern Annular Mode, represents sea level pressure anomalies across the Arctic and North Atlantic Oceans (>20°N). The Antarctic Oscillation (AAO) index or Southern Annular Mode represents the leading principle component of geopotential height anomalies south of 20°S (ref. Thompson and Wallace, 2000). High-pass convolution filters (window=9) were applied to all indices to remove high-frequency variability from the series.

We examined the effects of climate indices by taking yearly model predicted Chl in each of 10 regions (*i.e.* with seasonal, spatial, and depth effects controlled for), converting these to de-trended, normalized anomalies and cross-correlating them against relevant climate indices in each region.

Sea surface temperature (SST) data were extracted from the Hadley Centre Sea Surface Temperature data set (HadISST; 1899-2009); (ref. Rayner et al., 2003). Wind intensity data were extracted from the National Oceans and Atmospheric Administration (NOAA) Objectively Analyzed Air-Sea Fluxes (OAFlux) from the Global Oceans database (1958-2009); (ref. Yu et al., 2007). We calculated mixed layer depth (MLD) from subsurface ocean profiles of temperature and salinity extracted from Hadley EN3 v.2a (Met office; 1950 -2009); (Table A.1); (ref. Ingleby and Huddleston, 2007). We used a finite MLD definition based on Δ density (σ_t)=0.125 kg m (refs. Levitus, 1982; Kara et al., 2000). The finite difference criterion was chosen opposed to a gradient criterion to estimate MLD because it has been experimentally shown to be more stable (Bainerd and Gregg, 1995). The initial temperature and density values were chosen at a depth of 10 m to eliminate any potential bias in the profile due to 'skin effects' at the ocean surface (Fairall et al., 1996). Linear interpolation was used to calculate the exact values for MLD.

Global changes in physical variables were estimated by fitting linear models containing covariates for year and month to data in each 1° x 1° and 10° x 10° cell (Figure A.9). Regional changes were estimated by fitting additive models containing covariates for year, month, and location (latitude, longitude) in each region. Since these data were extracted on a global 180° x 360° grid, each individual 1° x 1° grid cell was area-weighted to account for this. To examine the effects of changing SST, MLD, and wind intensity on Chl, all datasets were merged by location (1° x 1° cell), year, and month, and both local and regional models were re-fitted with a physical driver

effect estimated. This approach allows isolation of the effects of physical drivers on Chl while removing variability associated with other model covariates (*i.e.* year, day, latitude, longitude and depth). Since VIF analysis indicated collinearity among some physical variables, individual models containing each physical variable were fit.

A.1.9 Potential Sources of Error.

Limitations in spatial and temporal data availability increase uncertainty in model inference. In the Southern Hemisphere for instance, confidence intervals were wider, estimates fluctuated more, and model residuals were greater, indicating increased uncertainty in these areas due to a relative scarcity of data. We have accounted for this uncertainty by inverse variance-weighting regional estimates when deriving the global mean Chl trends, and also by providing trend estimates using only post-1950 data for comparison. Despite these measures, the patchy nature of the data remains a potential source of uncertainty, especially in the Southern Hemisphere. Furthermore we note that our regional models estimate Chl trends averaged over larger spatial scales and provided little insight into mesoscale differences in trends. We attempted to partly remedy this issue by estimating 'local-scale' phytoplankton trends at 10° x 10° resolution (Figure A.2). Yet, these local-scale models made spatial comparisons difficult due to the different temporal data coverage among cells. Likewise, inconsistency of temporal sampling effort between provinces and cells raises the possibility that sampling intensity was not adequate to fully resolve temporal changes in some regions.

Another potential source of error may be associated with the change in filters used to separate phytoplankton for the extraction of Chl. The earlier use of Whatman GF/C glass fiber filters may have underestimated the concentration of Chl (ref. Venrick et al., 1987). This potential bias is only relevant for *in situ* data and would result in an apparent increase in Chl. Hence, if there were any biases introduced by changes in filters, it would render our estimates of Chl decline conservative.

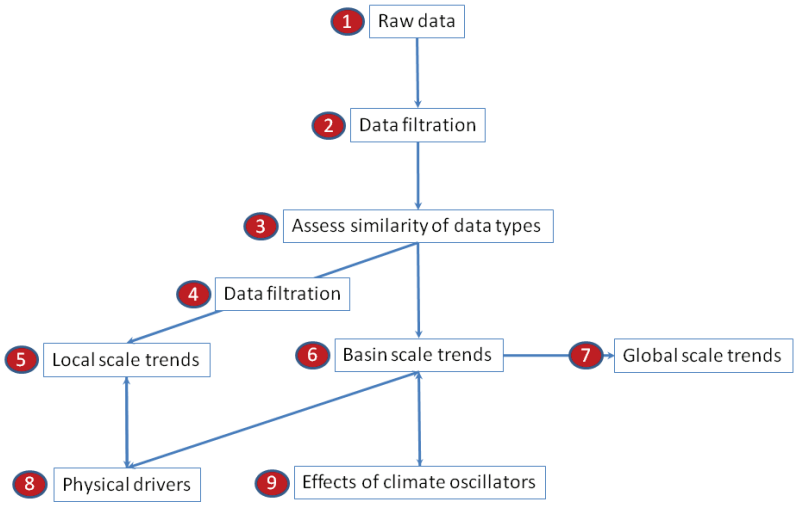

Step	Objective & Rationale	Implementation
1	**Data exploration**	-Plot spatial and temporal distribution of data, summary statistics.
2	**Remove biologically unrealistic data**	-Systematic filtration methods to remove biologically improbable outliers and those associated with optical or data entry errors
3	**Examine statistical similarity of individual Chl data types** - Combine data types to extend temporal and spatial scope of analysis.	-Calculate weighted mean Chl for each year, month, and 0.25 degree geographic bin. Fit model II regression to mean Chl data, examine correlation, slope, and intercept to determine isotropy. -Examine standardized residuals spatially and temporally. -Estimate Chl trends from each data type individually. -Regression tree analysis.
4	**Improve local scale model estimation** - Abundant, adequate data required to estimate trends.	- Remove 10 degree cells which have few data points, or where the number of available years or months of data is low.
5	**Estimate Chl trends in different local scale geographic areas to examine global spatial Chl trends**	- Fit GAMs to each 10 degree bin where adequate data exists.
6	**Estimate mean Chl trends in different basin scale ocean areas** -Flexible analysis framework needed to explain spatial and temporal variability in highly unbalanced data.	- Fit GAMs to each of 10 geographic basins encompassing the globe - Estimate Chl as a linear, categorical, and smooth function of time.
7	**Estimate global Chl trends** - Global Chl trends are realization of underlying random process.	- Combine individual estimates from basin scale trends using random effects meta-analysis. - Global estimate calculated as both variance- and area-weighted mean.
8	**Determine the effects of physical drivers on Chl trends** - SST, MLD, and Wind are likely proxies for many climate scale oceanographic changes and have strong effects on upper ocean nutrient concentrations.	- Estimate Chl and SST trends locally and regionally and compare trends. - Merge 1 degree physical data with available Chl data and fit local and regional models to determine SST effects on Chl.
9	**Examine effects of climate oscillators on Chl trends** - Longer term Chl trends required to examine relationships. -Useful model-verification tool.	- Examine correlation between standardized, de-trended Chl trends and relevant climate teleconnection indices.

Figure A.1: Schematic of statistical analyses.
Flowchart and table depicting the data processing steps, their objectives, rationale, and implementation.

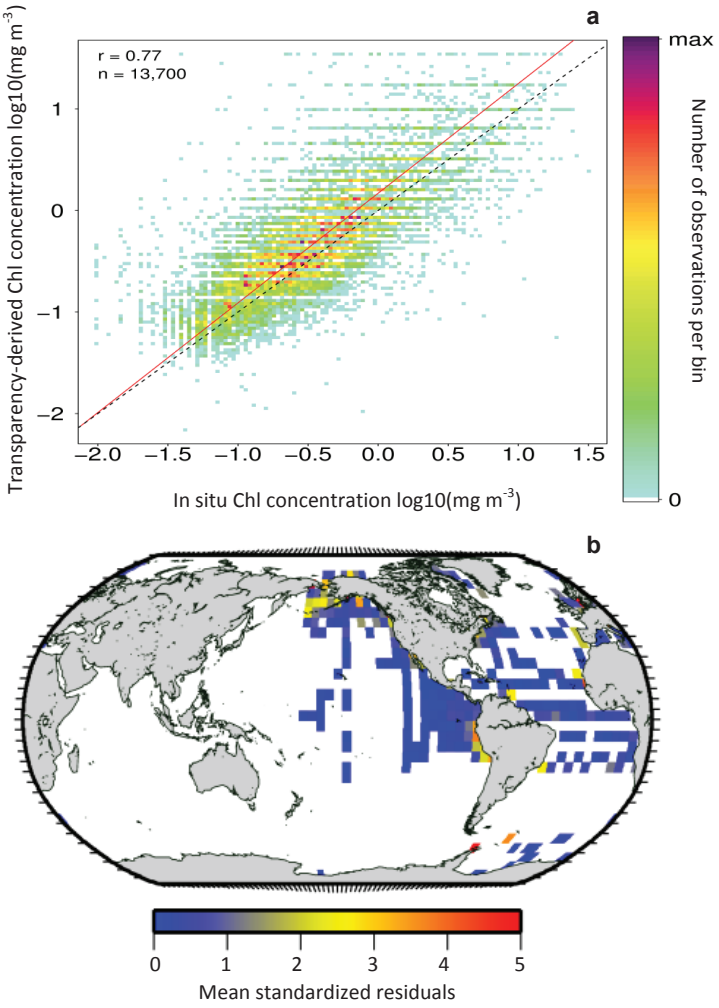

Figure A.2: Comparison between transparency- and *in situ*-derived Chl data. (A) Linear relationship between transparency- and *in situ*-derived Chl represented by model II major axis regression model (red line). Points are log10 mean Chl per year, month, and 0.25 degree cell. Color of the points represents the number of observations within each bin. Dashed line represents an idealized slope of 1. Pearson correlation coefficient (r) and sample size (n) are shown. **(b)** Absolute standardized mean model residuals from linear models in (A) binned to 5 degree cells. White areas are cells where no matchups exist.

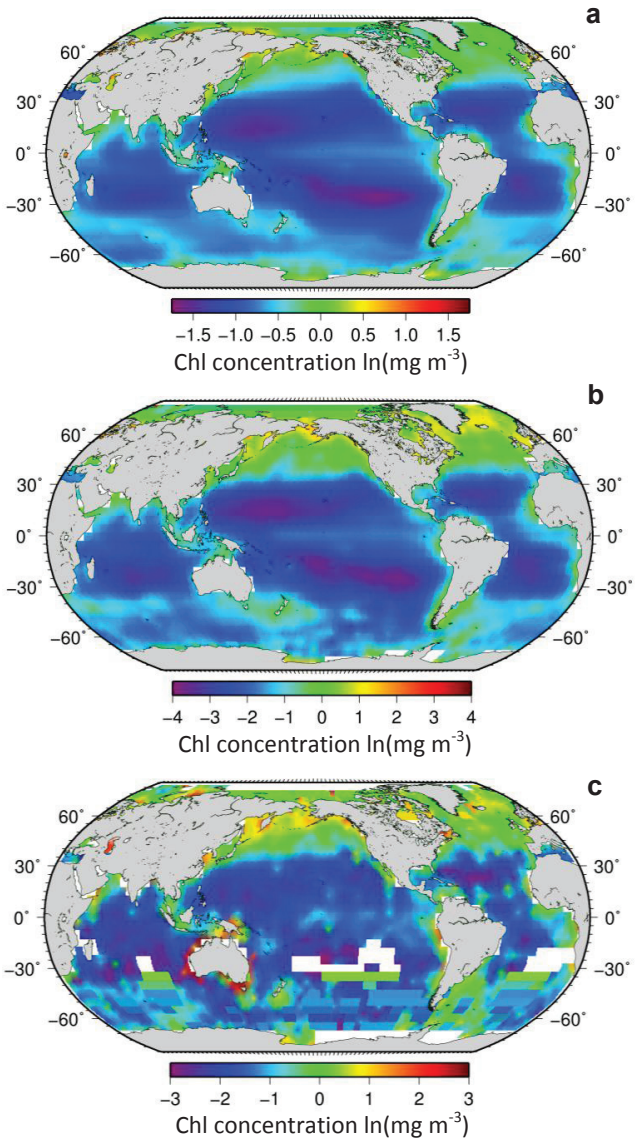

Figure A.3: Chl climatology comparisons.
(a-c) Averaged Chl concentration derived from (A) the Sea-viewing Wide Field of view Sensor (SeaWiFS), (B) the Coastal Zone Color Scanner (CZCS), and (C) blended transparency and *in situ* data. All data were log-transformed and averaged per 5 degree cell for comparison. Seasonal effects were not removed.

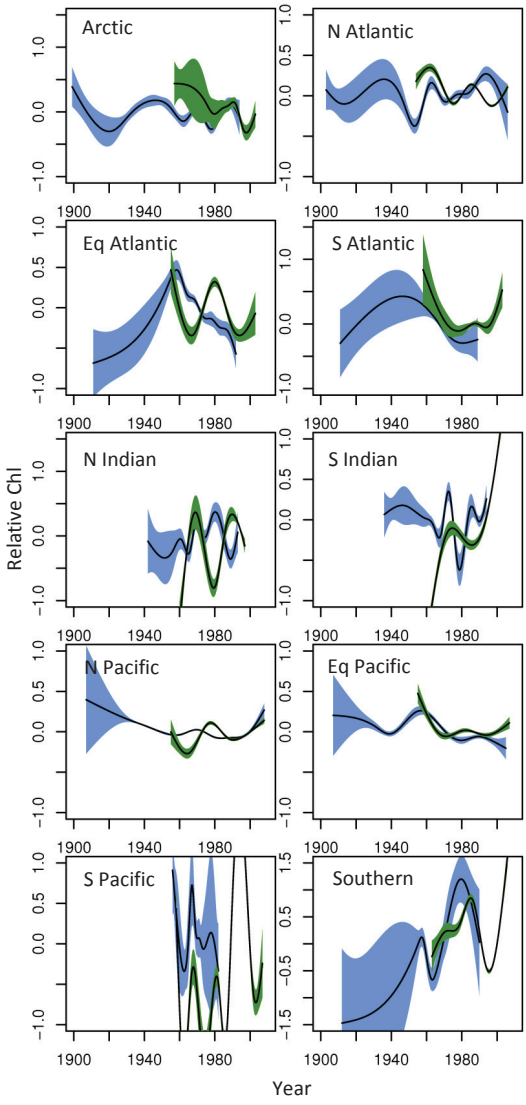

Figure A.4: Regional Chl trends by data source.
Estimated smooth rates of Chl change from GAM models fitted to each data source (n=2) and basin (n=10). Blue colors indicate trends estimated using transparency data and green using *in situ* data. Shaded areas are the 95% confidence limits for each trend.

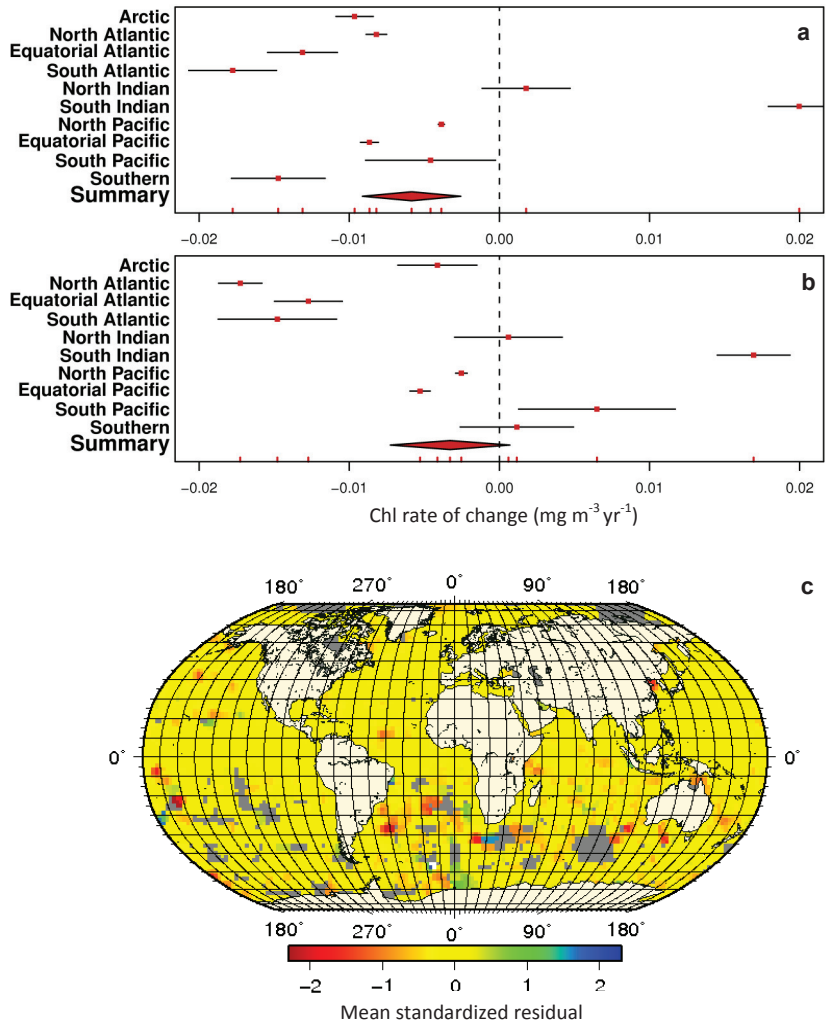

Figure A.5: Chl trends by ocean zone.
Estimated rates of Chl change in each region (n=10) from GAM models fitted to all available data (A), and using data in open ocean areas, where water depths are >200 m (B). Means and 95% confidence intervals are shown. (C) Mean standardized residuals from 10 regional models in (A) plotted on a 1° X 1° degree grid. Colors depict the mean magnitude of unexplained residual variation in each cell. Grey colors depict missing data.

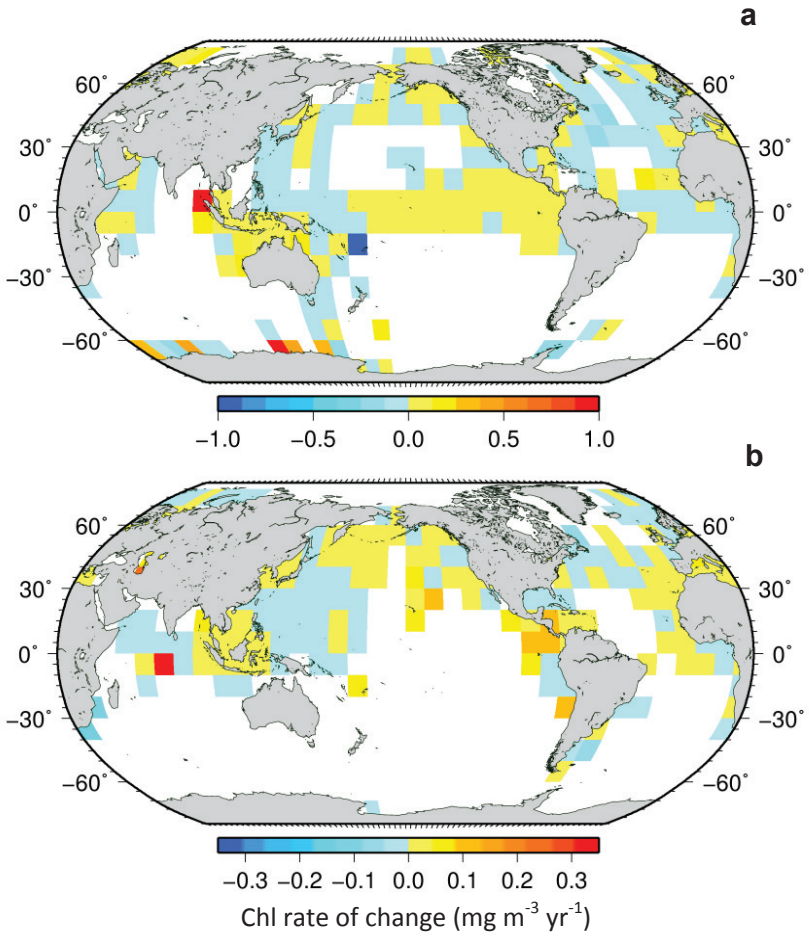

Figure A.6: Local Chl trends separated by data source.
Mean instantaneous rates of Chl change estimated for each 10°x10° cell containing adequate data. Trends were estimated for *in situ* (A) and transparency data (B). Yellow and red represent cells where Chl concentration has increased, blue represents Chl decrease, and white indicates cells lacking sufficient data.

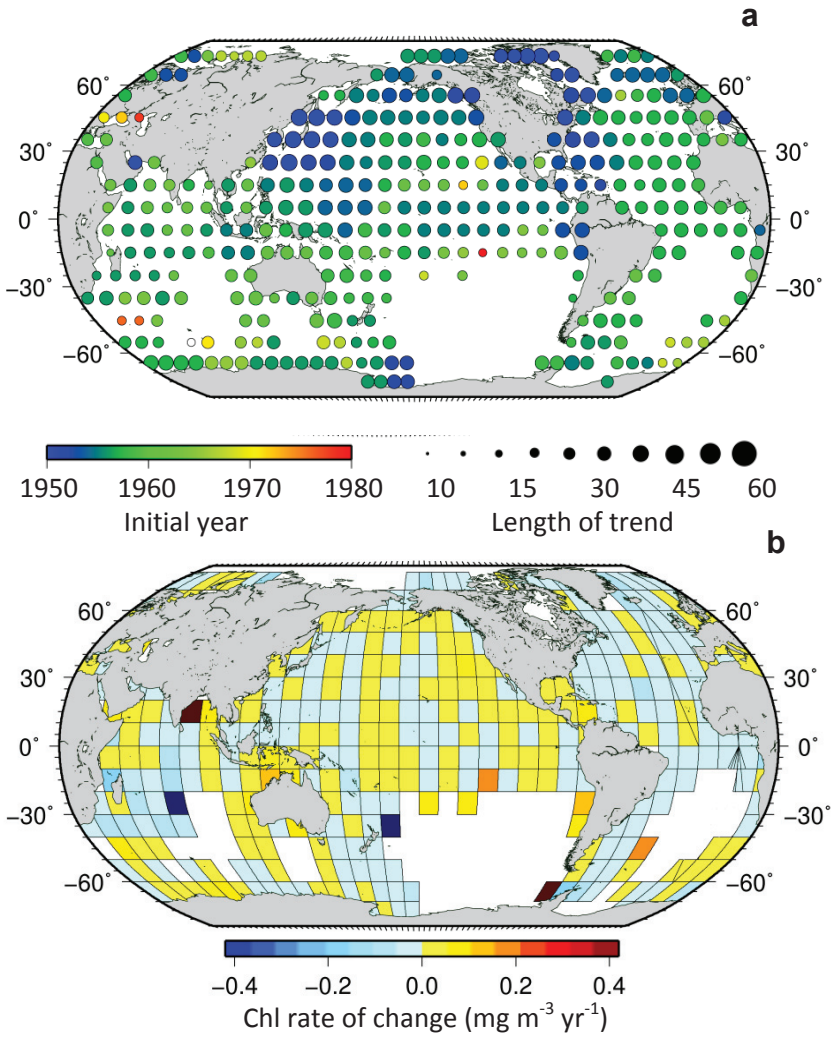

Figure A.7: Spatial variability in phytoplankton trends using post-1950 data. (a) Baseline year and temporal span of Chl data used in local models. (B) Mean instantaneous rates of Chl change estimated for each 10° x 10° cell (squares; n=358). Yellow and red indicate cells where Chl concentration has increased, blue indicates Chl decrease, and white indicates cells lacking sufficient data. Cells bordered in black denote statistically significant rates of change ($P<0.05$).

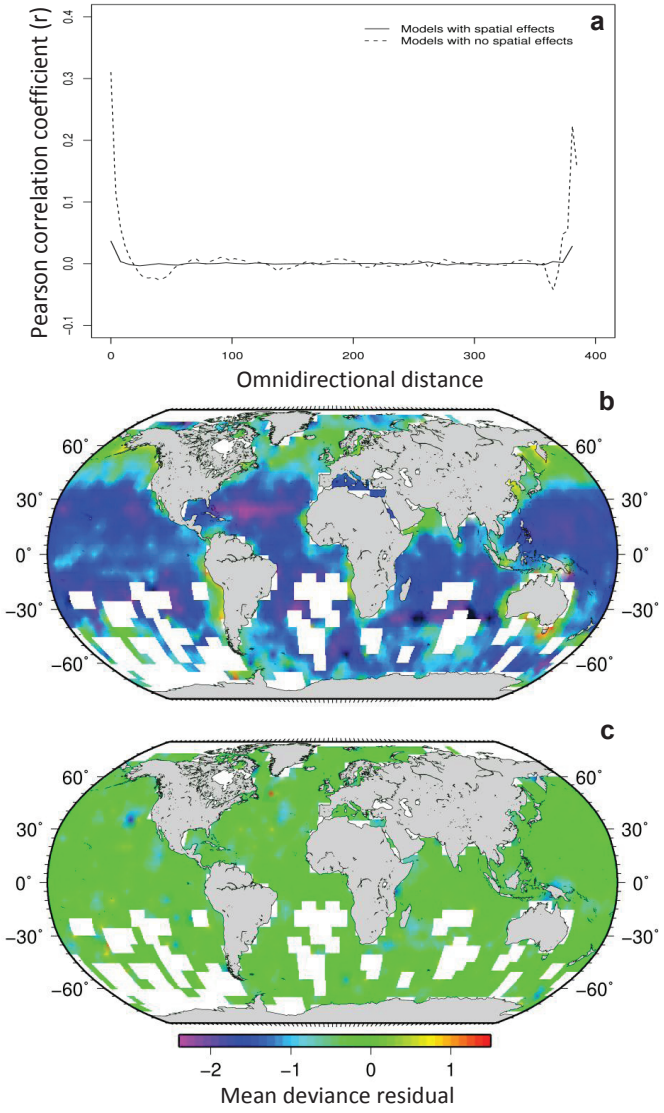

Figure A.8: Effects of removing spatial autocorrelation.
(a) Omnidirectional correlogram analysis of mean model residuals from all regional models per 1° cell before (dashed line) and after (solid line) including the spatial effect. (b-c) Spatial examination of regional GAM residuals before (B) and after (C) including the spatial effect. Colors depict the mean model residual in each 1° X 1° cell.

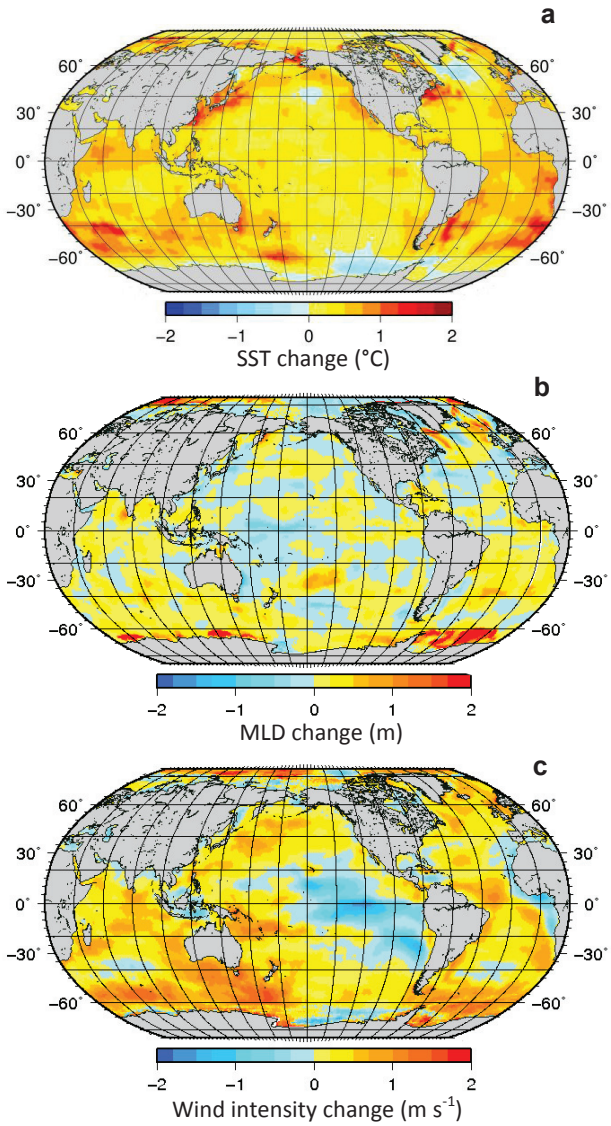

Figure A.9: Physical drivers.
(a) Estimated changes in SST (1° resolution 1899-2009), (B) MLD (1° resolution 1955-2009), and (C) Wind intensity (1° resolution 1958-2009) over the available time periods. Blue depicts declines and yellow and red depict increases.

Appendix B

Boyce et al. Reply

In their thoughtful responses to our article on global chlorophyll (Chl) trends (Boyce et al., 2010), Mackas (Mackas, 2011), Rykaczewski and Dunne (RD);(Rykaczewski and Dunne, 2011), and Mcquatter-Gollop and colleagues (McQuatters-Gollop et al., 2011) suggest that some of the variation observed in our analysis may be explained by a possible bias, whereby transparency-derived chlorophyll (Chl_T) measurements overestimate phytoplankton abundance relative to direct *in situ* chlorophyll (Chl_I)measurements. While we cannot entirely discount the possibility that changes in sampling methods may introduce fractional bias, extensive sensitivity analyses detailed below show that this is not responsible for the observed Chl declines. Furthermore, the accuracy of Chl_T as a proxy of surface Chl has been independently verified (Lewis et al., 1988; Falkowski and Wilson, 1992), and indicate that Chl_T explains only 0.5-1.5% less of the variance in surface Chl than precision measurements of water-leaving radiance (remotely sensed ocean color)(Falkowski and Wilson, 1992).

Mackas and RD suggest that a systematic bias between Chl_T and Chl_I, combined with unbalanced temporal sampling effort may have influenced the direction of Chl trends. However, multiple lines of evidence indicate that this is not the case. We adjusted Chl_T using the corrective algorithm suggested by Mackas (Mackas, 2011, Eqn. 3a, 3b) and re-estimated Chl trends. This improved the agreement between Chl_T and Chl_I (b=0.98; r^2=0.6) and did not change the direction of Chl trends in any of the regions. The magnitude of change varied in some regions and the proportion of declining cells dropped from 59% to 53%; however, our original conclusions remained valid. (2) In our paper we compared Chl_T and Chl_I using model II major axis regression, assuming error in both variables (Boyce et al., 2010, Figure 2A). However, the simulations performed by RD use our model II regression parameters to predict simulated Chl values using model I ordinary least squares (OLS) regression, which is

Published as: Boyce, D. G., M. R. Lewis, and B. Worm. 2011. Boyce et al. reply. Nature 472: E8E9.

based on a different set of statistical assumptions and will therefore bias their analysis (Ripley and Thompson, 1987). There are two ways to avoid this problem. First, simulated values can be computed using model I regression as RD have done, but using parameters estimated from a model I regression of Chl_T and Chl_I matchups. Such model I analysis reveals that Chl_T are lower on average than Chl_I (b=0.83; r^2=0.6); hence the simulation should adjust Chl_T measurements downward, rather than upward as RD have done. Alternatively, simulated values can be computed using model II regression with the appropriate parameters of our fitted model (Boyce et al., 2010). The error introduced by application of an inappropriate model is further highlighted by the observation that the Chl trends simulated by RD (Rykaczewski and Dunne, 2011, Fig. 2) appear opposite to our results[1] across much of the ocean; for example, their simulated declines in coastal areas were not reproduced by our analyses (Boyce et al., 2010, Figure 2B). Furthermore, while RD attribute Chl increases in the Indian Ocean to an increasing proportion of Chl_T measurements through time, we did not observe such a pattern in our database: like other regions, both Indian basins show a decreasing proportion of Chl_T and an increasing proportion of Chl_I measurements through time. (3) By removing all Chl measurements collected in shelf regions (<200 m depth) the agreement between Chl_T and Chl_I was improved (b=1.016, n=11,329 matchups). Re-fitting models to this filtered data set (n=283,681) did not alter the direction of trends in any of the regions examined, nor did it change the local trends, suggesting that the observed declines are robust. (4) Lastly, our statistical models reproduced with high fidelity the well-known seasonal cycles of Chl in different regions and demonstrated clear coherence between Chl and leading climate indicators; this would not be expected if a systematic bias were confounding the data.

In a related comment McQuatters *et al.* (MG); (McQuatters-Gollop et al., 2011) claim that the removal of all Chl_T observations changes the trends to positive in the Atlantic and Pacific regions. We caution that comparing trends from Chl_T or Chl_I individually may be misleading, since the length of time series, spatial coverage, and availability of data can be very different. However, estimating trends using only Chl_I measurements, changed the Chl trend to positive in the South Atlantic (P=0.10; 73% of all measurements) and North Pacific (P<0.05; 26% of all measurements) regions only. Likewise, estimating trends since 1980 (as suggested by MG) did not affect the

direction of change in any of the Atlantic regions.

Furthermore, MG present Continuous Plankton Recorder (CPR) color index data suggesting that phytoplankton abundance in the North Atlantic has increased, rather than decreased as we reported. However, there are important differences between the CPR data and those used in our analysis, which may explain some of the observed discrepancies. As MG mention, the CPR retains the largest phytoplankton cells (>270 μm; (refs. McQuatters-Gollop et al., 2011), and the vast majority of phytoplankton cells – which are much smaller - are not sampled quantitatively (Tarran et al., 2000). Thus a CPR-derived color index may not be strictly comparable to direct Chl or transparency measurements. Additionally, the CPR dataset almost exclusively contains measurements sampled north of 40° latitude (McQuatters-Gollop et al., 2011, Fig. 1a) , and many observations from inshore areas, which is contrary to our approach. The suggested phytoplankton increase across the Atlantic is also not supported by an independent analysis of *in situ* and satellite data collected over similar timescales (Gregg et al., 2003).

MG also observe that some shorter-term (∼20 yr) localized time series show increases rather than decreases in Chl. We do not dispute this but suggest that comparing such series to the longer-term (>50 yr), basin-scale trends we report may be misleading. Ours (Boyce et al., 2010) and others' (Behrenfeld et al., 2001; Martinez et al., 2009; Behrenfeld et al., 2006; Henson et al., 2010) analyses demonstrate that large-scale, long-term data sets are needed to isolate low-frequency trends from the yearly to decadal fluctuations which are often driven by climate oscillations. Comparisons of ours and other long-term regional estimates indicate broad agreement (Gregg et al., 2003; Gregg and Conkright, 2002; Falkowski and Wilson, 1992). Furthermore, since we included the cited BATS, HOTS, and CalCOFI time series in our analysis, the important contributions that these data make are fully accounted for. As shown both in our paper (Figure A.2B; Boyce et al., 2010), and in the CPR time series (McQuatters-Gollop et al., 2011; Reid et al., 1998), phytoplankton has increased in some areas and thus it should not be surprising that some time series reproduce this trend.

In conclusion, we welcome the critical suggestions offered by the authors and agree that the inter-calibration of different Chl measurement techniques is an ongoing and

important topic. The above-mentioned requirement for long time-series, the relatively low coverage of historic Chl measurements across the global oceans, and the multitude of available Chl measurement techniques necessitate the use of synthetic Chl time series for any global long-term analysis. Based on the extensive robustness analyses reported here and previously, we conclude that the observed global decline in Chl is independent of the data source used, and is not biased as a result of combining transparency and *in situ* data.

Appendix C

Oceanographic Drivers of Global Chlorophyll Changes Over the Past Century

Table C.1: Published phytoplankton time series and associated metadata.

Variable	Model used	Distribution	Link
EKE	GLM	Gamma	Log
Ice	GLM	Binomial	Logit
Salinity	Linear	Gaussian	
SST	Linear	Gaussian	
Frontal energy	Linear	Gaussian	
Stratification	GLM	Gamma	Log
Wind	GLM	Gamma	Log
Cloud	Linear	Gaussian	

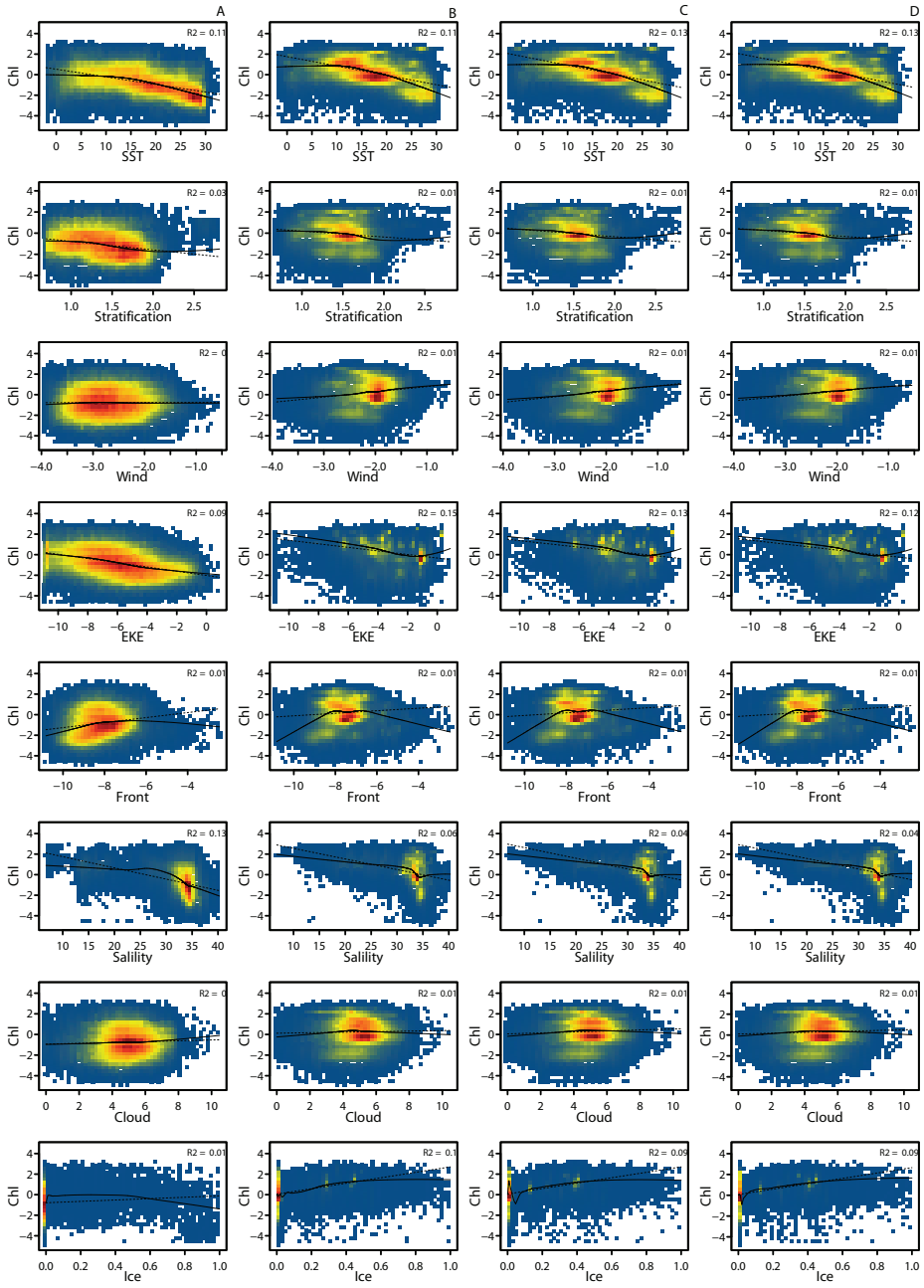

Figure C.1: Relationships between oceanographic variables and Chl.
All available space-, and time-matched oceanographic variables (x-axes), are plotted against Chl (y-axes). Columns are (A) Raw data, (B) seasonal and spatial variability accounted for, (C) seasonal, spatial, and long-term variability accounted for, and (D) seasonal, spatial, long-term, and climate variability accounted for. Colours depict the number of observations per pixel. Dashed line is the linear trend, and the dashed line is a non-linear (spline) trend fitted to the data. Variables have been transformed to approximate the normal distribution where necessary.

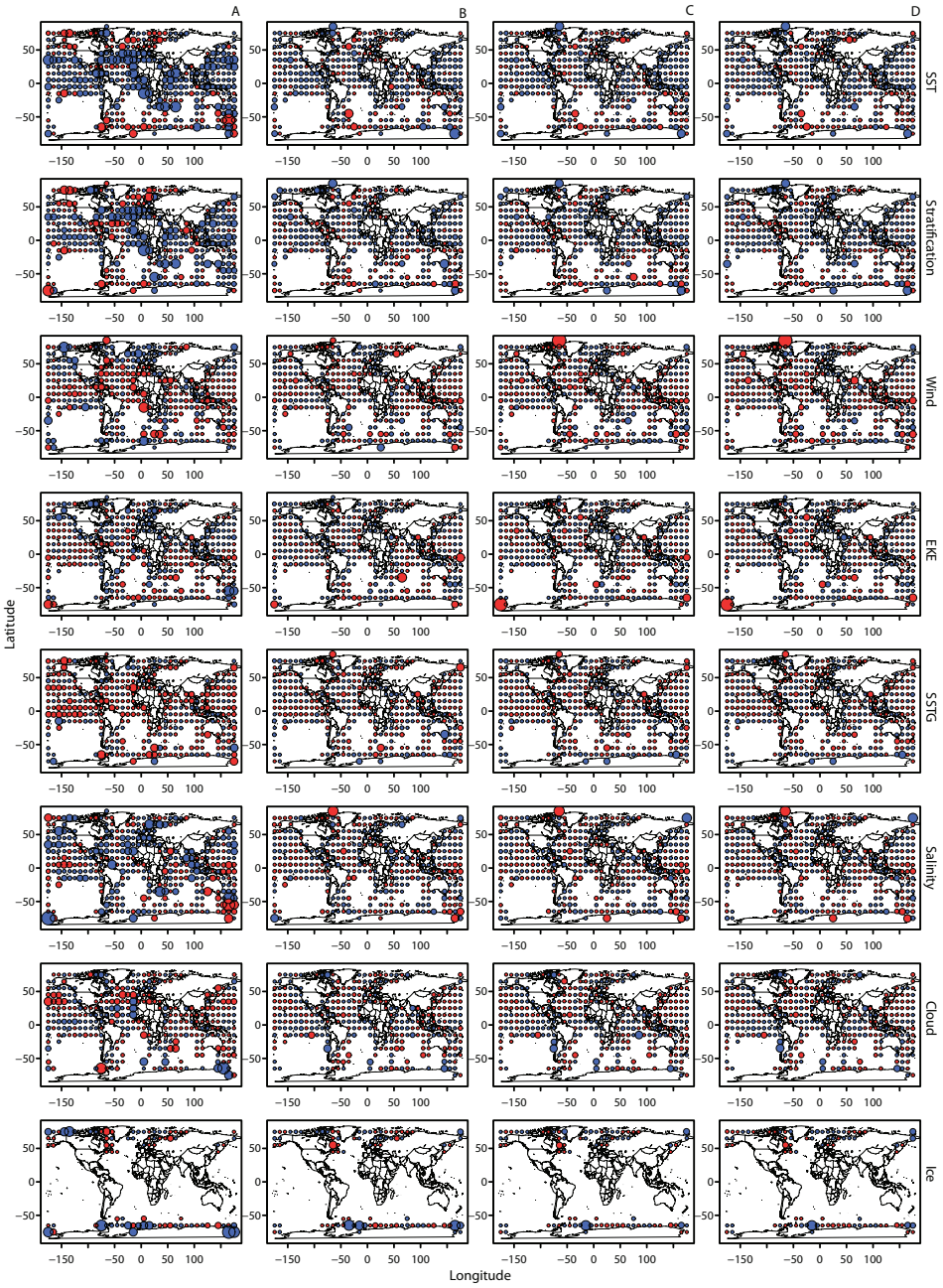

Figure C.2: Relationships between oceanographic variables and Chl as a function of latitude

Univariate linear relationships between all oceanographic variables and Chl in each 10° x 10° degree cell as a function of latitude. Columns are (A) Raw data, (B) seasonal and spatial variability accounted for, (C) seasonal, spatial, and long-term variability accounted for, and (D) seasonal, spatial, long-term, and climate variability accounted for. Colours depict the 10° latitude band where the relationship was observed.

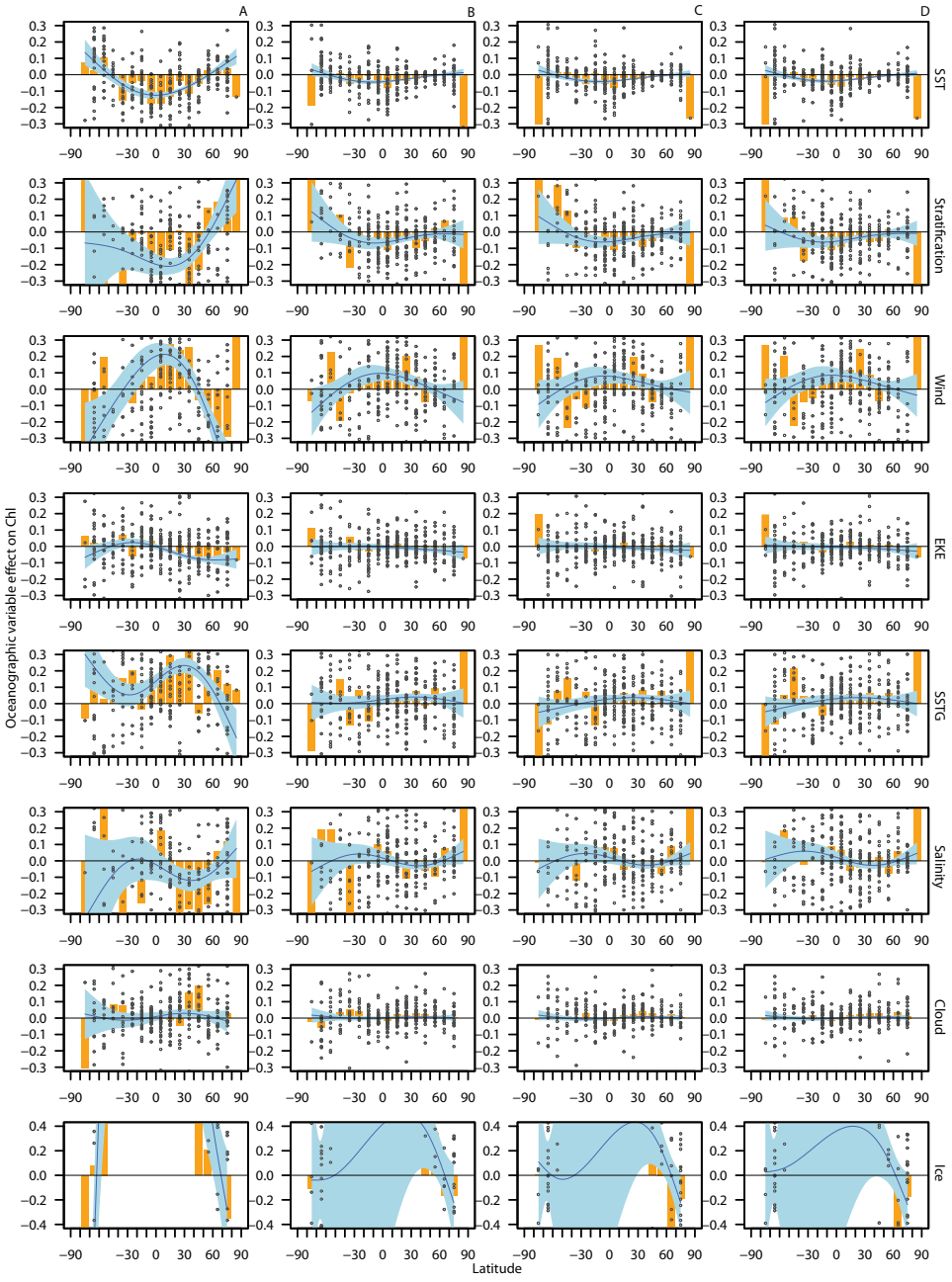

Figure C.3: Spatial distribution in the effects of oceanographic variables on Chl. Spatial distribution in the univariate effects of oceanographic variables on Chl. Columns are (A) Raw data, (B) seasonal and spatial variability accounted for, (C) seasonal, spatial, and long-term variability accounted for, and (D) seasonal, spatial, long-term, and climate variability accounted for. Red denotes negative effects of the driver on Chl and red denotes positive effects. The size of the symbol depicts the proportion of variance explained by the oceanographic variable (range: 0 to 1). White areas contain insufficient data from analysis.

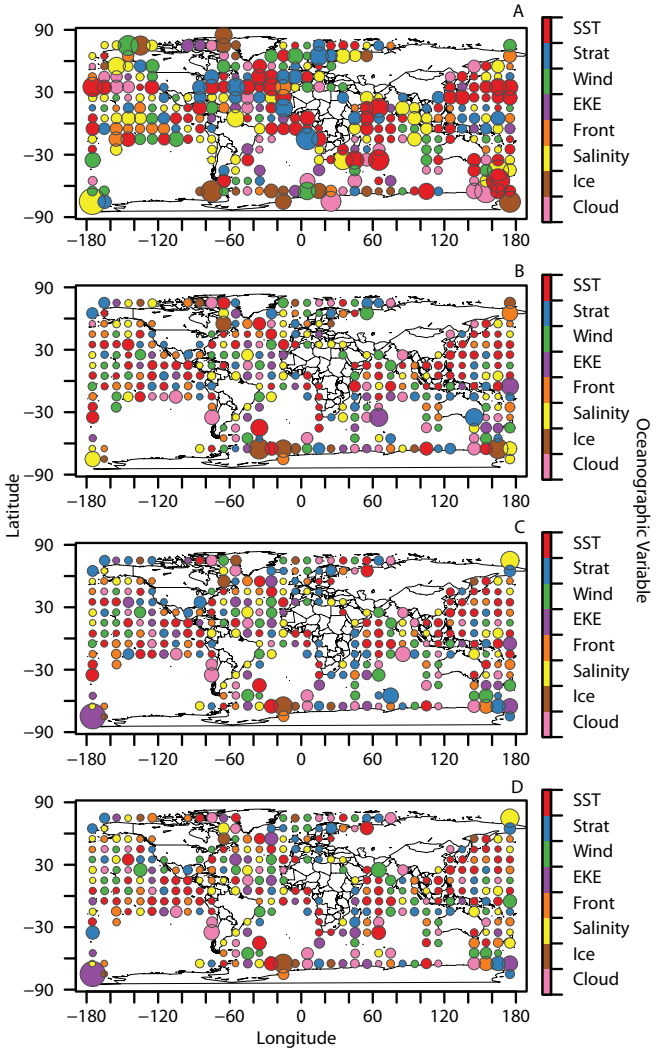

Figure C.4: Effects of the oceanographic variables on Chl as a function of latitude. Latitudinal gradient in the univariate effects of the oceanographic variables on Chl estimated on a 10° x 10° grid. Columns are (A) Raw data, (B) seasonal and spatial variability accounted for, (C) seasonal, spatial, and long-term variability accounted for, and (D) seasonal, spatial, long-term, and climate variability accounted for. Points are the estimated effect of the variable on Chl within each 10° x 10° cell. The shaded bars are the median effect values for each 10° latitude bin. Trend lines are GAMs estimates of the effects as weighted smooth functions of latitude; weightings are the inverse of the individual estimate standard errors. Blue shaded regions are the 95% confidence intervals for the trend lines.

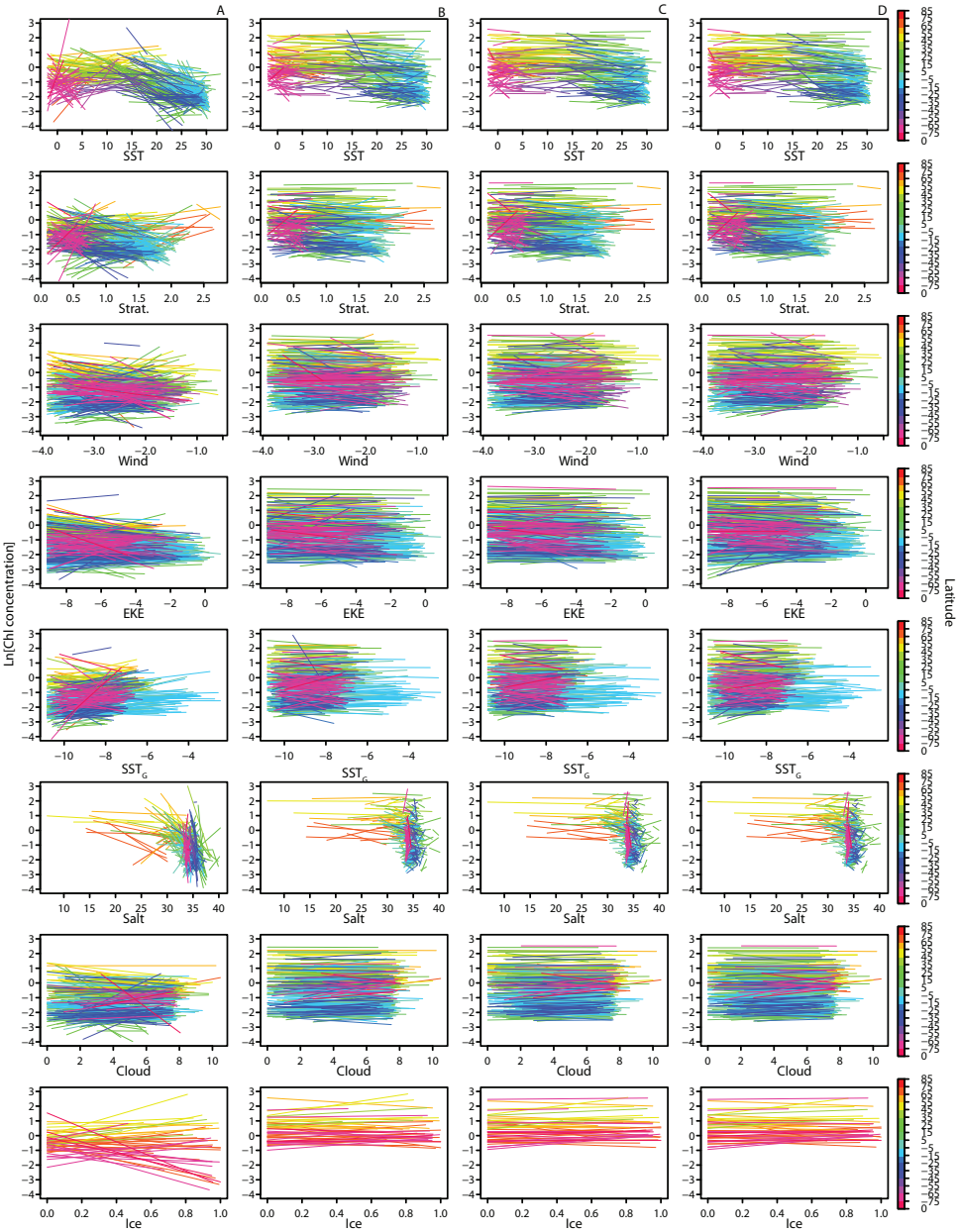

Figure C.5: Oceanographic variables explaining the largest proportion of Chl variability.

The oceanographic variables explaining the largest proportion of Chl variability within each 10° x 10° are cell plotted spatially. Rows are (A) Raw data, (B) seasonal and spatial variability accounted for, (C) seasonal, spatial, and long-term variability accounted for, and (D) seasonal, spatial, long-term, and climate variability accounted for. Colours depict the oceanographic driver and the size of the symbol depicts the proportion of Chl variance explained by that oceanographic variable. This procedure was undertaken (A) using the raw data, and (B) after accounting for spatial, seasonal, inter-annual, and climate variability.

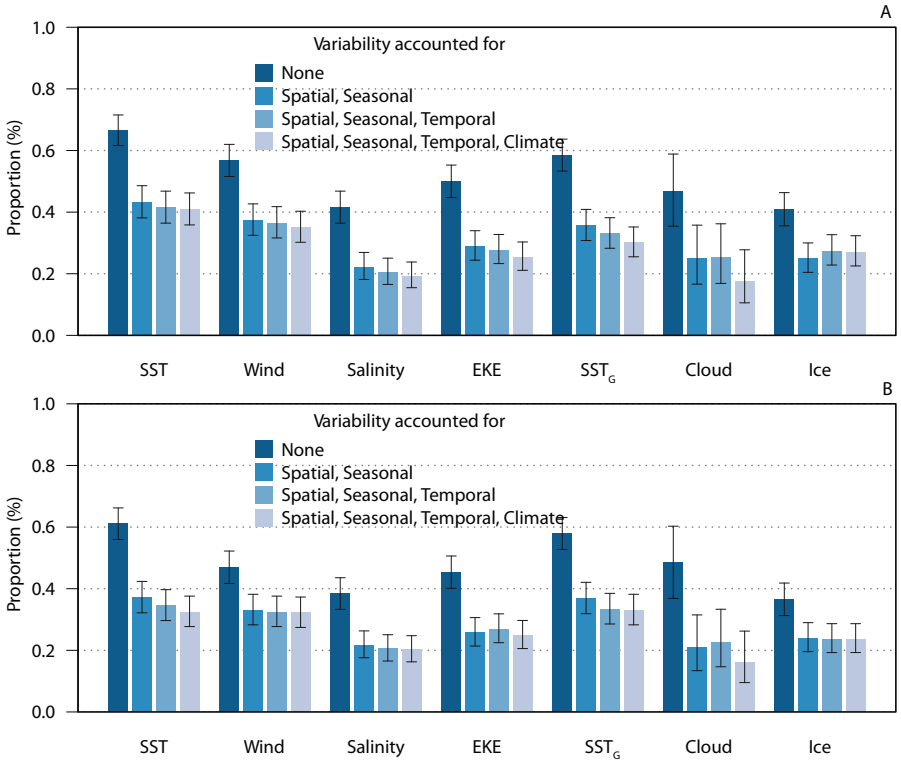

Figure C.6: Effect of oceanographic drivers on Chl after accounting for stratification effect.
Shaded bars depict the proportion of 10° x 10° cells where (C) each oceanographic variable was the strongest single predictor of Chl, and (D) the effect of each oceanographic variable on Chl was statistically significant ($p<0.05$) after accounting for the effects of stratification on Chl. Only the cells where analysis was possible were used. Colours depict the variability accounted for prior to the analysis, where dark blue is the raw data, and light blue is the data after accounting for spatial, seasonal, inter-annual, and climate variability. Vertical lines represent the 95% Wilson score confidence intervals for the proportions.

Appendix D

Effects of Sea Surface Warming on Marine Plankton

D.1 Mesocosm Experiment: Initial Conditions.

Table S1. Initial values of physical, chemical, and biological components. Start temperature in the cold treatment=8°C, and in the warm treatment=14°C.

D.2 Effects of Warming on Plankton Stability.

Here we interpret and discuss the effect of temperature on the temporal stability of measured variables. We calculated the coefficient of variation (CV) of each measured variable within each individual mesocosm as a measure of normalized temporal stability.

For each measured variable we used ordinary least squares regression equations to estimate temporal stability as a linear function of nutrients, temperature, and their interaction. Backward model selection was undertaken according the Akaike information criteria (AIC) score. Using this analysis, positive model effects are destabilizing and negative effects are stabilizing (Table S2).

Our analysis of temporal stability suggest that ocean warming has destabilizing effects on plankton communities, significantly on heterotrophs (copepods, ciliates and HNFs) and phytoplankton biomass (Figure D.2). This suggests that warming has not only an impact on the productivity, but it may also increase variability within pelagic ecosystems making future changes in the ocean productivity harder to predict.

Table S2. Temporal variability of selected biological components estimated as linear functions of warming. Significant model effects ($p<0.05$) are denoted in bold text.

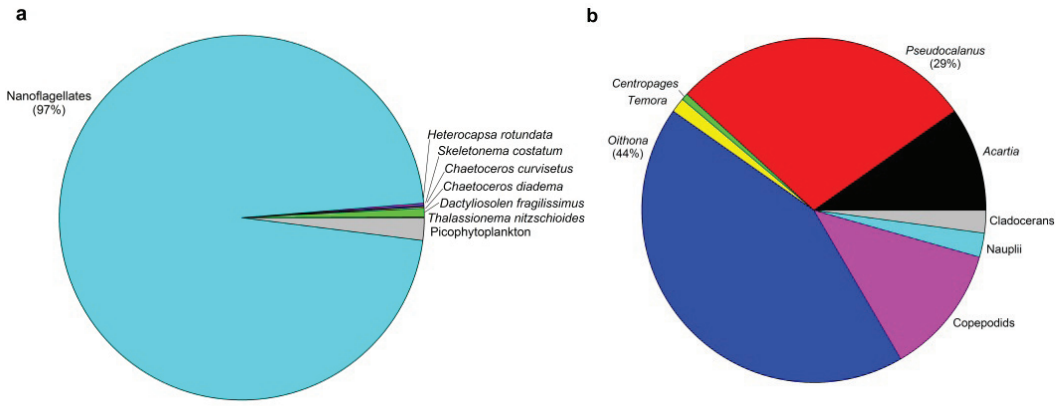

Figure D.1: Initial mesocosm community composition.
Initial community composition of phytoplankton (a) and mesozooplankton (b).

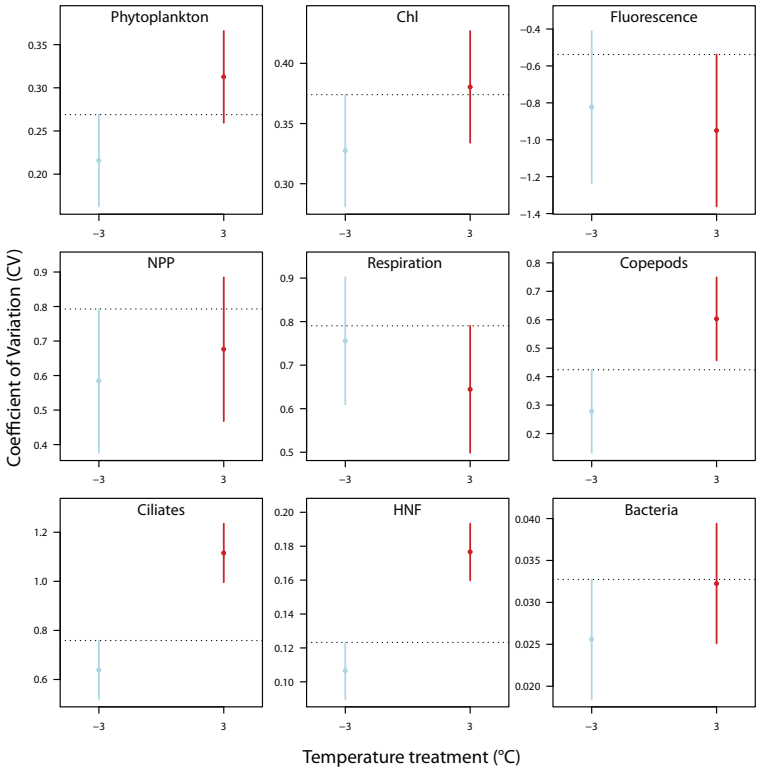

Figure D.2: Stability as a function of temperature and nutrients.
Coefficients of variation for selected biological components in cold (blue) and warm (red) mesocosms.

Appendix E

Patterns, Drivers and Ecosystem Consequences of Marine Phytoplankton Change

E.1 Data Sources and Methods

All data used in this were extracted from publicly available sources. Publication statistics used to produce figure 1 were extracted from SciVerse Scopus[1] and the Thomsom ISI Web of Science[2], which represent two of the largest abstract and citation data bases for peer-reviewed scientific literature. To standardize the proportion of publications for each marine taxa, the number of articles published in each year was divided by the total number of published articles in the same year and multiplied by 100. Temporal trends in the scientific literature on phytoplankton were estimated using generalized additive models (GAMs); (Hastie and Tibshirani, 1986). GAMs are an extension of generalized linear models (GLMs) which enable the specification of the response as a smooth function of covariates.

Phytoplankton abundance as indicated by chlorophyll-a (Chl; mg m^{-3}) was derived from remotely-sensed ocean-leaving radiances measured by the Sea-viewing Wide Field-of-view Sensor (SeaWiFS; (McClain et al., 2004). Climatological surface nitrate concentrations (N; μmol L-^{1}) were extracted from the NODC World Ocean Atlas (2009) and are available as global 1 by 1° objectively analyzed measurements. Zooplankton biomass measurements (mg C m^{-3}) were extracted from the COPEPOD database (O'Brien, 2005) and are available at a near-global 1° by 1° resolution.

Standardized time series of westerly weather, phytoplankton, zooplankton, herring, and kittiwake breeding success as reported by (Aebischer et al., 1990) were extracted as yearly averages using data digitization software[3]. Indices of the North Atlantic Oscillation Index (NAO), and the Atlantic Multidecadal Oscillation (AMO)

[1] www.info.sciverse.com/scopus
[2] www.apps.webofknowledge.com
[3] www.getdata-graph-digitizer.com

were extracted from the sources listed in Table S1. The NAO represents the first principle component from a rotated principle components analysis (RPCA) applied to monthly standardized pressure anomalies across the North Atlantic (20° to 90°N); (ref. Barnston and Livezey, 1987). The AMO represents the area-weighted SST average over the North Atlantic (0° to 70°N). To remove high-frequency temporal variability, all series were smoothed using GAMs. Following this smoothing procedure, all series were re-scaled such that they were represented on the same scale (between -1 and 1).

Appendix F

Copyright Permissions

F.1 Copyright Permissions: Chapter 3

From: daniel boyce [mailto:dboyce@dal.ca]
Sent: 11 June 2013 20:12
To: Lupp, Claudia
Subject: Copyright permission to include Nature publications in thesis.

Dear Dr. Lupp,
I am preparing my PhD thesis for submission to the Faculty of Graduate Studies at Dalhousie University, Halifax, Nova Scotia, Canada. I am seeking your permission to include a manuscript version of the following paper(s) as a chapter in the thesis: "Global patterns of marine phytoplankton change".

Boyce, D. G., M. R. Lewis, and B. Worm. 2010. Global phytoplankton decline over the past century. Nature 466: 591–596.

Boyce, D. G., M. R. Lewis, and B. Worm. 2011. Boyce et al. reply. Nature 472: E8–E9.

Canadian graduate theses are reproduced by the Library and Archives of Canada (formerly National Library of Canada) through a non-exclusive, world-wide license to reproduce, loan, distribute, or sell theses. I am also seeking your permission for the material described above to be reproduced and distributed by the LAC(NLC). Further details about the LAC(NLC) thesis program are available on the LAC(NLC) website (www.nlc-bnc.ca).
Full publication details and a copy of this permission letter will be included in the thesis.
Yours sincerely,
Daniel Boyce.

Dear Daniel,
Thank you for contacting Nature Publishing Group. As an author, you have the right to use this manuscript and figures, as per the licence-to-publish you signed:
Ownership of copyright in the article remains with the Authors, and provided that, when reproducing the Contribution or extracts from it, the Authors acknowledge first and reference publication in the Journal, the Authors retain the following non-exclusive rights:
a) To reproduce the Contribution in whole or in part in any printed volume (book or thesis) of which they are the author(s).
b) They and any academic institution where they work at the time may reproduce the Contribution for the purpose of course teaching.
c) To post a copy of the Contribution as accepted for publication after peer review (in Word or Tex format) on the Authors' own web site or institutional repository, or the Authors' funding body's designated archive, six months after publication of the printed or online edition of the Journal, provided that they also give a hyperlink from the Contribution to the Journals web site.
d) To reuse figures or tables created by them and contained in the Contribution in other works created by them.
Kind Regards,
Claire Smith
Permissions Assistant
nature publishing group
The Macmillan Building
4 Crinan Street, London N1 9XW
e: permissions@nature.com
p: + 44 207 014 4129

F.2 Copyright Permissions: Chapter 4

From: Daniel Boyce [mailto:dboyce@dal.ca]
Sent: Monday, July 29, 2013 12:49 PM
To: lomethods-editor@aslo.org; Boris Worm
Subject: Re: Copyright permission to include L&O: Methods paper in thesis.

Dear Dr. Kemp,
I am preparing my PhD thesis for submission to the Faculty of Graduate Studies at Dalhousie University, Halifax, Nova Scotia, Canada. I am seeking your permission to include a manuscript version of the following paper(s) as a chapter in the thesis: "Global patterns of marine phytoplankton change".

Boyce, D. G., M. Lewis, and B. Worm. 2012. Integrating global chlorophyll data from 1890 to 2010. Limnology and Oceanography: Methods 10: 840–852.

Canadian graduate theses are reproduced by the Library and Archives of Canada (formerly National Library of Canada) through a non-exclusive, world-wide license to reproduce, loan, distribute, or sell theses. I am also seeking your permission for the material described above to be reproduced and distributed by the LAC(NLC). Further details about the LAC(NLC) thesis program are available on the LAC(NLC) website (www.nlc-bnc.ca).
Full publication details and a copy of this permission letter will be included in the thesis.
Yours sincerely,
Daniel Boyce

Dear Mr. Boyce,
ASLO's policies allow authors to include articles published in ASLO journals in their thesis or dissertation. I see no conflict with this policy in your request.
Regards,
Paul Kemp
Editor, Limnology and Oceanography: Methods

,

Bibliography

Acker, J. G. and Leptoukh, G. (2007). Online analysis enhances use of NASA earth science data. *Transactions, American Geophysical Union*, 88:14–17.

Aebischer, N. J., Coulson, J. C., and Colebrook, J. M. (1990). Parallel long-term trends across four marine trophic levels and weather. *Nature*, 347:753–755.

Agusti, S., Satta, M. P., Mura, M. P., and Benavent, E. (1998). Dissolved esterase activity as a tracer of phytoplankton lysis: Evidence of high phytoplankton lysis rates in the northwestern Mediterranean. *Limnology and Oceanography*, 43(8):1836–1849.

Akima, H. (1978). A method of bivariate interpolation and smooth surface fitting for irregularly distributed data points. *ACM transactions on mathematical software*, 4(2):148–159.

Alvain, S., Moulin, C., Dandonneau, Y., and Bréon, F. (2005). Remote sensing of phytoplankton groups in case 1 waters from global SeaWiFS imagery. *Deep Sea Research Part I: Oceanographic Research Papers*, 52(11):1989–2004.

Alvain, S., Moulin, C., Dandonneau, Y., and Loisel, H. (2008). Seasonal distribution and succession of dominant phytoplankton groups in the global ocean: A satellite view. *Global Biogeochemical Cycles*, 22(3):GB3001.

Antoine, D., Morel, A., Gordon, H. R., Banzon, V. F., and Evans, R. H. (2005). Bridging ocean color observations of the 1980s and 2000s in search of long-term trends. *Journal of Geophysical Research*, 110:1–22.

Arrigo, K. R., Perovich, D. K., Pickart, R. S., Brown, Z. W., Dijken, G. L. V., Lowry, K. E., Mills, M. M., Palmer, M. A., Balch, W. M., Bahr, F., Bates, N. R., Benitez-nelson, C., Bowler, B., Brownlee, E., Ehn, J. K., Frey, K. E., Garley, R., Laney, S. R., Lubelczyk, L., Mathis, J., Matsuoka, A., Mitchell, B. G., Moore, G. W. K., Ortega-retuerta, E., Pal, S., Polashenski, C. M., Reynolds, R. A., Schieber, B., Sosik, H. M., Stephens, M., and Swift, J. H. (2012). Under Arctic Sea Ice. *Science*, 336(6087):1408.

Atkinson, A., Siegel, V., and Pakhomov, E. (2004). Long-term decline in krill stock and increase in salps within the Southern Ocean. *Nature*, 432(7013):100–103.

Atkinson, D. (1994). Temperature and organism size - A biological law for ectotherms. *Advances in Ecological Research, Vol 25*, 25:1–58.

Atkinson, D., Ciotti, B. J., and Montagnes, D. J. S. (2003). Protists decrease in size linearly with temperature: ca. 2.5% degrees C(-1). *Proceedings. Biological sciences / The Royal Society*, 270(1533):2605–11.

Augustin, N., A, Mugglestone, M., and Buckland, S. (1996). An autologistic model for the spatial distribution of wildlife. 33(2):339–347.

Azam, F., Fenchel, T., Field, J. G., Gray, J. S., Meyerreil, L. A., and Thingstad, F. (1983). The ecological role of water-column microbes in the sea. *Marine Ecology-Progress Series*, 10(3):257–263.

Bainerd, K. E. and Gregg, M. C. (1995). Surface mixed and mixing layer depths . *Deep Sea Research*, 9:1521–1543.

Bakun, A. (1990). Global climate change and intensification of coastal ocean upwelling. *Science*, 247:198–201.

Barber, R. T. and Chavez, F. R. (1986). Ocean variability in relation to living resources during the 1982-83 El Nino. *Nature*, 319:279–285.

Barnes, C., Maxwell, D., Reuman, D. C., and Jennings, S. (2010). Global patterns in predator-prey size relationships reveal size dependency of trophic transfer efficiency. *Ecology*, 91(1):222–32.

Barnston, A. G. and Livezey, R. E. (1987). Classification, seasonality and persistence of low-frequency atmospheric circulation patterns. *Monthly Weather Review*, 115:1083–1126.

Baum, J. K. and Worm, B. (2009). Cascading top-down effects of changing oceanic predator abundances. *Journal of Animal Ecology*, 78(4):699–714.

Beaufort, L., Lancelot, Y., Camberlin, P., Cayre, O., Vincent, E., Bassinot, F., and Labeyrie, L. (1997). Insolation cycles as a major control equatorial Indian Ocean primary production. *Science*, 278(5342):1451–1454.

Beaugrand, G. Ibaez, F. (2002). Spatial dependence of calanoid copepod diversity in the North Atlantic Ocean. *Marine Ecology-Progress Series*, 232:197â211.

Beaugrand, G., Brander, K. M., Alistair Lindley, J., Souissi, S., and Reid, P. C. (2003). Plankton effect on cod recruitment in the North Sea. *Nature*, 426(6967):661–4.

Beaulieu, C., Henson, S. a., Sarmiento, J. L., Dunne, J. P., Doney, S. C., Rykaczewski, R. R., and Bopp, L. (2013). Factors challenging our ability to detect long-term trends in ocean chlorophyll. *Biogeosciences*, 10(4):2711–2724.

Bedacht, E., Gulev, S. K., and Macke, A. (2007). Intercomparison of global cloud cover fields over oceans from the VOS observations and NCEP/NCAR reanalysis. *International Journal of Climatology*, 27(13):1707–1719.

Behrenfeld, M. (2011). Uncertain future for ocean algae. *Nature Climate Change*, 1(1):33–34.

Behrenfeld, M., Bale, A. J., Kolber, Z. S., Aiken, J., and Falkowski, P. G. (1996). Confirmation of iron limitation of phytoplankton photosynthesis in the equatorial Pacific Ocean. *Nature*, 383(6600):508–511.

Behrenfeld, M. and Falkowski, P. (1997). Consumers guide to phytoplankton primary productivity models. *Limnology and Oceanography*, 42:1479–1491.

Behrenfeld, M., O'Malley, R., Siegel, D., McClain, C., Sarmiento, J., Feldman, G., Milligan, A., Falkowski, P., Letelier, R., and Boss, E. (2006). Climate-driven trends in contemporary ocean productivity. *Nature*, 444(7120):752–5.

Behrenfeld, M. J., Boss, E., Siegel, D. A., and Shea, D. M. (2005). Carbon-based ocean productivity and phytoplankton physiology from space. *Global Biogeochemical Cycles*, 19:1–14.

Behrenfeld, M. J., Randerson, J. T., McClain, C. R., Feldman, G. C., Los, S. O., Tucker, C. J., Falkowski, P. G., Field, C. B., Frouin, R., Esaias, W. E., Dolber, D. D., and Pollack, N. H. (2001). Biospheric primary production during an ENSO transition. *Science*, 291:2594–2597.

Bidle, K. D. and Falkowski, P. G. (2004). Cell death in planktonic, photosynthetic microorganisms. *Nature*, 2:643–655.

Bigelow, K. A., Boggs, H., and He, X. I. (1999). Environmental effects on swordfish and blue shark catch rates in the US North Pacifc longline fishery. *Fisheries Oceanography*, (July 1997):178–198.

Bopp, L., Aumont, O., Cadule, P., Alvain, S., and Gehlen, M. (2005). Response of diatoms distribution to global warming and potential implications: A global model study. *Geophysical Research Letters*, 32(19).

Bopp, L., Monfray, P., Aumont, O., Dufresne, J.-L. L., Le Treut, H., Madec, G., Terray, L., and Orr, J. C. (2001). Potential impact of climate change on marine export production. *Global Biogeochemical Cycles*, 15(1):81–99.

Boyce, D., Dowd, M., Lewis, M., and Worm, B. (2013). Global chlorophyll change over the past century. *Progress in Oceanography (in review)*.

Boyce, D., Lewis, M., and Worm, B. (2010). Global phytoplankton decline over the past century. *Nature*, 466:591–596.

Boyce, D., Lewis, M. R., and Worm, B. (2011). Boyce et al. reply. *Nature*, 472(7342):E8–E9.

Boyce, D. G., Lewis, M., and Worm, B. (2012). Integrating global chlorophyll data from 1890 to 2010. *Limnology and Oceanography: Methods*, 10:840–852.

Boyd, P. W. and Doney, S. C. (2002). Modelling regional responses by marine pelagic ecosystems to global climate change. *Geophysical Research Letters*, 29(16).

Boyd, P. W., Watson, A. J., Law, C. S., Abraham, E. R., Trull, T., Murdoch, R., Bakker, D. C. E., Bowie, A. R., Buesseler, K. O., Chang, H., Charette, M., Croot, P., Downing, K., Frew, R., Gall, M., Hadfield, M., Hall, J., Harvey, M., Jameson, G., LaRoche, J., Liddicoat, M., Ling, R., Maldonado, M. T., McKay, R. M., Nodder, S., Pickmere, S., Pridmore, R., Rintoul, S., Safi, K., Sutton, P., Strzepek, R., Tanneberger, K., Turner, S., Waite, A., and Zeldis, J. (2000). A mesoscale phytoplankton bloom in the polar Southern Ocean stimulated by iron fertilization. *Nature*, 407(6805):695–702.

Boyer, T. P., Antonov, J. I., Baranova, O. K., Garcia, H. E., Johnson, D. R., Locarnini, R. A., Mishonov, A. V., O'Brien, T. D., Seidov, D., Smolyar, I. V., and Zweng, M. M. (2009). World ocean database 2009. Technical report, Silver Spring, MD.

Brander, K. M. (2007). Global fish production and climate change. *Proceedings of the National Academy of Sciences of the United States of America*, 104:19709–19714.

Brimblecombe, P. and Pitman, J. (1980). Long-term deposit at Rothamsted, Southern England. *Tellus*, 32(3):261–267.

Broecker, W. S., Sutherland, S., and Peng, T.-H. (1999). A possible 20th century slowdown of Southern ocean deep water formation. *Science*, 286:1132–1134.

Brown, J. H., Gillooly, J. F., Allen, A. P., Savage, V. M., and West, G. B. (2004). Toward a metabolic theory of ecology. *Ecology*, 85(7):1771–1789.

Buchanan, J. Y. (1910). Colour of the sea. *Nature*, 84:87–89.

Burnham, K. P. (2004). Multimodel Inference: Understanding AIC and BIC in Model Selection. *Sociological Methods & Research*, 33(2):261–304.

Burnham, K. P. and Anderson, D. R. (2002). *Model Selection and Multi-Model Inference: A Practical Information-Theoretic Approach*. Springer-Verlag, New York, 2nd edition.

Burrough, P. A., and McDonell, R. A. (1998). *Principles of Geographical Information Systems*. Oxford University Press, New York, USA.

Capone, D. G., Zehr, J. P., Paerl, H. W., Bergman, B., and Carpenter, E. J. (1997). Trichodesmium, a globally significant marine cyanobacterium. *Science*, 276(5316):1221–1229.

Carton, J. a. and Giese, B. S. (2008). A Reanalysis of Ocean Climate Using Simple Ocean Data Assimilation (SODA). *Monthly Weather Review*, 136(8):2999–3017.

Casini, M., Lovgren, J., Hjelm, J., Cardinale, M., Molinero, J.-C. C., Kornilovs, G., and Lövgren, J. (2008). Multi-level trophic cascades in a heavily exploited open marine ecosystem. *Proceedings of the Royal Society B-Biological Sciences*, 275(1644):1793–1801.

Cermeno, P., Dutkiewicz, S., Harris, R. P., Follows, M., Schofield, O., and Falkowski, P. (2008). The role of nutricline depth in regulating the ocean carbon cycle. *Proceedings of the National Academy of Sciences of the United States of America*, 105(51):20344–20349.

Charlson, R. J., Lovelock, J. E., Andreae, M. O., and Warren, S. G. (1987). Oceanic phytoplankton, atmospheric sulphur, cloud albedo and climate. *Nature*, 326:655–661.

Charpy-Roubaud, C. and Sournia, A. (1990). The comparative estimation of phytoplanktonic, microphytobenthic and macrophytobenthic primary production in the oceans. *Marine Microbial Food Webs*, 4(1):31–57.

Chassot, E., Bonhommeau, S., Dulvy, N. K., Mélin, F., Watson, R., Gascuel, D., and Le Pape, O. (2010). Global marine primary production constrains fisheries catches. *Ecology letters*, 13(4):495–505.

Chassot, E., Melin, F., Le Pape, O., and Gascuel, D. (2007). Bottom-up control regulates fisheries production at the scale of eco-regions in European seas. *Marine Ecology-Progress Series*, 343:45–55.

Chavez, F., Ryan, J., Lluch-Cota, S., and Niquen, C. (2003). From anchovies to sardines and back: multidecadal change in the Pacific Ocean. *Science*, 299(5604):217–21.

Chavez, F. P., Messie, M., and Pennington, J. T. (2011). Marine primary production in relation to climate variability and change. *Annual Review of Marine Science*, 3:227–260.

Chavez, F. P., Strutton, P. G., Friederich, C. E., Feely, R. A., Feldman, G. C., Foley, D. C., and McPhaden, M. J. (1999). Biological and chemical response of the equatorial Pacific Ocean to the 1997-98 El Nino. *Science*, 286(5447):2126–2131.

Chavez, F. P. and Toggweiler, J. R. (1995). Physical estimates of global new production: The upwelling contribution. In *Upwelling in the Ocean: Modern Processes and Ancient Records*, volume 18, pages 313–320.

Chisholm, S. W., Falkowski, P., and Cullen, J. J. (2001). Dis-crediting ocean fertilization. *Science*, 294:309–310.

Collier, A., Finlayson, G. M., and Cake, E. W. (1968). On the transparency of the sea. *Limnology and Oceanography*, 13(2):391–394.

Conkright, M. E., Brien, T. D. O., Locarnini, R. A., Boyer, T. P., and Antonov, J. I. (2002). NOAA Atlas NESDIS 54 WORLD OCEAN ATLAS 2001 VOLUME 6 : Chlorophyll. 6.

Conkright, M. E. and Gregg, W. W. (2003). Comparison of global chlorophyll climatologies: In situ, czcs, blended in situ-czcs and seawifs. *International Journal of Remote Sensing*, 24(5):969–991.

Cooper, H. and Hedges, L. V. (1994). *The handbook of research synthesis*. Russell Sage Foundation, New York.

Cox, P. M., Betts, R. A., Jones, C. D., Spall, S. A., and Totterdell, I. J. (2000). Acceleration of global warming due to carbon-cycle feedbacks in a coupled climate model. *Nature*, 408:184–187.

Cressie, N. A. C. (1993). *Statistics for spatial data*. John Wiley & Sons, New York.

Cullen, J. (1982). The deep chlorophyll maximum: comparing vertical profiles of chlorophyll a. *Can J Fish Aquat Sci*, 39:791–801.

Cushing, D. H. (1990). Plankton production and year-class strength in fish populations - an update of the match mismatch hypothesis. *Advances in Marine Biology*, 26:249–293.

Dewar, W. K., Bingham, R. J., Iverson, R. L., Nowacek, D. P., St. Laurent, L. C., and Wiebe, P. H. (2006). Does the marine biosphere mix the ocean? *Journal of Marine Research*, 64(4):541–561.

Diaz, R. J. and Rosenberg, R. (2008). Spreading dead zones and consequences for marine ecosystems. *Science*, 321(5891):926–9.

Dickson, R. R., Kelly, P. M., Colebrook, J. M., Wooster, W. S., and Cushing, D. H. (1988). North winds and production in the eastern North Atlantic. *Journal of Plankton Research*, 10(1):151–169.

Dippner, J. W. and Krause, M. (2013). Continuous plankton recorder underestimates zooplankton abundance. *Journal of Marine Systems*, 111-112:263–268.

Doney, S. C. (2006). Plankton in a warmer world. *Nature*, 444:695–96.

Doney, S. C., Glover, D. M., McCue, S. J., and Fuentes, M. (2003). Mesoscale variability of Sea-viewing Wide Field-of-view Sensor(SeaWiFS) satellite ocean color: Global patterns and spatial scales. *Journal of Geophysical Research-Oceans*, 108(C2):1–19.

Dormann, C. F. (2007). Assessing the validity of autologistic regression. *Ecological Modelling*, 207(2-4):234–242.

D'Ortenzio, F., Antoine, D., Martinez, E., and Ribera d'Alcalà, M. (2012). Phenological changes of oceanic phytoplankton in the 1980s and 2000s as revealed by remotely sensed ocean-color observations. *Global Biogeochemical Cycles*, 26(4):1–16.

Duce, R. A., Liss, P. S., Merrill, J. T., Buat-Menard, P., Hicks, B. B., Miller, J. M., Prospero, J. M., Arimoto, R., Church, T. M., Ellis, W., Galloway, J. N., Hanson, L., Jickells, T. D., Knapp, A. H., Rienhart, K. H., Schneider, B., Soudine, A., Tokos, J. J., Tsunogai, S., Wollast, R., and Zhou, M. (1991). The atmospheric input of trace species to the world ocean. *Global Biogeochemical Cycles*, 5:193–259.

Durham, W. M., Kessler, J. O., and Stocker, R. (2009). Disruption of vertical motility by shear triggers formation of thin phytoplankton layers. *Science*, 323:1067–1069.

Edwards, K. F., Thomas, M. K., Klausmeier, C. a., and Litchman, E. (2012). Allometric scaling and taxonomic variation in nutrient utilization traits and maximum growth rate of phytoplankton. *Limnology and Oceanography*, 57(2):554–566.

Edwards, M. (2004). Preface. *Marine Ecology Progress Series*, cpr:1–2.

Eppley, R. (1972). Temperature and phytoplankton growth in the sea. *Fishery Bulletin*, 70(4):1063–85.

Eppley, R. and Sloan, P. (1965). Carbon balance experiments with marine phytoplankton. *Journal of the Fisheries Research Board of Canada*, 22:1083–97.

Estes, J. a., Terborgh, J., Brashares, J. S., Power, M. E., Berger, J., Bond, W. J., Carpenter, S. R., Essington, T. E., Holt, R. D., Jackson, J. B. C., Marquis, R. J., Oksanen, L., Oksanen, T., Paine, R. T., Pikitch, E. K., Ripple, W. J., Sandin, S. a., Scheffer, M., Schoener, T. W., Shurin, J. B., Sinclair, A. R. E., Soule, M. E., Virtanen, R., Wardle, D. a., and Soulé, M. E. (2011). Trophic downgrading of planet earth. *Science*, 333(6040):301–306.

Etnoyer, P., Canny, D., Mate, B., and Morgan, L. (2004). Persistent pelagic habitats in the Baja California to Bering Sea (B2B) ecoregion. *Oceanography*, 17(1):90–101.

Evans, E. H. and Gordon, H. R. (1994). Coastal zone color scanner 'system calibration': A retrospective examination. *Journal of Geophysical Research*, 99(C4):7293–7307.

Fairall, C. W., Bradley, E. F., Godfrey, J. S., Wick, G. A., Edsom, J. B., and Young, G. S. (1996). Cool-skin and warm-layer effects on sea surface temperature. *Geophysical Research Letters*, 101:1295–1308.

Falkowski, P. (1998). Biogeochemical Controls and Feedbacks on Ocean Primary Production. *Science*, 281(5374):200–206.

Falkowski, P. (2012). The power of plankton. *Nature*, 483(7387):S17–S20.

Falkowski, P. and Wilson, C. (1992). Phytoplankton productivity in the North Pacific ocean since 1900 and implications for absorption of anthropogenic C02. *Nature*, 358:741–743.

FAO (2010). The state of the world fisheries and aquaculture. Technical report, Rome.

Field, C. B., Behrenfeld, M. J., and Randerson, J. T. (1998). Primary Production of the Biosphere : Integrating Terrestrial and Oceanic Components. *Science*, 281.

Finkel, Z. V., Katz, M. E., Wright, J. D., Schofield, O. M. E., and Falkowski, P. G. (2005). Climatically driven macroevolutionary patterns in the size of marine diatoms over the Cenozoic. *Proceedings of the National Academy of Sciences of the United States of America*, 102(25):8927–8932.

Forel, F. A. (1890). Une nouvelle forme de la gamme de couleur pour l'etude de l'eau des lacs. *Archives des sciences physiques et naturelles/Societe de physique et d'histoire naturelle de geneve*, 6(25).

Fortier, M., Fortier, L., Michel, C., and Legendre, L. (2002). Climatic and biological forcing of the vertical flux of biogenic particles under seasonal Arctic sea ice. *Marine Ecology Progress Series*, 225(1):1–16.

Frank, K., Petrie, B., Choi, J. S., and Leggett, W. C. (2005). Trophic cascades in a formerly cod-dominated ecosystem. *Science*, 308(5728):1621–1623.

Frank, K. T., Petrie, B., Fisher, J. a. D., and Leggett, W. C. (2011). Transient dynamics of an altered large marine ecosystem. *Nature*, 477(7362):86–9.

Frederiksen, M., Edwards, M., Richardson, A. J., Halliday, N. C., and Wanless, S. (2006). From plankton to top predators: bottom-up control of a marine food web across four trophic levels. *The Journal of animal ecology*, 75(6):1259–68.

Fromentin, J. M. and Planque, B. (1996). Calanus and environment in the eastern North Atlantic. 2. Influence of the North Atlantic Oscillation on C. finmarchicus and C. helgolandicus. *Marine Ecology Progress Series*, 134:111–118.

Fulton, T. L. and Strobeck, C. (2010). Multiple markers and multiple individuals refine true seal phylogeny and bring molecules and morphology back in line. *Proceedings. Biological sciences / The Royal Society*, 277(1684):1065–70.

Geider, R. J. (1987). Light and temperature-dependence of the carbon to chlorophyll-a ratio in microalgae and cyanobacteria - implications for physiology and growth of phytoplankton. *New Phytologist*, 106(1):1–34.

Gjosaeter, J. and Kawaguchi, K. (1980). A review of the world resources of mesopelagic fish. *FAO Fisheries Technical Paper*, 193:151.

Gnanadesikan, A., Vecchi, G. A., Anderson, W. G., Hallberg, R., and Emmanuel, K. (2010). How ocean color can steer Pacific tropical cyclones. *Geophysical Research Letters*.

Goes, J., Thoppil, P., and Gomes, H. R. (2005). Warming of the eurasian landmass is making the arabian sea more productive. *Science*, 308:545–548.

Grantham, B. A., Chan, F., Nielsen, K. J., Fox, D. S., Barth, J. A., Huyer, A., Lubchenco, J., and Menge, B. A. (2004). Upwelling-driven nearshore hypoxia signals ecosystem and oceanographic changes in the northeast Pacific. *Nature*, 429(6993):749–754.

Gregg, W. W., Casey, N. W., and McClain, C. R. (2005). Recent trends in global ocean chlorophyll. *Geophysical Research Letters*, 32:1–5.

Gregg, W. W. and Conkright, M. E. (2001). Warming of the eurasian landmass is making the arabian sea more productive. *J. Geophys. Res.*, 106(C2):2499–2515.

Gregg, W. W. and Conkright, M. E. (2002). Decadal changes in global ocean chlorophyll. *Geophysical Research Letters*, 29:1730–1734.

Gregg, W. W., Conkright, M. E., Ginoux, P., O'Reilly, J. E., and Casey, N. W. (2003). Ocean primary production and climate: Global decadal changes. *Geophysical Research Letters*, 30:1813–1909.

Guidi, L., Stemmann, L., Jackson, G. A., Ibanez, F., Claustre, H., Legendre, L., Picheral, M., and Gorsky, G. (2009). Effects of phytoplankton community on production, size, and export of large aggregates: A world-ocean analysis. *Limnology and Oceanography*, 54(6):1951–1963.

Gumpertz, M. L. M., Graham, J. J. M., and Ristaino, J. B. J. B. (1997). Autologistic model of spatial pattern of phytophthora epidemic in bell pepper: effects of soil variables on disease presence. *Journal of Agricultural Biological and Environmental Statistics*, 2(2):131–156.

Hamme, R. C., Webley, P. W., Crawford, W. R., Whitney, F. A., DeGrandpre, M. D., Emerson, S. R., Eriksen, C. C., Giesbrecht, K. E., Gower, J. F. R., Kavanaugh, M. T., Pena, M. A., Sabine, C. L., Batten, S. D., Coogan, L. A., Grundle, D. S., and Lockwood, D. (2010). Volcanic ash fuels anomalous plankton bloom in subarctic northeast Pacific. *Geophysical Research Letters*, 37:1–5.

Haney, J. C. (1986). Seabird aggregation at Gulf Stream frontal eddies. *Marine Ecology-Progress Series*, 28:279–285.

Hansen, H. (1999). *Determination of oxygen. In: Methods of seawater analysis, Edition 3*. WILEY-VCH Verlag GmbH, Weinheim.

Hastie, T. and Tibshirani, R. (1986). Generalized additive models. *Statistical Science*, 1:297–318.

Heiberger, R. and Holland, B. (2004). *Statistical analysis and data display: An intermediate course with examples in S-plus, R, and SAS*. Springer.

Henson, S. A., Sarmiento, J. L., Dunne, J. P., Bopp, L., Lima, I., Doney, S. C., John, J., and Beaulieu, C. (2010). Detection of anthropogenic climate change in satellite records of ocean chlorophyll and productivity. *Biogeosciences*, 7:621–640.

Herdman, A. W. A. and Url, S. (1909). Our Food from the Waters. *Science*, 30(778):740–749.

Hillebrand, H. (1999). Effect of biotic interactions on the structure of microphytobenthos. *Dissertation. Ber. Inst. Meeresk. Kiel*, 308:157.

Hillebrand, H. (2004). On the generality of the latitudinal diversity gradient. *American Naturalist*, 163(2):192–211.

Hjort, J. (1914). Fluctuations in the Great Fisheries of Northern Europe. *Rapports, Conceil Permanent International pour l'Exploration de la Mer*, 20:1–288.

Hofmann, M. and Maqueda, M. (2006). Performance of a second-order moments advection scheme in an Ocean General Circulation Model. *Journal of Geophysical Research*, 111(C5):1–26.

Hofmann, M., Worm, B., Rahmstorf, S., and Schellnhuber, H. J. (2011). Declining ocean chlorophyll under unabated anthropogenic CO2 emissions. *Environmental Research Letters*, 6(3).

Hooper, D. U., Adair, E. C., Cardinale, B. J., Byrnes, J. E. K., Hungate, B. a., Matulich, K. L., Gonzalez, A., Duffy, J. E., Gamfeldt, L., and O'Connor, M. I. (2012). A global synthesis reveals biodiversity loss as a major driver of ecosystem change. *Nature*, 486(7401):105–8.

Houben, A. J. P., Bijl, P. K., Pross, J., Bohaty, S. M., Passchier, S., Stickley, C. E., Röhl, U., Sugisaki, S., Tauxe, L., van de Flierdt, T., Olney, M., Sangiorgi, F., Sluijs, A., Escutia, C., Brinkhuis, H., Dotti, C. E., Klaus, A., Fehr, A., Williams, T., Bendle, J. a. P., Carr, S. a., Dunbar, R. B., Flores, J.-A., Gonzàlez, J. J., Hayden, T. G., Iwai, M., Jimenez-Espejo, F. J., Katsuki, K., Kong, G. S., McKay, R. M., Nakai, M., Pekar, S. F., Riesselman, C., Sakai, T., Salzmann, U., Shrivastava, P. K., Tuo, S., Welsh, K., and Yamane, M. (2013). Reorganization of Southern Ocean plankton ecosystem at the onset of Antarctic glaciation. *Science*, 340(6130):341–4.

Hovis, W. A., Clark, D. K., Anderson, F., Austin, R. W., Wilson, W. H., Baker, E. T., Ball, D., Gordon, H. R., Mueller, J. L., El-Sayed, S. Z., Sturm, B., Wrigley, R. C., and Yentsch, C. S. (1980). Nimbus-7 coastal zone color scanner: system description and initial imagery. *Science*, 210(4465):60–63.

Howarth, R. W., Billen, G., Townsend, A., Jaworski, N., Lajtha, K., Downing, J. A., Elmgren, R., Caraco, N., Jordan, T., Berendse, F., Freney, J., Kundeyarow, V., Murdoch, P., and Zhao-Liang, Z. (1996). Regional nitrogen budgets and riverine N and P fluxes for the drainages to the North Atlantic Ocean: natural and human influences. *Biogeochemistry*, 35:75–139.

Huot, Y., Babin, M., Bruyant, F., Grob, C., Twardowski, M. S., and Claustre, H. (2007). Does chlorophyll a provide the best index of phytoplankton biomass for primary productivity studies? *Biogeosciences Discussions*, 4:707–745.

Hyrenbach, K. D., Forney, K. A., and Dayton, P. K. (2000). Marine protected areas and ocean basin management. *Aquatic Conservation-Marine and Freshwater Ecosystems*, 10:437–458.

Ingleby, B. and Huddleston, M. (2007). Quality control of ocean temperature and salinity profiles - historical and real-time data. *Journal of Marine Systems*, 65:158–175.

I.O.C.C.G. (2007). Ocean-colour data merging . Technical report.

I.P.C.C. (2007). Climate change 2007: synthesis report. Summary for policymakers. Fourth Assessment Report. Technical report, Gland, Switzerland.

Irigoien, X., Huisman, J., and Harris, R. P. (2004). Global biodiversity patterns of marine phytoplankton and zooplankton. *Nature*, 429(6994):863–867.

Irwin, A. J. and Finkel, Z. V. (2009). Mining a sea of data: deducing the environmental controls of ocean chlorophyll. *Plos One*, 3(11):1–6.

Jacobs, S. S., Giulivi, C. F., and Mele, P. A. (2002). Freshening of the Ross Sea during the late 20th century. *Science*, 297(5580):386–389.

Jeffrey, S. W., Mantoura, R. F. C., and Wright, S. W. (1997). *Phytoplankton pigments in oceanography*, volume 10. UNESCO, Paris, France.

Ji, R., Davis, C., Chen, C., Townsend, D., Mountain, D., and Beardsley, R. (2008). Modeling the influence of low-salinity water inflow on winter-spring phytoplankton dynamics in the nova scotian shelf - gulf of maine region. *Journal of Plankton Research*, 30:1399–1360.

Jickells, T. D. (1998). Nutrient biogeochemistry of the coastal zone. *Science*, 281:217–222.

Johnson, N. A., Campbell, J. W., Moorre, T. S., Rex, M. A., Etter, R. J., McClain, C. R., and Dowell, M. D. (2007). The relationship between the standing stock of deep-sea macrobenthos and surface production in the western North Atlantic. *Deep-Sea Research Part I-Oceanographic Research Papers*, 54(8):1350–1360.

Kalnay, E. (1996). The NCEP/NCAR 40-year reanalysis project. *Bulletin of the American Meteorological Society*, 77:437–471.

Kara, A. B., Rochford, P. A., and Hurlburt, H. E. (2000). An optimal definition for ocean mixed layer depth. *Journal of Geophysical Research*, 105(C7):16,803–816,821.

Kim, Y. J. and Gu, C. (2004). Smoothing spline Gaussian regression: more stable computation via efficient approximation. *Journal of the Royal Statistical Society, Series B*, 66:337–356.

Klauschies, T., Bauer, B., Aberle-Malzahn, N., Sommer, U., and Gaedke, U. (2012). Climate change effects on phytoplankton depend on cell size and food web structure. *Marine Biology*, 159(11):2455–2478.

Kuhlbrodt, T., Rahmstorf, S., Zickfeld, K., Vikebø, F. B., Sundby, S., Hofmann, M., Link, P. M., Bondeau, A., Cramer, W., and Jaeger, C. (2009). An Integrated Assessment of changes in the thermohaline circulation. *Climatic Change*, 96(4):489–537.

Kunze, E., Dower, J. F., Beveridge, I., Dewey, R., and Bartlett, K. P. (2006). Observations of biologically generated turbulence in a coastal inlet. *Science*, 313(5794):1768–70.

Lasker, R. (1975). Field criteria for survival of anchovy larvae: the relation between inshore chlorophyll maximum layers and successful first feeding. *Fishery Bulletin*, 73(3):453–462.

Lee, S. H., Joo, H. M., Liu, Z., Chen, J., and He, J. (2012). Phytoplankton productivity in newly opened waters of the Western Arctic Ocean. *Deep Sea Research Part II: Topical Studies in Oceanography*, 8184(0):18–27.

Legendre, P. and Legendre, L. (1998). *Numerical ecology*. Elsevier Science, Amsterdam, 2nd edition.

Levitus, S. (1982). *Climatological atlas of the world ocean*, volume 13. U.S. Govt. Print. Off., Washington, D.C.

Levitus, S. (2000). Warming of the World Ocean. *Science*, 287(5461):2225–2229.

Levy, G. and Brown, R. A. (1986). A simple objective analysis scheme for scatterometer data. *J. Geophys. Res.*, 91:5153–5158.

Lewandowska, A., Boyce, D., Hofmann, M., Matthiessen, B., Sommer, U., and Worm, B. (2013). Effects of sea surface warming on marine plankton. *Ecology Letters (in review)*.

Lewis, M. R., Kuring, N., and Yentsch, C. (1988). Global patterns of ocean transparency: implications for the new production of the open ocean. *Journal of Geophysical Research*, 93:6847–6856.

Li, W. K. W., McLaughlin, F. A., Lovejoy, C., and Carmack, E. C. (2009). Smallest algae thrive as the Arctic Ocean freshens. *Science*, 326(5952):539.

Litzow, M. a. and Ciannelli, L. (2007). Oscillating trophic control induces community reorganization in a marine ecosystem. *Ecology letters*, 10(12):1124–34.

Llewellyn, C. A., Tarran, G. A., Galliene, C. P., Cummings, D. G., De Menezes, A., Rees, A. P., Dixon, J. L., Widdicombe, C. E., Fileman, E. S., and Wilson, W. H. (2008). Microbial dynamics during the decline of a spring diatom bloom in the Northeast Atlantic. *Journal of Plankton Research*, 30(3):261–273.

Loeb, V., Siegel, V., HolmHansen, O., Hewitt, R., Fraser, W., Trivelpiece, W., and Trivelpiece, S. (1997). Effects of sea-ice extent and krill or salp dominance on the Antarctic food web. *Nature*, 387(6636):897–900.

Lorenzen, C. L. (1966). A method for the continuous measurement of in vivo chlorophyll concentration. *Deep Sea Research*, 13(2):223–227.

Lozier, M. S., Dave, A. C., Palter, J. B., Gerber, L. M., and Barber, R. T. (2011). On the relationship between stratification and primary productivity in the North Atlantic. *Geophysical Research Letters*, 38.

Mackas, D. L. (2011). Does blending of chlorophyll data bias temporal trend? *Nature: Brief communications arising*, 472:E4–E5.

Mahadevan, A. and Campbell, J. W. (2002). Biogeochemical patchiness at the sea surface. *Geophysical Research Letters*, 29(19):31–32.

Mann, K. H. and Lazier, J. R. N. (1991). *Dynamics of marine ecosystems*. Blackwell, Oxford, UK.

Mantoura, R. F. C. and Llewellyn, C. A. (1983). The rapid determination of algal chlorophyll and carotenoid pigments and their breakdown products in natural waters by reverse-phase high-performance liquid chromatography. *Analytica Chimica Acta*, 151:297–314.

Marcott, S. a., Shakun, J. D., Clark, P. U., and Mix, A. C. (2013). A reconstruction of regional and global temperature for the past 11,300 years. *Science*, 339(6124):1198–201.

Martin, J. H., Coale, K. H., Johnson, K. S., Fitzwater, S. E., Gordon, R. M., Tanner, S. J., Hunter, C. N., Elrod, V. A., Nowicki, J. L., Coley, T. L., Barber, R. T., Lindley, S., Watson, A. J., Vanscoy, K., Law, C. S., Liddicoat, M. I., Ling, R., Stanton, T., Stockel, J., Collins, C., Anderson, A., Bidigare, R., Ondrusek, M., Latasa, M., Millero, F. J., Lee, K., Yao, W., Zhang, J. Z., Friederich, G., Sakamoto, C., Chavez, F., Buck, K., Kolber, Z., Greene, R., Falkowski, P., Chisholm, S. W., Hoge, F., Swift, R., Yungel, J., Turner, S., Nightingale, P., Hatton, A., Liss, P., and Tindale, N. W. (1994). Testing the iron hypothesis in ecosystems of the equatorial Pacific Ocean. *Nature*, 371(6493):123–129.

Martin, J. H. and Fitzwater, S. E. (1988). Iron deficiency limits phytoplankton growth in the northeast Pacific subarctic. *Nature*, 331(6154):341–343.

Martinez, E., Antoine, E., Ortenzio, F., and Gentili, B. (2009). Climate-driven decadal-scale oscillations of Oceanic Phytoplankton. *Science*, 326:1253–56.

Masotti, I., Moulin, C., Alvain, S., Bopp, L., Tagliabue, a., and Antoine, D. (2011). Large-scale shifts in phytoplankton groups in the Equatorial Pacific during ENSO cycles. *Biogeosciences*, 8(3):539–550.

McClain, C. R., Feldman, G. C., and Hooker, S. B. (2004). An overview of the SeaWiFS project and strategies for producing a climate research quality global ocean bio-optical time series. *Deep-Sea Res. II*, 51:5–42.

McGillicuddy, D. J., Anderson, L. A., Bates, N. R., Bibby, T., Buesseler, K. O., Carlson, C. A., Davis, C. S., Ewart, C., Falkowski, P. G., Goldthwait, S. A., Hansell, D. A., Jenkins, W. J., Johnson, R., Kosnyrev, V. K., Ledwell, J. R., Li, Q. P., Siegel, D. a., and Steinberg, D. K. (2007). Eddy/wind interactions stimulate extraordinary mid-ocean plankton blooms. *Science*, 316(5827):1021–6.

McQuatters-Gollop, A., Reid, P. C., Edwards, M. E., Burkhill, P. H., Castellani, C., Batten, S., Gieskes, W., Beare, D., Bidigare, R. R., Head, E., Johnson, R., Kahru, M., Koslow, A. J., and Angelica, P. (2011). Is there a decline in marine phytoplankton? *Nature: Brief communications arising*, 472:E6—-E7.

Menden-Deuer, S. and Lessard, E. (2000). Carbon to Volume Relationships for Dinoflagellates, Diatoms, and Other Protist Plankton. In *Limnology and Oceanography*, volume 45, pages 569–79.

Mitchell, G. and Holm-Hansen, O. (1990). Observation and modeling of the Antarctic phytoplankton crop in relation to mixing depth. *Deep Sea Research Part I: Oceanographic Research Papers*, 92(8):981–1007.

Montes-Hugo, M., Doney, S. C., Ducklow, H. W., Fraser, W., Martinson, D., Stammerjohn, S. E., and Schofield, O. (2009). Recent changes in phytoplankton communities associated with rapid regional climate change along the western Antarctic Peninsula. *Science*, 323(5920):1470–3.

Moore, C. M., Mills, M. M., Achterberg, E. P., Geider, R. J., LaRoche, J., Lucas, M. I., McDonagh, E. L., Pan, X., Poulton, A. J., Rijkenberg, M. J. A., Suggett, D. J., Ussher, S. J., and Woodward, E. M. S. (2009). Large-scale distribution of Atlantic nitrogen fixation controlled by iron availability. *Nature Geoscience*, 2(12):867–871.

Moran, X.A.G Lopez-Urrutia, A. L. W. (2010). Increasing importance of small phytoplankton in a warmer ocean. *Global Change Biology*, 16(3):1137–1144.

Morel, A. and Gentili, B. (2009). A simple band ratio technique to quantify the colored dissolved and detrital organic material from ocean color remotely sensed data. *Remote Sensing of Environment*, 113(5):998–1011.

Mundy, C. J., Gosselin, M., Ehn, J., Gratton, Y., Rossnagel, A., Barber, D. G., Martin, J., Tremblay, J.-E., Palmer, M., Arrigo, K. R., Darnis, G., Fortier, L., Else, B., and Papakyriakou, T. (2009). Contribution of under-ice primary production to an ice-edge upwelling phytoplankton bloom in the Canadian Beaufort Sea. *Geophysical Research Letters*, 36(17):L17601.

Munk, W. (1966). Abyssal recipes. *Deep Sea Research*, 13:707–730.

Murphy, E., Morris, D., Watkins, J., and Priddle, J. (1988). Scales of interaction between Antarctic krill and the environment. In Sahrhage, D., editor, *Antarctic Ocean and Resources Variability*, pages 120–303. Springer-Verlag, Berlin.

Murray, R. W., Leinen, M., and Knowlton, C. W. (2012). Links between iron input and opal deposition in the Pleistocene equatorial Pacific Ocean. *Nature Geoscience*, 5(4):270–274.

Murtugudde, R., Beauchamp, R. J., McClain, C. R., Lewis, M. R., and Busalacchi, A. (2002). Effects of penetrative radiation on the upper tropical ocean circulation. *Journal of Climate*, 15:470–486.

Nakicenovic, N. and Swart, R. (2000). *IPCC Special Report on Emissions Scenarios*. Cambridge University Press.

Ney, R. and Schoor, J. (2000). What course for carbon trading? *Environmental Science & Technology*, 34:177A–182A.

Nixon, S. W. (1995). Coastal marine eutrophication: a definition, social causes and future concerns. *Ophelia*, 41:199–219.

Nixon, S. W. and Pilson, M. E. Q. (1983). Nitrogen in estuarine and coastal marine systems. In Carpenter, E. J. and Capone, D. G., editors, *Nitrogen in the marine environment*. Academic Press, New York, USA.

Norris, R. D., Turner, S. K., Hull, P. M., and Ridgwell, A. (2013). Marine ecosystem responses to Cenozoic global change. *Science*, 341(6145):492–8.

O'Brien, T. (2005). Copepod: a global plankton database. Technical Report NMFS-F/SPO-73.

O'Connor, M. I., Piehler, M. F., Leech, D. M., Anton, A., and Bruno, J. F. (2009). Warming and Resource Availability Shift Food Web Structure and Metabolism. *Plos Biology*, 7(8).

Olonscheck, D., Hofmann, M., Worm, B., and Schellnhuber, H. J. (2013). Decomposing the effects of ocean warming on chlorophyll a concentrations into physically and biologically driven contributions. *Environmental Research Letters*, 8(1):014043.

O'Reilly, J. E., Maritorena, S., Siegel, D., O'Brien, M. C., Toole, D., Mitchell, B. G., Kahru, M., Chavez, F. P., Strutton, P., Cota, G., Hooker, S. B., McClain, C. R., Carder, K. L., Muller-Karger, F., Harding, L., Magnuson, A., Phinney, D., Moore, G. F., Aiken, J., Arrigo, K. R., Letelier, R., and Culver, M. (2000). Ocean color chlorophyll a algorithms for SeaWiFS, OC2, and OC4: Version 4. Technical report, Greenbelt, Maryland.

Oschlies, A. and Garcon, V. (1998). Eddy-induced enhancement of primary production in a model of the north Atlantic Ocean. *Nature*, 394(6690):266–269.

Otero, J., Alvarez-Salgado, X. A., Gonzalez, A. F., Miranda, A., Groom, S. B., Cabanas, J. M., Casas, G., Wheatley, B., and Guerra, A. (2008). Bottom-up control of common octopus Octopus vulgaris in the Galician upwelling system, northeast Atlantic Ocean. *Marine Ecology-Progress Series*, 362:181–192.

Pane, G. M. L. (2003). Ecology of planktonic heterotrophic flagellates. *Rivista di biologia, Biology forum*, 96:55–71.

Patterson, S. (1985). Surface circulation and kinetic energy distributions in the Southern Hemisphere Oceans from FGGE drifting buoys. *Journal of Physical Oceanography*, 15:865–884.

Pauly, D. (1995). Anecdotes and the shifting baseline syndrome of fisheries. *Trends in Ecology and Evolution*, 10:430.

Paytan, A., Mackey, K. R. M., Chen, Y., Lima, I. D., Doney, S. C., and Mahowald, N. (2009). Toxicity of atmospheric aerosols on marine phytoplankton. *Proceedings of the National Academy of Sciences of the United States of America*, 10(12):4601–4605.

Peierls, B., Caraco, N., Pace, M., and Cole, J. (1991). River nitrogen export linked to human population density. *Nature*, 350:386–87.

Perovich, D. K. and Richter-Menge, J. A. (2009). Loss of Sea Ice in the Arctic. *Annual Review of Marine Science*, 1(1):417–441.

Platt, T., Fuentes-Yaco, C., and Frank, T. (2003). Spring algal bloom and larval fish survival. *Nature*, 423:398–399.

Pollard, R. T., Salter, I., Sanders, R. J., Lucas, M. I., Moore, C. M., Mills, R. A., Statham, P. J., Allen, J. T., Baker, A. R., Bakker, D. C. E., Charette, M. A., Fielding, S., Fones, G. R., French, M., Hickman, A. E., Holland, R. J., Hughes, J. A., Jickells, T. D., Lampitt, R. S., Morris, P. J., Nedelec, F. H., Nielsdottir, M., Planquette, H., Popova, E. E., Poulton, A. J., Read, J. F., Seeyave, S., Smith, T., Stinchcombe, M., Taylor, S., Thomalla, S., Venables, H. J., Williamson, R., and Zubkov, M. V. (2009). Mesoscale vertical motion and the size structure of phytoplankton in the ocean. *Nature*, 457(7229):577–U81.

Polovina, J. J., Dunne, J. P., Woodworth, P. a., and Howell, E. a. (2011). Projected expansion of the subtropical biome and contraction of the temperate and equatorial upwelling biomes in the North Pacific under global warming. *ICES Journal of Marine Science*, 68(6):986–995.

Polovina, J. J., Howell, E. A., and Abecassis, M. (2008). Ocean's least productive waters are expanding. *Geophysical Research Letters*, 35:L03618.

Polovina, J. J., Howellb, E., Kobayashia, D. R., and Sekia, M. P. (2001). The transition zone chlorophyll front, a dynamic global feature defining migration and forage habitat for marine resources. *Progress in Oceanography*, 49:469–483.

Polovina, J. J., Kobayashi, D. R., Parker, D. M., Seki, M. P., and Balazs, G. H. (2000). Turtles on the edge: movement of loggerhead turtles (Caretta caretta) along oceanic fronts, spanning longline fishing grounds in the central North Pacific, 1997 - 1998. *Fisheries Oceanography*, 9:71–82.

Polovina, J. J. and Woodworth, P. a. (2012). Declines in phytoplankton cell size in the subtropical oceans estimated from satellite remotely-sensed temperature and chlorophyll, 1998 - 2007. *Deep Sea Research Part II: Topical Studies in Oceanography*, 77-80:82–88.

Pomeroy, L. R. (1998). The Microbial Loop. *Oceanography*, 20(2):28–33.

Post, E., Bhatt, U. S., Bitz, C. M., Brodie, J. F., Fulton, T. L., Hebblewhite, M., Kerby, J., Kutz, S. J., Stirling, I., and Walker, D. a. (2013). Ecological consequences of sea-ice decline. *Science*, 341(6145):519–24.

Preisendorfer, R. W. (1986). Secchi disk science: Visual optics of natural waters. *Limnology and Oceanography*, 31(5):909–926.

Quinn, P. K. and Bates, T. S. (2011). The case against climate regulation via oceanic phytoplankton sulphur emissions. *Nature*, 480(7375):51–56.

Raitsos, D. E., Reid, P. C., Lavender, S. J., Edwards, M., and Richardson, A. J. (2005). Extending the SeaWiFS chlorophyll data set back 50 years in the northeast Atlantic. *Geophysical Research Letters*, 32:1–4.

Rao, C. R. (1964). The use and interpretation of principal component analysis in applied research. *The Indian Journal of Statistics, Series A (1961-2002)*, 26:329–358.

Rayner, N. A., Parker, D. E., Horton, B., Folland, C. K., Alexander, L. V., Rowell, D. P., Kent, E. C., and Kaplan, A. (2003). Global analyses of sea surface temperature, sea ice, and night marine air temperature since the late nineteenth century. *Journal of Geophysical Research*, 108(D14):1–37.

Redfield, A. C. (1958). The biological control of chemical factors in the environment. *American Scientist*, 46(3):205–221.

Reich, P. B., Tilman, D., Isbell, F., Mueller, K., Hobbie, S. E., Flynn, D. F. B., and Eisenhauer, N. (2012). Impacts of biodiversity loss escalate through time as redundancy fades. *Science*, 336(6081):589–92.

Reid, P. C. (1975). Large-scale changes in north-sea phytoplankton. *Nature*, 257(5523):217–219.

Reid, P. C., Colebrook, J. M., Matthews, J. B. L., and Aiken, J. (2003). Continuous Plankton Recorder Team, the Continuous Plankton Recorder: concepts and history, from Plankton Indicator to undulating recorders. *Progress in Oceanography*, 58(2-4):117–173.

Reid, P. C., Edwards, M., Hunt, H. G., and Warner, A. J. (1998). Phytoplankton change in the North Atlantic. *Nature*, 391:546.

Richardson, A. J. and Schoeman, D. S. (2004). Climate impact on plankton ecosystems in the Northeast Atlantic. *Science*, 305:1609–1612.

Ripley, B. D. and Thompson, M. (1987). Regression techniques for the detection of analytical bias. *Analyst*, 112:377–383.

Rodriguez, J., Tintore, J., Allen, J., Blanco, J., Gomis, D., Reul, A., Ruiz, J., Rodriguez, V., Echevarria, F., and Jimenez-Gomez, F. (2001). Mesoscale vertical motion and the size structure of phytoplankton in the ocean. *Nature*, 410(6826):360–363.

Roemmich, D. and McGowan, J. (1995). Climatic warming and the decline of zooplankton in the california current. *Science*, 267(5202):1324–6.

Roman, J. and McCarthy, J. J. (2010). The whale pump: marine mammals enhance primary productivity in a coastal basin. *PloS one*, 5(10):e13255.

Roman, J. and Palumbi, S. R. (2003). Whales before whaling in the North Atlantic. *Science*, 301:508–510.

Romero, O. E., Leduc, G., Vidal, L., and Fischer, G. (2011). Millennial variability and long-term changes of the diatom production in the eastern equatorial Pacific during the last glacial cycle. *Paleoceanography*, 26(2):1–11.

Rosenzweig, C., Karoly, D., Vicarelli, M., Neofotis, P., Wu, Q., Casassa, G., Menzel, A., Root, T. L., Estrella, N., Seguin, B., Tryjanowski, P., Liu, C., Rawlins, S., and Imeson, A. (2008). Attributing physical and biological impacts to anthropogenic climate change. *Nature*, 453(7193):353–7.

Ruhl, H. A., Ellena, J. A., and Smith, K. L. (2008). Connections between climate, food limitation, and carbon cycling in abyssal sediment communities. *Proceedings of the National Academy of Sciences of the United States of America*, 105(44):17006–17011.

Rykaczewski, R. and Dunne, J. P. (2011). A measured look at ocean chlorophyll trends. *Nature: Brief communications arising*, 472:E5–E6.

Ryther, J. H. (1969). Photosynthesis and fish production in the sea. *Science*, 166(3901):72–6.

Ryther, J. H. and Yentsch, C. S. (1957). The estimation of phytoplankton production in the ocean from chlorophyll and light data. *Limnology and Oceanography*, 2(3):281–286.

Saba, V. S., Marjorie, A., Freidrichs, A., Carr, M.-E. M. E., Antoine, D., Armstrong, R. a., Asanuma, R., Aumont, O., Bates, N. N. R., Behrenfeld, M. J. M. J., Bennington, V., Bopp, L., Bruggeman, J., Buitenhuis, E. E. T., Church, M. J. M. J., Ciotti, A. M. A. M., Doney, S. C., Dowell, M., Dunne, V., Friedrichs, M. A. M., Asanuma, I., Dunne, J., Dutkiewicz, S., Gregg, W., Hoepffner, N., Hyde, K. J. W., Ishizaka, J., Kameda, T., Karl, D. M., Lima, I., Lomas, M. W., Marra, J., McKinley, G. a., Melin, F., Moore, J. K., Morel, A., O'Reilly, J., Salihoglu, B., Scardi, M., Smyth, T. J., Tang, S. L., Tjiputra, J., Uitz, J., Vichi, M., Waters, K., Westberry, T. K., Yool, A., and Mélin, F. (2010). Challenges of modeling depth-integrated marine primary productivity over multiple decades: A case study at BATS and HOT. *Global Biogeochemical Cycles*, 24(3):1–21.

Saba, V. S., Spotila, J. R., Chavez, F. P., and Musick, J. a. (2008). Bottom-up and climatic forcing on the worldwide population of leatherback turtles. *Ecology*, 89(5):1414–27.

Sabine, C. L., Feely, R. A., Gruber, N., Key, R. M., Lee, K., Bullister, J. L., Wanninkhof, R., Wong, C. S., Wallace, D. W. R., Tilbrook, B., Millero, F. J., Peng, T.-H., Kozyr, A., Ono, T., and Rios, A. F. (2004). The oceanic sink for anthropogenic CO2. *Science*, 305(5682):367–371.

Sachs, J. P. and Anderson, R. F. (2005). Increased productivity in the subantarctic ocean during Heinrich events. *Nature*, 434(7037):1118–21.

Saji, N. H., Goswami, B. N., Vinayachandran, P. N., and Yamagata, T. (1999). A dipole mode in the tropical Indian Ocean. *Nature*, 401:360–363.

Sarmiento, J. L., Slater, R., Barber, R., Bopp, L., Doney, S. C., Hirst, a. C., Kleypas, J., Matear, R., Mikolajewicz, U., Monfray, P., Soldatov, V., Spall, S. a., and Stouffer, R. (2004). Response of ocean ecosystems to climate warming. *Global Biogeochemical Cycles*, 18(3).

Saulquin, B., Fablet, R., Mangin, A., Mercier, G., Antoine, D., and D'Andon, F. (2013). Detection of linear trends in multi-sensor time series in presence of autocorrelated noise : application to the chlorophyll-a SeaWiFS and MERIS datasets and extrapolation to the incoming Sentinel 3 - OLCI 1 Introduction. *Journal of Geophysical Research-Oceans*.

Schmittner, A. (2005). Decline of the marine ecosystem caused by a reduction in the Atlantic overturning circulation. *Nature*, 434:628–633.

Schmittner, A., Oschlies, A., Matthews, H. D., and Galbraith, E. D. (2008). Future changes in climate, ocean circulation, ecosystems, and biogeochemical cycling simulated for a business-as-usual CO2 emission scenario until year 4000 AD. *Global Biogeochemical Cycles*, 23.

Schwarz, G. (1978). Estimating the dimension of a model. *The Annals of Statistics*, 6(2):461–64.

Secchi, A. (1886). Sul Moto Ondoso del Mare e su le Correnti di esso Specialmente Auquelle Littorali.

Sibert, J., Hampton, J., Kleiber, P., and Maunder, M. (2006). Biomass, size, and trophic status of top predators in the Pacific Ocean. *Science*, 314(5806):1773–6.

Siegel, D., Behrenfeld, M., Maritorena, S., McClain, C., Antoine, D., Bailey, S., Bontempi, P., Boss, E., Dierssen, H., Doney, S., Eplee, R., Evans, R., Feldman, G., Fields, E., Franz, B., Kuring, N., Mengelt, C., Nelson, N., Patt, F., Robinson, W., Sarmiento, J., Swan, C., Werdell, P., Westberry, T., Wilding, J., and Yoder, J. (2013). Regional to global assessments of phytoplankton dynamics from the SeaWiFS mission. *Remote Sensing of Environment*, 135:77–91.

Siegel, D. A., Maritorena, S., Nelson, N. B., and Behrenfeld, M. J. (2005). Independence and interdependence of global ocean color properties; Reassessing the bio-optical assumption. *Journal of Geophysical Research*, 110:C07011.

Six, K.D. MaierReimer, E. (1996). Effects of plankton dynamics on seasonal carbon fluxes in an ocean general circulation model. *Global Biogeochemical Cycles*, 10:559–583.

Smart, W. M. (1960). *Text-book on spherical astronomy, 6th edition*. Cambridge University Press, Cambridge, England.

Smetacek, V. (2008). *Impacts of Global Warming on Polar Ecosystems*.

Sokal, R. R. and Rohlf, F. J. (1995). *Biometry - The principles and practice of statistics in biologial research*. W.H. Freeman, New York, 3rd edition.

Sommer, U. (2002). Experimental systems in aquatic ecology. *Encyclopedia of life sciences*.

Sommer, U., Aberle, N., Engel, A., Hansen, T., Lengfellner, K., Sandow, M., Wohlers, J., Zollner, E., and Riebesell, U. (2007). An indoor mesocosm system to study the effect of climate change on the late winter and spring succession of Baltic Sea phyto- and zooplankton. *Oecologia*, 150(4):655–667.

Sommer, U., Aberle, N., Lengfellner, K., and Lewandowska, A. (2012). The Baltic Sea spring phytoplankton bloom in a changing climate: an experimental approach. *Marine Biology*, 159:2479–2490.

Sommer, U. and Lengfellner, K. (2008). Climate change and the timing, magnitude, and composition of the phytoplankton spring bloom. *Global Change Biology*, 14(6):1199–1208.

Sommer, U. and Sommer, F. (2006). Cladocerans versus copepods: the cause of contrasting top-down controls on freshwater and marine phytoplankton. *Oecologia*, 147(2):183–194.

Steinacher, M., Joos, F., Frolicher, T. L., Bopp, L., Cadule, P., Cocco, V., Doney, S. C., Gehlen, M., Lindsay, K., Moore, J. K., Schneider, B., and Segschneider, J. (2010). Projected 21st century decrease in marine productivity: a multi-model analysis. *Biogeosciences*, 7(3):979–1005.

Stibor, Herwig Vadstein, O. D. S. G. A. H. T. H. F. K. A. L. B. L. K. P. C. R. W. S. M. S.-H. L. O. Y. (2004). Copepods act as a switch between alternative trophic cascades in marine pelagic food webs. *Ecology Letters*, 7:321–328.

Stoecker, P. M. D. (1989). An experimentally determined carbon-volume ratio for marine oligotrichous ciliates from estuarine and coastal waters. *Limnology and Oceanography*, 34:403–434.

Stokes, G. G. (1864). On the supposed identity of biliverdin with chlorophyll with remarks on the constitution of chlorophyll. *Proceedings of the Royal Society B-Biological Sciences*, 13:144–145.

Strass, V. H. and Niithig, E.-M. (1996). Seasonal shifts in ice edge phytoplankton blooms in the Barents Sea related to the water column stability. *Polar Biology*, 16(409):409–422.

Stroeve, J. C., Kattsov, V., Barrett, A., Serreze, M., Pavlova, T., Holland, M., and Meier, W. N. (2012). Trends in Arctic sea ice extent from CMIP5, CMIP3 and observations. *Geophysical Research Letters*, 39(16):L16502.

Sund, P. N., Blackburn, M., and Williams, F. (1981). Tunas and their environment in the Pacific Ocean: a review. *Oceanography and Marine Biology: an Annual Review*, 19:443–512.

Suttle, C. A. (1994). The significance of viruses to mortality in aquatic microbial communities. *Microbial Ecology*, 28(2):237–243.

Suttle, C. A. (2007). Marine viruses - major players in the global ecosystem. *Nature Reviews Microbiology*, 5(10):801–812.

Sverdrup, H. U. (1953). On conditions for the vernal blooming of phytoplankton. *Journal du conseil international pour l'exploration de la mer*, 18:287–295.

Tarran, G. A., Zubkov, M. V., Sleigh, M. A., Burkhill, P. H., and Yallop, M. (2000). Microbial community structure and standing stocks in the NE Atlantic in June and July of 1996. *Deep-Sea Res. Part II: Tropical studies in oceanography*, 48(4-5):963–985.

Taucher, J. and Oschlies, A. (2011). Can we predict the direction of marine primary production change under global warming? *Geophysical Research Letters*, 38.

Taylor, A. H., Allen, J. I., and Clark, P. A. (2002). Extraction of a weak climatic signal by an ecosystem. *Nature*, 416(6881):629–632.

Thomas, M. K., Kremer, C. T., Klausmeier, C. a., and Litchman, E. (2012). A global pattern of thermal adaptation in marine phytoplankton. *Science*, 338(6110):1085–8.

Thompson, D. W. J. and Wallace, J. M. (2000). Annular modes in the extratropical circulation. Part I: Month-to-month variability. *J. Clim.*, 13:1000–1016.

Tilman, D. (1996). Biodiversity: population versus ecosystem stability. *Ecology*, 77(2):350–363.

Trees, C. C., Kennicutt, M. C. I., and Brooks, J. (1985). Errors associated with the standard fluorometric determination of chlorophylls and phaeopigments. *Marine Chemistry*, 17:1–12.

Tyler, J. E. (1968). The Secchi disk. *Limnology and Oceanography*, 13(1):1–6.

Uitz, J., Claustre, H., Gentili, B., and Stramski, D. (2010). Phytoplankton class-specific primary production in the world's oceans: Seasonal and interannual variability from satellite observations. *Global Biogeochemical Cycles*, 24(3):GB3016.

Uitz, J., Claustre, H., Griffiths, F. B., Ras, J., Garcia, N., and Sandroni, V. (2009). A phytoplankton class-specific primary production model applied to the Kerguelen Islands region (Southern Ocean). *Deep Sea Research Part I: Oceanographic Research Papers*, 56(4):541–560.

Vantrepotte, V. and Melin, F. (2009). Temporal variability of 10-year global SeaWiFS time-series of phytoplankton chlorophyll a concentration. *ICES Journal of Marine Science*, 66:1547–1556.

Vecchi, G. a., Soden, B. J., Wittenberg, A. T., Held, I. M., Leetmaa, A., and Harrison, M. J. (2006). Weakening of tropical Pacific atmospheric circulation due to anthropogenic forcing. *Nature*, 441(7089):73–6.

Venrick, E., McGowan, J., Cayan, D., and Hayward, T. (1987). Climate and Chlorophyll a: Long-Term Trends in the Central North Pacific Ocean. *Science*, 238(4823):70–2.

Vermeij, G. J. (2011). Shifting sources of productivity in the coastal marine tropics during the Cenozoic era. *Proceedings of the Royal Society B-Biological Sciences*, 278(1716):2362–2368.

Walsh, W. A. and Kleiber, P. (2001). Generalized additive model and regression tree analyses of blue shark (Prionace glauca) catch rates by the Hawaii-based commercial longline fishery. *Fisheries Research*, 53:115–131.

Wang, M., Overland, J. E., and Bond, N. A. (2010). Climate projections for selected large marine ecosystems. *Journal of Marine Systems*, 79(3-4):258–266.

Ware, D. M. and Thomson, R. E. (2005). Bottom-up ecosystem trophic dynamics determine fish production in the Northeast Pacific. *Science*, 308(5726):1280–1284.

Welschmeyer, N. A. (1994). Fluorometric analysis of chlorophyll a in the presence of chlorophyll b and phaeopigments. *Limnology and Oceanography*, 39:1985–1992.

Wernand, M., van der Woerd, H., and Gieskes, W. (2013). Trends in ocean colour and chlorophyll concentration from 1889 to 2000, worldwide. *PloS one*, 8(6):1–20.

Wernand, M. R. and Woerd, H. J. v. D. (2010). Ocean colour changes in the North Pacific since 1930. *Journal of the European Optical Society: Rapid Publications*, 5:10015s.

Wiggert, J. D., Murtugudde, R. G., and Christian, J. R. (2006). Annual ecosystem variability in the tropical Indian Ocean: results of a coupled bio-physical ocean general circulation model. *Deep-Sea Res. II*, 53:644–676.

Wilson, E. (1927). Probable inference, the law of succession, and statistical inference. *Journal of the American Statistical Association*, 22(158):209–212.

Wiltshire, K., Harsdorf, S., Smidt, B., Blocker, G., Reuter, R., and Schroeder, F. (1998). The determination of algal biomass (as chlorophyll) in suspended matter from the Elbe estuary and the German Bight: A comparison of high-performance liquid chromatography, delayed fluorescence and prompt fluorescence methods. *Journal of Experimental Marine Biology and Ecology*, 222:113–131.

Wood, R. and Bretherton, C. S. (2006). On the relationship between stratiform low cloud cover and lower-tropospheric stability. *Journal of Climate*, 19(24):6425–6432.

Wood, S. N. (2003). Thin plate regression splines. *Journal of the Royal Statistical Society: Series B (Statistical Methodology)*, 65(1):95–114.

Wood, S. N. (2004). Stable and Efficient Multiple Smoothing Parameter Estimation for Generalized Additive Models. *Journal of the American Statistical Association*, 99(467):673–686.

Woodruff, S. D., Worley, S. J., Lubker, S. J., Ji, Z., Eric Freeman, J., Berry, D. I., Brohan, P., Kent, E. C., Reynolds, R. W., Smith, S. R., and Wilkinson, C. (2011). ICOADS Release 2.5: extensions and enhancements to the surface marine meteorological archive. *International Journal of Climatology*, 31(7):951–967.

Woodworth-Jefcoats, P. a., Polovina, J. J., Dunne, J. P., and Blanchard, J. L. (2013). Ecosystem size structure response to 21st century climate projection: large fish abundance decreases in the central North Pacific and increases in the California Current. *Global change biology*, 19(3):724–33.

Worm, B., Barbier, E. B., Beaumont, N., Duffy, J. E., Folke, C., Halpern, B. S., Jackson, J. B. C., Lotze, H. K., Micheli, F., Palumbi, S. R., Sala, E., Selkoe, K. a., Stachowicz, J. J., and Watson, R. (2006). Impacts of biodiversity loss on ocean ecosystem services. *Science*, 314(5800):787–90.

Worm, B., Hilborn, R., Baum, J. K., Branch, T. a., Collie, J. S., Costello, C., Fogarty, M. J., Fulton, E. a., Hutchings, J. a., Jennings, S., Jensen, O. P., Lotze, H. K., Mace, P. M., McClanahan, T. R., Minto, C., Palumbi, S. R., Parma, A. M., Ricard, D., Rosenberg, A. a., Watson, R., and Zeller, D. (2009). Rebuilding global fisheries. *Science*, 325(5940):578–85.

Yentsch, C. S. and Menzel, D. W. (1963). A method for the determination of phytoplankton chlorophyll and phaeophytin by fluorescence. *Deep Sea Res.*, 10(3):221–231.

Yoder, J. A. and Kennelly, M. A. (2003). Seasonal and ENSO variability in global ocean phytoplankton chlorophyll derived from 4 years of SeaWiFS measurements. *Global Biogeochemical Cycles*, 17(4):1–24.

Yu, J. Y., Vodyanik, M. A., Smuga-Otto, K., Antosiewicz-Bourget, J., Frane, J. L., Tian, S., Nie, J., Jonsdottir, G. A., Ruotti, V., Stewart, R., Slukvin II, and Thomson, J. A. (2007). Induced pluripotent stem cell lines derived from human somatic cells. *Science*, 318(5858):1917–1920.